

Liquid Crystals on paper  
(and cellulose nanofibres)

Harry Edward Albert Toynton, MChem

MSc by Research

University of York

Chemistry

January 2017

## Abstract

This work has built upon previous surface initiated atom transfer radical polymerisations (SI-ATRP) of side chain liquid crystal polymers (SCLCPs) from cellulose (paper) biofibres utilising developments in ATRP chemistry. Activator ReGenerated by Electron Transfer (ARGET) ATRP has been utilised to provide robust conditions for the grafting. Grafts with terminally attached and more sterically restricted laterally attached mesogenic units have been achieved. A new mixing protocol has been developed to allow for the polymerisations in the presence of regenerated cellulose electrospun fibres. Adsorption has been confirmed for both laterally and terminally attached SCLCPs to cellulose with graft-from polymerisations evidenced for the laterally attached regime. Graft-from polymerisations have been achieved with terminally attached mesogens as side chains; however, for the terminally attached SCLCPs physisorption of the sacrificial polymer is also observed. All adsorptions (graftings) were confirmed by FT-IR, with special attention given to the carbonyl peak at  $\sim 1730\text{ cm}^{-1}$ . Cellulose (paper and electrospun fibres) surfaces were characterised by SEM; in addition, the ESF surfaces were studied by polarising optical microscopy (POM). Sacrificial initiator was used to monitor the extent of surface grafting and characterisation of the sacrificial polymer was carried out by gel permeation chromatography,  $^1\text{H}$  NMR and POM.

## Table of Contents

Abstract	2
Table of Contents	3
List of Tables	5
List of Figures	6
List of Schemes	15
List of Equations	17
Acknowledgements	18
Declaration	19
1. Introduction	20
1.1. Liquid Crystals	20
1.2. Polymers	23
1.3. Polymeric Liquid Crystals	27
1.4. Functional Materials	29
1.5. Surface Modification Approaches	33
1.6. Covalent graft modification of Cellulose	34
1.7. Controlled Radical Polymerisation	35
1.8. Surface initiated ATRP, SI-ATRP	39
1.9. Pairing surface grafting and liquid crystals for the functionalisation of cellulose.	41
1.10. Applications	42
1.11. Characterisation Techniques	44
2. Aims	47
3. Results and Discussion	50
3.1. Synthesis of Monomers	52
3.2. Substrate Characterisation	56
3.3. SI-ATRP of the end-on monomer without sacrificial initiator (Entry 1)	64
3.4. SI-ATRP of the end-on monomer with sacrificial initiator (Entry 2)	69
3.5. Potential of Me <sub>6</sub> TREN as an alternative complexing ligand (Entry 3)	74

3.6.	Potential of anisole as an alternative solvent (Entry 4).	81
3.7.	Surface initiated (SI) ARGET ATRP of the end-on acrylate monomer (Entry 7).	85
3.8.	Surface initiated (SI) ARGET ATRP of the side-on acrylate monomer (Entry 8).	90
3.9.	Vacuum Alternative to Mechanical Stirring (VALMS)	97
3.10.	ARGET-ATRP in the absence of controlled mixing (Entry 5).	98
3.11.	ARGET-ATRP with vacuum assisted mixing (Entry 6).	102
3.12.	Model Substrates	105
3.13.	Regeneration of cellulose from cellulose acetate ESF.	107
3.14.	Polymer grafting from regenerated cellulose ESF	108
3.15.	ReGC-ESF graft-from ARGET ATRP polymerisation of the end-on acrylate monomer, 2, in the absence of controlled mixing (Entry 9)	110
3.16.	ReGC-ESF graft-from ARGET ATRP polymerisation of the end-on acrylate monomer, 2, with vacuum assisted mixing (Entry 10)	115
3.17.	ReGC-cellulose ESF graft-from ARGET ATRP polymerisation of the side-on acrylate monomer, 6 ,with vacuum assisted mixing (Entry 11)	119
4.	Mesophase behaviour of polymeric materials	123
4.1.	Sacrificial polymer properties	123
4.2.	Properties of the substrate from the ReGC-ESF graft-from ARGET ATRP polymerisation of the end-on acrylate monomer in the absence of controlled mixing (Entry 9).	140
4.3.	Properties of the substrate from the ReGC-ESF graft-from ARGET ATRP polymerisation of the end-on acrylate monomer with VALMS (Entry 10).	142
4.4.	Properties of the substrate from the ReGC-ESF graft-from ARGET ATRP polymerisation of the side-on acrylate monomer with VALMS (Entry 11).	144
4.5.	Liquid Crystal behaviour conclusions	146
5.	Conclusions	147
5.1.	Future Work	148
6.	Experimental	149
6.1.	Chemical analysis and purification	149
6.2.	Characterisation of Liquid Crystal behaviour	150
6.3.	Synthesis of monomers	151
6.4.	Substrate Synthesis	157
	Abbreviations	188
	References	190

## List of Tables

Table 1: GPC data for the sacrificial LCPs previously reported as previously analysed and using the same polystyrene calibration used for the analysis of subsequent polymers.	63
Table 2: GPC data for the sacrificial LCPs formed in the grafting reactions.	77
Table 3: Phase transition temperatures of the sacrificial polymers, showing good conversion of the end-on acrylate monomer, onsets obtained by DSC on the first cooling from the isotropic, $T_g$ obtained from onset on second heating, at heating/cooling rate of $10\text{ }^\circ\text{C min}^{-1}$ .	126
Table 4: Phase transition temperatures of the sacrificial polymers, showing good conversion of the side-on acrylate monomer, I-N onsets were obtained by DSC on the first cooling from the isotropic, $T_g$ obtained onset on second heating, at heating/cooling rate of $10\text{ }^\circ\text{C min}^{-1}$ .	135
Table 5: Overview of polymerisation variables	186-7

## List of Figures

Figure 1: Representation of the shape of calamitic and discotic liquid crystals.	21
Figure 2: Schematic representation of a simple series of thermotropic phase transformations. a. crystal, b. smectic, c. nematic and d. isotropic.	21
Figure 3: Template of calamitic liquid crystal cores. Modified from [2]. Where A and B are rigid elements (mesogenic cores), X, Z and where deployed Y are linking units, R and R' are terminal chains and N and M substituents.	22
Figure 4: General mechanism for chain growth polymerisation.	23
Figure 5: Example of step growth polymerisation with general diacid and diol monomers.	23
Figure 6: Distribution of molecular weight produced by conventional radical polymerisation and Controlled Radical Polymerisation (specifically RAFT) of the same substrate under comparable polymerisation conditions. [Reproduced from 9].	25
Figure 7: Schematic representation of a comb-shaped side-chain polymer.	26
Figure 8: Schematic representation of linear and branched block copolymers.	27
Figure 9: Schematic representation of a. main chain liquid crystal polymers.	27
Figure 10: Schematic representation of side chain liquid crystal polymers with a. terminally attached side groups, b. laterally attached side groups.	28
Figure 11: Structure of a section of a cellulose polymer.	29
Figure 12: Crystal structure and hydrogen-bonding system in cellulose I $\beta$ from synchrotron X-ray and neutron fibre diffraction [reproduced from 21].	30
Figure 13: The hierarchical structure of cellulose modified from [27].	31
Figure 14: Schematic comparison of the graft-from (a) and graft-to (b) approaches.	34
Figure 15: Comparison of NMP, ATRP and RAFT in the areas related to the synthesis of high molecular weight polymers (HMW), low molecular weight polymers (LMW), end functional polymers (End Funct), block copolymers (Blocks), range of polymerizable monomers (Mon Range), synthesis of various hybrid materials (Hybrids), environmental issues (Env) and polymerization in aqueous media (Water) [reproduced from 8].	36
Figure 16: Structures of the two widely favoured ATRP ligands.	38
Figure 17: Example of the concept of regions of catalyst control, in the case of aqueous systems. This example shows restrictions imposed on catalyst choice by bromide concentration, solution pH and the thermodynamics of the catalytic complex disassociation. Reproduced from [72].	38
Figure 18: Schematic representation of cellulose substrate initiation with grafted initiators.	40
Figure 19: Schematic representation of graft-from polymerisation using a cellulose macroinitiator <i>via</i> ATRP.	40

Figure 20: Schematic representation of graft-from polymerisation of 11-(4'-cyanophenyl-4-phenoxy)undecyl acrylate monomers using a cellulose macroinitiator <i>via</i> ATRP.	42
Figure 21: Schematic representation of pore retention in a GPC column [reproduced from 95].	45
Figure 22: Schematic representation of cellulose side on LCP graft targets.	47
Figure 23: Structures of the target monomers a. 11-(4'-cyanophenyl-4-phenoxy)undecyl acrylate and b. 2-((4-(acryloyloxy)butoxy)carbonyl)-1,4-phenylene bis(4-butoxybenzoate).	49
Figure 24: GPC triple detection trace of the end-on acrylate monomer 2: showing right angle light scattering (RALS), differential pressure (DP) and refractive index (RI).	52
Figure 25: GPC triple detection trace of the end-on acrylate monomer 2 with toluene as an internal standard: showing right angle light scattering (RALS), differential pressure (DP) and refractive index (RI).	53
Figure 26: GPC triple detection trace of the side-on acrylate monomer 6: showing right angle light scattering (RALS), differential pressure (DP) and refractive index (RI).	55
Figure 27: GPC triple detection trace of the side-on acrylate monomer 6 with toluene as an internal standard: showing right angle light scattering (RALS), differential pressure (DP) and refractive index (RI).	55
Figure 28: SEM images of the washed Whatman (I) filter paper at 70× magnification showing visible fibres. Regions 1 and 2 identified ahead of enlargement see Figures 30 & 31.	56
Figure 29: SEM images showing an enlargement of a smooth region of pristine cellulose paper (Figure 27) at a. 330×, b. 750×, c. 2000×, d. 3000×, and e. 8000× magnification.	57
Figure 30: SEM images showing an enlargement of a rougher region of pristine cellulose paper (Figure 27) at a. 330×, b. 750×, c. 2000×, d. 3000×, and e. 8000× magnification.	57
Figure 31: FT-IR of a. pristine and b. initiator grafted filter paper.	59
Figure 32: GPC triple detection trace from the sacrificial polymer formed in Experiment LCP 2 of the previous work: showing right angle light scattering (RALS), differential pressure (DP) and refractive index (RI).	61
Figure 33: SEM images of the surface formed in Experiment LCP 2 of the previous work at a. 330×, b. 750×, c. 2000×, d. 3000×, and e. 8000× magnification.	61
Figure 34: GPC triple detection trace from the sacrificial polymer formed in Experiment LCP 3 of the previous work: showing right angle light scattering (RALS), differential pressure (DP) and refractive index (RI).	62
Figure 35: SEM images of the surface formed in Experiment LCP 3 of the previous work at a. 330×, b. 750×, c. 2000×, d. 3000×, and e. 8000× magnification.	62

Figure 36:  $^1\text{H}$  NMR of the sacrificial polymer from the ATRP of compound **2** with [Cu(I)/PMDETA] in toluene with a macroinitiator and no sacrificial initiator. 65

Figure 37: GPC triple detection trace of sacrificial polymer from the ATRP of compound **2** with [Cu(I)/PMDETA] in toluene with a paper-macroinitiator and no sacrificial initiator: showing right angle light scattering (RALS), differential pressure (DP) and refractive index (RI). 65

Figure 38: FT-IR of substrate achieved from the ATRP of compound **2** with [Cu(I)/PMDETA] in toluene with a macroinitiator and no sacrificial initiator, with insets showing the carbonyl region for the washed filter paper (green), paper-macroinitiator (red) and product substrate (blue). 66

Figure 39: SEM images of the surface obtained from the SI-ATRP reaction of compound **2** with [Cu(I)/PMDETA] in toluene without sacrificial initiator (Entry **1**) at a. 330 $\times$ , b. 750 $\times$ , c. 2000 $\times$ , d. 3000 $\times$ , and e. 8000 $\times$  magnification. 67

Figure 40: Structure of PMDETA. 69

Figure 41: a. Complete  $^1\text{H}$  NMR spectrum of the sacrificial polymer from the synthesis of substrate **4** *via* the ATRP polymerisation of compound **2**. b.  $^1\text{H}$  NMR spectrum for the monitoring region of the sacrificial polymer used to monitor the progress of the reaction. 70

Figure 42: GPC triple detection trace of sacrificial initiator from the synthesis of substrate **4** *via* the ATRP polymerisation of compound: showing right angle light scattering (RALS), differential pressure (DP) and refractive index (RI). Insert shows the relative responses of the signal at 14.31 mL compared to the negative system peaks. 71

Figure 43: FTIR of the substrate obtained *via* the synthesis of substrate **4** *via* the ATRP polymerisation of compound **2**, with an inset showing the carbonyl region for the product substrate (blue). 72

Figure 44: SEM images of the surface obtained from the SI-ATRP reaction of compound **2** with [Cu(I)/PMDETA] in the presence of sacrificial initiator in toluene (Entry **2**) at a. 330 $\times$ , b. 750 $\times$ , c. 2000 $\times$ , d. 3000 $\times$ , and e. 8000 $\times$  magnification. 73

Figure 45: a. Complete  $^1\text{H}$  NMR spectrum of the sacrificial polymer from the synthesis of substrate **5** *via* the ATRP polymerisation of compound **2** using  $\text{Me}_6\text{TREN}$  as the complexing ligand for the Cu(I) catalyst. b.  $^1\text{H}$  NMR spectrum for the monitoring region of the sacrificial polymer used to monitor the progress of the reaction. 75

Figure 46: GPC triple detection trace of sacrificial initiator from the synthesis of substrate **5** *via* the ATRP polymerisation of compound **2** using  $\text{Me}_6\text{TREN}$  as the complexing ligand for the Cu(I) catalyst: showing right angle light scattering (RALS), differential pressure (DP) and refractive index (RI). 76

Figure 47: FT-IR of the substrate obtained from the synthesis of substrate **5** *via* the ATRP 78

polymerisation of compound **2** using Me<sub>6</sub>TREN as the complexing ligand for the Cu(I) catalyst, with an inset showing the carbonyl region for the product substrate (blue).

Figure 48: SEM images of the surface obtained from the SI-ATRP reaction of compound **2** with [Cu(I)/Me<sub>6</sub>TREN] in the presence of sacrificial initiator in toluene (Entry **3**) at a. 330×, b. 750×, c. 2000×, d. 3000×, and e. 8000× magnification. 79

Figure 49: Structures of copper(I) and copper(II) complexes derived from previously characterised complexes. [Modified from 71] 80

Figure 50: Monitoring region of the sacrificial polymer <sup>1</sup>H NMR monitoring region from the synthesis of substrate **6** *via* the ATRP polymerisation of compound **2** in anisole. 81

Figure 51: GPC triple detection trace of sacrificial initiator from the synthesis of substrate **6** *via* the ATRP polymerisation of compound **2** in anisole: showing right angle light scattering (RALS), differential pressure (DP) and refractive index (RI). 82

Figure 52: FT-IR of the substrate achieved from the synthesis of substrate **6** *via* the ATRP polymerisation of compound **2** in anisole, with an inset showing the carbonyl region for the product substrate (blue). 83

Figure 53: SEM images of the surface obtained from the SI-ATRP reaction of compound **2** with [Cu(I)/PMDETA] in the presence of sacrificial initiator in anisole (Entry **4**) at a. 330×, b. 750×, c. 2000×, d. 3000×, and e. 8000× magnification. 84

Figure 54: Monitoring region of the sacrificial polymer <sup>1</sup>H NMR monitoring region from the synthesis of substrate **9** *via* the ARGET ATRP of compound **2**. 86

Figure 55: GPC triple detection trace of sacrificial initiator from the synthesis of substrate **9** *via* the ARGET ATRP of compound **2**: showing right angle light scattering (RALS), differential pressure (DP) and refractive index (RI). 86

Figure 56: FT-IR of the substrate achieved *via* the synthesis of substrate **9** *via* the ARGET ATRP of compound **2**. 87

Figure 57: SEM images of the surface obtained from the SI-ARGET ATRP reaction of compound **2** with [Cu(II)/PMDETA] – ascorbic acid in the presence of sacrificial initiator in anisole (Entry **7**) at a. 330×, b. 750×, c. 2000×, d. 3000×, and e. 8000× magnification. 88

Figure 58: a. Complete <sup>1</sup>H NMR spectrum of the sacrificial polymer from the synthesis of substrate **10** *via* the ATRP polymerisation of compound **6**. b. <sup>1</sup>H NMR spectrum for the monitoring region of the sacrificial polymer used to monitor the progress of the reaction. 91

Figure 59: GPC triple detection trace of sacrificial initiator from the synthesis of **10** *via* the ARGET ATRP of compound **6**: showing right angle light scattering (RALS), differential pressure (DP) and refractive index (RI). 92

Figure 60: FT-IR of from the substrate achieved *via* the SI-ARGET ATRP of compound **6**, with an inset showing the carbonyl region for the product substrate (blue). 94

Figure 61: SEM images of the surface obtained from the SI-ARGET ATRP reaction of compound **6** with [Cu(II)/PMDETA] – ascorbic acid in the presence of sacrificial initiator in anisole (Entry **8**) at a. 330×, b. 750×, c. 2000×, d. 3000×, and e. 8000× magnification. 95

Figure 62: Monitoring region of the sacrificial polymer <sup>1</sup>H NMR monitoring region from the synthesis of substrate **7** *via* the ARGET polymerisation of compound **2** in the absence of controlled mixing. 98

Figure 63: GPC triple detection trace of sacrificial initiator from the synthesis of substrate **7** *via* the ARGET polymerisation of compound **2** in the absence of controlled mixing: showing right angle light scattering (RALS), differential pressure (DP) and refractive index (RI). 99

Figure 64: FT-IR of the substrate obtained from the synthesis of substrate **7** *via* the ARGET polymerisation of compound **2** in the absence of stirring, with an inset showing the carbonyl region for the product substrate (blue). 99

Figure 65: SEM images of the surface obtained from the SI-ARGET ATRP reaction of compound **2** with [Cu(II)/PMDETA] – ascorbic acid, in the presence of sacrificial initiator in anisole (Entry **5**), without controlled mixing, at a. 330×, b. 750×, c. 2000×, d. 3000×, and e. 8000× magnification. 100

Figure 66: Monitoring region of the sacrificial polymer <sup>1</sup>H NMR monitoring region from the synthesis of substrate **8** *via* the ARGET-ATRP of compound **2** with vacuum assisted mixing. 102

Figure 67: GPC triple detection trace of sacrificial initiator from the synthesis of substrate **8** *via* the ARGET polymerisation of compound **2** mixed utilising the vacuum alternative to mechanical stirring: showing right angle light scattering (RALS), differential pressure (DP) and refractive index (RI). 103

Figure 68: FT-IR of the substrate achieved from the synthesis of substrate **8** *via* the ARGET polymerisation of compound **2** mixed utilising the vacuum alternative to mechanical stirring. 103

Figure 69: SEM images of the surface obtained from the SI-ARGET ATRP reaction of compound **2** with [Cu(II)/PMDETA] – ascorbic acid, in the presence of sacrificial initiator in anisole/toluene (Entry **6**), with VALMS at a. 330×, b. 750×, c. 2000×, d. 3000×, and e. 8000× magnification. 104

Figure 70: SEM images of ESF cellulose acetate mat, at a. 70× b. 330×, c. 2000× and d. 8000× magnification. Analysed following the boiling toluene, ethanol wash cycle. 106

Figure 71: SEM images of the regenerated cellulose fibres obtained from the NaOH treatment of cellulose acetate ESF. at a. 330×, b. 750×, c. 2000×, d. 3000×, and e. 8000× magnification. 107

Figure 72: FT-IR showing a. the initial cellulose acetate, b. the regenerated cellulose ESF and c. an ESF macroinitiator (substrate <b>12b</b> ).	109
Figure 73: <sup>1</sup> H NMR monitoring region from the synthesis of substrate <b>13</b> <i>via</i> the ARGET-ATRP polymerisation of compound <b>2</b> in the absence of stirring.	110
Figure 74: GPC triple detection trace of sacrificial initiator from the synthesis of substrate <b>13</b> <i>via</i> the ARGET polymerisation of compound <b>2</b> in the absence of stirring: showing right angle light scattering (RALS), differential pressure (DP) and refractive index (RI).	111
Figure 75: FT-IR of a. Compound <b>2</b> , b. Sacrificial polymer from the monitoring of the graft-from modification of substrate <b>13</b> , c. Regenerated electrospun fibre, d. Electrospun fibre macroinitiator, e. scaled summation of b. and c. to predict the infrared spectra of sacrificially formed polymer physisorbed on the substrate surface, f. substrate <b>13</b> synthesised <i>via</i> the ARGET-ATRP of compound <b>2</b> in the absence of stirring following the initial washing, g. substrate <b>13</b> following an additional washing procedure of boiling toluene and ethanol.	112
Figure 76: SEM images of the surface obtained from the SI-ARGET ATRP reaction of compound <b>2</b> with [Cu(II)/PMDETA] – ascorbic acid, in the presence of sacrificial initiator in anisole (Entry <b>9</b> ), without controlled mixing, at a. 330×, b. 750×, c. 2000×, d. 3000×, and e. 8000× magnification. Analysed following the boiling toluene, ethanol wash cycle.	113
Figure 77: Monitoring region of the sacrificial polymer <sup>1</sup> H NMR monitoring region from the synthesis of substrate <b>14</b> <i>via</i> the ARGET-ATRP of compound <b>2</b> mixed utilising the vacuum alternative to mechanical stirring.	115
Figure 78: GPC trace of sacrificial initiator from the synthesis of substrate <b>14</b> <i>via</i> the ARGET atom transfer radical polymerisation of compound <b>2</b> mixed utilising the vacuum alternative to mechanical stirring: showing right angle light scattering (RALS), differential pressure (DP) and refractive index (RI).	116
Figure 79: FT-IR of a. Compound <b>2</b> , b. Sacrificial polymer from the monitoring of the graft-from modification of substrate <b>14</b> , c. Regenerated electrospun fibre, d. Electrospun fibre macroinitiator, e. scaled summation of b. and c. to predict the infrared spectra of sacrificially formed polymer physisorbed on the substrate surface, f. substrate <b>14</b> synthesised <i>via</i> the ARGET-ATRP of compound <b>2</b> in the absence of stirring following the initial washing, g. substrate <b>14</b> following an additional washing procedure of boiling toluene and ethanol.	116
Figure 80: SEM images of the surface obtained from the SI-ARGET ATRP reaction of compound <b>2</b> with [Cu(II)/PMDETA] – ascorbic acid, in the presence of sacrificial initiator in anisole (Entry <b>10</b> ), with VALMS, at a. 330×, b. 750×, c. 2000×, d. 3000×, and e. 8000× magnification. Analysed following the boiling toluene, ethanol wash cycle.	117

- Figure 81: Monitoring region of the sacrificial polymer  $^1\text{H}$  NMR monitoring region from the synthesis of substrate **15** *via* the ARGET ATRP of compound **6** mixed utilising the vacuum alternative to mechanical stirring. 119
- Figure 82: GPC trace of sacrificial initiator from the synthesis of substrate **15** *via* the ARGET atom transfer radical polymerisation of compound **6** mixed utilising the vacuum alternative to mechanical stirring: showing right angle light scattering (RALS), differential pressure (DP) and refractive index (RI). 120
- Figure 83: FT-IR of a. Compound **6**, b. Sacrificial polymer from the monitoring of the graft-from modification of substrate **15**, c. Regenerated electrospun fibre, d. Electrospun fibre macroinitiator, e. scaled summation of b. and c. to predict the infrared spectra of sacrificially formed polymer physisorbed on the substrate surface, f. substrate **15** synthesised *via* the ARGET-ATRP of compound **6** in the absence of stirring following the initial washing, g. substrate **15** following an additional washing procedure of boiling toluene and ethanol. 121
- Figure 84: SEM images of the surface obtained from the SI-ARGET ATRP reaction of compound **6** with  $[\text{Cu}(\text{II})/\text{PMDETA}] - \text{ascorbic acid}$ , in the presence of sacrificial initiator in anisole (Entry **11**), with VALMS, at a. 330 $\times$ , b. 750 $\times$ , c. 2000 $\times$ , d. 3000 $\times$ , and e. 8000 $\times$  magnification. Analysed following the boiling toluene, ethanol wash cycle. 122
- Figure 85: DSC trace of the sacrificial polymer (1.22 mg) formed in the  $\text{CuI}/\text{Me}_6\text{TREN}$  catalysed polymerisation of the end-on monomer acrylate (Entry **3**), showing the: second heat (blue), first cool (red), third heat (yellow) and second cooling (purple) cycles. 124
- Figure 86: DSC trace of the sacrificial polymer (1.37 mg) formed in the ARGET-ATRP reaction in the absence of controlled mixing (Entry **5**), showing the: second heat (blue), first cool (red), third heat (yellow) and second cooling (purple) cycles. 124
- Figure 87: DSC trace of the sacrificial polymer (1.12 mg) formed in the ARGET-ATRP reaction with vacuum assisted mixing (Entry **6**), showing the: second heat (blue), first cool (red), third heat (yellow) and second cooling (purple) cycles. 125
- Figure 88: DSC trace of the sacrificial polymer (1.78 mg) formed in the surface initiated (SI) ARGET ATRP of the end-on acrylate monomer (Entry **7**), showing the: second heat (blue), first cool (red), third heat (yellow) and second cooling (purple) cycles. 125
- Figure 89: DSC trace of the sacrificial polymer (1.04 mg) formed in ReGC-ESF graft-from ARGET ATRP polymerisation of the end-on acrylate monomer with vacuum assisted mixing (Entry **10**), showing the: second heat (blue), first cool (red), third heat (yellow) and second cooling (purple) cycles. 125
- Figure 90: Focal-conic domain and sections through the domain for the case of an ellipse and hyperbola [reproduced from 117]. 127

Figure 91: Photomicrographs of sacrificial polymer from the paper initiated ARGET ATRP of compound **2**, with stirring (Entry **7**), showing the development of the SmA phase on cooling from the isotropic liquid at 122.3 (a), 117.7 (b), 110.0 (c), 100.5 (d), 92.8 (e), 72.5 (f) °C, at magnification ×100. 128

Figure 92: Photomicrographs of sacrificial polymer from the RegC ESF initiated ARGET ATRP of compound **2**, in the absence of mixing (Entry **9**), showing the development of the SmA phase on cooling from the isotropic liquid at 115.8 °C and 110.0 °C, at magnification ×100. 129

Figure 93: Photomicrographs of sacrificial polymer from the RegC ESF initiated ARGET ATRP of compound **2**, with VALMS (Entry **10**), on cooling from the isotropic liquid. Showing a focal conic texture of the SmA phase at 131.9 °C (a) and the broken-fan texture of the SmC phase at 28.8 °C (b) confined between two layers, and the SmA phase at 131.9 °C (c) on a single surface at magnification ×100. Note different regions are observed in all photomicrographs. 130

Figure 94: Photomicrographs of the ‘Frozen’ smectic (glass) phases observed from the cooling (~ 5 °C (a) and room temperature for one week (b)) of a. paper initiated, with stirring (Entry **7**) and b. ESF initiated without mixing (Entry **9**) at magnification ×100. For the same regions previously observed. 131

Figure 95: Schematic representation of the interdigitated (a) and double-layer (b) alternatives for mesogenic group arrangement at the interface of terminally attached SCLCPs. 132

Figure 96: Representation of the intermolecular interactions between adjacent cyanobiphenyloxy groups in an interdigitated smectic phase. 132

Figure 97: DSC trace of the sacrificial polymer (1.63 mg) formed in the surface initiated (SI) ARGET ATRP of the side-on acrylate monomer (Entry **8**), showing the: second heat (blue), first cool (red), third heat (yellow) and second cooling (purple) cycles. 134

Figure 98: DSC trace of the sacrificial polymer (2.28 mg) formed in the ReGC-cellulose ESF graft-from ARGET ATRP polymerisation of the side-on acrylate monomer with vacuum assisted mixing (Entry **11**), showing the: second heat (blue), first cool (red), third heat (yellow) and second cooling (purple) cycles. 134

Figure 99: Photo micrographs of sacrificial polymer from the paper initiated ARGET ATRP of compound **6**, with stirring, on cooling from the isotropic liquid at 103.6 °C on a single surface at magnification ×100. 136

Figure 100: Photo micrographs of sacrificial polymer from the RegC ESF initiated ARGET ATRP of compound **6**, with VALMS, with the cross polarisers at 50° (a), 90° (b) and 130° (c) and at 105.0 °C and on cooling from the isotropic liquid at 105.5 °C under crossed 137

polarisers (d) at magnification  $\times 100$ .

Figure 101: Photomicrographs of the 'Frozen' nematic (glass) phases observed from 138 cooling ( $\sim 5\text{ }^{\circ}\text{C}$  (a) and room temperature for one week (b)) of sample paper initiated (a), and RegC initiated (b) ARGET ATRP at magnification  $\times 100$ .

Figure 102: Schematic representation of the backbone jacketing by laterally attached 139 mesogenic side-groups.

Figure 103: Photomicrography of substrate **14** taken at (left to right)  $150.0\text{ }^{\circ}\text{C}$ ,  $140.7\text{ }^{\circ}\text{C}$  140 and  $50.4\text{ }^{\circ}\text{C}$ ) at (from top to bottom) 1008 ms exposure, crossed polarisers, 304 ms exposure crossed polarisers and 144 ms exposure parallel polarisers. All photomicrographs were taken with the bright field at the same illumination.

Figure 104: Photomicrography of substrate **15** taken at (left to right)  $150.0\text{ }^{\circ}\text{C}$ ,  $142.2\text{ }^{\circ}\text{C}$  142 and  $50.0\text{ }^{\circ}\text{C}$ ) at (from top to bottom) 1008 ms exposure, crossed polarisers, 304 ms exposure crossed polarisers and 144 ms exposure parallel polarisers. All photomicrographs were taken with the bright field at the same illumination.

Figure 105: Photomicrography of substrate **16** taken at (left to right)  $150.0\text{ }^{\circ}\text{C}$ ,  $140.7\text{ }^{\circ}\text{C}$  144 and  $50.4\text{ }^{\circ}\text{C}$ ) at (from top to bottom) 1008 ms exposure, crossed polarisers, 304 ms exposure crossed polarisers and 144 ms exposure parallel polarisers. All photomicrographs were taken with the bright field at the same illumination.

Figure 106: 4'-((11-hydroxyundecyl)oxy)-[1,1'-biphenyl-yl]carbonitrile. 151

Figure 107: 11-((4'-cyano-[1,1'-biphenyl]-4-yl)oxy)undecyl acrylate. 152

Figure 108: Benzyl-2,5-dihydroxybenzoate. 153

Figure 109: Benzyl-2,5-di(4-butoxybenzoyloxy)benzoate. 154

Figure 110: 2,5-bis((4-butoxybenzoyl)oxy)benzoic acid. 155

Figure 111: 2-((4-(acryloyloxy)butoxy)carbonyl)-1,4-phenylene bis(4-butoxybenzoate). 156

Figure 112: Cellulose(paper) macroinitiator. 158

Figure 113: Cellulose(paper) macroinitiator. 159

Figure 114: Regenerated cellulose ESF mat. 176

Figure 115: Cellulose(ESF) macroinitiator. 177

## List of Schemes

Scheme 1: General Mechanism for above. ATRA, and below ATRP modified from [66].	37
Scheme 2: Mechanism for ARGET ATRP as proposed by Jakubowski et al.	39
Scheme 3: Total synthetic route for the synthesis of the cyanobiphenyl acrylate, <b>2</b> , from 4'-cyano-4'-hydroxybiphenyl.	52
Scheme 4: Total synthetic route for the synthesis of side-on acrylate, <b>6</b> , from 2,5-dihydroxybenzoic acid.	54
Scheme 5: Reaction scheme for the Cu(I)Br/PMDETA activated ATRP of substrate <b>3</b> via the graft from polymerisation of substrate <b>1a</b> with compound <b>2</b> without sacrificial initiator.	64
Scheme 6: Reaction scheme for the Cu(I)Br/PMDETA activated ATRP of substrate <b>4</b> via the graft from polymerisation of substrate <b>1b</b> with compound <b>2</b> in the presence of sacrificial initiator.	70
Scheme 7: Reaction scheme for the Cu(I)/Me <sub>6</sub> TREN activated ATRP of substrate <b>5</b> via the graft from polymerisation of substrate <b>1c</b> with compound <b>2</b> in the presence of sacrificial initiator.	74
Scheme 8: Reaction scheme for the Cu(I)Br/PMDETA activated ATRP of substrate <b>6</b> via the graft from polymerisation of substrate <b>6</b> in the presence of sacrificial initiator.	81
Scheme 9: Reaction scheme for the Cu(II)Br <sub>2</sub> /PMDETA activated ATRP of substrate <b>9</b> via the graft from polymerisation of substrate <b>2ai</b> with compound <b>2</b> in the presence of sacrificial initiator.	85
Scheme 10: Reaction scheme for the Cu(II)Br <sub>2</sub> /PMDETA activated ARGET ATRP of substrate <b>10</b> via the graft from polymerisation of substrate <b>2ai</b> with compound <b>6</b> in the presence of sacrificial initiator.	90
Scheme 11: Potential R-R termination routes for radical polymerisations within the context of this work.	93
Scheme 12: SI-ATRP of compound <b>2</b> , from cellulose (paper) macroinitiator using Cu(I)/PMEDTA in toluene, under argon (with stirring).	160
Scheme 13: SI-ATRP of compound <b>2</b> , from cellulose (paper) macroinitiator using Cu(I)/PMEDTA in toluene, with sacrificial initiator (ebib) under argon (with stirring).	162
Scheme 14: SI-ATRP of compound <b>2</b> , from cellulose (paper) macroinitiator using Cu(I)/Me <sub>6</sub> TREN in toluene, with sacrificial initiator, ebib, under argon (with stirring).	164
Scheme 15: SI-ATRP of compound <b>2</b> , from cellulose (paper) macroinitiator using Cu(I)/PMEDTA in anisole, with sacrificial initiator, ebib, under argon (with stirring).	166
Scheme 16: SI-ARGET ATRP of compound <b>2</b> , from cellulose (paper) macroinitiator using Cu(II)/PMEDTA – ascorbic acid in anisole/toluene, with sacrificial initiator, ebib, under	168

argon (without mechanical mixing).

Scheme 17: SI-ARGET ATRP of compound **2**, from cellulose (paper) macroinitiator using Cu(II)/PMEDTA – ascorbic acid in anisole/toluene, with sacrificial initiator, ebib, under vacuum (without mechanical mixing). 170

Scheme 18: SI-ARGET ATRP of compound **2**, from cellulose (paper) macroinitiator using Cu(II)/PMEDTA – ascorbic acid in anisole, with sacrificial initiator, ebib, under argon (with stirring). 172

Scheme 19: SI-ARGET ATRP of compound **6**, from cellulose (paper) macroinitiator using Cu(II)/PMEDTA – ascorbic acid in anisole, with sacrificial initiator, ebib, under argon (with stirring). 174

Scheme 20: SI-ARGET ATRP of compound **2**, from cellulose (ESF) macroinitiator using Cu(II)/PMEDTA – ascorbic acid in anisole/toluene, with sacrificial initiator, ebib, under argon (without mixing). 178

Scheme 21: SI-ARGET ATRP of compound **2**, from cellulose (ESF) macroinitiator using Cu(II)/PMEDTA – ascorbic acid in anisole/toluene, with sacrificial initiator, ebib, under argon (without mixing). 180

Scheme 22: SI-ARGET ATRP of compound **2**, from cellulose (ESF) macroinitiator using Cu(II)/PMEDTA – ascorbic acid in anisole/toluene, with sacrificial initiator, ebib, under vacuum (without mechanical mixing). 182

Scheme 23: SI-ARGET ATRP of compound **6**, from cellulose (ESF) macroinitiator using Cu(II)/PMEDTA – ascorbic acid in anisole/toluene, with sacrificial initiator, ebib, under vacuum (without mechanical mixing). 184

## List of Equations

Equation 1: Equation for number average molar mass.	24
Equation 2: Equation for mass average molar mass.	24
Equation 3: Equation for polydispersity.	25
Equation 4: Hookes Law. Where $\sigma$ is the applied stress, E is the material constant (Young's modulus) and $\epsilon$ is the resulting strain.	26

## Acknowledgements

This thesis would not have been possible without the support and encouragement of all my nearest and dearest. I am mindful of how fortunate I am that my family have always supported me in pursuing my passions. The support and love (and worry) of my parents, grandparents, brothers and other family members means more to me than can ever be expressed.

My unreserved thanks go to Isabel Saez for having the faith to accept me as a student; the scientific interest that has made this work as novel as possible and the scientific rigour to ensure that this work tells as complete a story as was possible in the time available. I'd like to thank Stephen Cowling for acting as my IPM and offering his scientific insights.

It would not have been possible to explore the grafting of liquid crystal polymers from electrospun fibres without the generosity of Maria Godinho and the members of the Soft and biofunctional materials group at the New University of Lisbon for providing the electrospun cellulose acetate mats used in this work, and enthusiasm for this project.

My thanks go to Meg Stark and Karen Hodgkinson for accommodating me during my SEM studies and the Langwith welfare team for agreeing to have our team meetings at 9 am every Monday, to accommodate my lab work.

Thank you to everyone who has ensured that this period of my life has been so rewarding. My thanks go to the members of the York Liquid Crystals and Functional Materials group who have had the questionable pleasure of my company on a day to day basis and have provided many an enjoyable conversations on scientific and trivial matter. Particular thanks go to Richard Mandle who is always interested in discussing any scientific issues and who ran the HPLCs of the side-on monomer, to Julia Sarju (who no matter how busy always made time and provided valuable feedback), Rachel Bean, Iman Khazal and Craig Archbald for friendship and help.

Alessio Riccobono and Ellie Byrne for offering me shelter over the Christmas period. Jessica Andrews for reading more of my thesis than can possibly be fair and to Harry Rackham and Jordan Herod who have also read their fair share.

I'd like to also thank Duncan Bruce, Paul Walton and John Goodby for nurturing my passion for science. To David Pugh and the teaching lab technicians for helping me develop more broadly.

To all of my closest friends for their understanding and the escapes they have provided to me when they were most needed. I want to express special gratitude to those who have endured my impatience and impetuosity – particularly while I have been writing up.

## **Declaration**

I declare that this thesis is a presentation of original work and I am the sole author. This work has not previously been presented for an award at this, or any other, University. All sources are acknowledged as References. Some of the results have previously been presented in the form of a poster entitled "Functionalisation of Paper via Liquid Crystal Attachment" as part of the KMS Prize Winners Seminar in the chemistry department of the University of York. SEM was conducted in the 'Imagine and Cytometry facility' of the Biology Department of the University of York, instrument set up and sputter coatings were performed by Meg Stark and Karen Hodgkinson.

## 1. Introduction

Cheap versatile sensing devices are desirable for a wide range of applications. Medical operations in remote, low population density areas and large data set 'citizen science' are both currently restricted by the availability of economically viable sensing devices. Liquid crystals offer a route to light weight, single unit devices. Interest is growing about the potential of surface polymer brushes for furthering sensor technology.<sup>1</sup> Cellulose derived substrates offer a route to combine the desirable properties of LCs with readily available support substrates.

### 1.1. Liquid Crystals

The liquid crystal state exists as an intermediate state between the solid and isotropic liquid phases (states) of matter. Liquid crystal phases are closely linked to anisotropy (direction dependence) in the molecular shape or distribution of charge (microphase segregation).

Molecules in condensed phases pack to maximise the favourable interactions between neighbouring molecules and to minimise unfavourable interactions. The anisotropy of the molecules introduces a packing preference which results in local direction dependent order. The packing restraints caused by anisotropy result in a degree of long-range order; additional dynamics can result in orientational order and/or positional order.

Liquid crystals have the disorder associated with the liquid phase showing a degree of translational freedom, but still retain certain orientational order (akin to a crystal).

Orientational order is measured in terms of the favourability of a molecular axis to point in a preferred direction. This statistically preferred direction is known as the director. In a case where the molecules are perfectly aligned the value of the director is 1; in a completely randomly aligned sample the value is 0; this is the case in the liquid state. Liquid crystals being an intermediate phase exhibit intermediate degrees of orientational order.

Liquid crystals can be classified by the stimulus that induces the phase transformations. In some materials mesophase formation is driven by the presence of a solvent (lyotropic liquid crystals). In other materials mesophase formation is driven by changes in temperature (thermotropic liquid crystals).

#### 1.1.1. Thermotropic Liquid Crystals

The term mesophase is a comprehensive term, *meso* meaning middle reflects that mesophases are stable between the solid and liquid phases. The structural properties of a liquid crystalline phase are the *mesomorphic* properties, while molecular species capable of assembling in liquid crystal phases are mesogenic. Mesogenic materials have sufficient rigidity and favourable molecular shape properties to assemble to form *mesophases*.

Thermotropic liquid crystals can be classified by their molecular shape (aspect ratio) either as calamitic (rod-like) or discotic (disc-like). Calamitic liquid crystals have a high aspect ratio resulting from a long thin shape; discotic liquid crystals have the alternative anisotropy of a short length and large diameter (Figure 1).

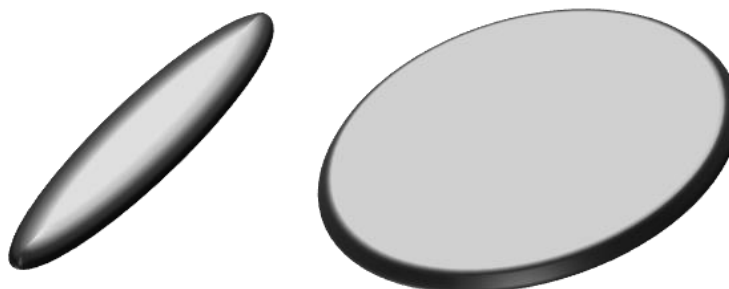


Figure 1: Representation of the shape of calamitic and discotic liquid crystals.

The most abundant class of liquid crystals are calamitic liquid crystals. Calamitic liquid crystals exhibit a rich variety of liquid crystal phases, although the most commonly encountered phases are the nematic and the smectic phases.

The intermolecular transformations that occur with increasing temperature in some common calamitic materials are shown in Figure 2. A crystalline solid (a) has long range order across a 3-D lattice and complete orientational order. On increasing temperature it transforms to a smectic phase (b). The smectic phases maintain statistical layer ordering in 2-D layers and orientational ordering, but now show translational order within the layers. As the energy of the system is further increased, molecules gain free translational order in all directions, resulting in a nematic phase (c). Nematics maintain their orientational order. When molecules do not have appropriate interactions to promote the formation of layers only the nematic phases are exhibited. The final phase in the continuum is the liquid phase (isotropic) where all ordering in the system breaks down (d).

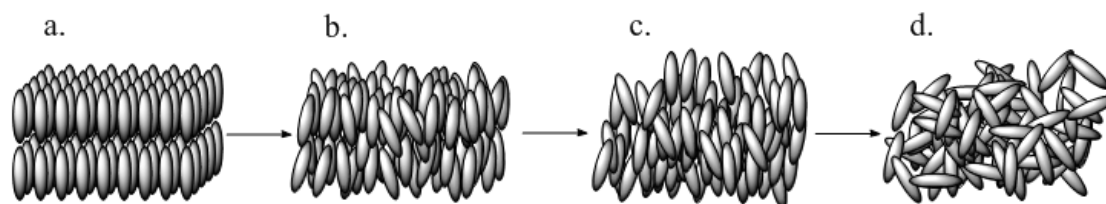


Figure 2: Schematic representation of a simple series of thermotropic phase transformations. a. crystal, b. smectic, c. nematic and d. isotropic.

In order to exploit desirable phases an understanding of how structural modifications at the molecular level can be utilised to impart favourable phase behaviour on a bulk must be obtained. A common feature in thermotropic liquid crystals is the presence of a rigid core. If the core is sufficiently rigid it will have a significant enough influence on the molecule's shape promote the

formation of liquid crystalline phases. Traditionally phenyl and/or cyclohexyl rings form part of the mesogenic core (Figure 3).

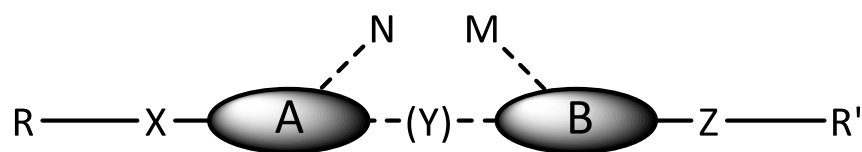


Figure 3: Template of calamitic liquid crystal cores. Modified from [2]. Where A and B are rigid elements (mesogenic cores), X, Z and where deployed Y are linking units, R and R' are terminal chains and N and M substituents.

Mesogenic units with enhanced ability to support mesophases can be achieved by linking additional core components or by supporting better polarisable conjugation with end substituents.

Additional components can be included to favour the formation of layers (lamellar phase), chiral behaviour (chiral group inclusion) or tilting of molecular alignment.<sup>3-5</sup>

Anisotropic materials have, due to their shape, two or more refractive indices. For this purpose, we will consider, rod-like, calamitic liquid crystals with two refractive indices. In a rod-like molecule the first refractive index is that parallel to the long axis of the molecule, this parallel refractive index is known as the extraordinary refractive index  $n_e$ . A second refractive index exists perpendicular to the long axis this is known as the ordinary refractive index  $n_o$  - for a rod-like molecule two degenerate ordinary refractive indices exist. Where the two refractive indices,  $n_e$  and  $n_o$ , are non-degenerate they refract light to different degrees. The magnitude of the difference is quantified by the birefringence:

$$\Delta n = n_e - n_o$$

When an incident ray of light encounters an anisotropic material, each polarisation component of the incident light interacts with the different refractive indices perpendicular to each other with different degrees of refraction. The different routes of the two polarization components result in path length of different multiples of the wavelength. The difference in phase velocity of the extraordinary ray from the ordinary ray, results in constructive and destructive interference.

The interaction of the medium with the light is dependent on the angle at which the light encounters the molecules, if the molecules are aligned with directional order a birefringence affect can occur through the medium. By placing a cross polariser perpendicular to the incident light polarization, only refracted light can be detected. This can be used to identify liquid crystal phases and is used commercially for display devices.<sup>6</sup>

## 1.2. Polymers

Polymers are extended molecules constructed from large numbers of small fragments, known as monomers. The construction of the simplest polymers is represented by the degree of polymerisation  $\overline{X}_n$  where  $n$  is the number of repeat units.

Synthetic and natural polymers are known, the most abundant natural polymer on earth is cellulose (Section 1.4.1). Polymers show a huge range of tailorable properties; amongst these are viscosity, stress-strain profiles (including plastics) and conductance. As a result of their huge tailorability and favourable economic factors, polymers have become the material of the modern age.

### 1.2.1. Classification

There are two broad methods of synthesising polymers from their constituent monomers. Chain growth polymerisation, otherwise known as addition polymerisation, is the process where a monomer adds to the living end of a propagating chain (Figure 4).<sup>7</sup>

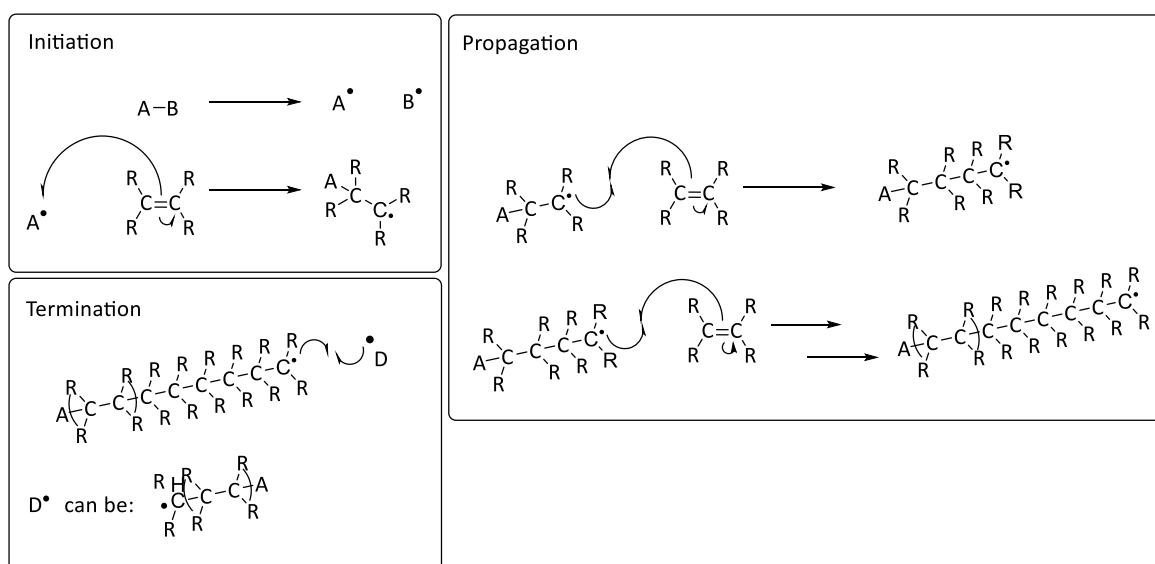


Figure 4: General mechanism for chain growth polymerisation.

However, step growth polymerisation, historically known as condensation polymerisation, differs from the above as a small molecule is eliminated as the reactive functional groups combine in the polymerisation reaction; this is entropically favoured which drives the process (Figure 5).

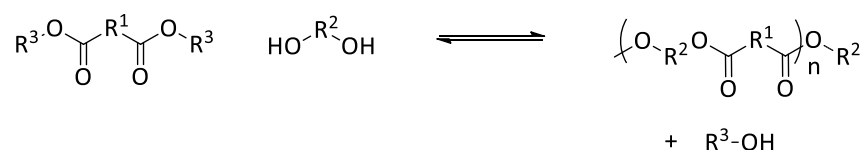


Figure 5: Example of step growth polymerisation with general diacid and diol monomers.

## 1.2.2. Properties: Chain Distribution

Polymers exhibit a wide range of tuneable physical properties as well as some unique properties. These properties are determined by factors including size and intermolecular interactions.

Dispersity in polymer chain length means that different masses can be used to describe the polymers properties.

The number average molar mass is the simple mean of all mass of all polymer chains (Equation 1).

$$\bar{M}_n = \frac{\sum_i N_i M_i}{\sum_i N_i}$$

*Equation 1: Equation for number average molar mass.*

The mass average molar mass better describes some properties a polymer exhibits, where they are dominated by larger mass polymers, by assigning them a higher weighting (Equation 2).

$$\bar{M}_w = \frac{\sum_i N_i M_i^2}{\sum_i N_i M_i}$$

*Equation 2: Equation for mass average molar mass.*

The inability to assign a particular molecular weight to a polymer is one of the key distinguishing features of polymerisation, since polymer chains with different numbers of repeat units are formed. Recently effectively controlled radical polymerisations have been developed, that made it possible to significantly narrowed the range of molecular weights produced in the polymerisation reaction.<sup>8</sup> However, variation does still lead to a distribution in chain lengths in even the best controlled systems (Figure 6).

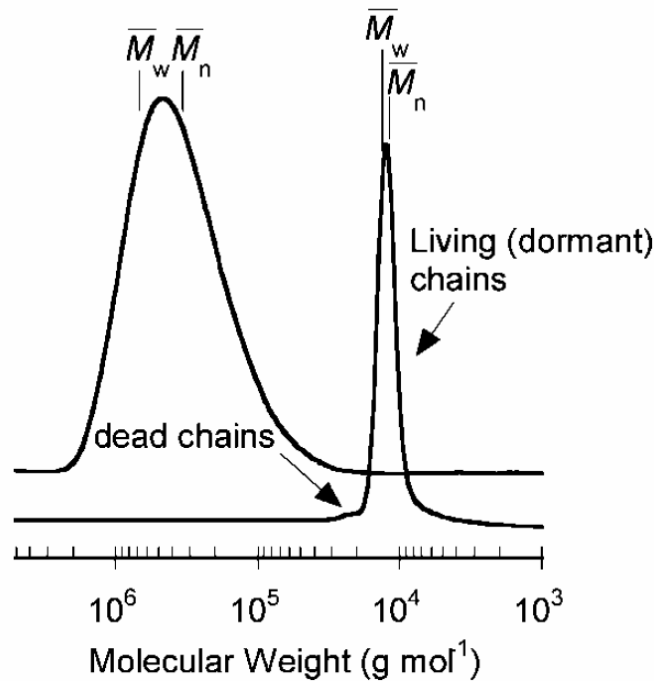


Figure 6: Distribution of molecular weight produced by conventional radical polymerisation and Controlled Radical Polymerisation (specifically RAFT) of the same substrate under comparable polymerisation conditions. [Reproduced from 9].

By comparing the difference between  $M_n$  and  $M_w$  we can quantify the polymer distributions. The ratio of  $M_w$  to  $M_n$  is known as the polydispersity index, polydispersity or more broadly dispersity (Equation 3).<sup>10</sup> The metric of polydispersity allows us to compare how well the two masses correspond. An ideal polymer would have both represented by the same value and therefore a ratio of one. The larger the variation the higher the polydispersity index.

$$\text{PDI} = \mathfrak{D}_M = M_w/M_n$$

Equation 3: Equation for polydispersity.

The relationship is not as rigorous in reverse, as such molecular weight distribution can only imply a higher polydispersity.<sup>11</sup>

### 1.2.3. Thermal and mechanical properties of polymers

In most applications the potential of polymers is reduced to utilisation of their mechanical properties. The two most important mechanical properties are tensile strength and elasticity. Increases in tensile strength are usually achieved with increases in chain length and cross linking. In polymeric materials the elasticity is modelled by Hooke's law (Equation 4) until the elastic limit, after the elastic limit some materials begin to deform irreversibly, this behaviour defines them as plastics.

$$\sigma = E\epsilon$$

*Equation 4: Hookes Law. Where  $\sigma$  is the applied stress,  $E$  is the material constant (Young's modulus) and  $\epsilon$  is the resulting strain.*

Polymeric materials have a specific phase transition known as the glass-transition temperature. In application the glass-transition temperature is a range over which polymer chains gain kinetic freedom and pass from a 'glassy' state into a 'rubbery' state. The glass-transition temperature is defined by IUPAC as 'the temperature at which the viscosity of the glass is  $10^{13}$  dPa s'.

Branches in the polymer disturb the packing of the polymer chains. Increased levels of branching result in reduced polymer transition temperatures. Free radicals can abstract hydrogen from the polymer backbone; this creates a new living end which can lead to branching.

Branching can be utilised to 'cross-link' multiple chains together. A short unit involved independently in multiple polymer chains restricts the movement of the chains it is incorporated in, thereby increasing the overall order of the system, increasing phase transitions.

#### 1.2.4. Comb-shaped polymers

Comb-shaped polymers are a special class of branched polymers where the branches are sufficiently long and regular to impart new specific properties on the polymer. The branches, now known as side chains, are in close special proximity, supporting side chain-side chain interactions. The backbone of the polymer maintains aspects of its linear properties, including flexibility. This results in a duality of character. The spacing and nature of the side chains can influence how much backbone character is exhibited. Where the side chains have a sufficiently large interaction, the tight packing can result in the chain flexibility being constrained with the side chain interactions driving the shape.<sup>12</sup> (Figure 7).

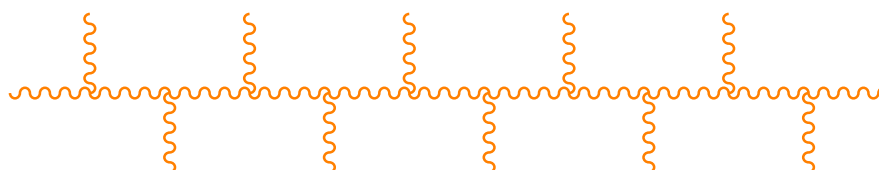


*Figure 7: Schematic representation of a comb-shaped side-chain polymer.*

#### 1.2.5. Block-co-polymers

Co-polymers are polymers constituted of two or more polymer components. Copolymers can exist as two joint regions of polymer with different composition or as polymer(s) of different composition branching from a polymeric backbone (Figure 8). Any conceivable combination of each type can exist, allowing continuous permutations. Like comb-shaped polymers, co-polymers show properties resulting from the competing or complementary properties of each component.

When a comb-shaped polymer contains side-chain polymers of different composition to that of the main backbone, they are termed graft-copolymers.

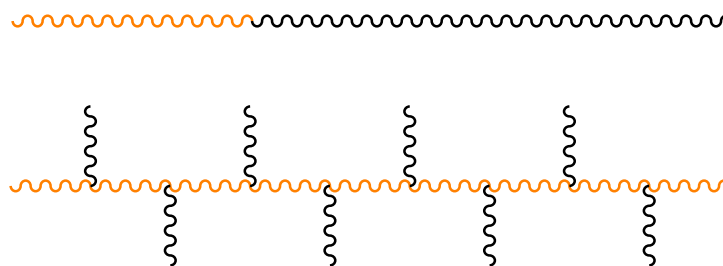


Figure 8: Schematic representation of linear and branched block copolymers.

### 1.3. Polymeric Liquid Crystal

Introduction of rigid units, such as mesogenic units, into either the backbone of the polymer or as pendant groups limits the movement of the polymer chain and encourage more effective packing this increases intermolecular interactions and in turn the phase transitions. A converse relationship is seen with flexible side chains which increase the free space in the system and favour higher energy phases.

Liquid crystal polymers combine the structural requirements of polymers and the mesogenic properties of liquid crystals to create polymers exhibiting mesophases. The balancing of the complex polymeric liquid crystal interactions results in property complexity that is more than the sum of the two parts. Like conventional polymers, many polymeric liquid crystals exhibit glass transition temperatures; however, crystallinity has a requirement for stereoregularity which is sometimes depressed by the mesogenic inclusion. This may lead to both crystalline and amorphous regions. The inherent polydispersity of PLCs leads to wider phase transitions than their lower molecular weight counterparts. Depending on the manner of the mesogenic unit attachment, several structural types are formed.

#### 1.3.1. Main-chain Liquid Crystal Polymers

Main-chain Liquid Crystal polymers include mesogenic units within the backbone of the polymer (Figure 9) either as a chain growth unit or as one/or both components of a step growth synthesis. Consideration of MCLPs as a spectrum from conventional polymers to conventional liquid crystals can be used to consider the ratios of conventional backbone (spacer to mesogenic units. The rigidity of mesogenic units means that increased mesogenic inclusion leads to increased polymer rigidity as discussed with conventional polymers they can support more effective space filling.



Figure 9: Schematic representation of a main chain liquid crystal polymer.

### 1.3.2. Side-chain Liquid Crystal Polymers

Mesogenic units can be added as side chains either as an alternative to back bone inclusion or in addition to main chain inclusion, this tends to add to further complexity in the phase behaviour<sup>11, 12, 13, 14</sup>. Mesogenic inclusion is best achieved by utilising the regularity associated with comb-shaped polymers. Where mesogenic units are used as the side chains, the ordered packing associated with the mesogenic interactions can result in strong interactions between the branches. The restricted branches can affect a strong effect on the chain properties.

In order for the mesophase to exist, the mesogenic components require freedom to arrange according to the packing requirements of that phase. This is antagonistic to (in conflict with) the preference of the main-chain (backbone) for which the preference is to maximise entropy, by adopted a coiled confirmation.<sup>15</sup> When mesogenic units are attached to the polymeric chain this leads to an antagonism between the two alternative arrangements. Side-chain liquid crystal polymers offer the potential to decouple these two antagonistic factors, through separation utilising spacers (Figure 10). However, the backbone influence on the phase behaviour cannot be eliminated completely.<sup>15-18</sup>

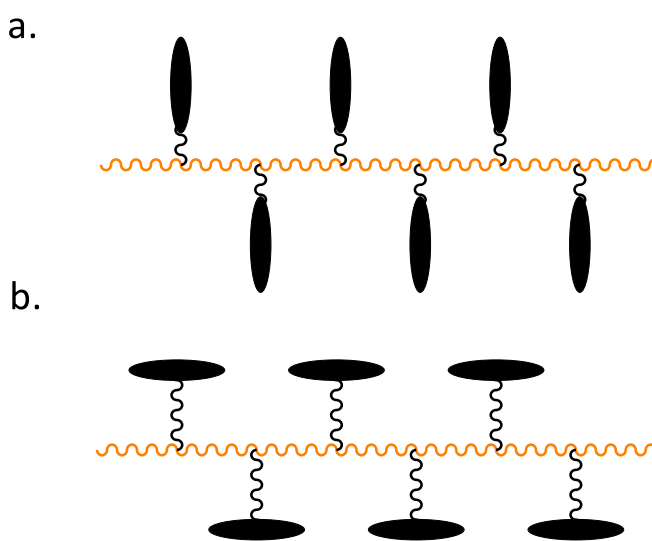


Figure 10: Schematic representation of side chain liquid crystal polymers with a. terminally attached side groups, b. laterally attached side groups.

Flexible spacers act to decouple the motions of the mesogenic units from those of the backbone and, in so doing allow for mesomorphic behaviour to exist. Where the spacers are still relatively short the similarity to low molecular weight thermotropic liquid crystals is reflected in the odd-even relationship shown by the mesophases.

As has been discussed LCPs (regardless of type) include a backbone, mesogenic units and potentially various degrees of mesogenic component separation. This complexity is

supplemented in SCLPs by further options for the method of mesogenic attachment and significantly affects the organisation of the mesogenic units. In side-chain liquid crystal polymers the effects of branching on glass transition temperatures appear to hold true.

### 1.3.2.1. Terminally attached mesogenic units

In terminally-attached side-chain LC polymers, the mesogenic units are attached to the polymer backbone through a flexible spacer, to one end of the core (Figure 10a.). Since polymerisation results in increased order, it is often observed that mesogenic monomers that show a nematic phase, if polymerised often form a smectic phase.

### 1.3.2.2. Laterally attached mesogenic units

A different topology can be accomplished through the lateral attachment of the mesogen to the core, normally, *via* a flexible spacer (Figure 10b.).<sup>19</sup> Laterally attached mesogenic units show very different behaviour compared to their terminally attached counterparts. Regardless of the spacer length smectic behaviour is poorly supported, and instead the nematic phase dominates. It has been suggested that this is a result of the mesogenic units jacketing the backbone as a scaffold and forming a sheath.<sup>18</sup>

## 1.4. Functional Materials

Functional materials are often synthesised or optimised with a specific application in mind. One class of functional materials are intelligent materials, these materials can adjust their behaviour to respond to changes in internal or external 'parameters' (stimuli).<sup>20</sup>

### 1.4.1. Cellulose

Cellulose has been widely utilised as a material for several thousand years. In 1838 Anselme Payen ascertained the chemical formula, knowledge of the structure of cellulose and its chemistry has been growing ever since. The greatest development in the chemical understanding of cellulose was the determination of the polymeric structure, by Hermann Staudinger, in 1920.

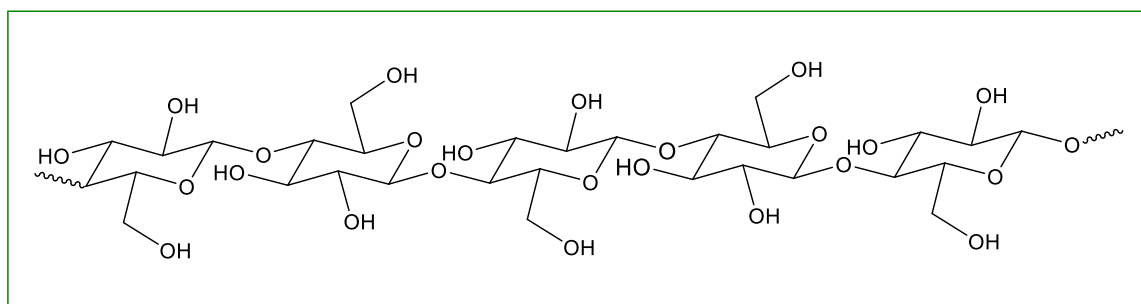


Figure 11: Structure of a section of a cellulose polymer.

Cellulose has long been known as a versatile material, it can be modified by mechanical and chemical methods. Cellulose has very strong intermolecular chain interaction. High linearity allows the chains to pack highly effectively in addition hydroxyl groups can form extensive hydrogen bonding networks.<sup>21</sup>

#### 1.4.1.1. Morphology

There are five known forms of cellulose. Cellulose from natural sources has a form known as cellulose I, consisting of parallel chains. These can be converted to the most stable crystalline form, cellulose II consisting of antiparallel chains, by hydrolysis (mercerization) with aqueous sodium hydroxide.<sup>22-24</sup>

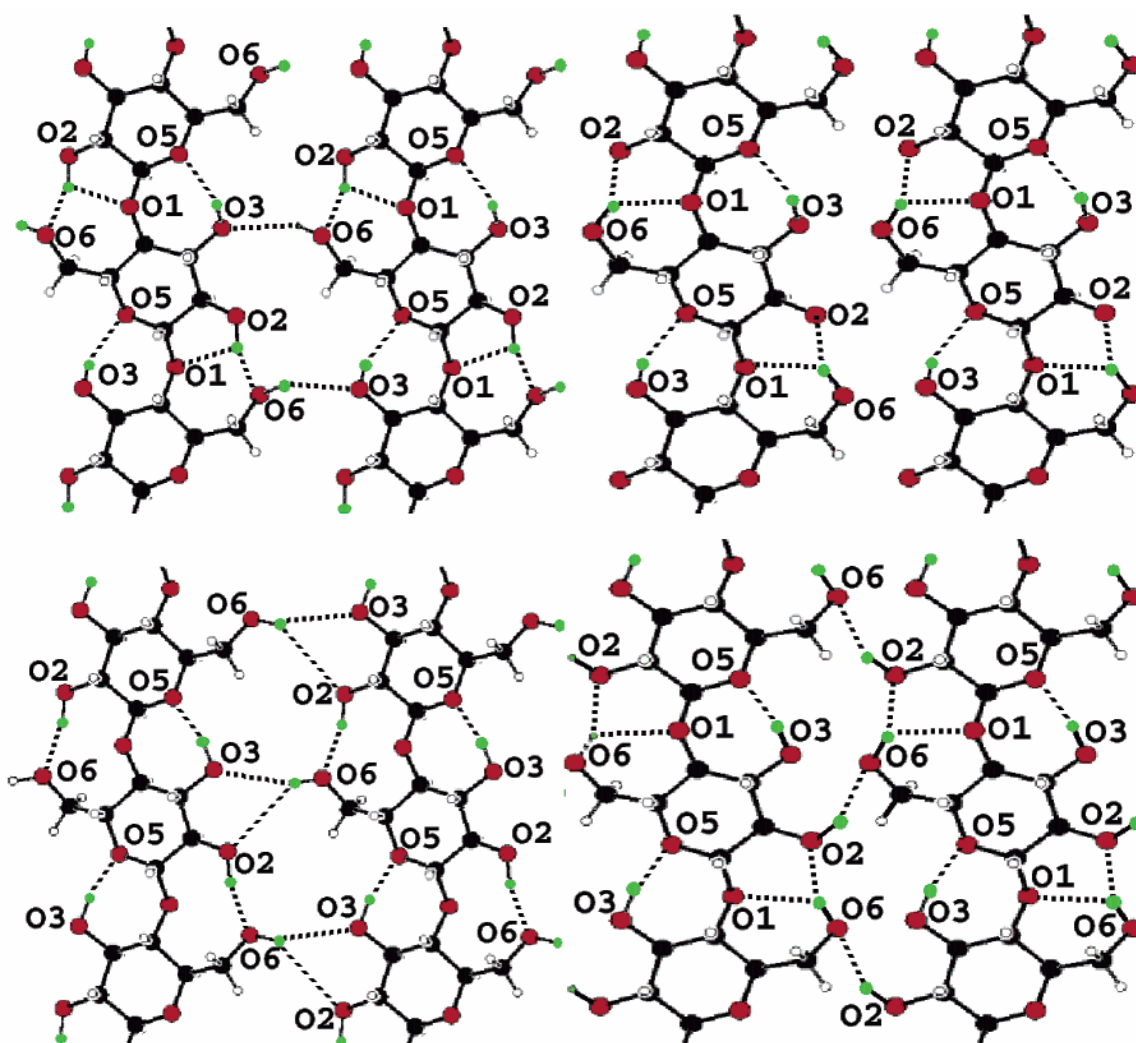


Figure 12: Crystal structure and hydrogen-bonding system in cellulose II from synchrotron X-ray and neutron fibre diffraction [reproduced from 21].

Beyond any property considerations, cellulose is a favourable material as it is a renewable feedstock. It is only relatively recently in the history of anthropogenic cellulose use that we have had the understanding to go beyond traditional uses and target value added materials by introducing favourable chemical properties to the material.

Crystalline cellulose can be encountered as one of four potential polymorphs. These polymorphs constitute crystalline parts of elementary fibrils alongside amorphous regions. Cellulose adopts a hierarchical structure with elementary fibrils arranging into microfibrils (Figure 13). These then wind together with a defined microfibril angle, but non-defined direction, to form nanoscale fibres which intertwine to form mechanical interlocks or fibril bridges.<sup>25</sup> These nanoscale interactions of locking and twisting give rise to bulk properties dependent on the cellulose source and processing.<sup>26</sup>

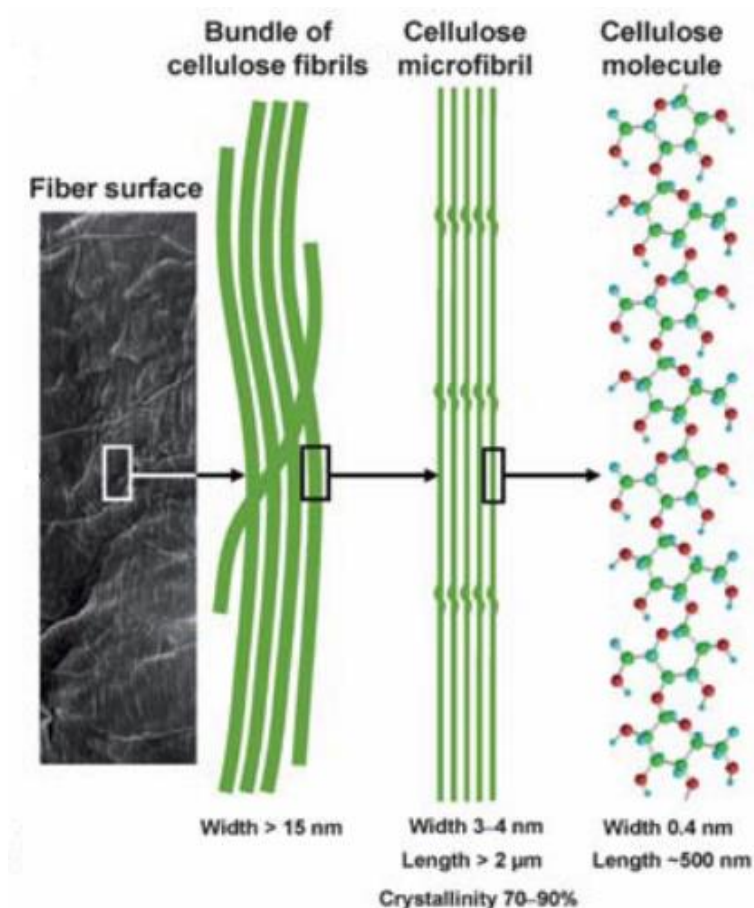


Figure 13: The hierarchical structure of cellulose modified from [27].

#### 1.4.1.2. Microfibrillated cellulose

Microfibrillated (MFC) is a cellulosic material with a homogenous fibre diameter,<sup>23</sup> typically in the range 10-40 nm, placing it between microcrystalline cellulose and an individual microfibril which are typically 10-100 times larger, and 1-20 times smaller respectively.<sup>28</sup>

Specific surface area (SSA) is a property of solids measuring the total surface area of a material per unit mass. Due to its composition of large numbers of nanocomposites/cellulosic materials, each with a small diameter and therefore high surface area, MFC has a much higher SSA than unprocessed cellulose<sup>23</sup>. Specific surface area is understood to be quite hard to measure for microfibrillated cellulose due to aggregation effects.<sup>23</sup>

### 1.4.1.2.1. Regenerated Cellulose Electrospun fibre

Electrospinning is one of the most versatile forms of microfibrillation.<sup>29</sup> Electrospinning is capable of producing extended fibres of homogenous diameter.<sup>30</sup> In the electrospinning process the material to be fabricated, typically a polymer, is dissolved in solution and fed through a spinneret. The solution is charged using a high voltage electrode. The charged solution develops repulsive force greater than the surface tension, at the critical voltage a jet of solution is ejected from the spinneret. The ejected jet is drawn across an electrochemical potential, stretching and drying in the process, where it is deposited. Due to the difficulty of dissolving cellulose it is usually electrospun as cellulose acetate and subsequently regenerated by hydrolysis with aqueous sodium hydroxide.<sup>29, 31, 32</sup>

Heat treated electrospun fibres have been shown to have potential as filtration membranes due to the high porosity.<sup>31</sup> Electrospun poly(vinylpyrrolidone) fibres with a core of liquid crystals have been developed,<sup>33</sup> and subsequently shown to have a sensing response,<sup>34</sup> including to volatile organic compounds.<sup>35</sup> Cellulose offers the potential to attach functionality covalently.

### 1.4.2. Cellulose derivatives

One way of creating a functional material is to integrate additional properties with those of a 'host' material. Functional materials have been made from cellulose with combinations of economic and social factors, and material properties fuelling research. Some recent applications of functional materials based on cellulose have included self-folding paper,<sup>36, 37</sup> and low cost sensors.<sup>38</sup> including graphite coating-derived conductance controlled sensors.<sup>39</sup>

The ability to modify cellulose chemically offers the potential to go beyond conventional physical approaches to the synthesis of covalently functionalised materials. Cellulose is modified through the reaction of OH groups of the glucose units. Steric effects in cellulose have been shown, in esterification studies,<sup>40</sup> to result in very marked trend in hydroxyl groups reactivity (Relationship 1).<sup>41, 42</sup> The C6 OH-group reacts an order of magnitude faster than the other C2 and C3 OH-groups.<sup>43</sup>



*Relationship 1: Hydroxyl group reactivity.*

Cellulose is prone to crystallisation.<sup>44</sup> This has led to studies of cellulose considering it mostly as a surface in heterogeneous conditions. Although under some conditions it can be involved in homogeneous reaction as well. Homogeneous graft modifications of cellulose have mostly been performed in DMAc/LiCl or ionic liquids.<sup>45</sup>

Heterogeneous conditions do present the complication of reaction components aggregating; this can lead to lower conversions and graft densities. By maintaining the mechanical structure of the cellulose precursor material heterogeneous conditions can maintain large amounts of the material properties which we associate with cellulose, some of which come from the complex hydrogen bond networks.

## **1.5. Surface modification approaches**

In order to maintain the favourable mechanical properties of cellulose and complement them with other properties, either to introduce new character or to suppress inherent character. It is important to not adversely disturb the intermolecular forces and packing.

In order to maintain this character, the only viable route to functionalization is surface modifications. Surface can be modified by mechanical or chemical means.<sup>46</sup> Using surface interactions to functional components including tailorable soft materials can be immobilised onto the surface - a process known as adsorption. Adsorption can take the form of physisorption or chemisorption. Chemisorption involves a selective chemical interaction at the surface.

Physisorption is the attractive forces driven process by which molecules can be deposited on a surface. As molecules are physisorbed they are attracted to the surface by non-covalent interactions. The principle of physisorption is utilised in electrospin coating surface modification. The adsorption of polymers with complementary surface units introduced onto cellulose demonstrates the utility of the approach.<sup>47</sup> A potential future route to physisorption is Chemical Vapour Deposition.<sup>48</sup>

### **1.5.1. Polymer grafting at surface**

In addition to the architecture of graft co-polymers discussed it can be possible to introduce the concept of a surface as covalently attached tier in the block hierarchy.

In order to achieve a covalent bond between a surface and a polymeric chain either a graft polymerization method (*graft-from*) or graft coupling method (*graft-to*) approach can be undertaken (figure 14).<sup>49</sup>

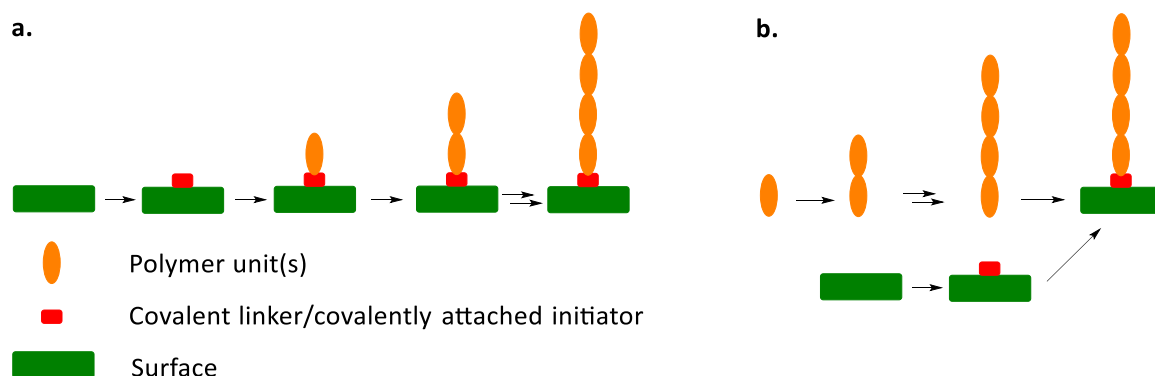


Figure 14: Schematic comparison of the graft-from (a) and graft-to (b) approaches.

### 1.5.1.1. Graft-to approaches

Graft-to polymerisation is the linking of preformed polymer to a surface, typically this will be via a condensation reaction from both the surface and the polymer. The use of preformed polymers allows for low polydispersity and as such property control, however large steric repulsions limit higher graft densities.<sup>50</sup>

### 1.5.1.2. Graft-from approaches (surface initiated chain grown polymerisations)

The highest graft density is a polymer brush,<sup>49, 51</sup> usually accessed *via* graft-from polymerisation<sup>41</sup>. Graft-from polymerization involves converting the surface into a macroinitiator. Polymerization can then initiate from the initiator sites on the surface. As the polymer grows it is attached to the surface by the initiation site. These have the potential to achieve high graft densities and grow complex and sterically bulky architectures. Traditional polymers and higher generation dendrons have been grafted from cellulose, producing sensitive biosensing substrates from filter paper.<sup>52</sup>

Grafting metrics can often be calculated accurately to quantify the extent of polymer grafting.<sup>53</sup>

## 1.6. Covalent graft modification of Cellulose

Functionality has been conferred on cellulose surface through chemical modification of the alcohol units on the cellulose surface,<sup>54, 55</sup> including through polymerisation.

One of the most common methods of polymerisation is the free radical polymerisations.<sup>56</sup> In the homogenous approach, an initiator is produced as a radical. After the initiation the polymerisation enters the 'propagation' step where a monomer is added to the radical site. Upon addition the radical is 'pushed' along the backbone where this step can be repeated until finally the radical comes into contact with another source of a free electron radical and they terminate. This process is much the same in the graft-from method which can be applied effectively to cellulose in both

homogenous and heterogeneous conditions. The key aspect is that the initiator is covalently bound to the cellulose polymer backbone. Free radical polymerisation, although favourable for its simplicity, is also disadvantaged because of the lack of control of polydispersities.

### **1.6.1. Initiation**

In order to capitalise on the potential of radical polymerisations for cellulose graft copolymers 'radical formation on the cellulose backbone *via* chemical activation' can be used. This avoids using the chain transfer or radiation induced methods both of which lead to high polydispersities.<sup>56</sup>

A number of polymerisation approaches have been explored with respect to polymerisation from surfaces. Some, such as ring opening polymerisation (ROP) and ionic polymerisation, have stringent criteria or conditions. A much more accessible class of polymerisations can be found in the living radical polymerisations (LRPs).

## **1.7. Controlled Radical Polymerisation**

"Living" radical polymerisations are a versatile category of polymerisation techniques. Living polymerisations were first described by Szwarc as 'chain growth process, without chain breaking reactions such as chain transfer or irreversible termination'.<sup>57</sup> Living radical polymerisations are a controlled radical polymerisation process, showing the transfer of an active radical site along a growing polymer chain.<sup>58</sup> Living radical polymerisations are controlled by limiting the number of active chains through equilibrium of the active and dormant chain terminals.<sup>59</sup>

The most popular living radical polymerisation techniques are nitroxide mediated polymerisations (NMP), atom transfer radical polymerisation (ATRP) and radical addition-fragmentation chain transfer polymerisation (RAFT) the different strengths of the alternative techniques determines the synthetic approach adopted (Figure 15).<sup>56</sup> These are radical processes and therefore have an inevitable degree of termination processes, therefore the term "living" is not strictly appropriate. When the active chains in the equilibrium are at sufficiently low concentrations the statistical deviation of chains can be narrowed preventing broad polydispersity profiles. By limiting the chain growth of all chains, by equilibrium to the dormant species, each chain is given an opportunity to polymerise. More accessible chains, with the same chemistry, are more likely to be activated however they also have a shorter active lifetime, with quicker deactivation, resulting in comparable molecular weights. A second condition, to achieve narrow polydispersity is the fast initiation relative to propagation to allow for simultaneous growth of all polymers. Living radical polymerisations, by limiting the number of active species, also limit self-termination reactions.

An additional benefit of living radical polymerisation is that they can serve to prevent the Trommsdorf effect, an auto acceleration event which can occur in free radical polymerisations due to the localised viscosity increases preventing termination reactions.<sup>60</sup>

In some cases multiple LRP polymerisation techniques can be used interchangeably.<sup>61</sup> The most comprehensively studied polymerisation technique is ATRP due to its robust and versatile nature.<sup>62</sup>

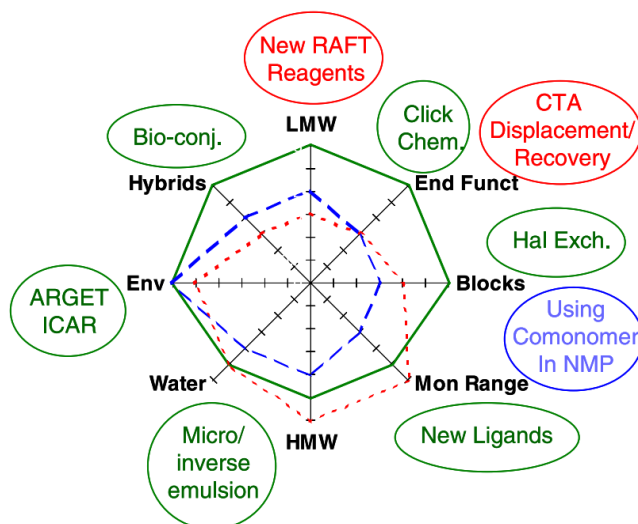
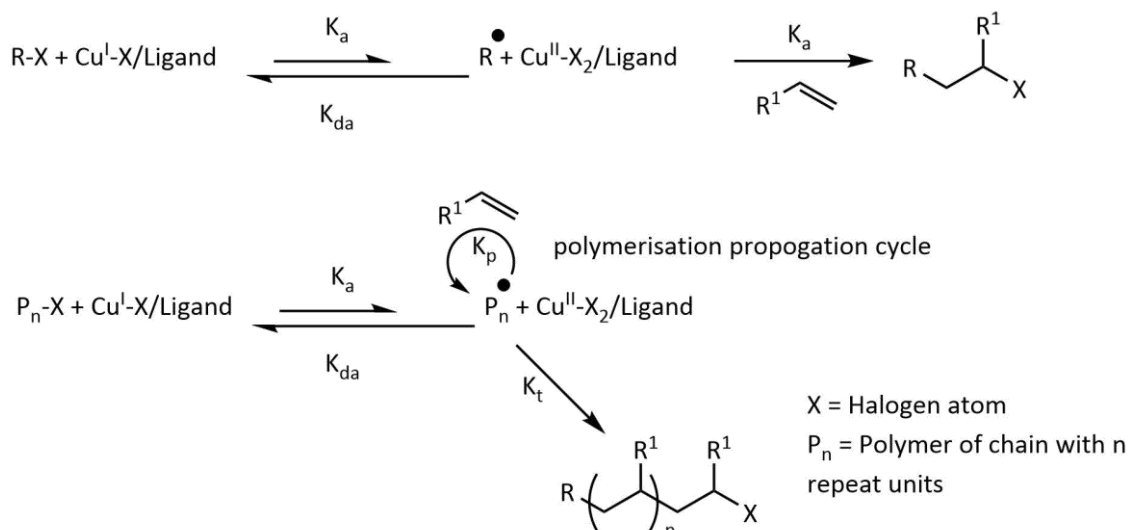


Figure 15: Comparison of NMP, ATRP and RAFT in the areas related to the synthesis of high molecular weight polymers (HMW), low molecular weight polymers (LMW), end functional polymers (End Funct), block copolymers (Blocks), range of polymerizable monomers (Mon Range), synthesis of various hybrid materials (Hybrids), environmental issues (Env) and polymerization in aqueous media (Water) [modified from 8].

### 1.7.1. Atom Transfer Radical Polymerisation (ATRP)

Progression of atom transfer radical addition (ATRA) reactions to polymer synthesis was achieved independently by two groups in 1995.<sup>63</sup> Both of these initial studies used methyl methacrylate. The first one, by Kamigaito's group, used a ruthenium based catalyst.<sup>64</sup> The second one by Matyaszewsk *at al.*, used the now popular copper halide catalyst.<sup>65</sup> Matyaszewski describes ATRP as 'a special case of ATRA',<sup>66</sup> and goes on to describe that ATRP requires the reactivation of the initial adduct and additionally discuss the requirement for propagation of growth by additional monomers from the radical terminated polymer growth sites.<sup>67</sup>

ATRP initiates with the catalytic abstraction of a halogen atom from an initiator, the abstraction of a halogen forms a radical terminated chain. This radical then propagates through addition of olefin units, with a radical being continually regenerated at the end of the chain as a new 'active site' (Scheme 1).



Scheme 1: General Mechanism for above. ATRA, and below ATRP modified from [66].

The distinguishing feature of ATRP approaches is the low number of active growth sites. This results from a fast deactivation of the active growth sites. By combining this with an appropriately slow rate of reactivation, an equilibrium can be established with a sufficiently low concentration of intermittent active sites. The position of the equilibrium can be tailored; the choice of equilibrium constant is a compromise between rate and polydispersity.

The robustness and living chain ends of ATRP makes it highly suited to the growth of block copolymers. ATRP has been adopted for the purpose of cellulose modification both surface (heterogeneous) and of dissolved fibres (homogeneous).

Good degrees of control can be achieved over polymerisation with ATRP using an appropriate choice of initiator, solvent, catalyst and ligand are all important as well as general considerations such as temperature and concentration.

#### 1.7.1.1. Initiator

Extensive work has been reported regarding the structural properties of the initiator on the rates of activation for ATRP.<sup>68, 69</sup> A good overview of this work can be found in a review by Braunecker and Matyjaszewski.<sup>8</sup> The stands out trends are that effective stabilisation of the radical and leaving group are key. More substituted alkyl groups provide a high rate of dissociation as do more deactivating groups. The larger halogens with alkyl bromide (and iodide) having rates several times those of chlorides.

#### 1.7.1.2. Catalyst

Upon abstracting a halide ion, in the chain activation process, the oxidation and coordination numbers of the metal will increase by one. ATRP of acrylates has been reported using several transition metals (copper, ruthenium and iron). The fast deactivation of acrylic radical by cupric

halides has been suggested as favouring lower polydispersity polyacrylates than those obtained with ruthenium or iron.<sup>70</sup> It has been suggested that ‘the active copper(I) complex must be four-coordinate complex bearing no halide ligands in order for the reaction to be truly catalytic and reversible’.<sup>71, 72</sup>

A wide range of ligands have been explored for the complexation of copper(I), in order to understand and optimise the equilibrium conditions for the catalyst.<sup>68</sup> Most polymerisations are performed using tris[2-(dimethylamino)ethyl]amine (Me<sub>6</sub>TREN) or tris(2-pyridylmethyl)amine (TPMA) (Figure 16) due to the high rates of activation alongside the maintenance of favourable equilibria with high rates of deactivation. However these are not always the optimal ligands, the choice of ligand is application specific. Each ligand has system specific operating ranges, over which they offer catalytic control, reflecting differences in ligand stability and active concentrations (Figure 17).

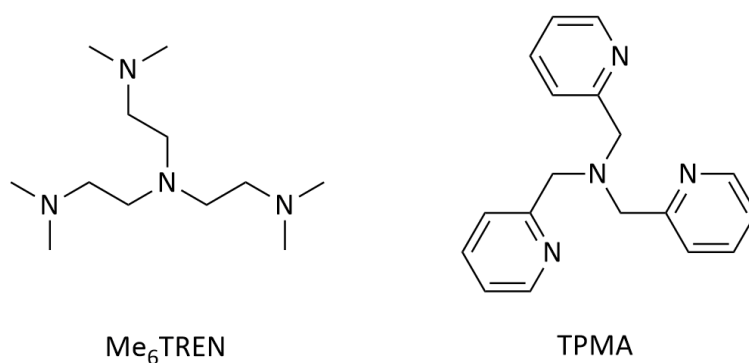


Figure 16: Structures of the two widely favoured ATRP ligands.

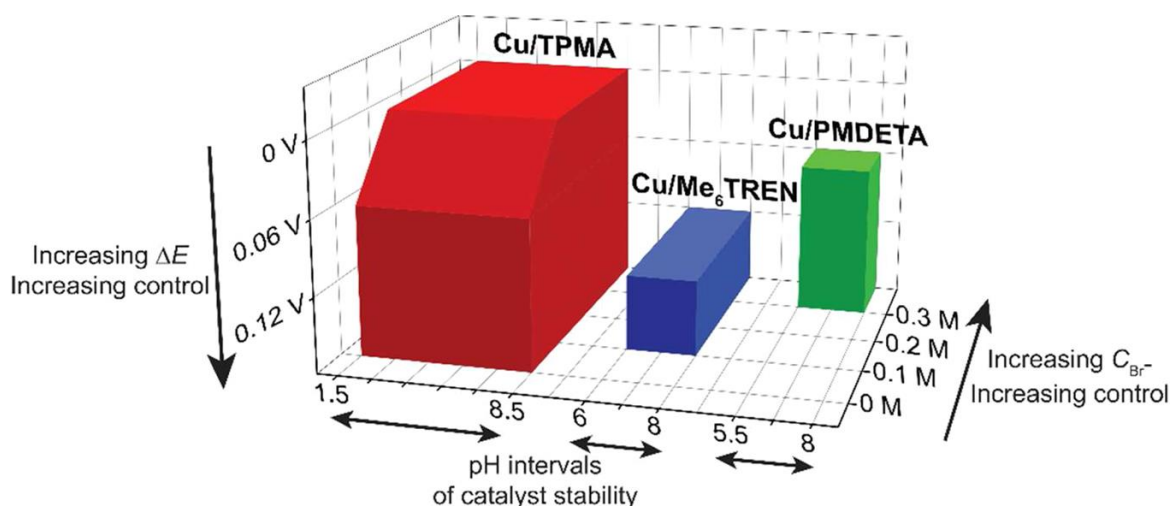


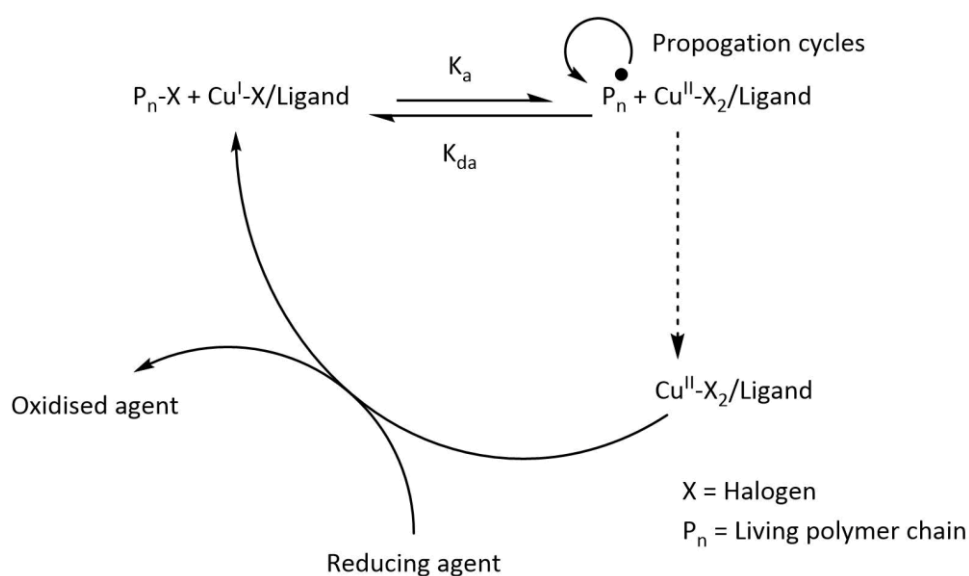
Figure 17: Example of the concept of regions of catalyst control, in the case of aqueous systems. This example shows restrictions imposed on catalyst choice by bromide concentration, solution pH and the thermodynamics of the catalytic complex disassociation. Reproduced from [72].

### 1.7.1.3. Solvent

More polar solvents have been shown to favour higher activation rates and lower deactivation rates in ATRP in experiments with a Cu(I)Br and 1,1,4,7,10,10-hexamethyltriethylenetetramine (HMTETA).<sup>73</sup> It appears that the interactions with the more substituted catalyst are more important than those with the polymer or initial inorganic compound.<sup>74</sup>

### 1.7.1.4. Reducing agents (ARGET)

In ATRP reactions the catalyst is unavoidably converted to the non-active Cu(II) species in the termination process of active chains. This redox reaction can be reversed through a reaction with a reducing agent (Scheme 2).<sup>75</sup> Typically tin(II) 2-ethylhexanoate or ascorbic acid have been used for this purpose, as well as excess of the nitrogen based ligands.<sup>76</sup>



*Scheme 2: Mechanism for ARGET ATRP as proposed by Jakubowski et al.<sup>77</sup>*

The choice of reducing agent is important to avoid significant reductions in control for the underlying ATRP process. Uncontrolled reduction of Cu(II) to Cu(I) results in an increased concentration of dissociated radical halides and reduces polymerisation control. Ascorbic acid, as a strong reducing agent, performs this process with a high rate, potentially disturbing the Cu(II) concentration balance ideally involving no termination; slow reduction processes and the 'active site' capping being dominant. The rate of reduction with ascorbic acid can be limited by the limited solubility of ascorbic acid in organic solvents such as anisole.<sup>78</sup>

## 1.8. Surface initiated ATRP, SI-ATRP

Surface functionalised materials can provide accessible routes for complex or novel architectures. Surface initiated ATRP provides a very efficient route to attach polymeric species to surfaces in a controlled and predictable way. The potential of SI-ATRP extends to brushes and block copolymers,<sup>62</sup> capable of enhancing the surface properties of substrates<sup>79</sup>.

Surface initiated ATRP (SI-ATRP) was first described in 1998,<sup>80</sup> this is a special case of graft from polymerizations. Since then SI-ATRP has been successfully conducted from a wide range of organic, polymeric, inorganic and metallic substrates,<sup>81</sup> in both homogeneous and heterogeneous conditions.

In order to set up a graft ATRP from a surface, the initial halogen abstraction to generate the radical initiator must occur from the surface. In order to allow this, most surfaces require the introduction of appropriate initiator units (Figure 18).

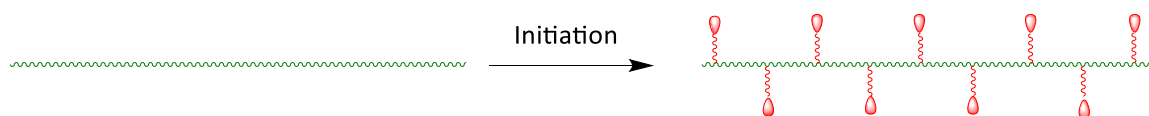


Figure 18: Schematic representation of cellulose substrate initiation with grafted initiators.

### 1.8.1. Surface initiated ATRP from cellulose

The hemiacetal and glycol hydroxyl groups offer potential sites on cellulose for radical formation (Figure 11). It is also possible to affix an initiator functional unit onto the cellulose to support favourable initiation protocols. For cellulose this is often done with alkyl halides, typically the halogen atom will be chlorine or bromine but iodine is also known.<sup>82</sup> ATRP was first reported from a cellulose substrate by Carlmark and Malmström in 2002 and has established predominance since then (Figure 19).<sup>83</sup> SI-ATRP has been successfully conducted from a number of cellulosic substrates, including nanocrystals,<sup>81</sup> microfibrils and regenerated cellulose electrospun fibres.<sup>84, 85</sup>

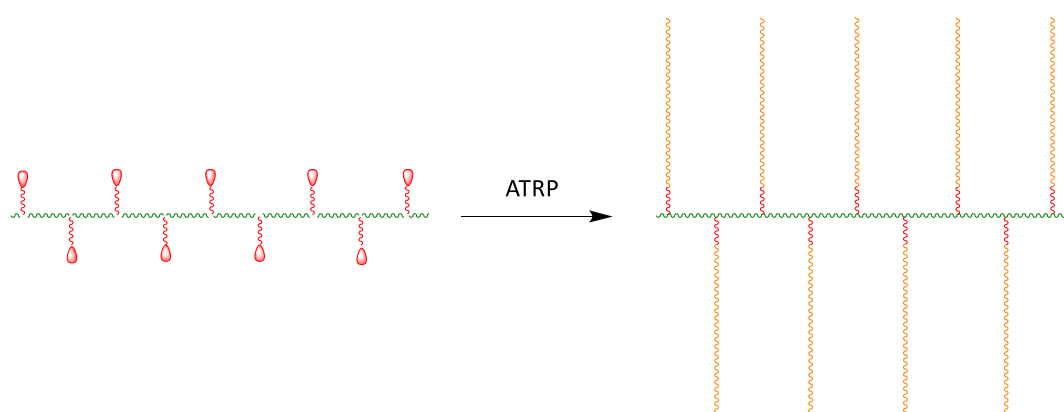


Figure 19: Schematic representation of graft-from polymerisation using a cellulose macroinitiator via ATRP.

## 1.9. Pairing surface grafting and liquid crystals for the functionalisation of cellulose.

### 1.9.1. Properties of liquid Crystals at Surface Interfaces

Interaction between surface and liquid crystals can be categorised as 'bulk' alignment interaction or more localised interactions at the interface.

At the interface the interactions are predicted by the semi-empirical relationship presented in the Friedel-Creagh-Kmetz (FCK) rule (Relationship 2).

$$\gamma_s < \gamma_{LC} \rightarrow \text{homeotropic alignment}$$

$$\gamma_s > \gamma_{LC} \rightarrow \text{parallel alignment}$$

*Relationship 2: Friedel-Creagh-Kmetz (FCK) rule, where  $\gamma_s$  is the surface substrate energy and  $\gamma_{LC}$  is the surface tension of the liquid crystal.*

The combined surface tension/energy of the liquid crystals and the surface is minimised. Where the surface tension of the liquid crystals is greater homeotropic alignment is favoured to maximise the intermolecular interactions between the molecules. Where the surface tension of the substrate is greater than that of the liquid crystals the molecules align parallel to the surface to maximise the interactions with the surface.

Surface anisotropy from the polymer orientation can propagate an alignment in the bulk in a manner analogous to epitaxial layer growth.<sup>86</sup>

### 1.9.2. Grafting liquid crystals from surfaces

Direct covalent grafting of liquid crystal monomeric species has been successfully performed directly onto surfaces.<sup>87</sup> As discussed with SCLCPs for the mesophase to successfully develop, the mesogenic units require the freedom to self-organize.

Surface initiated living radical polymerisations have been successfully deployed in the growth of liquid-crystalline polymer brushes on silica substrates,<sup>88</sup> including successful utilisation of SI-ATRP<sup>89</sup>. Among the varied monomers polymerised from cellulosic surfaces, graft-from liquid crystal polymers were reported by Malmström and Saez.<sup>90</sup>

Graft liquid crystals polymers from cellulose (filter paper) have been explored with respect to 11-(4'-cyanophenyl-4-phenoxy)undecyl acrylate monomers utilising ATRP (Figure 20).<sup>90</sup> The methodology involved covalent attachment of bromoisobutyrate bromide, BIBB, onto the cellulose surface and initiation of polymer growth. The ATRP ligand used, in this case, was PMDETA. The successful polymerisation resulted in value added cellulose with strong

hydrophobicity. Higher graft densities were achieved through block copolymerisation by introducing a PMA spacer close to the surface.

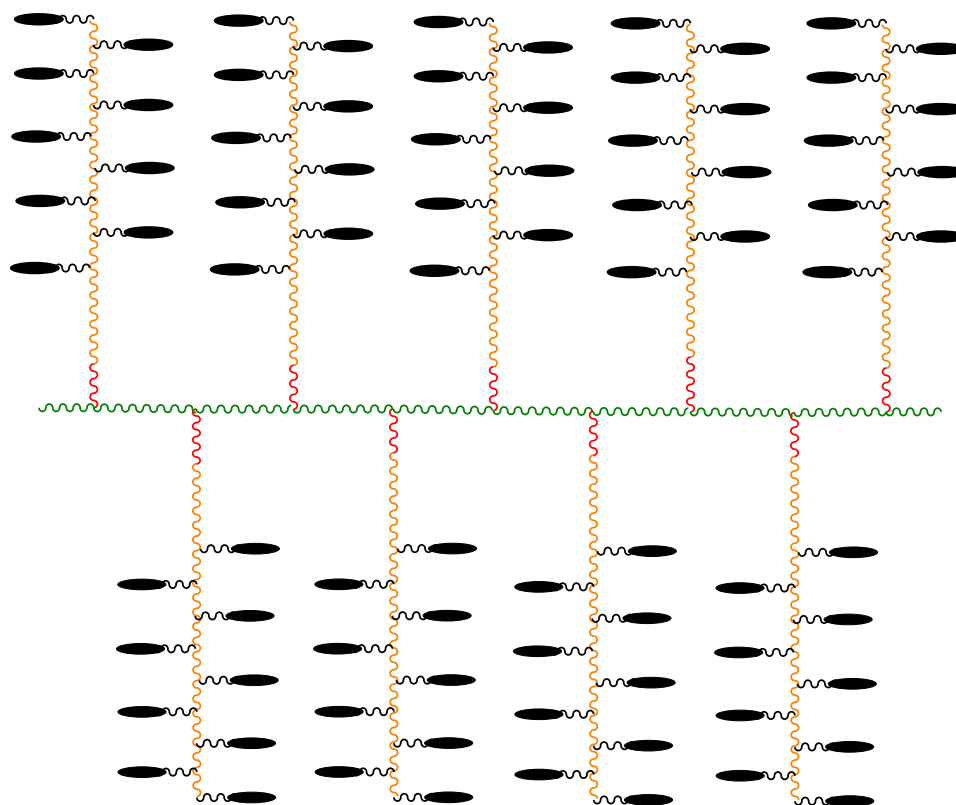


*Figure 20: Schematic representation of graft-from polymerisation of 11-(4'-cyanophenyl-4-phenoxy)undecyl acrylate monomers using a cellulose macroinitiator via ATRP.*

## 1.10. Applications

Applications for 'Intelligent' responsive copolymers based on cellulose have been discussed with respect to their response to stimuli ranging from electricity, to pH and temperature.<sup>91</sup> Applications have been suggested for responsive cellulose from responsive membranes<sup>92</sup> to grafted polymers for drug delivery systems,<sup>93</sup> triplology modification, shape memory materials as well as sensors.<sup>1</sup>

Responsive cellulose based on copolymers has been targeted for sensing applications. The high specific surface area of electrospun fibres offers the potential for significant increases in graft per cellulose unit. By increasing the loading of responsive units, it is envisaged that a stronger response could be induced. Liquid crystals are a delicate state of matter, sensitive to purity and guest host behaviour. Combining the sensitivity of liquid crystals with the mechanical properties of cellulose substrates and potentially high graft densities of electrospun fibres offers potential for highly powerful sensing devices.

It can be envisaged that surface initiated polymerisations from liquid crystalline electropun fibres could offer the potential for permeable alignment layers. A permeable alignment layer could be used for inducing mesophase behaviour on a flowing liquid crystal.

## **1.11. Characterisations Techniques**

### **1.11.1. Nuclear Magnetic Resonance**

Nuclear magnetic resonance (NMR) spectroscopy can be used for the characterisation of organic molecules and macromolecules and for the monitoring of polymerisations. NMR spectroscopy can be used for the monitoring of the degree of polymerisation by comparing the integration of monomer functional units to that of the polymer.<sup>94</sup> In some cases end group analysis can also be conducted to assess the degree of polymerisation by comparing the end group intensity to that of the monomer backbone. For NMR to be truly quantitative all nuclei must be excited and allowed to fully relax, therefore appropriately long  $T_1$  values must be used.

### **1.11.2. Differential Scanning Calorimetry (DSC)**

The intermediate phase transitions of polymeric and liquid crystal liquid crystal behaviour can be characterised by their changes in energy. The onsets, entropy and enthalpy of these transitions can be attained by DSC.

A sample is run against a reference standard of known heat capacity. Differences in the heating required to raise the temperature (heat flow) of a sample relative to the known reference is plotted against temperature. On DSC plots the area under the peak can be calculated using integration and with knowledge of the sample mass the enthalpy change of the transition can be calculated. This can in turn be used to calculate the entropy of the transition.

### **1.11.3. Polarising Optical Microscopy**

Polarising optical microscopy can be used to observe the interactions of polarised light with a birefringent medium. Medium defects can often be used to infer the molecular alignment properties and therefore phases of materials.

### **1.11.4. Gel Permeation Chromatography (GPC)**

Gel permeation chromatography (GPC) is a specific type of size exclusion chromatography, used to separate polymers into fractions based on size and measuring their abundance, it can be used to determine a samples molar mass distribution (MMD). GPC is a widely used technique for polymer analysis due to its rapid data collection and effective resolution. GPC is favourable as the full molar mass distribution can provide polydispersity, number average molar mass and number average molar mass.

As a size exclusion chromatography method GPC works by passing a highly dilute solution of the polymer product through a column of non-ionic spheres with a distribution of pore sizes. Smaller

polymers penetrate the pores further and as such have their elution retarded to a greater extent than larger polymers which cannot penetrate as far (Figure 21).

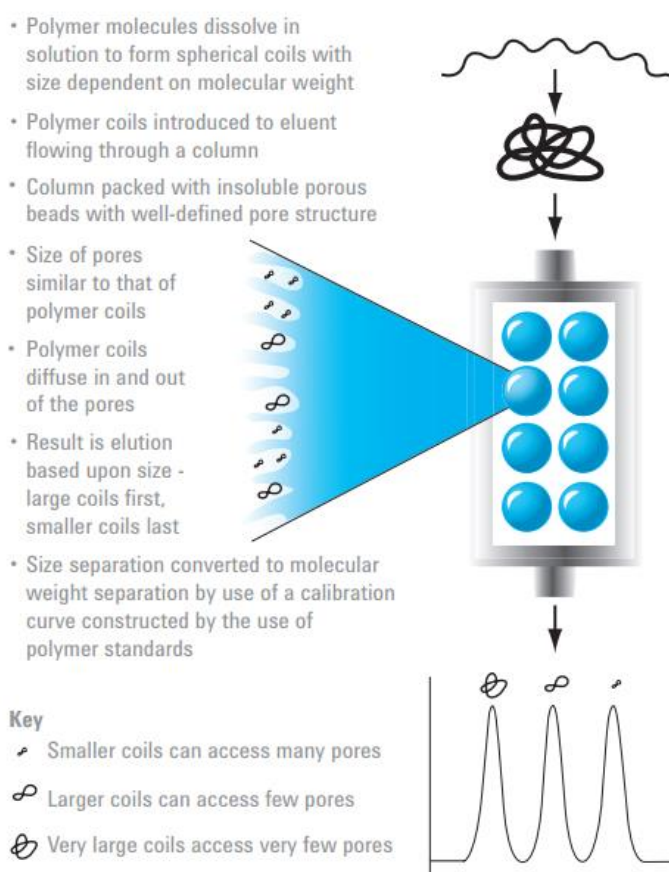


Figure 21: Schematic representation of pore retention in a GPC column [reproduced from 95].

GPC is at its most powerful when it is coupled with multiple in line detection techniques. Triple detection is widely utilised and can be used to provide a very rich and comprehensive data set about the properties of the polymer. Triple detection couples at least one light scattering detection, a viscometry detection and refractive index detection.

#### 1.11.4.1. Refractive index

Refractive index detection is a form of concentration detection. Solutions have a refractive index dependent on their relative composition. The detector simultaneously analyses a reference sample of solution and the column eluent. The response is proportional to the difference in composition; this provides a concentration dependent response.

#### 1.11.4.2. Light scattering

Light scattering detectors complement the results of a concentration detector to better represent the molecular weight of the elute, using a  $M_w$  proportional detection method.

Right angle light scattering detects at 90 degrees. This fails to account for the dissymmetry of scattering caused by destructive interference at higher angles from the incident ray, thus underestimating the scattering for larger molecules.

#### **1.11.4.3. Viscometry detection**

Viscometry detection measures the difference in the viscosity of reference solvent against the viscometry of the column eluent.

#### **1.11.4.4. Triple detection analysis**

The response obtained from a refractive index detector is proportional to the sample concentration. By coupling the RI response with a light scattering detector we can obtain a measurement of absolute molecular weight.

Viscometry detection uses a Mark-Houwink plot to correct the calculated molecular weight achieved from light scattering using an estimate of the molecular size calculated from the directly measured viscosity.

#### **1.11.5. Scanning Electron Microscopy (SEM)**

Scanning electron microscopy (SEM) is a high performance microscopy technique capable of resolution better than 1 nm. SEM works by moving an electron beam over a sample a detecting the sample response to the beam. The most common detection mode is secondary electron mode. Low energy, secondary electrons are emitted by the sample as a result of inelastic scattering of the electron beam. The low energy electrons are collected and passed through a photomultiplier, to enhance the signal, before detection. The detected beams are mapped onto pixels corresponding to the position of the initial electron beam to produce an image of the surface. In order to detect non-conducting surfaces, the surface must first be coated with a conducting species.

#### **1.11.6. Polymer Analysis**

The use of sacrificial initiators offers complementary information about surface polymerisations. Making the assumption that both the grafted and free polymer grow at the same rate the free polymer formed in solution can be analysed to infer the properties of the grafted polymers.<sup>96, 97</sup> The polymer can be analysed using solution phase analytical techniques such as <sup>1</sup>H-NMR and GPC.

## 2. Aims

Cellulose grafted side chain liquid crystal polymers have the potential to significantly increase the value of the cellulose, and a number of applications have been discussed.<sup>98</sup> Previous work has shown that terminally attached cyanobiphenyl (end-on) mesogenic units can be grafted as a side chain liquid crystal polymer on the surface of cellulose paper (filter paper, Whatmann No 1) and inferred that smectic phases are exhibited, by analysis of the sacrificial polymer formed during the SI-ATRP reaction. Progression from terminally attached mesogenic units towards laterally attached (side-on) mesogenic units can be predicted to support the nematic phase and allow for some new potentially sensing opportunities (Figure 22). On the other hand different cellulosic substrates, such as electrospun fibres which have much higher surface to volume ratios than paper can support much higher loading and potentially allows for intelligent devices with much higher responses than paper devices.

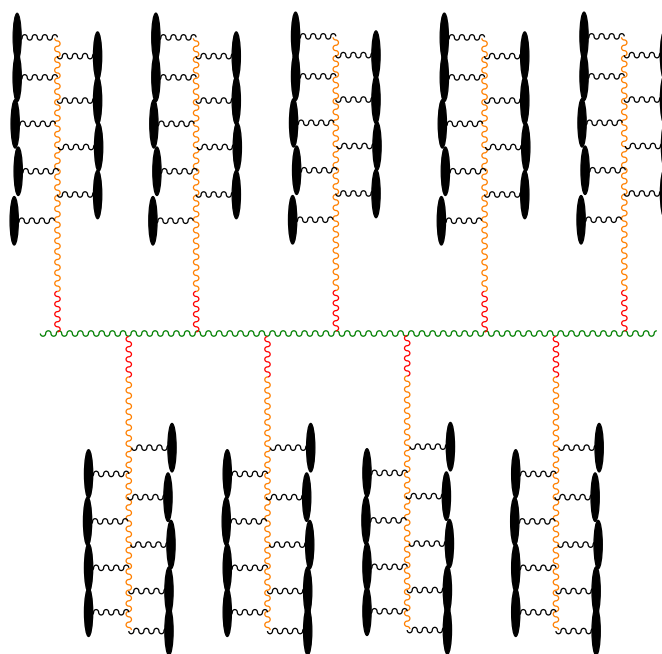


Figure 22: Schematic representation of cellulose side on LCP graft targets.

This work will explore the synthesis and properties of new paper and electrospun cellulose systems with liquid crystal polymer brushes attached to the cellulose substrates.

Work will be conducted to build upon the successful SI-ATRP of cyanobiphenyl-based SCLP from cellulose previously reported<sup>90</sup> and vary the substrates and the LC grafts. Liquid crystal acrylates monomers will be used to carry out the polymerisations.

1. To synthesis end-on and side-on acrylates previously reported as favourable monomers for SCLCPs.
2. To synthesis graft-from liquid crystal polymers with terminally attached side groups, using ATRP from paper as previously reported in the literature.
3. To utilise recent advances in ATRP chemistry to establish robust conditions.
4. To attempt to synthesis graft-from liquid crystal polymers with laterally attached side groups,<sup>99</sup> from paper substrates.
5. To attempt to synthesis graft-from liquid crystal polymers from electrospun fibre substrates.
  1. To attempt to synthesis graft-from liquid crystal polymers with terminally attached side groups, from electrospun fibre substrates.
  2. To attempt to synthesis graft-from liquid crystal polymers with laterally attached side groups, from electrospun fibre substrates.
6. To use the electrospun fibre grafted substrates to gain insights into the mesophase behaviour of the LCP grafted paper surfaces.
7. To compare the properties of grafted LCP with laterally attached side groups (side-on acrylates) to their terminally attached side groups (end-on acrylates) analogues.

The literature monomers 11-(4'-cyanophenyl-4-phenoxy)undecyl acrylate and 2-((4-(acryloyloxy)butoxy)carbonyl)-1,4-phenylene bis(4-butoxybenzoate) (Figure **23**) will be synthesised using preparations similar to those in the literature.<sup>99, 100</sup> Surface initiated graft-from polymerisations will be attempted in two stages: firstly converting the surface cellulose into a macroinitiator using bromoisobutryl bromide (bibb). The initiator sites on the surface of the macroinitiator will then be used to conduct graft-from polymerisations of the target monomers under ATRP conditions.

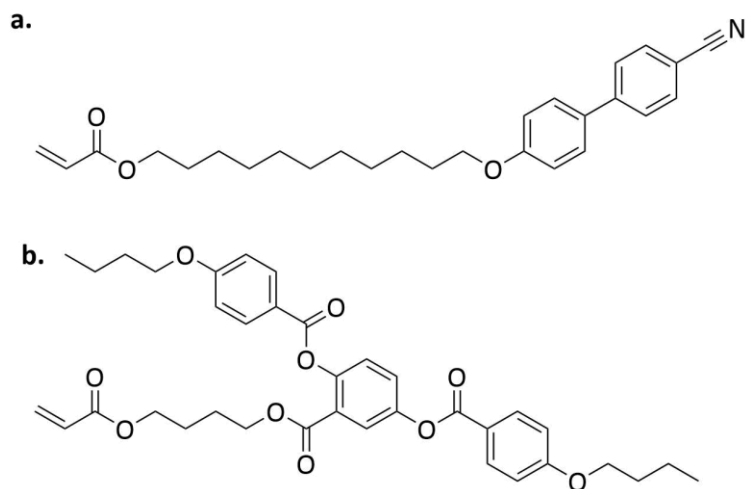


*Figure 23: Structures of the target monomers a. 11-(4'-cyanophenyl-4-phenoxy)undecyl acrylate and b. 2-((4-(acryloyloxy)butoxy)carbonyl)-1,4-phenylene bis(4-butoxybenzoate).*

Sacrificial initiator will be used to monitor the progress of the surface polymerisations. Surface initiations will be analysed by FT-IR and SEM, where appropriate the surfaces will be analysed by POM. The sacrificial polymer will be analysed by GPC, DSC,  $^1\text{H}$  NMR and FT-IR to infer an understanding of the surface and POM to aid the interpretation of the DSC.

### 3. Results and Discussion

Atom Transfer Radical Polymerisations (ATRPs) are a type of living radical polymerisation.

ATRP proceeds *via* the homolytic transfer of a halide from the terminal of a polymer chain to an active metal complex, increasing its oxidation state by one electron. In the course of the halide transfer the polymer chain becomes terminated by a free radical which in turn activates the chain to propagate the polymerisation. The polymerisation exists in equilibrium; the “living” chain can accept the return of the complexed halide, thus capping the chain. In this way the number of active chains can be limited to control polydispersity. For chain propagation to proceed the chain must be in the activate/radical form.

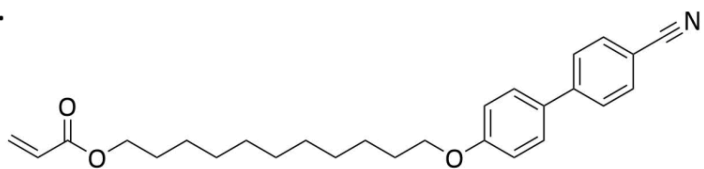
For this work an end-on monomer acrylate and a side-on monomer acrylate were chosen.

The end-on monomer **2** was chosen for initial studies to build upon previous results.<sup>90</sup> Polymers with the end-on monomer, **2**, repeat unit are known to have the following transitions:  $T_g$  15 SmC 20-25 SmA 125-140 Iso. The range of transition temperatures of the phase transitions is dependent on the degree of polymerisation and chain length.<sup>101</sup> By using a well understood monomer, greater potential exists for meaningfully interpreting results obtained from the grafting protocol.

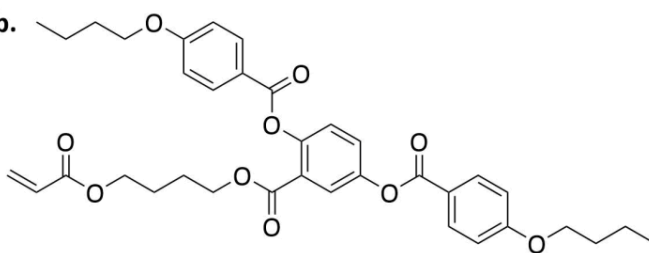
ATRP reactions have been conducted with the mesogen jacketed liquid crystal polymers, MJLCPs, a special type of SCLCP with a laterally attached side group with little or, as in the case, of the 2,5-bis[4-methoxyphenyl]-oxycarbonyl)styrene monomer, no spacer.<sup>102</sup> An unidentified liquid-crystalline mesophase was reported. The lack of spacer is understood to restrict the chain movement *via* the rigid and bulky mesogenic units and cause a stiff chain conformation. Building on the reported application of ATRP with no spacer, it is reasonable to expect polymerisation with an increased spacer to be achievable.

The use of side-on acrylate, **6**, has been reported for the synthesis of LC elastomers.<sup>99</sup> Upon polymerisation a nematic elastomer with the following transitions has been reported:  $T_g$  71.9 N 98.3 Iso. Side-on acrylate, **6**, is used in this work to attempt to graft a nematic liquid crystal polymer from the surface.

a.



b.

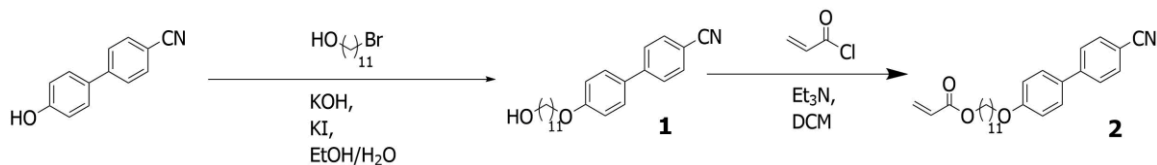


*Structures of a. end-on monomer 2 and b. side-on monomer 6.*

### 3.1. Synthesis of monomers

The monomers for this work were synthesised *via* general routes similar to those previously reported in the literature (Scheme 2),<sup>100</sup> and (Scheme 3).<sup>99</sup>

#### 3.1.1. End-on acrylate monomer



Scheme 3: Total synthetic route for the synthesis of the cyanobiphenyl acrylate, 2, from 4'-cyano-4'-hydroxybiphenyl.

Compound 1 was synthesised from commercially available 4'-cyano-4'-hydroxybiphenyl by Williamson etherification with 10-bromodecanol in the presence of a strong base.

The end-on acrylate monomer, 2, was synthesised *via* the esterification of compound 1 using an acid chloride. The highly reactive acid chloride species means the reaction proceeds quickly and cleanly. This made for a simple work up, with no major by-products or impurities.

The end-on monomer was analysed by GPC and had a retention volume of 17.6 mL (Figure 24) this was clearly distinguishable from the toluene internal standard at 20.3 mL (Figure 25), all GPCs in this work were run with THF as the solvent.

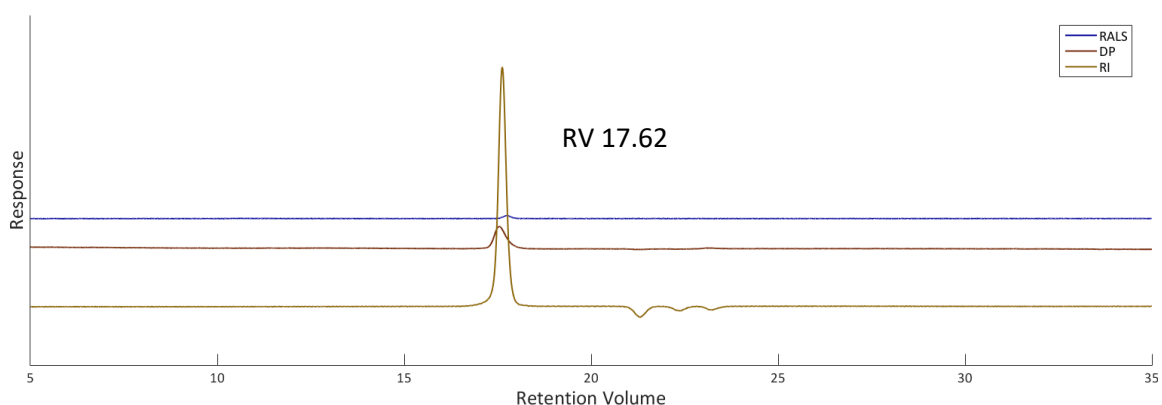


Figure 24: GPC triple detection trace of the end-on acrylate monomer 2: showing right angle light scattering (RALS), differential pressure (DP) and refractive index (RI).

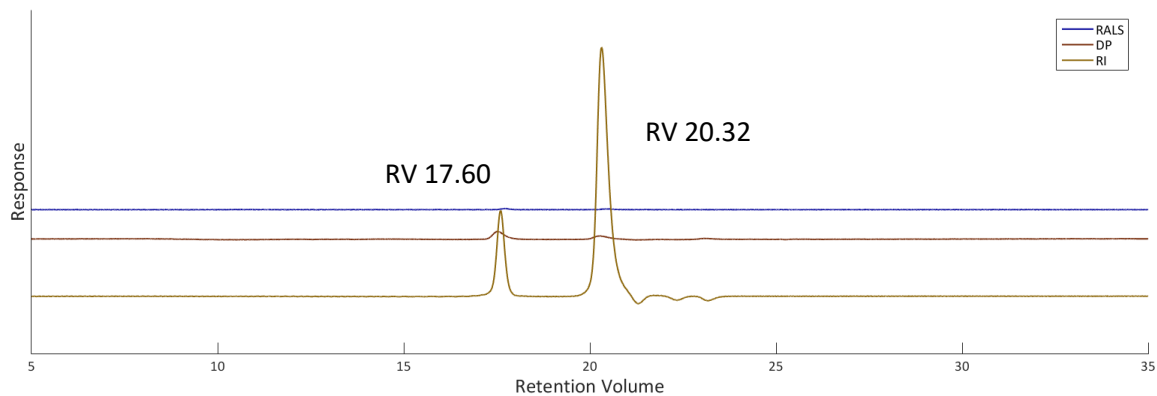
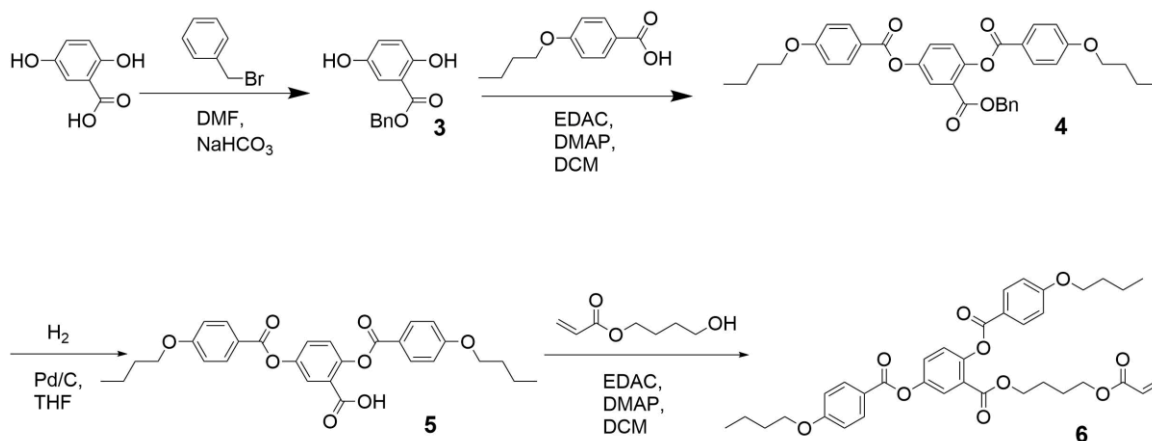


Figure 25: GPC triple detection trace of the end-on acrylate monomer **2** with toluene as an internal standard: showing right angle light scattering (RALS), differential pressure (DP) and refractive index (RI).

Retention volume is shown on the x-axis instead of time to remove the flow rate dependency. As all traces in this work were recorded at  $1 \text{ mL min}^{-1}$  the values are directly convertible into minutes.

### 3.1.2. Side-on acrylate monomer



Scheme 4: Total synthetic route for the synthesis of side-on acrylate, **6**, from 2,5-dihydroxybenzoic acid.

The side-on acrylate monomer, 2-((4-(acryloyloxy)butoxy)carbonyl)-1,4-phenylene bis(4-butoxybenzoate), **6**, was synthesised *via* successive carbodiimide catalysed esterification using 1-ethyl-3-(3-dimethylaminopropyl)carbodiimide (EDAC), (Scheme 3), according to the route reported in the literature with minor variations,<sup>99</sup> including the carbodiimide used. In order to prevent the 1,4-dihydroxybenzoic acid from esterifying with itself, the carboxylic acid was protected.

A benzyl protecting group was employed to selectively cap the carboxylic acid allowing transformations to be exclusively performed on the alcohols at the 1 and 4 positions. The benzyl protecting group is introduced *via* the nucleophilic substitution of the carboxylic acid with benzyl bromide. The phenol groups were reacted by EDAC mediated esterification with 4-butoxybenzoic acid. Following the esterification, the benzyl group was removed by hydrogenolysis catalysed by Pd on carbon to yield compound **5**. The side-on benzoic acid, compound **5**, was esterified with the commercially available acrylate terminated alcohol, 4-hydroxybutyl acrylate, 90%, to yield the side-on acrylate monomer, **6**. Electrospray ionisation (ESI) mass spectrometry showed a molecular weight species with an additional 14 mass units, this was assigned to C5 spacer suspected to have been introduced with the acrylate terminated alcohol; high performance liquid chromatography (HPLC) was used to define a ratio of C4 to C5 of 13.8:1.

The side-on monomer was analysed by GPC and had a retention of 17.2 mL (Figure 26) this was clearly distinguishable from the toluene internal standard at 20.3 mL (Figure 27).

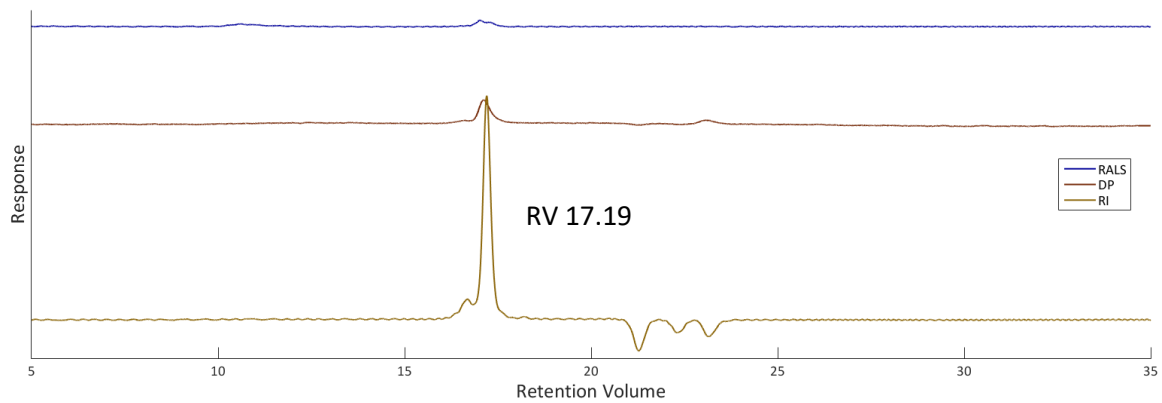


Figure 26: GPC triple detection trace of the side-on acrylate monomer 6: showing right angle light scattering (RALS), differential pressure (DP) and refractive index (RI).

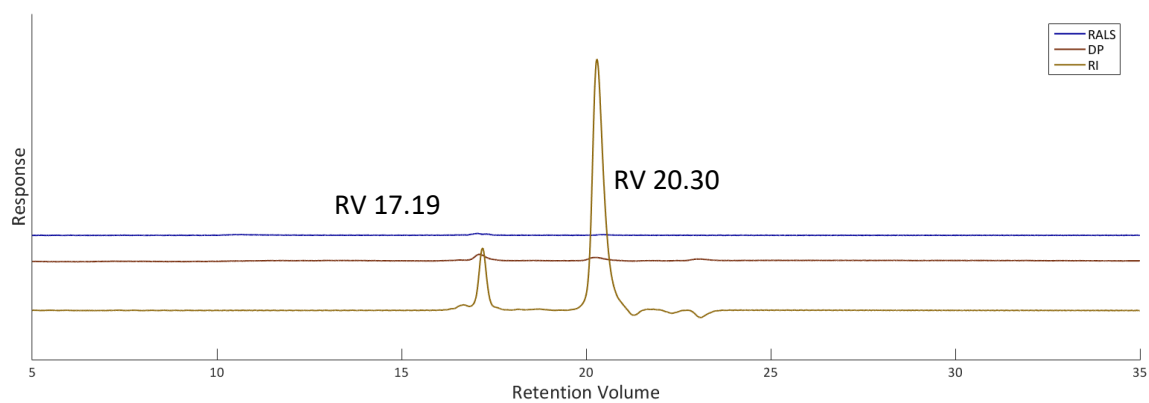


Figure 27: GPC triple detection trace of the side-on acrylate monomer 6 with toluene as an internal standard: showing right angle light scattering (RALS), differential pressure (DP) and refractive index (RI).

## 3.2. Substrate Characterisation

### 3.2.1. Paper substrate (cellulose) characterisation

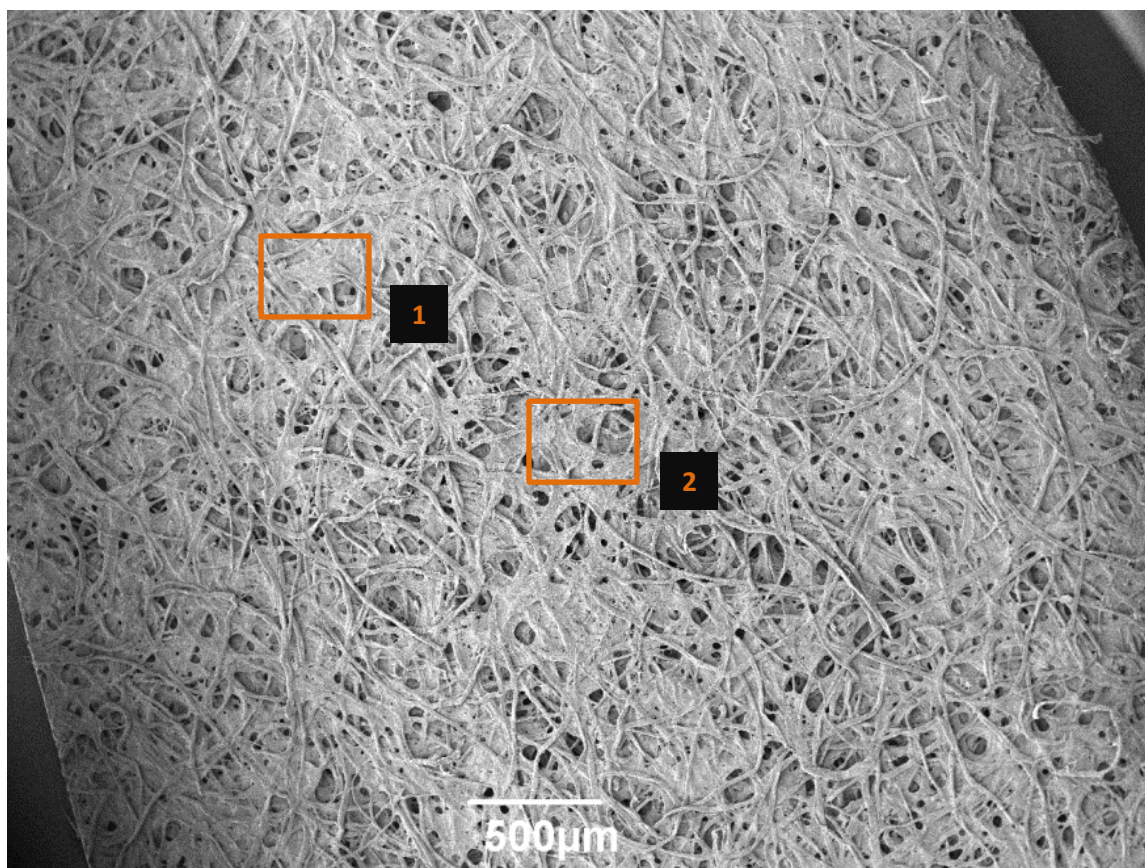


Figure 28: SEM images of the washed Whatman (l) filter paper at 70× magnification showing visible fibres. Regions 1 and 2 identified ahead of enlargement see Figures 30 & 31.

Washed paper was used as the substrate for variants of surface initiated atom transfer radical polymerisation. The surface was prepared by washing with acetone and DCM to remove any major contaminants from the surface. The pristine cellulose proceeded with is an inhomogenous surface made of fibres with a wide range of morphologies. The structure of the fibres is hierarchical, consisting of internal structures and only exposed functionalities are chemically active. Hence the surface is the reaction site of interest. The cellulose, and therefore the surface, is comprised of cellulose polymers (Figure 11). The alcohol units offer an accessible route to chemical modification.

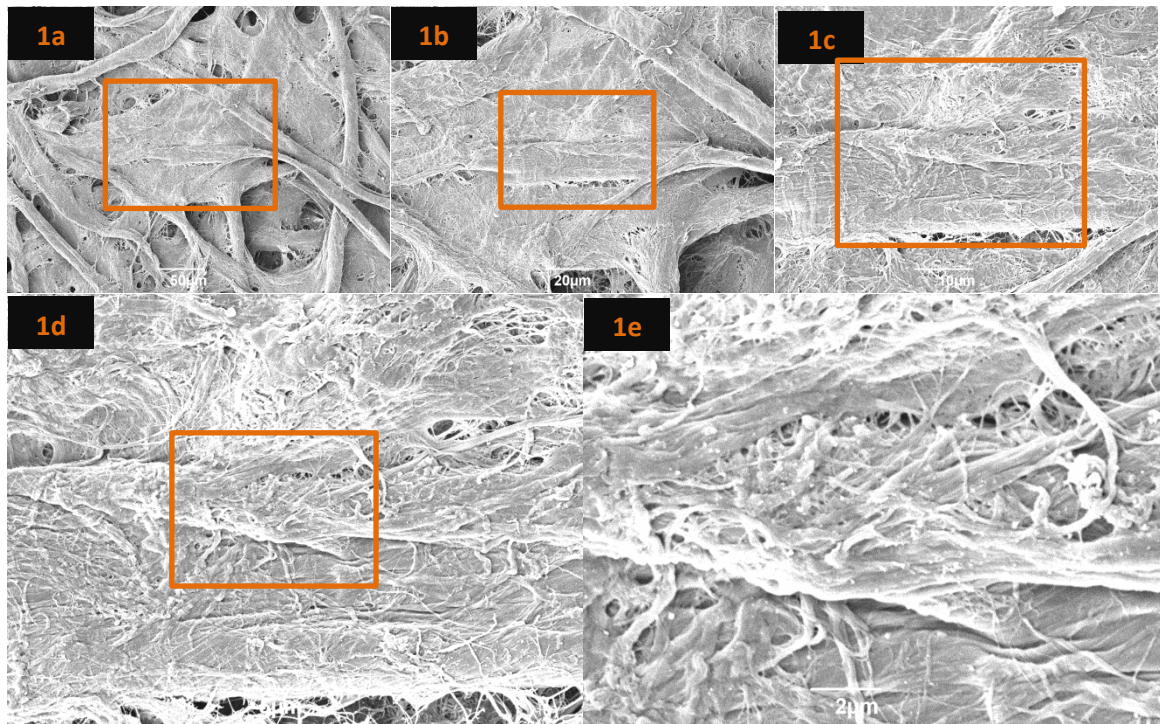


Figure 29: SEM images showing an enlargement of a smooth region of pristine cellulose paper (Figure 27) at a. 330 $\times$ , b. 750 $\times$ , c. 2000 $\times$ , d. 3000 $\times$ , and e. 8000 $\times$  magnification.

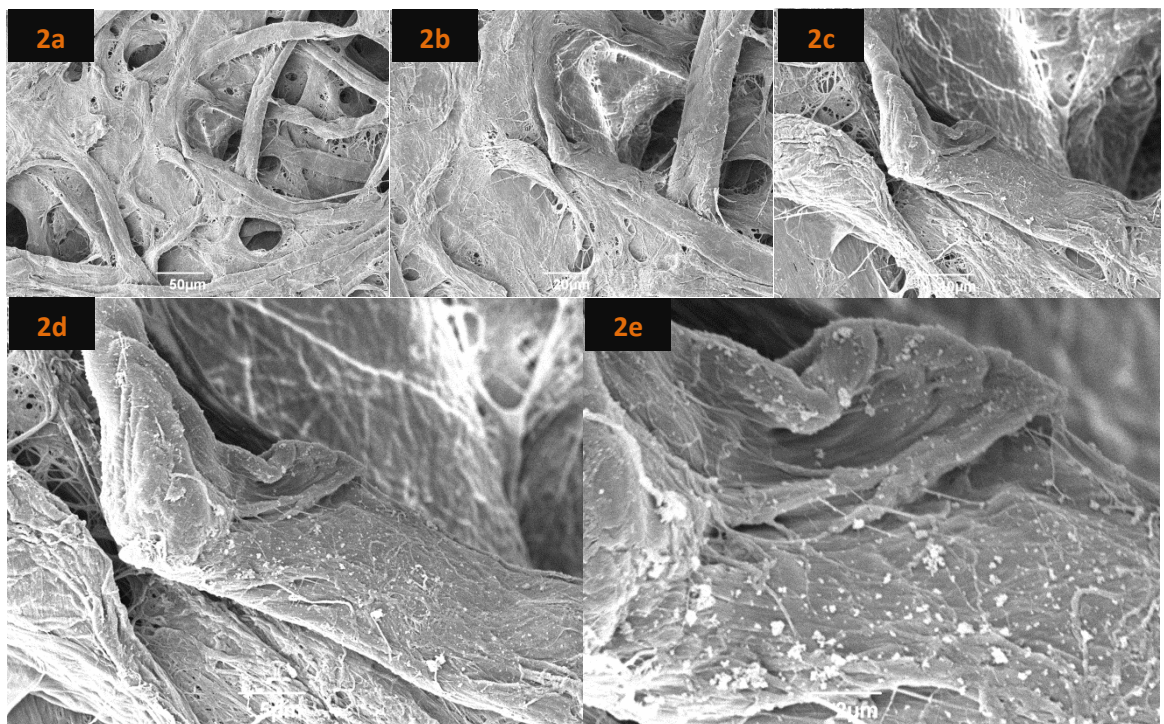


Figure 30: SEM images showing an enlargement of a rougher region of pristine cellulose paper (Figure 27) at a. 330 $\times$ , b. 750 $\times$ , c. 2000 $\times$ , d. 3000 $\times$ , and e. 8000 $\times$  magnification.

SEM images from the washed Whatman (I) filter paper show macrofibrils with the top end of the length range extending well into the mm regime, the inhomogeneity of the substrate is visible at all magnifications examined. There are two distinct surface topologies; the first show a smooth surface, the second a rougher surface. Two sets of SEM images are shown to illustrate the morphology. Region 1 and the accompanying enlargement series show a typical smooth region

and how it is comprised of multiple fibres intersecting with amorphous areas filling the vacancies. Region 2 and the accompanying enlargement series show the boundary of a rougher surface. In this rougher region the SEM images show grainy morphological features previously identified as 'microfibril bundles'.<sup>103</sup> In both regions there are 'loose' nanofibrils and the surface is sufficiently random that no suggestion of surface trenches are observed<sup>1</sup>. These observations provide a background for future interpretations of filter paper derived substrate surfaces. The inhomogeneous nature of the surface means that future observations are compared to similar regions in the pristine filter paper.

### 3.2.2. Covalently modified cellulose

As can be seen from Figure 31, it proved unviable to characterise the cellulose macroinitiator by infrared spectroscopy (FT-IR). It might be expected that a carbonyl peak would develop on the surface with the binding of initiator. This proved not to be the case because the carbonyl peak is obscured by the strength of the bulk cellulose signal. This is consistent with the loadings targeted due to the low surface area to volume ratio. The initiation was retrospectively confirmed later by proceeding to the polymerisations where the cumulative carbonyl stretches from the repeat unit were visible against the bulk of the cellulose background (Figure 38).

In order to prove whether the polymerisation was successfully initiating from the surface the resulting cellulose-polymer substrate it was washed to remove any sacrificial polymer and unreacted monomer. The paper samples were isolated and washed sequentially with THF, water, THF/Water (1:1), THF and ethanol (with sonication), three times each with ten millilitres of solvent per wash. This has been shown to be an effective washing protocol for removing the sacrificial polymer by stirring pristine paper in dissolved sacrificial polymer to produce a control sample and subsequently performing the same work up on the control sample. The sample stirred in the sacrificial polymer did not show stretches used to characterise the graft-from scenario.<sup>104</sup>

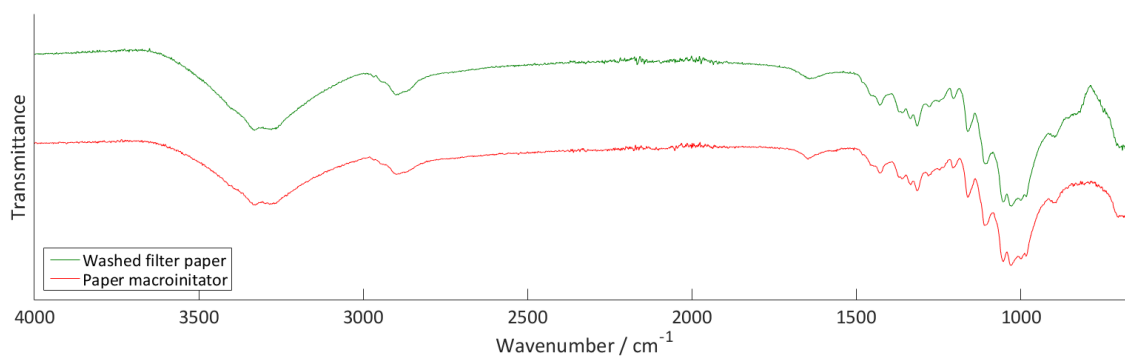
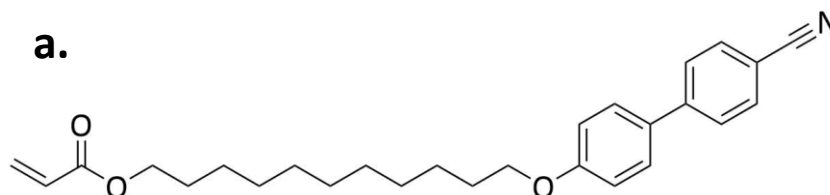


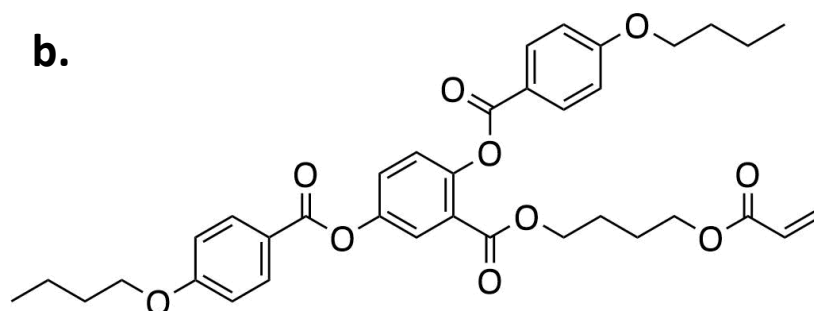
Figure 31: FT-IR of a. pristine and b. initiator grafted filter paper.

### 3.2.3. Establishing context for results

In order to probe the challenges of polymerisation with liquid crystal acrylates more meaningfully the previously studied 11-((4'-cyano-[1,1'-biphenyl]-4-yl)oxy)undecyl acrylate (compound **2**) was utilised<sup>90</sup>. For this work it was important to establish appropriate comparisons with the previous work.<sup>90</sup>



Atom transfer radical polymerisations of **2** with a variety of Cu(II)/ligand systems as catalysts, effect of different solvents and new variants of the ATRP process were investigated. Once favourable conditions to conduct the polymerisation were established, for monomer **2**, the polymerisation of side on acrylate, **6**, from the surface of cellulose paper substrates was studied.



#### Literature comparison

In order to establish a meaningful comparison the polymers obtained by polymerisation in the previous work were analysed by gel permeation chromatography (GPC) Figure **32**.<sup>90</sup> GPC is a comparative technique and as such meaningful comparisons are instrumentation dependent.

Figure **32** shows the GPC of the sacrificial polymer from the previously reported graft polymerisation of end-on monomer from paper (cellulose), LCP 2).

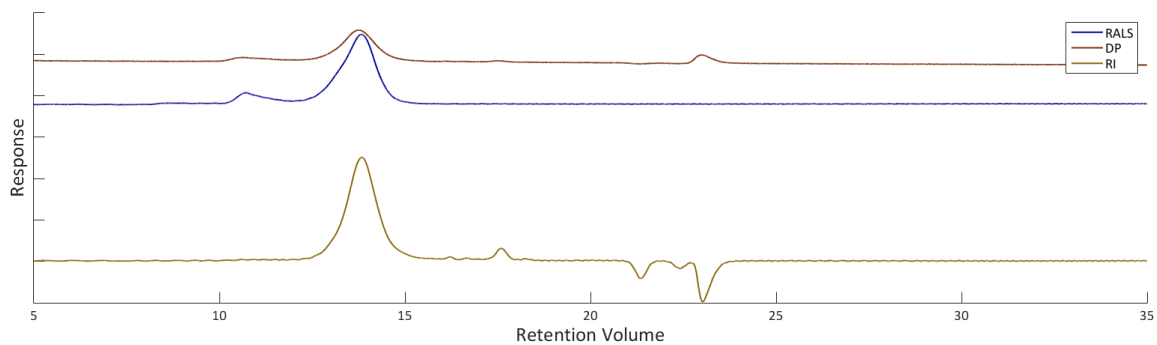


Figure 32: GPC triple detection trace from the sacrificial polymer formed in experiment LCP 2 of the previous work: showing right angle light scattering (RALS), differential pressure (DP) and refractive index (RI).

Figure 33 shows SEM images for a typical region of the surface obtained from the previously reported graft polymerisation of end-on monomer from paper (cellulose), LCP 2) at various magnifications.

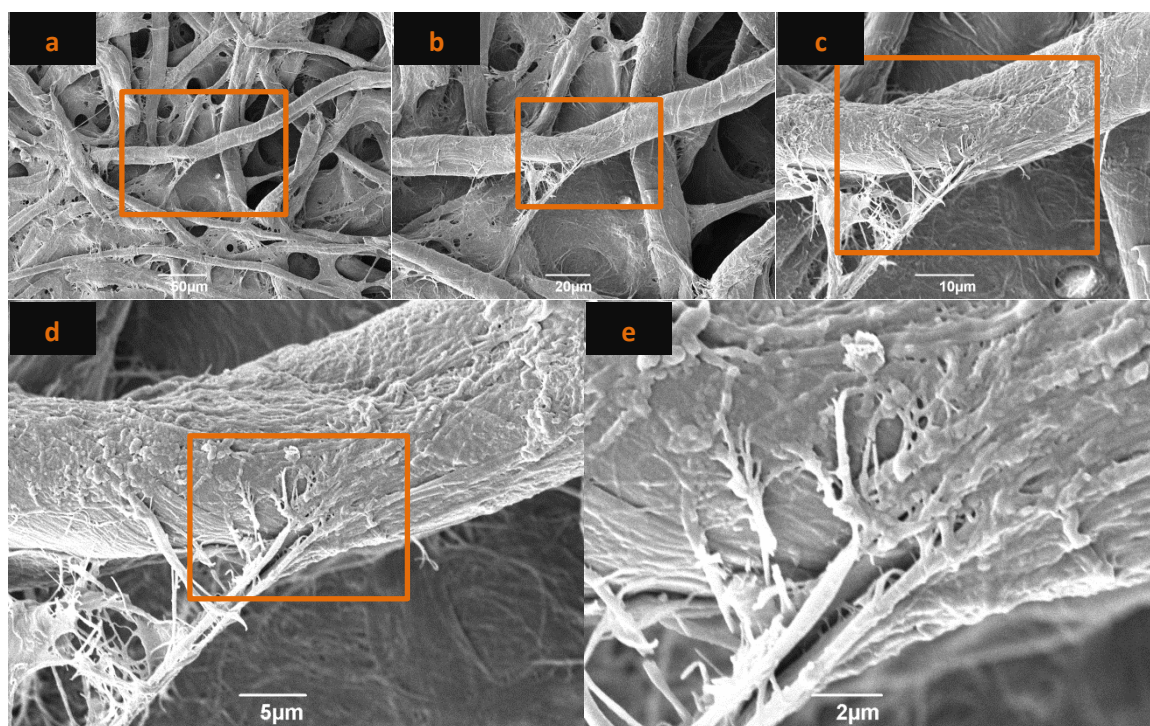


Figure 33: SEM images of the surface formed in experiment LCP 2 of the previous work at at a. 330 $\times$ , b. 750 $\times$ , c. 2000 $\times$ , d. 3000 $\times$ , and e. 8000 $\times$  magnification.

Figure 34 shows the GPC of the sacrificial polymer from the previously reported graft polymerisation of end-on monomer from paper (cellulose), LCP 3).

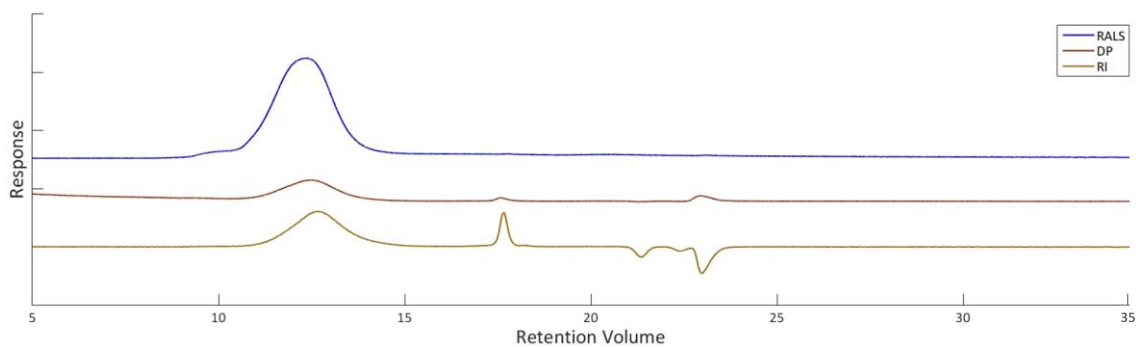


Figure 34: GPC triple detection trace from the sacrificial polymer formed in experiment LCP 3 of the previous work: showing right angle light scattering (RALS), differential pressure (DP) and refractive index (RI).

Figure 35 shows SEM images for a typical region of the surface obtained from the previously reported graft polymerisation of end-on monomer from paper (cellulose), LCP 3) at various magnifications.

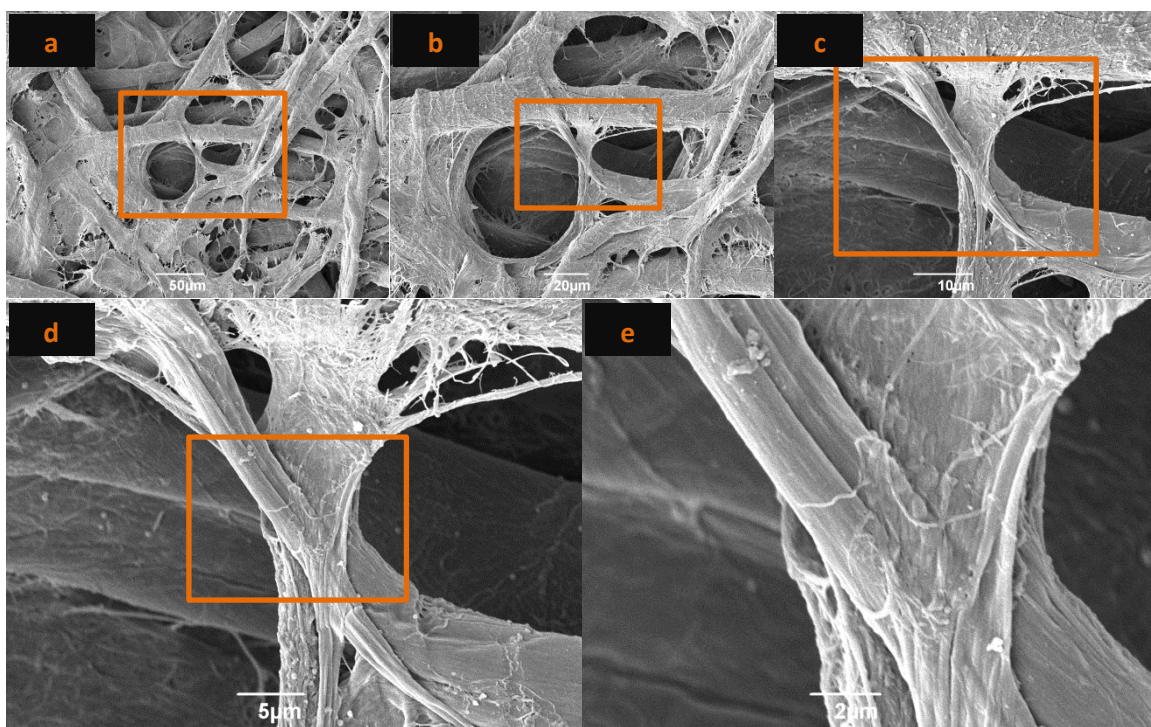


Figure 35: SEM images of the surface formed in experiment LCP 3 of the previous work at a. 330 $\times$ , b. 750 $\times$ , c. 2000 $\times$ , d. 3000 $\times$ , and e. 8000 $\times$  magnification.

Fresh GPC analysis of the previously analysed polymers gave  $M_n$  values of 16,587 and 48,852 for the elutions at 13.8 mL and 12.6 mL respectively for the sacrificial polymers of LCP 2 and LCP 3 respectively (Table 1). These results show that the calibration, against a polystyrene standard, for the instrument varies from that achieved in the previous studies (it did not prove possible to achieve a robust calibration). For LCP2 the  $M_n$  measured corresponds to the same degree of polymerisation as before for LCP3 the  $M_n$  measured is off by a scale factor of 1.48 the combined errors of the  $M_n$  and  $M_w$  error an increase in the calculated PDI. This is attributable to machine

error, the start delay is not functioning, efforts have been made to account for this with fresh calibrations. Any interpretation of polydispersity for subsequent experiments must be taken with extreme caution.

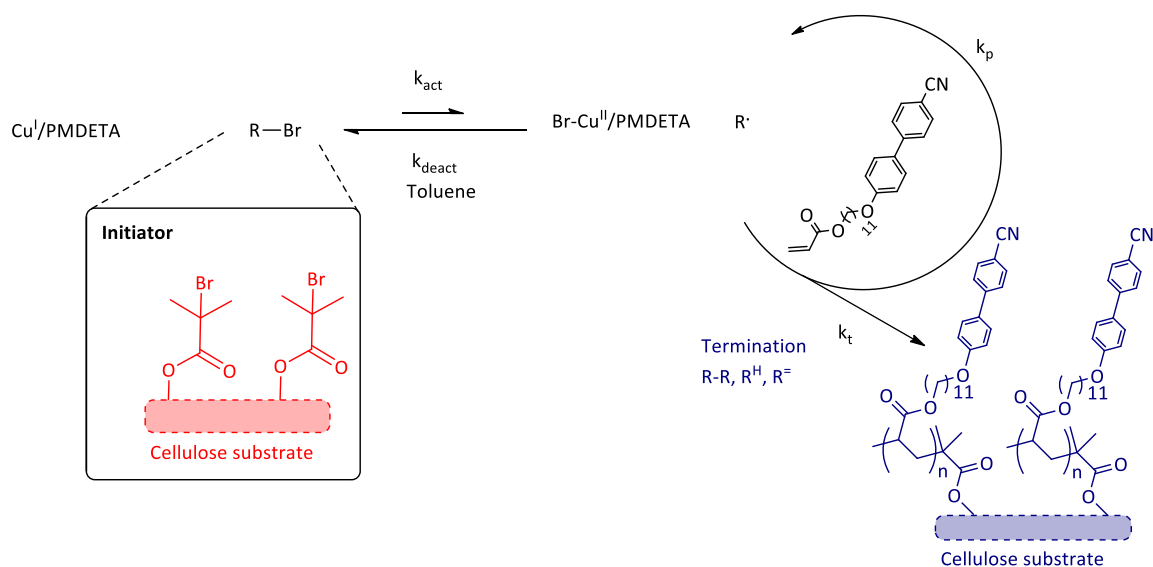
The surface obtained from the previous polymerisations (Figure **33** & **35**) begins to show the smoothing of the surface and flattening of microfibril bundles as well as a reduction in visible loose nanofibrils as they become thicker. Both of these observations appear to result from the features becoming incorporated in the competitive 'swelling' of the dominant fibres in the local morphological environment.

Table 1: GPC data for the sacrificial LCPs previously reported as previously analysed and using the same polystyrene calibration used for the analysis of subsequent polymers.

Entry	Mn <sub>prev</sub>	PDI <sub>prev</sub>	DP <sub>prev</sub>	Mn <sub>meas</sub>	Mw <sub>meas</sub>	PDI <sub>meas</sub>	DP <sub>meas</sub>
LCP 2	16370	1.21	39	16,587	22,401	1.35	40
LCP 3	33250	1.82	79	48,852	81,533	1.70	117

### 3.3. SI-ATRP of the end-on monomer without sacrificial initiator (Entry 1).

Surface initiated atom transfer radical polymerisation (SI-ATRP) was conducted from a cellulose (paper) macroinitiator using Cu(I)/PMDETA (108  $\mu$ mol:96  $\mu$ mol) and end-on acrylate monomer (4.77 mmol) in toluene, with stirring (Scheme 5).



Scheme 5: Reaction scheme for the Cu(I)Br/PMDETA activated ATRP of substrate **3** via the graft from polymerisation of substrate **1a** with compound **2** without sacrificial initiator.

In order to provide a benchmark for the polymerisations presented in this work, a graft was conducted from a paper-macroinitiator with no solution ‘sacrificial’ initiator. From the lack of sacrificial initiator it can be anticipated that thermal polymerisations do not occur in the system. Therefore evidence of polymerisation would only be expected to occur on the cellulose macroinitiator.

A stirred suspension of the end-on acrylate monomer in 0.5 mL of toluene was heated to 100 °C and worked up in the same manner as the crude solution. The crude solution showed the polymerisation was not occurring.

#### Solution polymerisation

The <sup>1</sup>H NMR of the crude isolated from the SI-ATRP reaction shows exclusively the presence of unreacted acrylate, **2**, indicating that in the absence of sacrificial initiator polymerisations did not occur (Figure 36).

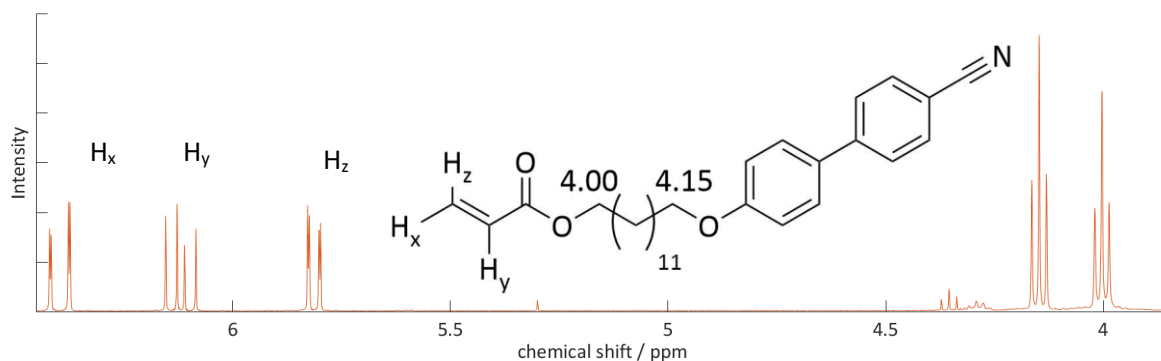


Figure 36:  $^1\text{H}$  NMR of the sacrificial polymer from the ATRP of compound **2** with  $[\text{Cu}(\text{I})/\text{PMDETA}]$  in toluene with a macroinitiator and no sacrificial initiator.

A  $^1\text{H}$  NMR ‘monitoring region’ was chosen for polymerisations with the end-on monomer of 3.85 – 4.20 ppm against 5.77-6.44 ppm. The  $^1\text{H}$  NMR spectrum shows triplets in the region 3.85–4.20 ppm assigned to the  $\text{CH}_2$  in the aliphatic chain next to the ether (4.00 ppm) and the ester (4.15 ppm) groups of the unreacted monomer. A ratio was taken of the total integration between 3.85 ppm and 4.20 ppm to the total integration between 5.77 ppm and 6.44 ppm of 1.36:1, this is very similar to an equivalent ratio for the stirred suspension of the end-on acrylate monomer in 0.5 mL of toluene was heated to 100 °C of 1.33 showing very little, if any change in the composition of the sample with respect to the olefin and  $\text{CH}_2\text{O}$  groups.

Whereas  $^1\text{H}$  NMR provides an indication as to the degree of monomer conversion, it does not provide information about the molecular weight or polydispersity of the polymers achieved. GPC is used to ascertain polymer characteristics (Mw, Mn and polydispersity). The analysis of the polymers produced in the previous work confirms that the characteristics presented in this work can only be meaningful when restricted to comparisons against other polymers produced within this work. Figure 37 shows the GPC trace of the crude isolated from the polymerisation reaction.

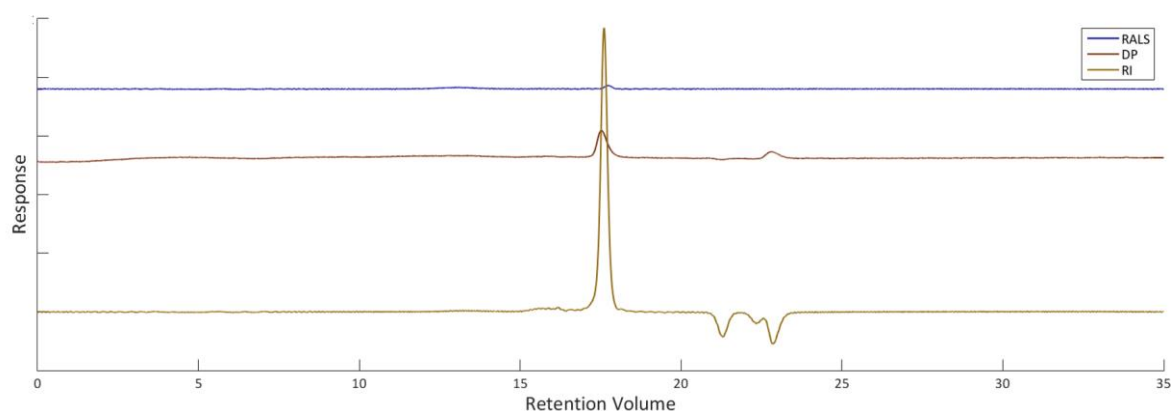


Figure 37: GPC triple detection trace of sacrificial polymer from the ATRP of compound **2** with  $[\text{Cu}(\text{I})/\text{PMDETA}]$  in toluene with a paper-macroinitiator and no sacrificial initiator: showing right angle light scattering (RALS), differential pressure (DP) and refractive index (RI).

GPC showed the absence of polymer formed in solution, characterised by a single species eluting at 17.6 mL this is consistent with the monomer. It can be concluded that there is no thermal initiation of the polymerisation in the solution under the conditions used, in the absence of sacrificial initiation. Consequently, it is appropriate to conclude that with sacrificial initiator, polymer formed in solution results from the ATRP-initiated polymerisation and not from thermal polymerisation of the acrylate monomer. Therefore it can be assumed that the characteristics of polymer formed in solution, due to the presence of sacrificial initiator (the sacrificial polymer) represent reasonably accurately (although not fully) the polymer on the substrate surface (formed from the surface-anchored initiator sites)<sup>96</sup>.

## Substrate polymerisation

The cellulose substrate was analysed by FT-IR and SEM. Figure 38 shows the IR spectrum of the paper substrate isolated from the polymerisation reaction (line e., blue). For comparison purposes the spectrum of the cellulose paper loaded with initiator is also shown (line d., red), as well as the IR spectra of the acrylate monomer (line a., black), the crude product, unreacted monomer, isolated from the polymerisation (line b, orange) and the washed filter paper (c., green).

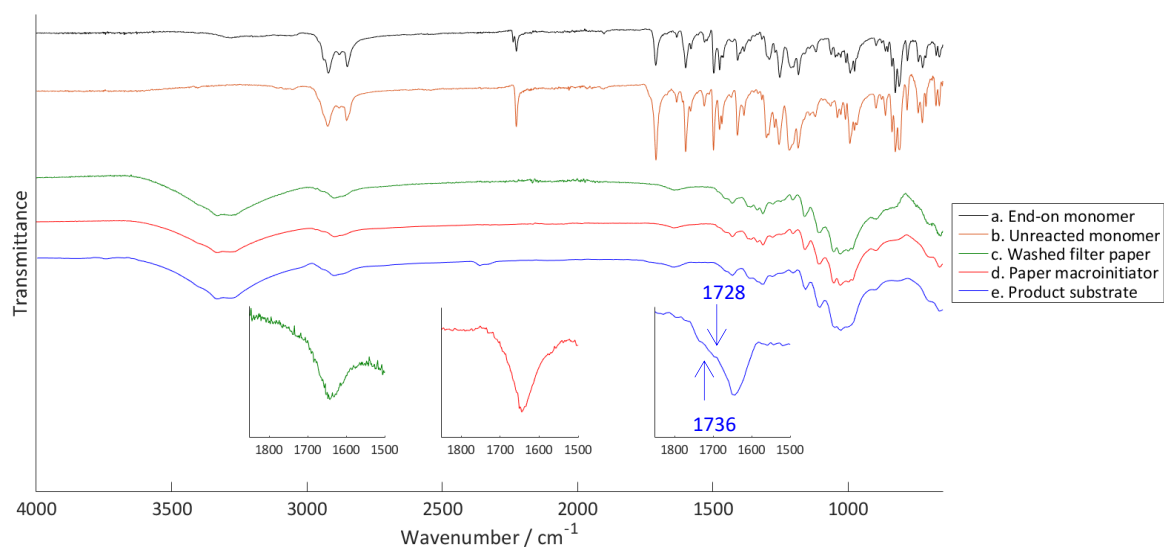


Figure 38: FT-IR of substrate achieved from the ATRP of compound 2 with [Cu(I)/PMDETA] in toluene with a macroinitiator and no sacrificial initiator, with insets showing the carbonyl region for the washed filter paper (green), paper-macroinitiator (red) and product substrate (blue).

The resulting substrate shown was washed using the previously established protocol (described in Section 3.2.2). In this and subsequent FT-IR figures, product substrate (shown last) refers to the paper substrate isolated from the reaction. FT-IR of the resulting substrate (see Figure 38, line e insert) shows the clear development of a broad absorption shoulder at  $\sim 1730\text{ cm}^{-1}$ , this was assigned to the stretching vibration of the carbonyl (C=O) on the side of the background cellulose O-H bend contribution<sup>105</sup> (local transmittance minima was found to be  $1736\text{ cm}^{-1}$ , this reflects a

combination of the two signals, the C=O stretch, O-H bend inflection point occurred at  $1728\text{ cm}^{-1}$ ).  $\nu_{\text{CN}} = 2230\text{ cm}^{-1}$  and  $\nu_{\text{Ar}} = 1610\text{ cm}^{-1}$ , previously observed in graft studies of the monomer from cellulose,<sup>90</sup> were not observed on the surface – this reflects their relative intensity relative to the  $\nu_{\text{CO}}$  signal and the lower loadings achieved, indicated by the  $\nu_{\text{CO}}$  intensity compared to the previously reported polymerisations.

SEM images of the paper substrate are shown in Figure 39 displaying a representative area of the surface at 330 $\times$  (a), 750 $\times$  (b), 2000 $\times$  (c), 3000 $\times$  (d), and 8000 $\times$  (e) magnifications these enlargements will be presented for subsequent substrates. The SEM images showed the systematic loss of microfibril bundles as they became engulfed in the wider morphology. Boundary edges continue to be observed between regions (see Figure 39di) at greater magnifications (see Figure 39d, e) trenches develop on the surface, these appear to be the result of competitive coating of fibres with some increasing in diameter independently and others fusing (Figure 39ei). There also appear to be incidents involving the ‘deposition’ of engorged nanofibrils, which have become too massive to favourably maintain a separation from the bulk Figure 39eii). These extreme case observations can be used to consider how alternative polymerisation systems demonstrate progress for the key analytical methods.

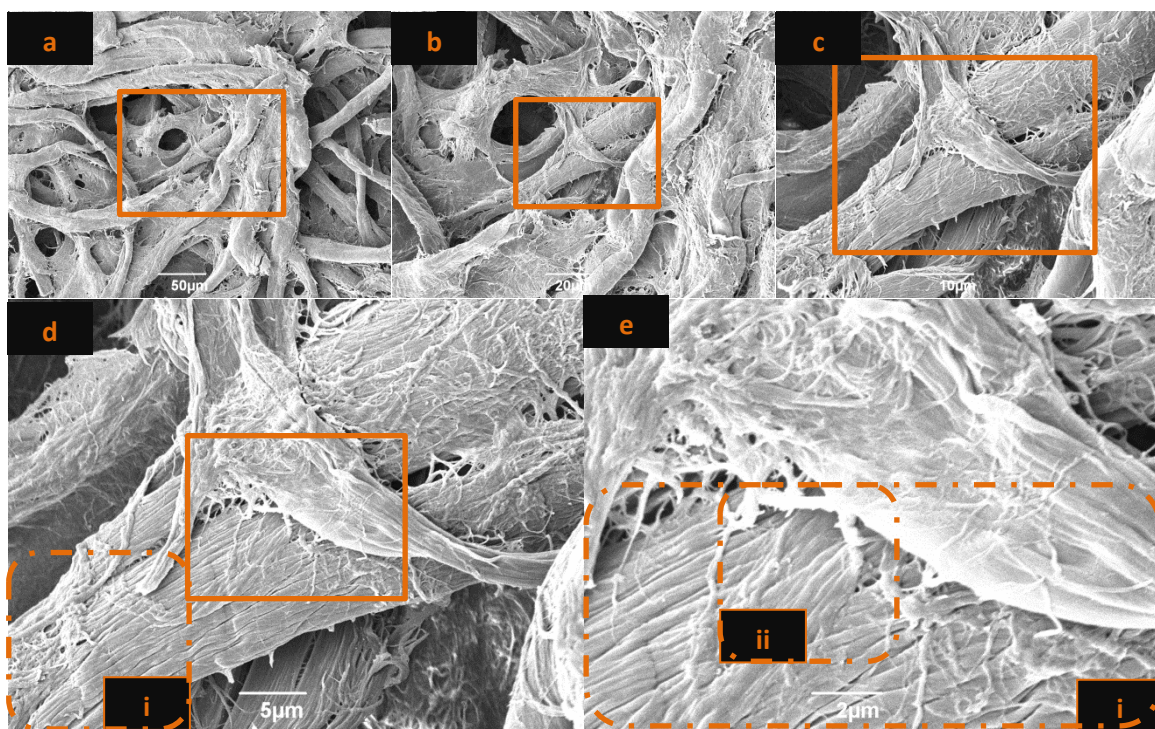


Figure 39: SEM images of the surface obtained from the SI-ATRP reaction of compound 2 with [Cu(I)/PMDETA] in toluene without sacrificial initiator (Entry 1) at a. 330 $\times$ , b. 750 $\times$ , c. 2000 $\times$ , d. 3000 $\times$ , and e. 8000 $\times$  magnification.

It was observed that the substrate mass decreased, this is not chemically meaningful. The mass loss is attributed to mechanical damage of the substrate. Observations of mass gain/loss appeared sporadic throughout the work, potentially due to substrate degradation; as such no

attempt was made at calculating graft metrics – as no confidence could be assigned to the meaningfulness of such metrics.

### 3.4. SI-ATRP of the end-on monomer with sacrificial initiator (Entry 2).

Sacrificial initiator is used throughout the rest of this work to produce a sacrificial polymer to allow us to monitor the progress of the reaction on the surface.<sup>96</sup> An additional benefit of sacrificial initiator is the ability to achieve greater control and therefore reduced polydispersity in reactions with sacrificial initiator.<sup>97</sup>

Previously reported work was developed in order to develop the polymerisation methodology and to ensure the robustness of the analysis methodology deployed, we carried out several scaled down variants of the polymerisation of the end-on cyanobiphenyl acrylate, **2**. ATRP requires very exacting condition, with very low levels of oxygen present. In order to achieve thorough degassing under a normal laboratory environment freeze-vacuum-thaw degassing cycles were employed throughout this work. As well as providing confidence of thorough degassing, these restrict the loss of volatile components and therefore allow for greater reproducibility of concentrations. Progressing from a robust experimental methodology allows more meaningful conclusions to be drawn about the potential of the living radical polymerisations for controlled grafting of liquid crystal polymers from surfaces. The previously reported work utilised a Cu<sup>I</sup>/PMDETA catalyst in toluene and achieved well controlled polymerisations, noting that the conditions were yet to be optimised<sup>90</sup>.

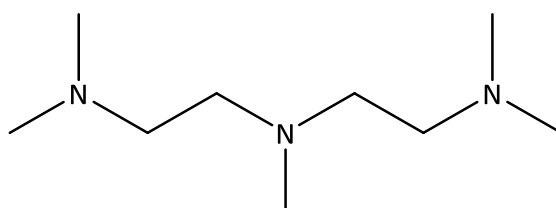
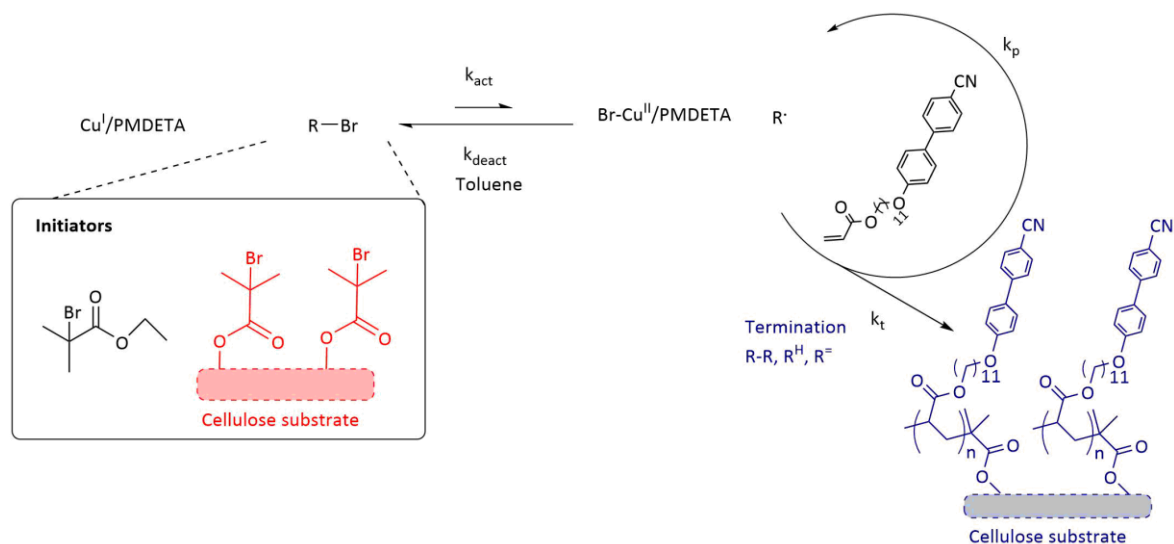


Figure 40: Structure of PMDETA.

Surface initiated atom transfer radical polymerisation (SI-ATRP) was conducted from a cellulose (paper) macroinitiator using Cu(I)/PMDETA (22.1  $\mu\text{mol}$ :35  $\mu\text{mol}$ ) and end-on acrylate monomer (1.09 mmol) in toluene, in presence of sacrificial initiator, EBIB (33  $\mu\text{mol}$ ), with stirring (Scheme 6).



*Scheme 6: Reaction scheme for the Cu(I)Br/PMDETA activated ATRP of substrate **4** via the graft from polymerisation of substrate **1b** with compound **2** in the presence of sacrificial initiator.*

### Solution polymerisation

Figure **41** shows the  $^1\text{H}$  NMR of the crude product isolated from Entry **2**. Figure **41b** shows the monitoring region used to monitor the progress of the polymerisation.

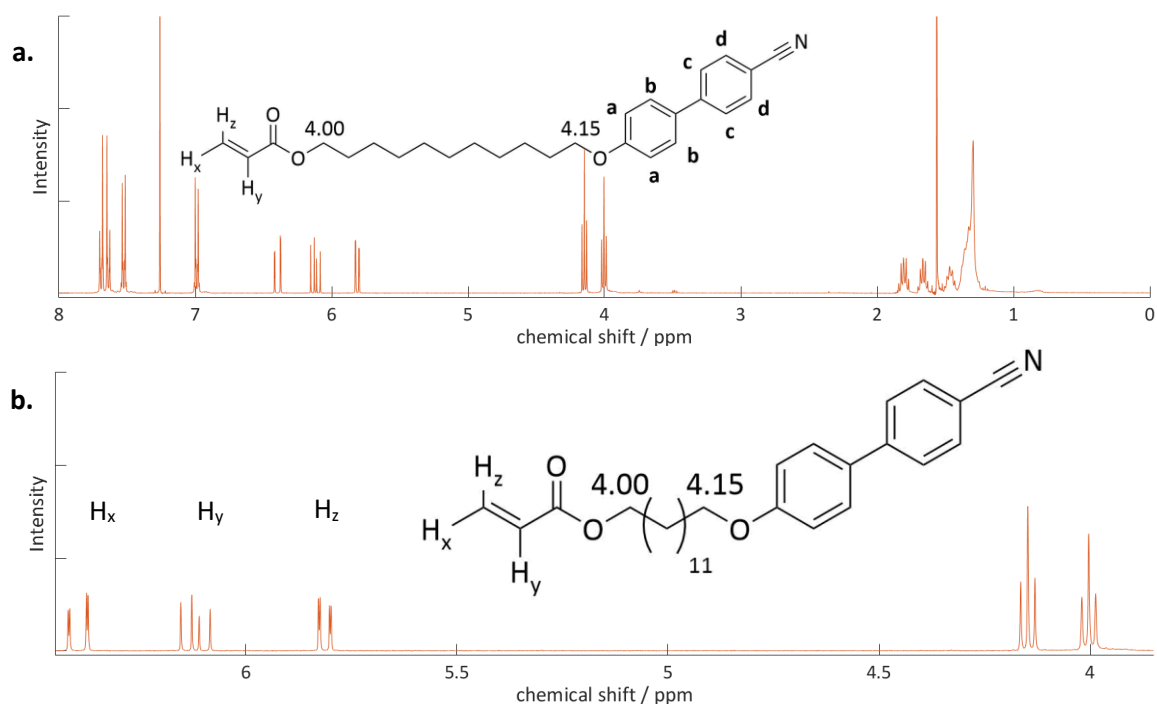


*Figure 41: a. Complete  $^1\text{H}$  NMR spectrum of the sacrificial polymer from the synthesis of substrate **4** via the ATRP polymerisation of compound **2**. b.  $^1\text{H}$  NMR spectrum for the monitoring region of the sacrificial polymer used to monitor the progress of the reaction.*

The  $^1\text{H}$  NMR spectrum shows that mostly monomer has been recovered from the polymerisation, since no signals due to the polymer are observed. In attempting to reproduce the literature experiment with scaled down conditions, no discernible polymerisation was seen in the monitoring region of the  $^1\text{H}$  NMR (Figure 41b). A monitoring ratio of 1.44:1 was calculated suggesting a small change from the background integration ratio, this is not reliable evidence given the size of the ratio change and the lack of discernible evidence in any of the signals (Figure 41a).

Figure 42 shows the GPC trace of the reaction crude isolated from the reaction.

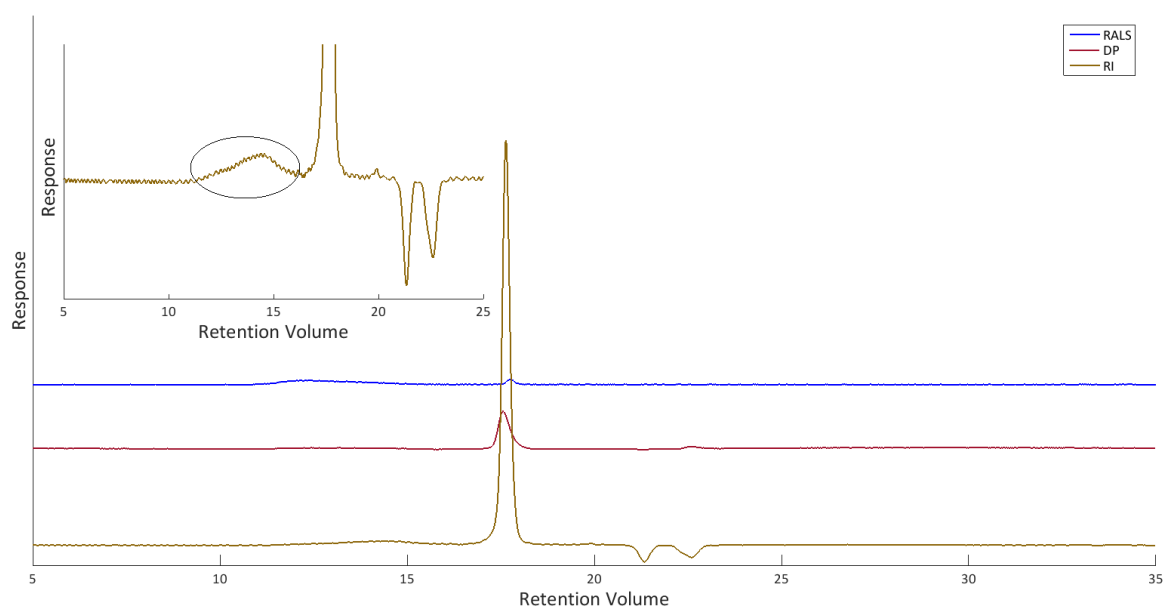


Figure 42: GPC triple detection trace of sacrificial initiator from the synthesis of substrate 4 via the ATRP polymerisation of compound: showing right angle light scattering (RALS), differential pressure (DP) and refractive index (RI). Insert shows the relative responses of the signal at 14.31 mL compared to the negative system peaks.

GPC proved more successful in observing a higher molecular weight species, as a very broad signal with a lower retention volume of 14.31 mL (shown in the expansion in figure 42) compared to the monomer at 17.61 mL. A lower retention volume value indicates a macromolecule with a higher hydrodynamic volume; this allows us to deduce that some macromolecule has been formed. In comparing the retention volume to those of the polystyrene standards we make the assumption that the polymer sample behaves similarly to the standard in terms of chemistry, density and folding, we can calculate a 'Polystyrene Equivalent' molecular weight or relative molecular weight ( $M_w$ ) for this sample the relative molecular weight was calculated as 1 because of the limitations of universal calibration. The very low intensity of the peak on all three GPC detection channels, with particular consideration given to the concentration (RI) channel, shows that the presence of the higher molecular weight species is very low compared to the monomer.

## Substrate polymerisation

Analysis of the cellulose paper resulting from this polymerisation was carried out by FT-IR and SEM. Figure 43 shows the IR spectra of the reagents and subsequent species as before.

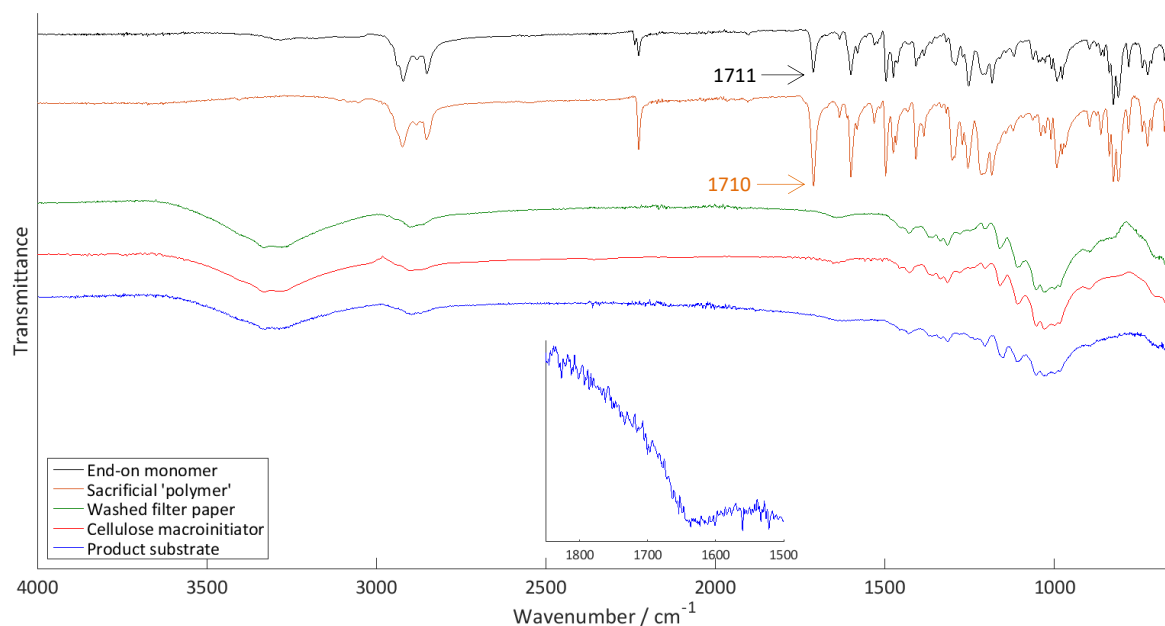


Figure 43: FTIR of the substrate obtained via the synthesis of substrate 4 via the ATRP polymerisation of compound 2, with an inset showing the carbonyl region for the product substrate (blue).

The FT-IR of the substrate shows no distinct shoulder around 1730 cm<sup>-1</sup>, where a peak has previously been observed in reported functionalisations of cellulose paper by ATRP it has been assigned to the carbonyl stretches;<sup>83</sup> the lack of identifiable carbonyl peak is in agreement with the low levels of polymer formed in solution as ascertained by GPC. It may be possible that scarce polymerisation occurred on the surface, below the signal to noise threshold resulting from the relative cellulose background-graft polymer loadings.

Figure 44 shows the SEM images of the paper surface at a. 330×, b. 750×, c. 2000×, d. 3000×, and e. 8000× magnification, with the magnification regions indicated.

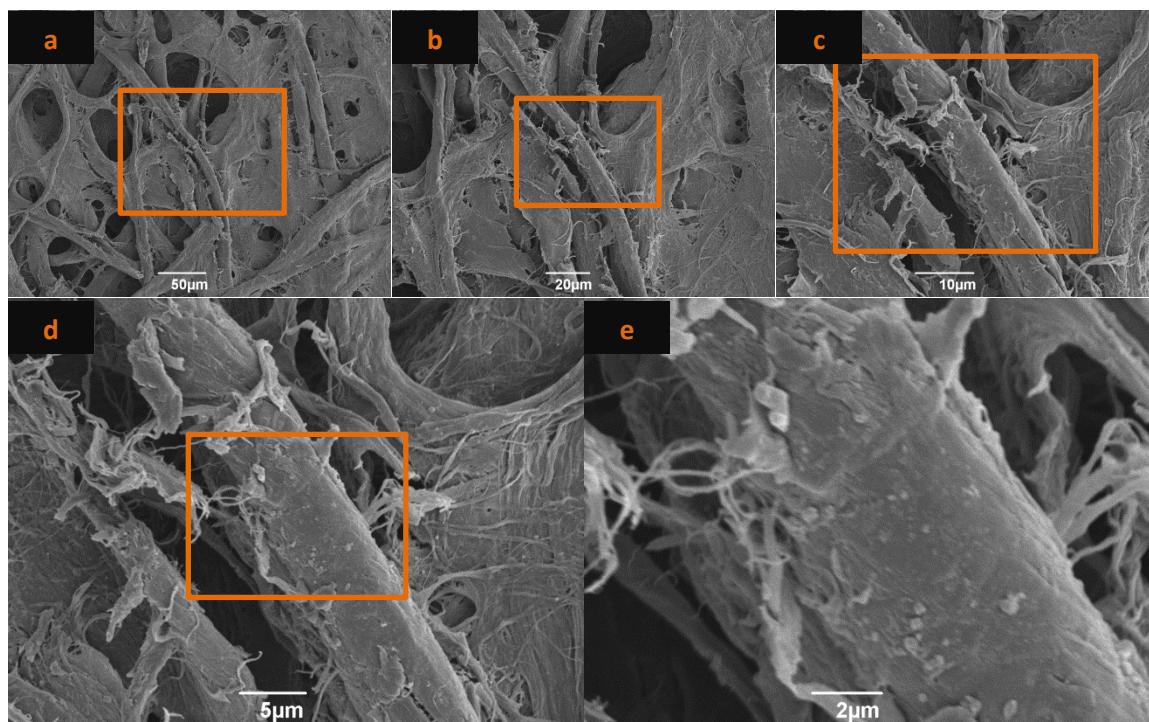


Figure 44: SEM images of the surface obtained from the SI-ATRP reaction of compound **2** with [Cu(I)/PMDETA] in the presence of sacrificial initiator in toluene (Entry **2**) at a. 330 $\times$ , b. 750 $\times$ , c. 2000 $\times$ , d. 3000 $\times$ , and e. 8000 $\times$  magnification.

Potentially some degree of smoothing of the surface could be deduced as shown from SEM images d. 3000  $\times$  and e. 8000  $\times$  magnification, however this is not conclusive evidence. The substrate surface appears broadly unchanged at low magnifications with fine fibres still retained widely throughout the sample.

## Conclusions

The lack of evidence for polymerisation, judged by evidence of the polymer in solution or on the paper substrate, could suggest that the catalyst is not successfully (re)generating the active sites, under the conditions used. The conditions vary significantly from the polymerisation in the absence of sacrificial initiator by the presence of sacrificial initiator and scale and additionally with the reagent ratios, and advantageously with the more thorough degassing method. The lack of catalytic activity could indicate catalyst death or oxygen poisoning or reflect one of the other conditions varied. In order to gain an insight into the catalyst activity an alternative ligand was used.

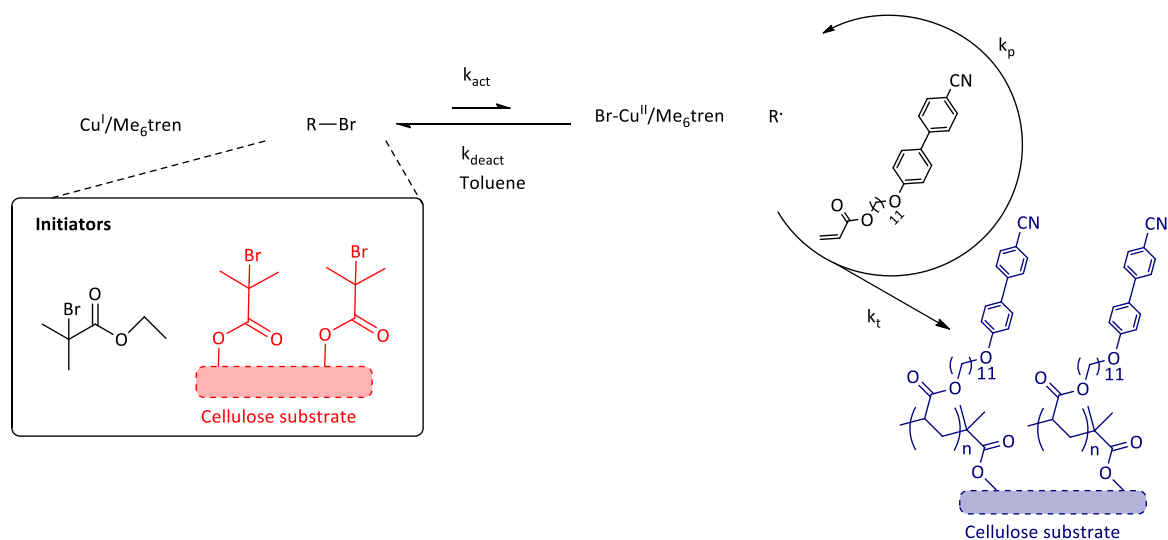
### 3.5. Potential of Me<sub>6</sub>TREN as an alternative complexing ligand (Entry 3).

Alongside PMDETA, Me<sub>6</sub>TREN has risen to prominence as a favoured ligand for ATRPs. In the previous work PMDETA was chosen because of its higher stability at higher temperatures.<sup>90</sup>

We employed Me<sub>6</sub>TREN to assess whether this concern was warranted.

Scheme 7 shows the surface-initiated polymerisation of end-on acrylate **2** using Cu(I)/Me<sub>6</sub>TREN as the catalytic system.

The surface initiated atom transfer radical polymerisation (SI-ATRP) was conducted from a cellulose (paper) macroinitiator using Cu(I)/Me<sub>6</sub>TREN (18.7 μmol:21 μmol) and end-on acrylate monomer (0.840 mmol) in toluene, in presence of sacrificial initiator, EBIB (22 μmol), with stirring.



Scheme 7: Reaction scheme for the Cu(I)/Me<sub>6</sub>TREN activated ATRP of substrate **5** via the graft from polymerisation of substrate **1c** with compound **2** in the presence of sacrificial initiator.

#### Solution polymerisation

Figure 45 shows the <sup>1</sup>H NMR spectrum of the sacrificial polymer formed in this reaction, which shows the complete disappearance of the olefinic protons of the acrylate group between 5.77 and 6.44 ppm and the appearance of a broad signal between 3.85 and 4.20 ppm.

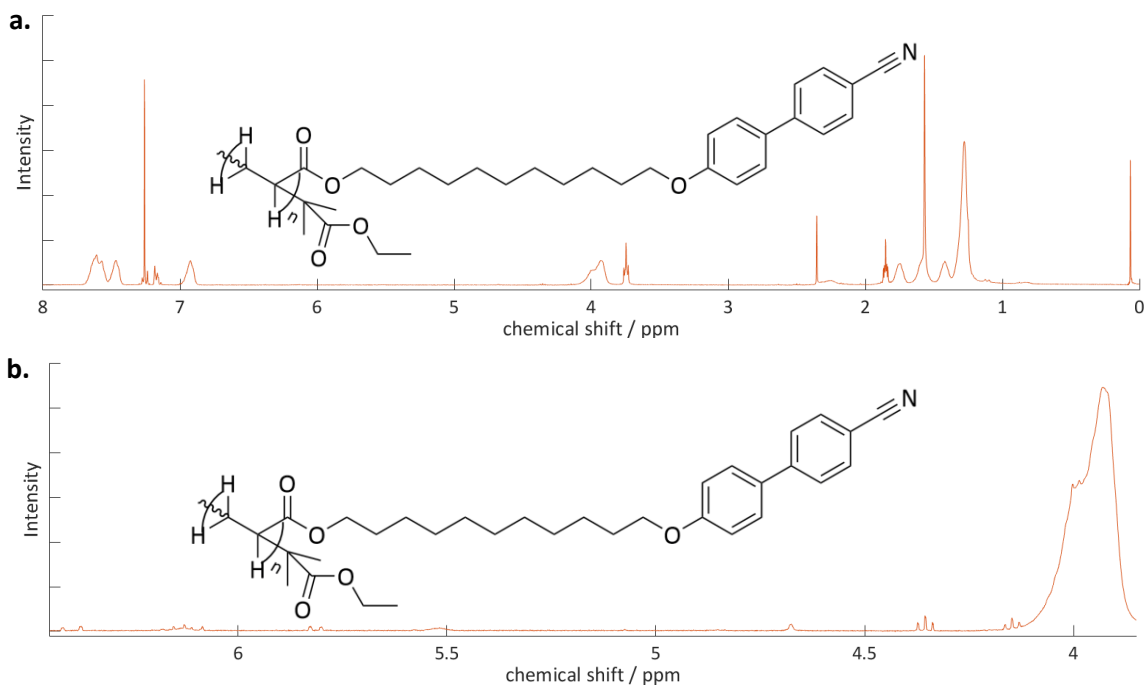


**Figure 45:** a. Complete  $^1\text{H}$  NMR spectrum of the sacrificial polymer from the synthesis of substrate **5** via the ATRP polymerisation of compound **2** using  $\text{Me}_6\text{TREN}$  as the complexing ligand for the  $\text{Cu(I)}$  catalyst. b.  $^1\text{H}$  NMR spectrum for the monitoring region of the sacrificial polymer used to monitor the progress of the reaction.

The  $\text{CH}_2$  protons would be expected to be retained in a successful polymerisation but with loss of resolution due to slight variation in the environment resulting from the position of the repeat units in the chain. Upon successful polymerisation a loss of the vinyl proton environments is expected, as the associated environments are converted to the substituted aliphatic backbone, with signals developing in the  $\text{CH}_2$  region. The increase of the  $\text{CH}_2$  proton integrations and reduction of the vinyl proton integrations upon polymerisation provides a ratio with a causal relationship to monomer conversion, although this might not be expected to be fully robust due to the incomplete relaxation of protons in the  $^1\text{H}$  NMR a characteristic regression, with a positive Spearman rank correlation coefficient, is obtained which can help to assess the degree of monomer conversion.

In contrast to the  $\text{Cu(I)}/\text{PMDETA}$  system the  $^1\text{H}$  NMR spectrum shows nearly complete conversion of the olefin protons to aliphatic protons, with a relative integration of 30.3 indicating a near complete conversion of monomer. The conversion of the acrylate vinyl region alone cannot definitely confirm polymerisation was successful as these conversions could have resulted in dimers or short oligomer chains. The successful polymerisation was ascertained by GPC, as shown in Figure 46.

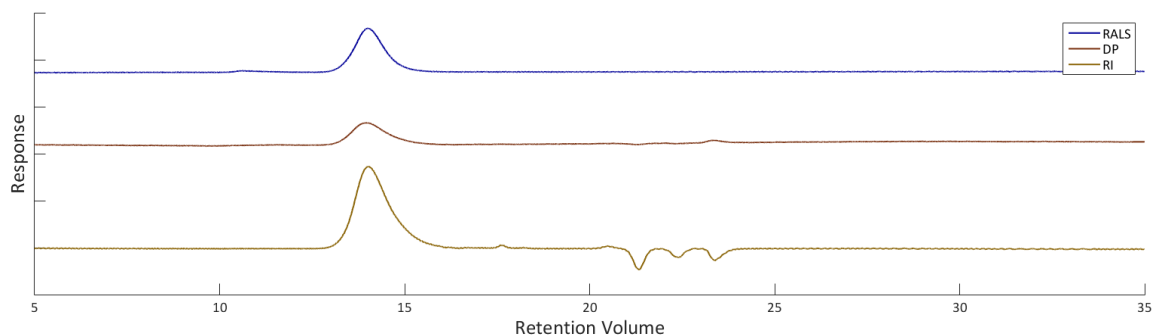


Figure 46: GPC triple detection trace of sacrificial initiator from the synthesis of substrate **5** via the ATRP polymerisation of compound **2** using Me<sub>6</sub>TREN as the complexing ligand for the Cu(I) catalyst: showing right angle light scattering (RALS), differential pressure (DP) and refractive index (RI).

The GPC trace agrees with the observations of the <sup>1</sup>H NMR spectrum and gives an indication of the degree of polymerisation. The monomer peak at 17.61 mL has reduced to a very low intensity signal, this indicates that it is due to a very low concentration of residual monomer. The substance with retention volume of 14.03 mL indicates the formation of a polymeric species. The peak is symmetric in the RALS and DP traces but shows a slight broadening to the lower Mw on RI. The molecular weight of the compound has increased with nearly all of the components eluting at 14.03 mL,  $Mn_{meas} = 9,730$  and  $Mw_{meas} = 15,556$ ;  $Mw/Mn_{meas} = 1.60$ . This retention is similar to that being eluted, at low concentrations in the Cu<sup>I</sup>/PMDETA system, this suggests that, on the rare occasion, when a chain was activated in the Cu<sup>I</sup>/PMDETA systems a similar degree of polymerisation occurs. As discussed in Section 3.2.3 it appears that the GPC calibration has resulted in a systematic error of the measured LCP molar masses. The measurements are reported (Table 2); nonetheless, to provide a comparative overview of the polymerisations, no interpretation can be meaningfully made of the results except the relative retention volume and therefore the relative Mn of the free polymer formed due to the sacrificial initiator.

Table 2: GPC data for the sacrificial LCPs formed in the grafting reactions.

Entry	DP <sub>theo</sub>	Mn <sub>theo</sub>	Mn <sub>meas</sub>	Mw <sub>meas</sub>	PDI (Mw/Mn)	DP <sub>meas</sub>
3	38	16,000	9,730	15,600	1.60	23
5	85	36,000	7,090	13,300	1.88	17
6	85	36,000	10,400	18,600	1.79	25
7	45	19,000	15,200	53,600	3.52	36
8 <sup>†</sup>	28	18,000	4,610	16,400	3.56	7
9	86	36,000	16,000	56,600	3.54	38
10	45	19,000	13,900	42,200	3.03	33
11 <sup>†</sup>	28	18,000	5,020	7,760	1.55	8

<sup>†</sup>side-on monomer

## Substrate polymerisation

FT-IR of the paper substrate resulting from the Cu(I)/Me<sub>6</sub>TREN catalysed polymerisation is shown in Figure 47.

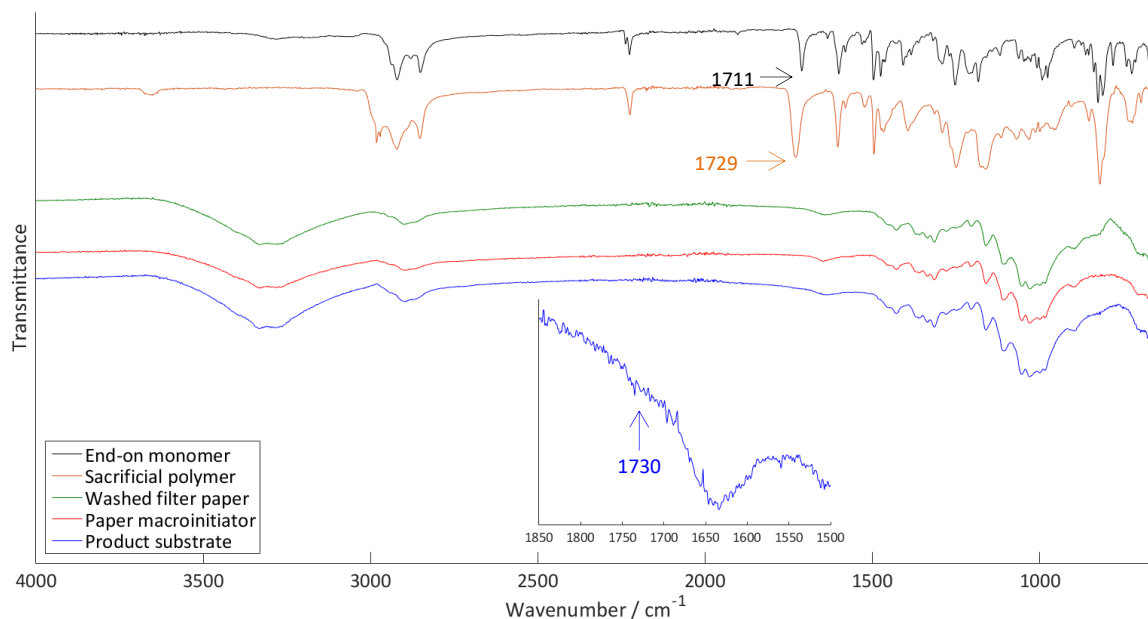


Figure 47: FT-IR of the substrate obtained from the synthesis of substrate **5** via the ATRP polymerisation of compound **2** using Me<sub>6</sub>TREN as the complexing ligand for the Cu(I) catalyst, with an inset showing the carbonyl region for the product substrate (blue).

The FT-IR of the substrate shows a discernible shoulder at 1730 cm<sup>-1</sup>, this corresponds with our expectation of a successful polymerisation as has been assigned in previous work.<sup>83, 90</sup> The  $\nu_{\text{CO}}$  observed is very weak in comparison with the background cellulose.

The intensity of absorption, due to C=O stretching of the polymer, depends on the degree of polymerisation achieved. In this reaction the degree of polymerisation achieved is less than that of the previous work the previous work (Table 1) therefore it is to be expected that the intensity of the peak is even smaller in this case.

The low intensity of this absorption means that this technique cannot be relied upon, in isolation, to confirm the presence of polymer on the surface. The morphology of the surface was studied by SEM. Figure 48 shows representative SEM images of the morphology obtained of the paper, enlargements are highlighted and shown at greater magnification.

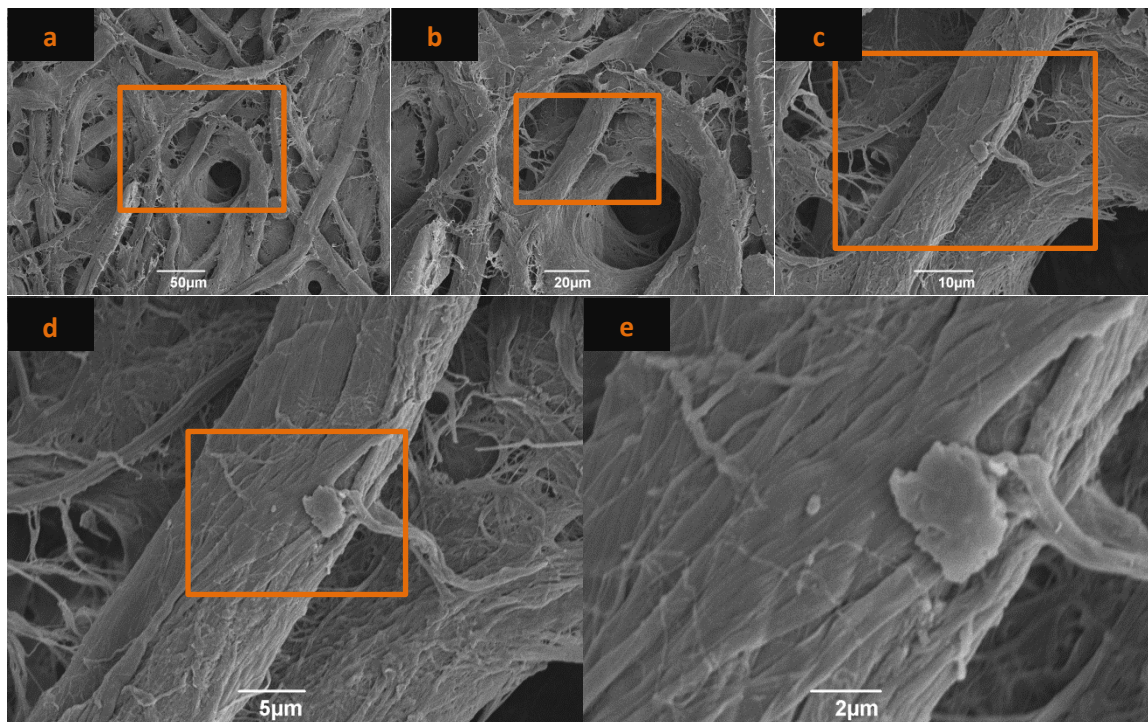


Figure 48: SEM images of the surface obtained from the SI-ATRP reaction of compound **2** with [Cu(I)/Me<sub>6</sub>TREN] in the presence of sacrificial initiator in toluene (Entry **3**) at a. 330 $\times$ , b. 750 $\times$ , c. 2000 $\times$ , d. 3000 $\times$ , and e. 8000 $\times$  magnification.

The SEM images of the surface obtained *via* the ATRP reaction shows visible thickening and deposition of the fibres. The thickening appears to have caused a smoothing, as the closest fibres have swelled and merged into each other. In regions where neighbouring fibres have a greater spatial separation, the development of trenches between the conglomerates is observed. This corroborates the observation in the FT-IR, that polymer grafts are present on the surface.

## Conclusions

The formation of the sacrificial polymer in the ATRP reaction with PMDETA and Me<sub>6</sub>TREN show that the Me<sub>6</sub>TREN was significantly more successful at catalysing the polymerisation, successfully obtaining polymer at high conversion, with a relatively low provisional calculated polydispersity. The conversions in these studies show that over the timescale used for the polymerisation Me<sub>6</sub>TREN remains stable.

The results of the toluene PMDETA relative to the toluene Me<sub>6</sub>TREN is consistent with suggestions that for ATRP to be truly reversible it requires that “the active copper(I) complex must be four-coordinate complex bearing no halide ligands”<sup>71</sup> (Figure 49). Under rigorous conditions Me<sub>6</sub>TREN can create the required valence shell independently, in contrast the PMDETA ligand requires an additional contribution to complete the valence shell, often this is provided by water. Alternative coordination contributions are found in ‘all’ coordinating solvents<sup>72</sup>.

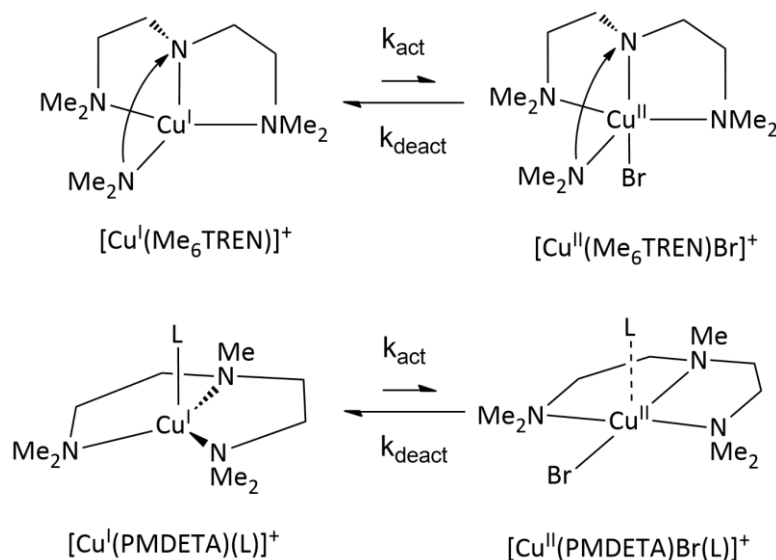


Figure 49: Structures of copper(I) and copper(II) complexes derived from previously characterised complexes.

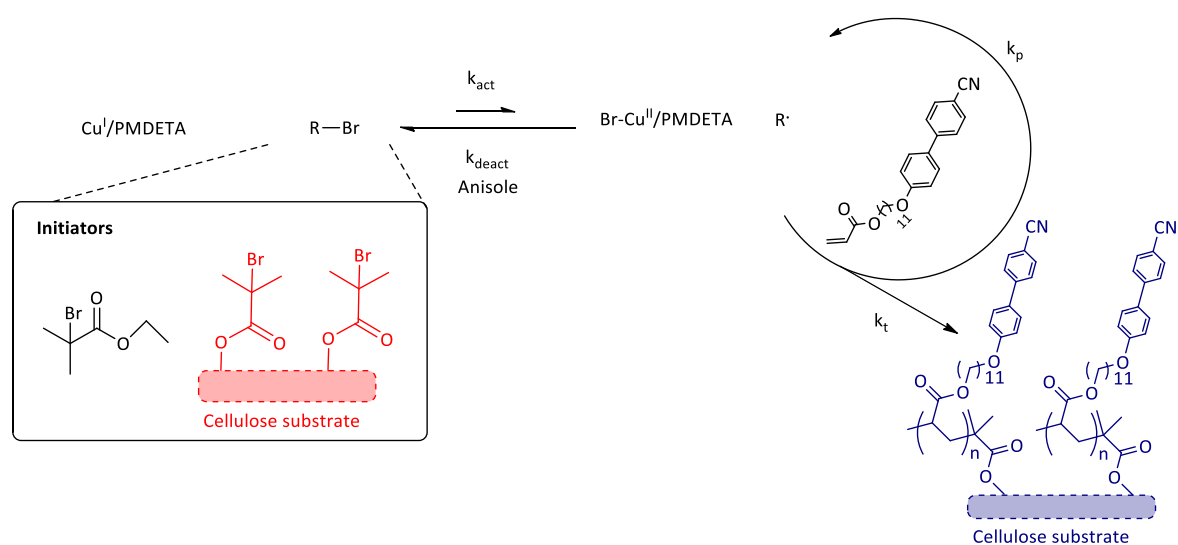
[Modified from 71].

As would be expected from our observations of the surface for the macro-initiated polymerisation without sacrificial initiation and trenches have developed on the surface of the paper. All evidence for the Me<sub>6</sub>TREN catalysed polymerisation agrees with the SEM observations. This is in contrast to the PMDETA complexed catalyst, which did not show evidence of polymerisation by FT-IR or clear evidence by <sup>1</sup>H NMR. This allows us to be confident that the polymerisation using a Cu(I)/Me<sub>6</sub>TREN catalyst occurred from the surface and that our predictions for the surface topology following a successful graft-from polymerisation are accurate.

### 3.6. Potential of anisole as an alternative solvent (Entry 4).

In order to try and improve the [Cu(I)PMDETA] systems, anisole was used as an alternative solvent. Anisole has a boiling point of 153.8 °C; this allows polymerisations to be conducted at the same temperature as with the toluene studies. Anisole is potentially capable of coordinating to the metal centre and completing the valence shell.

The surface initiated atom transfer radical polymerisation (SI-ATRP) was conducted from a cellulose (paper) macroinitiator using Cu(I)Br/PMDETA (18.4 μmol:17 μmol) and end-on acrylate monomer (0.840 mmol) in anisole, in presence of sacrificial initiator, EBIB (22 μmol), with stirring (Scheme 8).



Scheme 8: Reaction scheme for the Cu(I)Br/PMDETA activated ATRP of substrate **6** via the graft from polymerisation of substrate **6** in the presence of sacrificial initiator.

### Solution polymerisation

The concentrated crude reaction product collected after elution through silica was analysed for evidence of polymerisation. Figure 50 shows the <sup>1</sup>H NMR spectrum of the crude product.

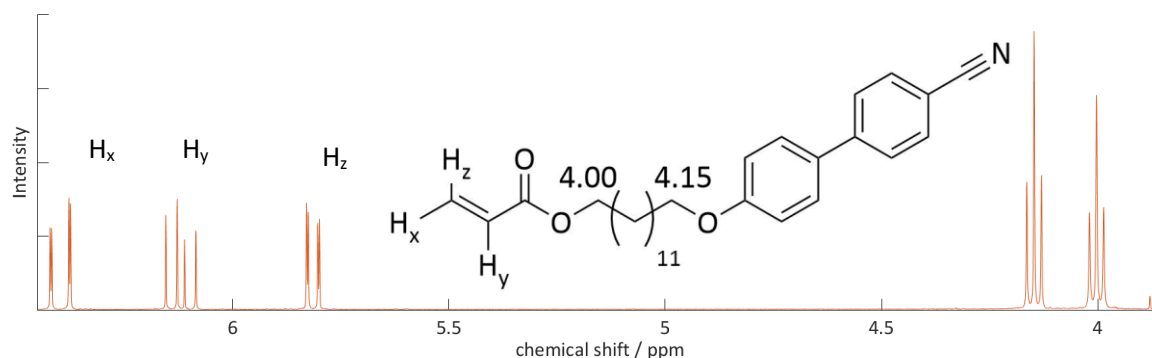


Figure 50: Monitoring region of the sacrificial polymer <sup>1</sup>H NMR monitoring region from the synthesis of substrate **6** via the ATRP polymerisation of compound **2** in anisole.

The use of anisole as a solvent for the Cu(I)/PMDETA] ATRP of compound **2** shows no evidence of polymerisation in the solution phase. The  $^1\text{H}$  NMR spectrum showed no indication of peaks other than those of the monomer used for the polymerisation, a monitoring ratio of 1.35:1 was observed. The same picture was seen in the GPC, no evidence of polymerisation was observed with a single species eluting at 17.60 mL this corresponds to the monomer. Sacrificial initiator is not observed by either monitoring technique - this is consistent with expectations for a species at such substantial dilutions. No attributable variations were observed between the NMR of the sacrificial monitoring reaction with sacrificial initiator and the monomer species added (Figure 50). The sacrificial reaction monitoring shows no evidence of polymerisation for the Cu<sup>I</sup>/PMDETA system when using anisole as the solvent. The GPC trace of the reaction crude reaction is shown in figure 51.

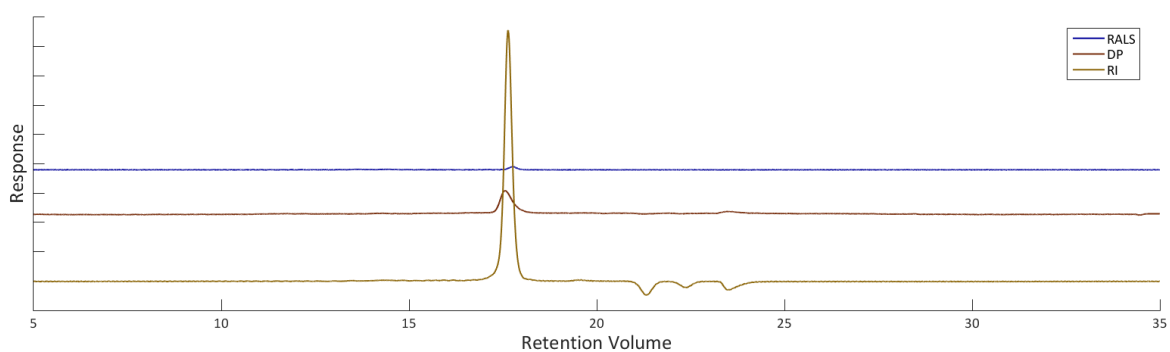


Figure 51: GPC triple detection trace of sacrificial initiator from the synthesis of substrate **6** via the ATRP polymerisation of compound **2** in anisole: showing right angle light scattering (RALS), differential pressure (DP) and refractive index (RI).

## Substrate polymerisation

FT-IR of the substrate from the attempted polymerisation showed no evidence of polymer present on the surface (Figure 52).

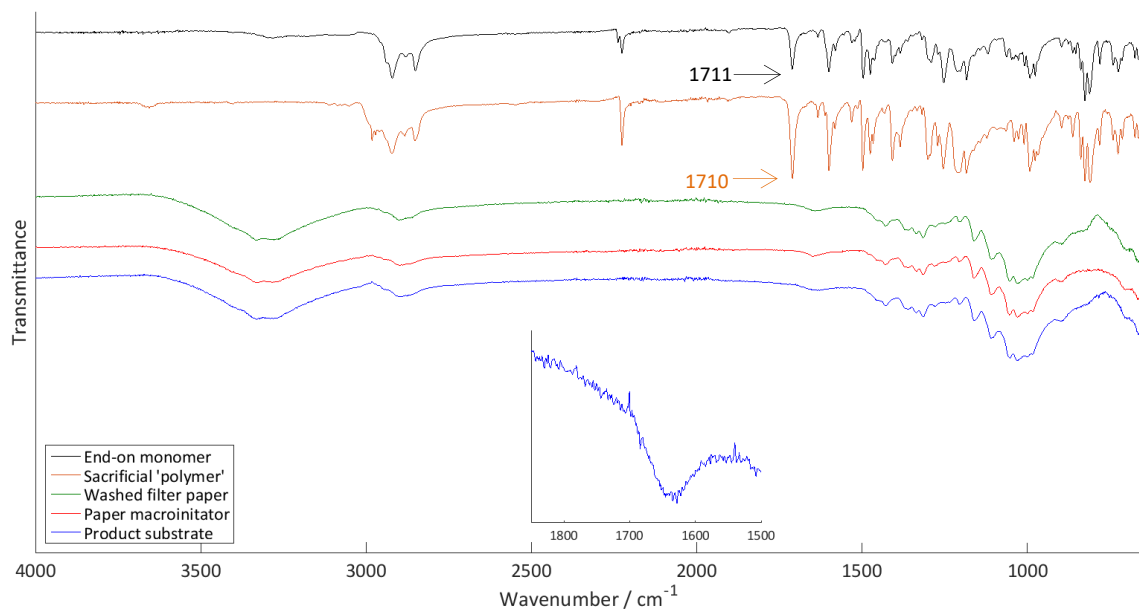


Figure 52: FT-IR of the substrate achieved from the synthesis of substrate **6** via the ATRP polymerisation of compound **2** in anisole, with an inset showing the carbonyl region for the product substrate (blue).

No evidence was seen of graft-from modification of the substrate following the attempted SI-ATRP of compound **2** with the [Cu(I)PMDTA] in anisole system. There was no evidence of a carbonyl (C=O) stretch on the substrate, either at the 1730  $\text{cm}^{-1}$  previously identified for earlier surface initiated polymerisation,<sup>83</sup> or from the monomer features present in the monitoring species, following the washing procedure.

SEM was conducted on the surface to provide morphology information to provide context to the FT-IR (Figure 53).

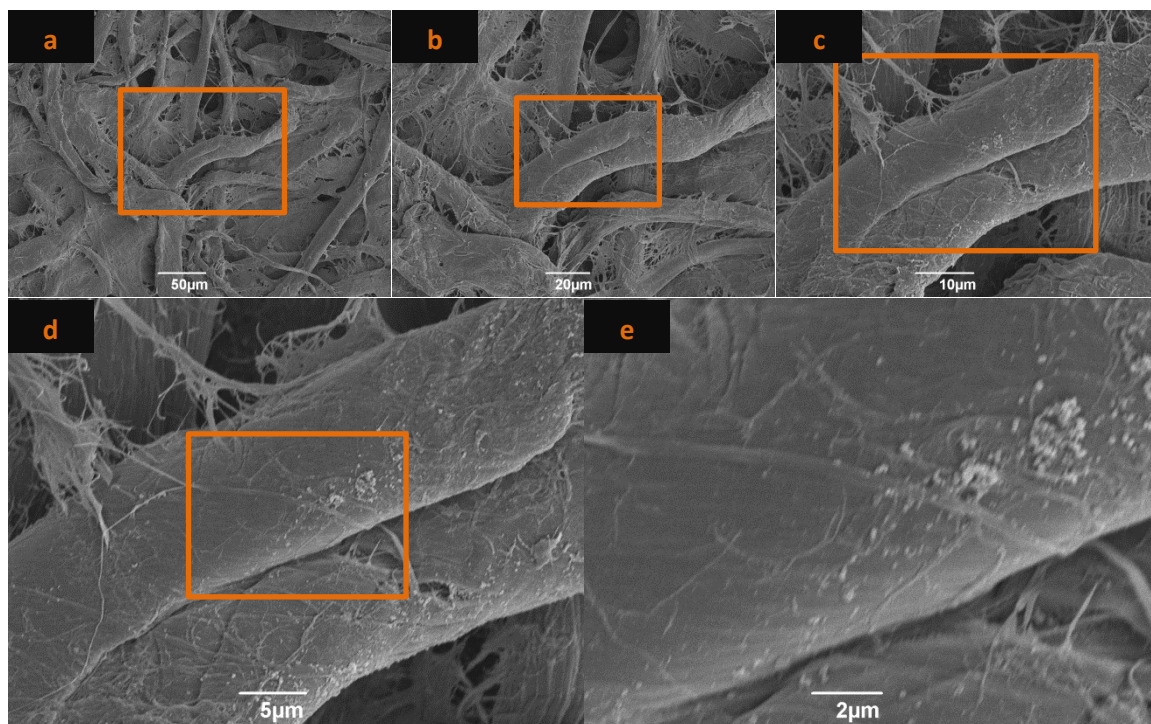


Figure 53: SEM images of the surface obtained from the SI-ATRP reaction of compound 2 with [Cu(I)/PMDETA] in the presence of sacrificial initiator in anisole (Entry 4) at a. 330x, b. 750x, c. 2000x, d. 3000x, and e. 8000x magnification.

SEM of the surface shows no variation from expectations of the pristine initiated surface, there appears to be no reduction in numbers of fine, loose microfibers observed and there appears to be a greater presence of the features attributable to microfibril bundles, potentially suggesting a reduction of amorphous regions.

A potential cause of amorphous material removal might be that anisole, being more polar, is able to solvate the amorphous regions which therefore get eroded with more ease.

## Conclusions

No benefit was observed from using anisole as the solvent. This may be that the anisole wasn't sufficiently coordinating to prevent catalyst's deactivation.

[Cu(I)PMDETA] has a low  $K_{ATRP}$  relative to [Cu(I)Me<sub>6</sub>TREN], [Cu(I)(PMDETA)] has a greater tendency towards disproportionation and therefore active catalyst loss.<sup>72</sup> However [Cu(II)PMDETA] can, under comparable conditions, produce polymers with more controlled polydispersity than [Cu(I)Me<sub>6</sub>TREN] with a high rate of polymerisation.<sup>72</sup>

These two factors lead towards studies using the Cu(II)PMDETA system as a catalyst. In order to use the Cu(II)PMDETA catalytic systems a suitable agent to reduce Cu(II) to Cu(I) needs to be present. Therefore Activator ReGenerated by Electron Transfer (ARGET) ATRP<sup>96</sup> was utilised next. ARGET-ATRP is well reported to result in polymerisations more tolerant of oxygen.<sup>106</sup>

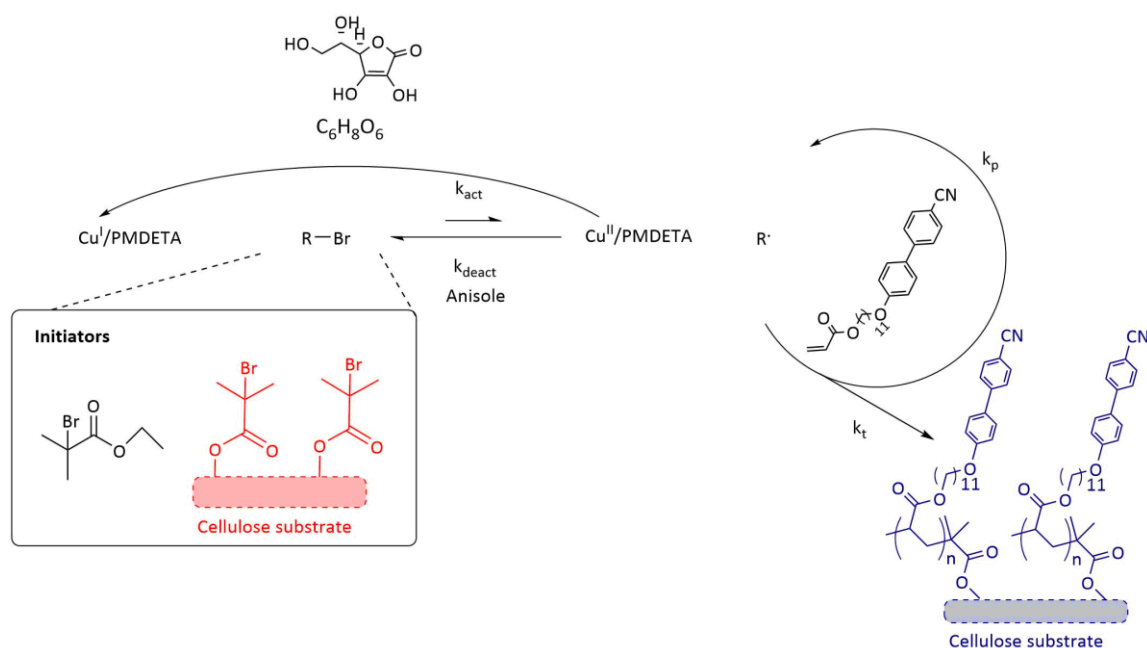
### 3.7. Surface initiated (SI) ARGET ATRP of the end-on acrylate monomer (Entry 7).

Activator ReGenerated by Electron Transfer (ARGET) ATRP utilises a reducing agent such as tin(II) 2-ethylhexanoate or ascorbic acid to regenerate Cu(I)/ligand lost from the polymerisation equilibrium through the competitive oxidation of Cu(I) to Cu(II). The regeneration of the active Cu(I) makes the ARGET system significantly more tolerant of oxygen and allows for reduced catalytic loadings.<sup>106</sup>

Ascorbic acid was chosen as the reducing agent because it is easier to handle and less toxic than tin (II) 2-ethylhexanoate.

Anisole was chosen as the solvent for the ARGET ATRP as it is well reported in the literature that the low solubility of ascorbic acid in organic solvents is important in maintaining control of the polydispersity with the strongly reducing ascorbic acid. Anisole has previously been deployed for this purpose with good results<sup>78</sup>.

The surface initiated ARGET-ATRP of **2** from cellulose (paper) macroinitiator was carried out using Cu(II)Br<sub>2</sub>/PMDETA (2.0 μmol:17 μmol), ascorbic acid (21.9 μmol) and end-on acrylate monomer (0.980 mmol) in anisole, in presence of sacrificial initiator, EBIB (22 μmol), with stirring (Scheme 9). These are of the same magnitudes as those used by Matyjaszewski et al. for the grafting of butyl acrylate.<sup>106</sup>



Scheme 9: Reaction scheme for the Cu(II)Br<sub>2</sub>/PMDETA activated ATRP of substrate **9** via the graft from polymerisation of substrate **2ai** with compound **2** in the presence of sacrificial initiator.

## Solution polymerisation

The sacrificial polymer obtained in the ascorbic acid ARGET-ATRP of the end-on cyanobiphenyl acrylate, **2**, was analysed by  $^1\text{H}$  NMR and GPC. Figure 54 shows the  $^1\text{H}$  NMR spectrum of the crude product isolated from the reaction.

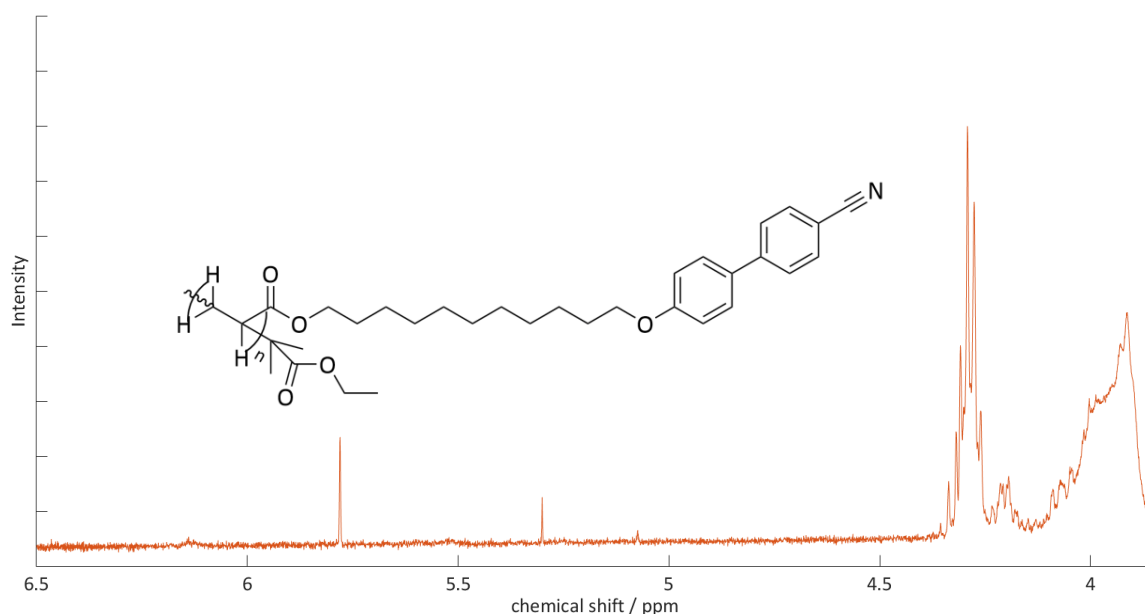


Figure 54: Monitoring region of the sacrificial polymer  $^1\text{H}$  NMR monitoring region from the synthesis of substrate **9** via the ARGET ATRP of compound **2**.

The ARGET ATRP system allowed for the complete conversion of monomer olefin units as monitored by  $^1\text{H}$  NMR of the sacrificial polymer (Figure 54). The monitoring region of 3.85-4.20 ppm to 5.77-6.44 ppm showed a ratio of 2.38:1. Qualitatively the spectrum showed no unreacted acrylate and the broad multiplet expected at  $\sim 4$  ppm. GPC analysis of the crude product was run to provide a comparison on the polymers achieved, against those of other reactions (figure 55).

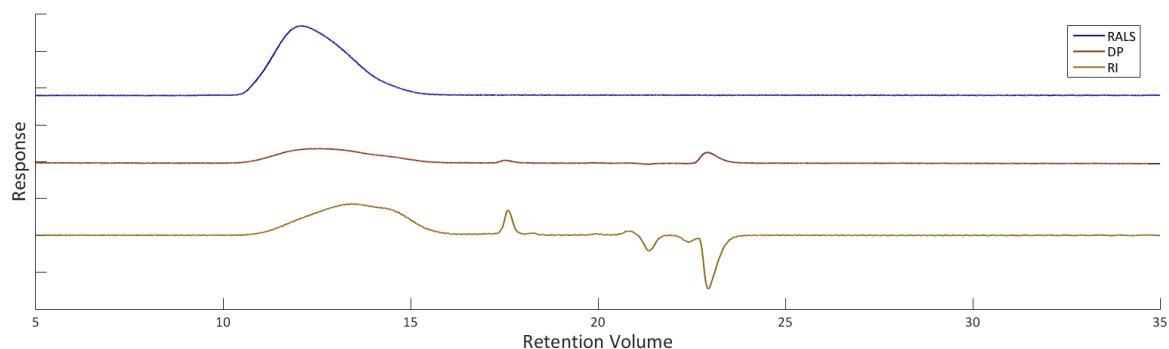


Figure 55: GPC triple detection trace of sacrificial initiator from the synthesis of substrate **9** via the ARGET ATRP of compound **2**: showing right angle light scattering (RALS), differential pressure (DP) and refractive index (RI).

GPC analysis of the sacrificial polymer showed a peak at a retention volume of 13.40 mL corresponding to  $M_{n,meas} = 15,200$ ;  $M_{w,meas} = 53,611$ ; with a shoulder at 14.4 mL resulting in a calculated PDI of 3.52. Significant levels of residual monomer was eluted at 17.60 mL, this is consistent with the monitoring ratio of the  $^1H$  NMR but not the qualitative interpretation.

The detection of the light scattering techniques relies on Rayleigh scattering to scatter light which is observed at the detector. For RALS the detector is at ninety degrees to the incident light. The Rayleigh equation tells us that the response is directly proportional to the molecular weight. Due to the high degree of scattering required for the detector to observe the scattered light RALS gives a disproportionately large response for higher molecular weight species. This explains the positive skew in the polymer peak under the RALS detection.

### Substrate polymerisation

FT-IR of the substrate obtained from the SI-ARGET ATRP of paper is shown in Figure 56.

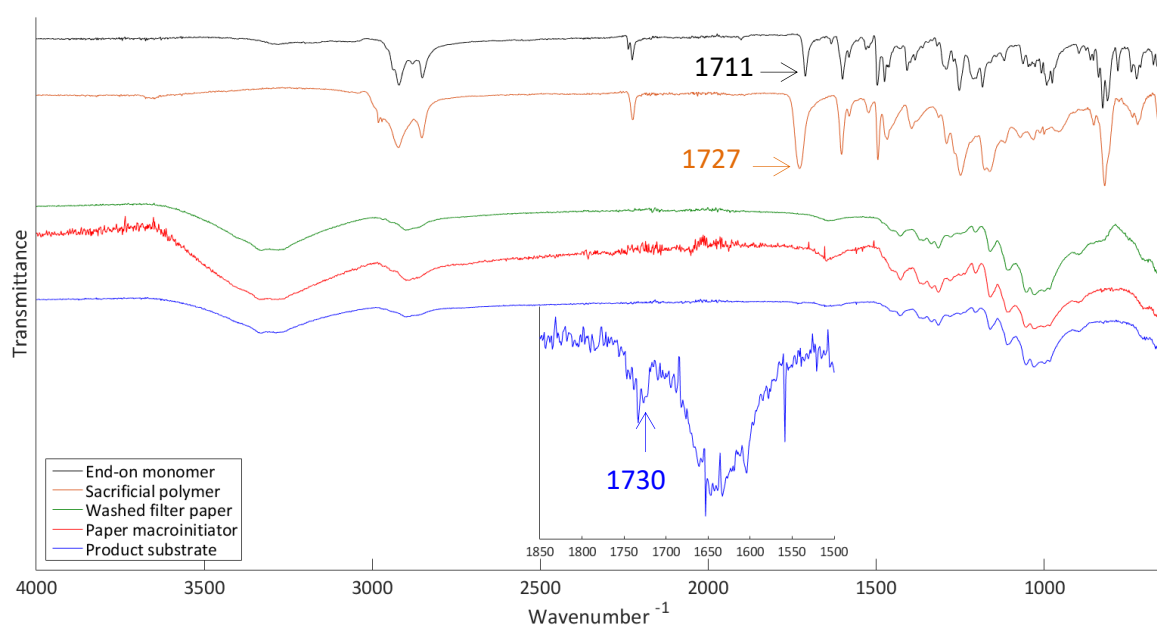


Figure 56: FT-IR of the substrate achieved via the synthesis of substrate 9 via the ARGET ATRP of compound 2.

The FT-IR of the substrate showed a significant peak at  $\sim 1730\text{ cm}^{-1}$  (inset of Figure 56), this was attributed to the C=O stretch of the polymer carbonyl units. The slight increase in the wavenumber relative to the sacrificial polymer ( $\nu_{CO} = 1727\text{ cm}^{-1}$ ) could be due to the environment of the material (solid powder versus a grafted film on the paper surface). FT-IR spectroscopy detects interaction with wavelengths of light corresponding to bending and stretching frequencies. It is speculated that the bending and stretching frequencies may become influenced

by the restrictions resulting from surface attachment, this could account for any minor shifts in frequencies.

Figure 57 shows the SEM images of a representative area from the paper surface at different magnification (330 $\times$ , b. 750 $\times$ , c. 2000 $\times$ , d. 3000 $\times$ , and e. 8000 $\times$  magnification).

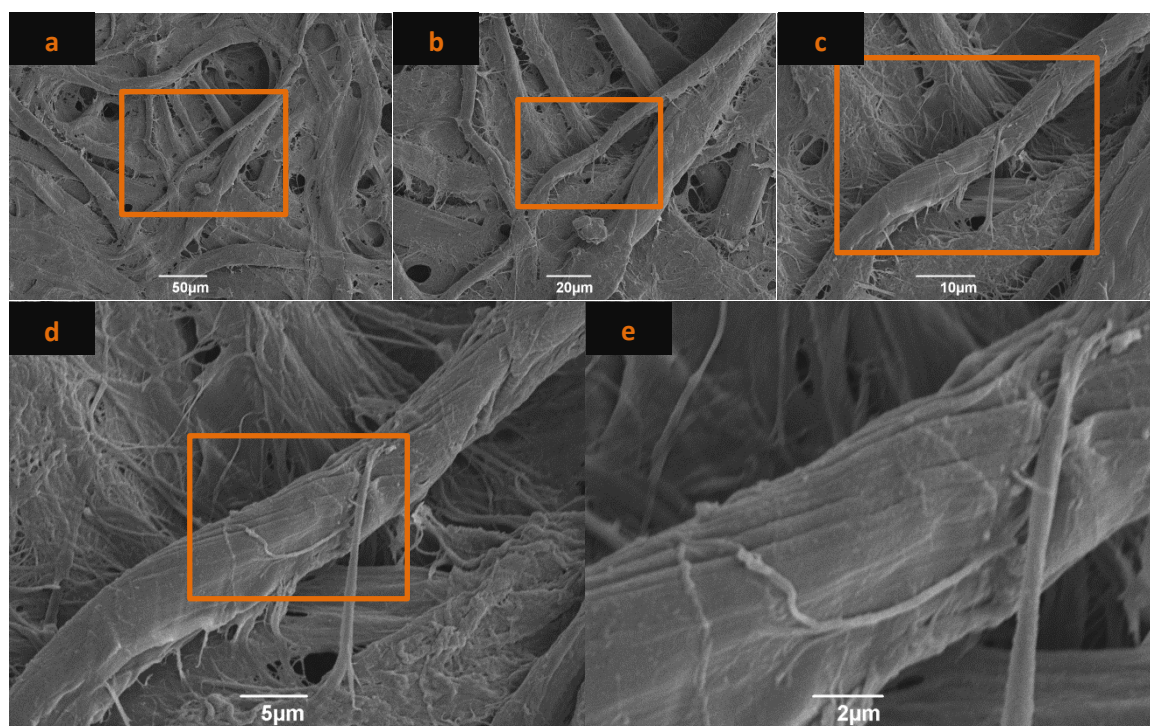


Figure 57: SEM images of the surface obtained from the SI-ARGET ATRP reaction of compound 2 with [Cu(II)/PMDETA] – ascorbic acid in the presence of sacrificial initiator in anisole (Entry 7) at a. 330 $\times$ , b. 750 $\times$ , c. 2000 $\times$ , d. 3000 $\times$ , and e. 8000 $\times$  magnification.

SEM corroborates the findings by FT-IR. At high magnification (Figure 57e.) there appears to be evidence of microfibril engulfment and the early stages of conglomeration. As was expected from the initial studies, SEM of the surface showed a thickening of the microfibrils, with ridges developing on the surface and a general smoothing of the broad topological environment (Figure 57). This is consistent with the evidence of surface grafting seen by FT-IR.

## Conclusions

All of the evidence from the surface initiated ARGET-ATRP (SI-ARGET ATRP) of compound 2 supports the conclusion that a polymerisation was successfully conducted from the surface. Analysis of the sacrificial polymer suggests that the polymerisation proceeded without significant loss of catalytic activity to produce a polymer with PDI = 2.60.

It can be confidently interpreted that the active Cu(I) species was successfully generated from the Cu(II)Br<sub>2</sub> reagent before withdrawing a halide, initially from the initiator and subsequently from the polymer chains, to produce the active polymerisation sites.<sup>75</sup> The use of these ARGET ATRP conditions allowed the polymerisation to proceed with catalytic loadings much lower than those

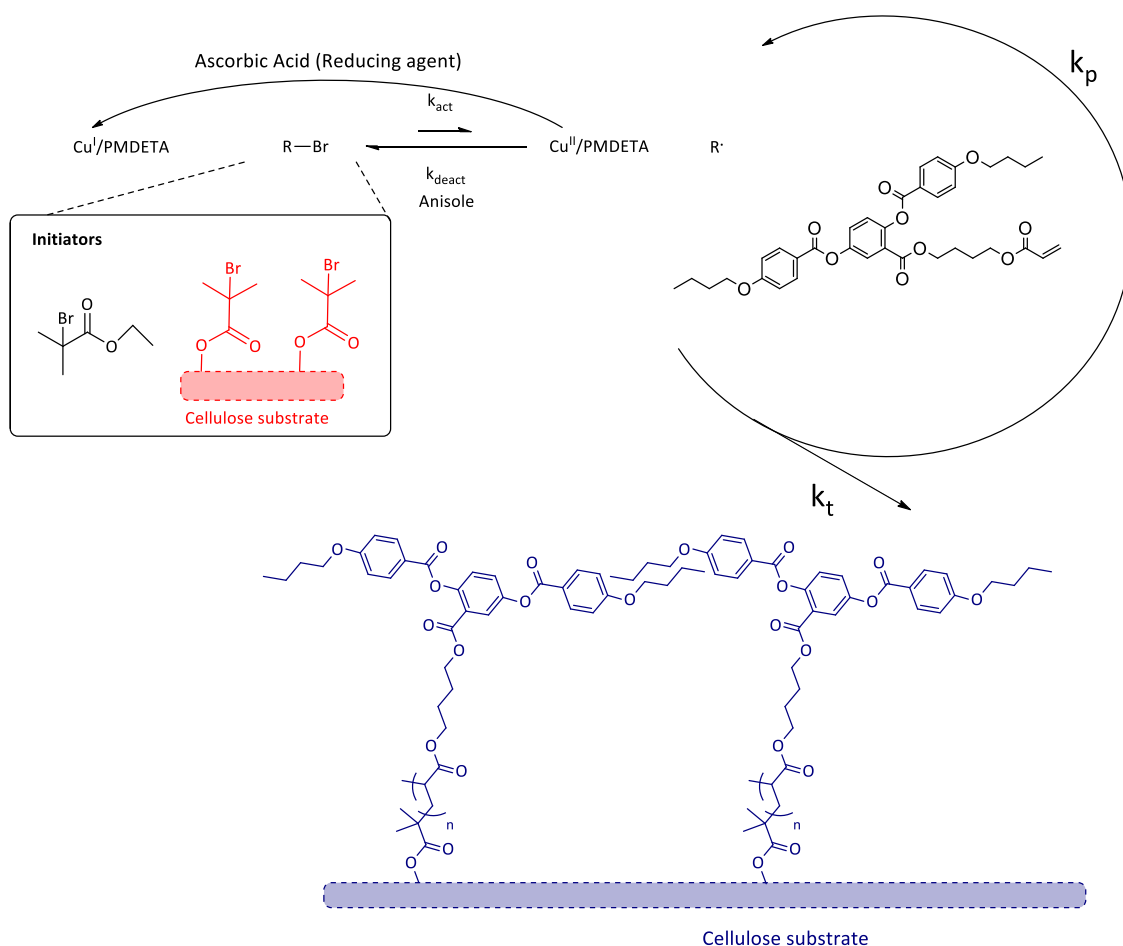
of the unsuccessful/severely compromised ATRP polymerisations with the same active copper complex<sup>106</sup> and the same monomer.

Since the Cu(I)Br ATRP polymerisation in anisole was not successful, it can be concluded that the success of the ARGET-ATRP of cyanobiphenyl acrylate, under conditions otherwise comparable condition to previous experiment is due to the nature of the polymerisation (regeneration of the Cu(I active species by ascorbic acid) rather than a solvent effect.

### 3.8. Surface initiated (SI) ARGET ATRP of the side-on acrylate monomer (Entry 8).

Having established favourable conditions for the polymerisation of the cyanobiphenyl acrylate monomer, **2**, on paper regarding Cu(II)/PMDEATA, ascorbic acid, EBIB and toluene [2.0  $\mu\text{mol}$ /17  $\mu\text{mol}$ , 21.9  $\mu\text{mol}$ , 22  $\mu\text{mol}$ ], the polymerisation of the side-on acrylate, **6**, from the cellulose surface was studied. The purpose of this study was to produce side-chain liquid crystal polymer brushes with laterally attached mesogenic units grafted onto the cellulose (paper) surface (Scheme 10).

Side-on liquid crystal acrylate was polymerised from cellulose surface (paper) loaded with initiator sites by ARGET-ATRP using Cu(II)Br<sub>2</sub>/PMDETA (2.1  $\mu\text{mol}$ :17  $\mu\text{mol}$ ), ascorbic acid (23.6  $\mu\text{mol}$ ) and side-on acrylate monomer (0.62 mmol) in anisole, in presence of sacrificial initiator, EBIB (22  $\mu\text{mol}$ ), with stirring.



Scheme 10: Reaction scheme for the Cu(II)Br<sub>2</sub>/PMDETA activated ARGET ATRP of substrate **10** via the graft from polymerisation of substrate **2ai** with compound **6** in the presence of sacrificial initiator.

The presence of sacrificial initiator in the polymerisation reaction yields a polymer that represents the characteristics of the polymer grafted from the cellulose surface.

## Solution Polymerisation

The  $^1\text{H}$  NMR spectrum of the crude product isolated from the reaction showed intense doublet of doublets at 5.58 ppm with coupling constants of 5.9 Hz and 1.9 Hz, that was not present in the acrylate monomer (Figure 58).

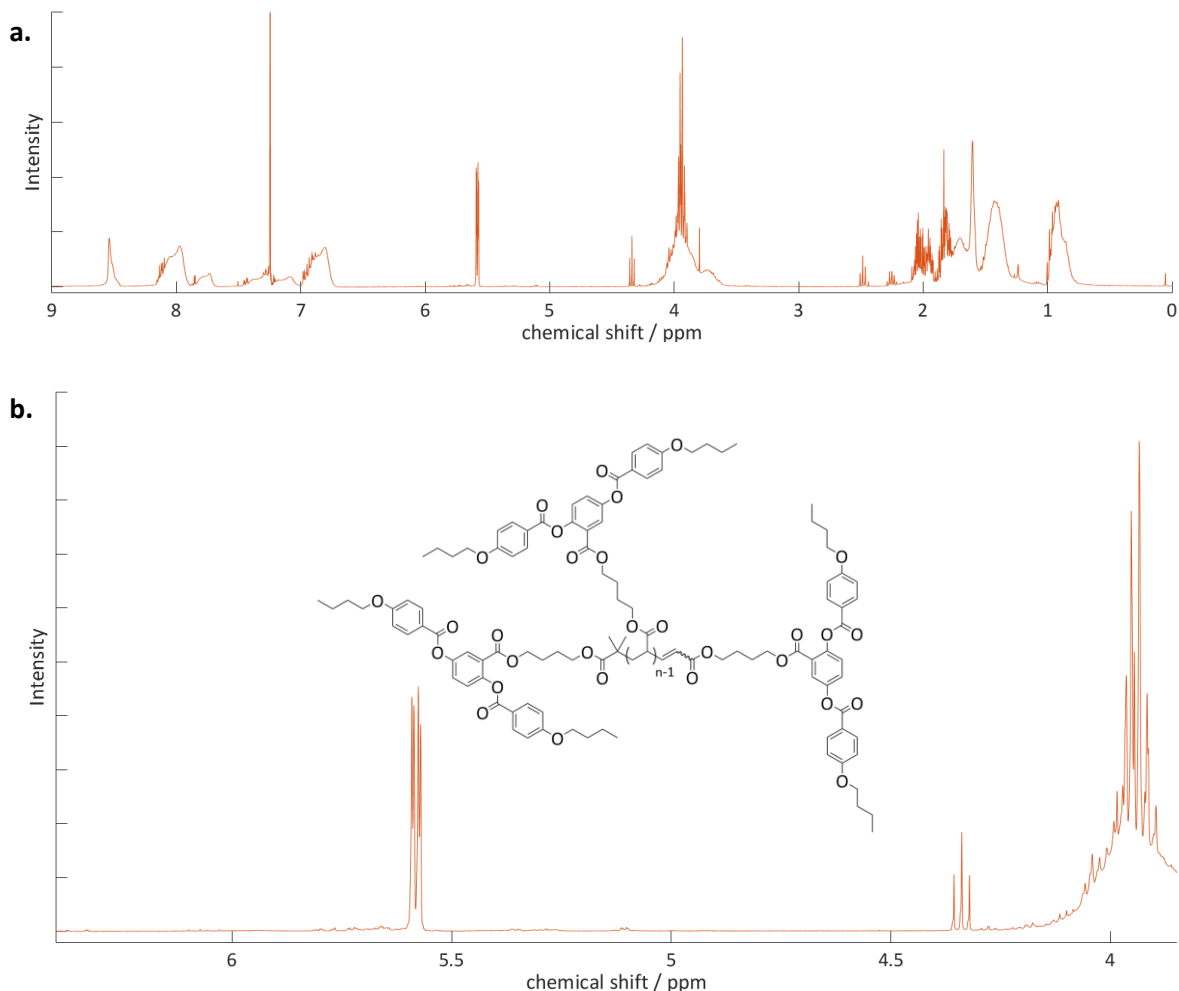


Figure 58: a. Complete  $^1\text{H}$  NMR spectrum of the sacrificial polymer from the synthesis of substrate **10** via the ATRP polymerisation of compound **6**. b.  $^1\text{H}$  NMR spectrum for the monitoring region of the sacrificial polymer used to monitor the progress of the reaction.

The resonance at 5.58 ppm is the characteristic  $\text{H}_a$  signal expected of a disproportionation product  $\text{D}_a$  as identified by Nakamura *et al.* (Scheme 11).<sup>107</sup> The  $\text{H}_{\text{btrans}}$  proton is expected at  $\sim 6.8$  ppm which would be obscured by the aromatic region. There is no sign of the cis-product, which should appear at  $\sim 6.15$  ppm.<sup>107</sup> The GPC trace of the crude product isolated from the reaction mixture is shown in Figure 59.

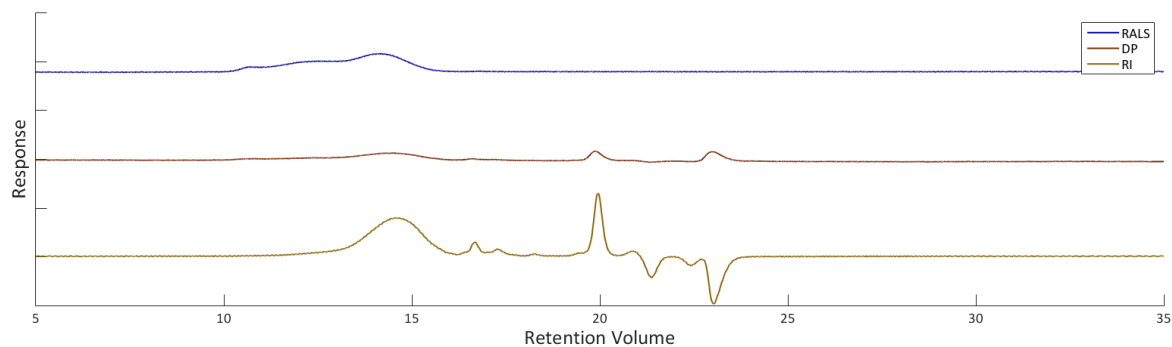
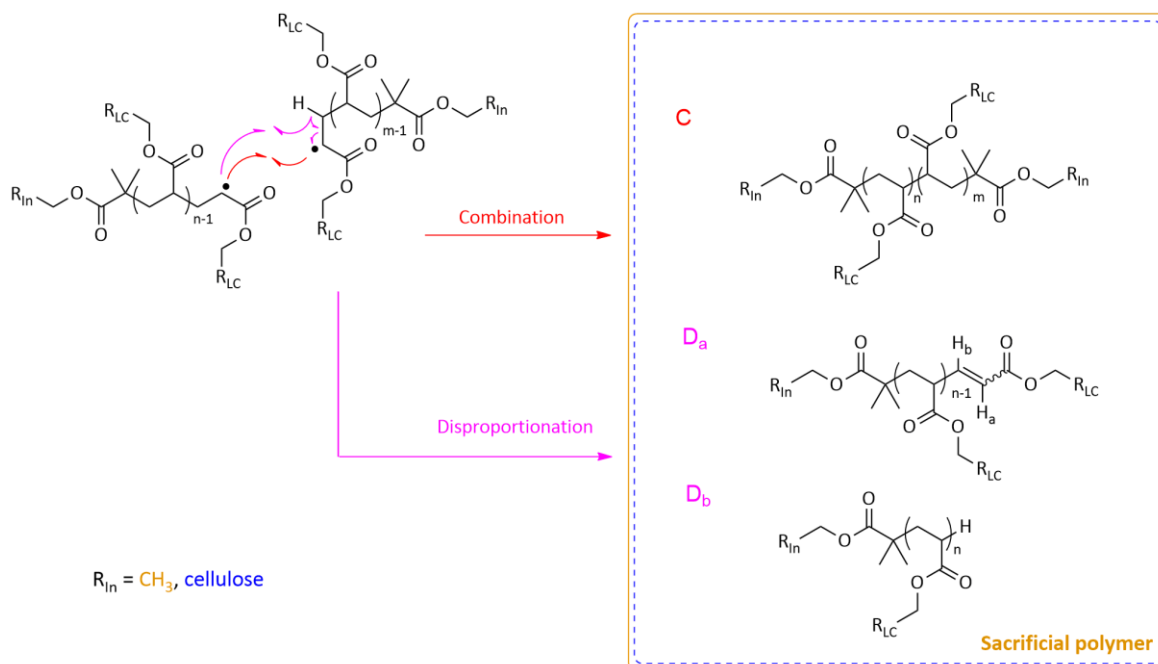


Figure 59: GPC triple detection trace of sacrificial initiator from the synthesis of **10** via the ARGET ATRP of compound **6**: showing right angle light scattering (RALS), differential pressure (DP) and refractive index (RI).

From the RI trace of the GPC it is observed that polymer is eluted first, followed by a minimal amount of residual monomer and an intermediate molecular weight species. The elution at 19.9 mL is attributed to residual anisole. Whereas the RI trace shows a symmetrical distribution of molecular weight, the RALS detection shows the polymer eluting as three distinct fractions. The polymer eluted at 14.6 mL comparison against the polystyrene standard gave Mn: 4,613; Mw: 16,431; with a convoluted distribution, with the polymer range eluted showing a combined calculated polydispersity of 3.56. Analytical techniques have been developed for the deconvolution of polymodal GPC traces by combining the results with those obtained by MALDI-MS.<sup>108</sup> Careful analysis by MALDI-MS and accurate GPC data would be required before conclusions could be offered from the distribution in this experiment.

It appears from the GPC that the primary termination route(s) results in an oligomer approaching the short polymer classification, with an approximately Gaussian distribution of polydispersities at 14.6 mL. It is worth noting that instrumental error resulted in an overestimation for the mass of higher molecular weight polymer and relatively accurate assessment of the lower molecular weight polymer. Acknowledging the limitations of extrapolation, it may be the case that error is resulting in an under estimation of the molecular weight of the relatively low molecular weight species formed in this reaction. Minor shoulders at retention volumes 12.0 mL and 10.5 mL can also be seen in the RALS trace, due to higher molecular weight species. This molecular weight profile could represent combination terminations, and this would be consistent with the distribution shape predicted by the theory of random coupling<sup>109</sup>.

It has been discussed in the literature that, at high loadings, polymer chains grafted from a surface causes spring-like elongation of the chains to minimise their free energy.<sup>51</sup> Bearing this in mind, an alternative explanation for the bands present is that, speculatively, the strain could cause disassociation of the amorphous cellulose regions together with their graft polymer chains from the surface.



*Scheme 11: Potential R-R termination routes for radical polymerisations within the context of this work.*

There is a discrepancy between the  $^1\text{H}$  NMR integrations of the  $\text{H}_a$  proton which appears to significantly overestimate it against the  $\text{CH}_2$  resonance at  $\sim 5.58$  ppm against the aromatics and the monitoring region at  $\sim 4$  ppm, compared to the molecular weights indicated by GPC. The better detection of higher molecular weight species in RALS means that it is unambiguous that the higher molecular weight species are very minimal; therefore, it is clear the highest molecular weight peak is less prominent than the intermediate molecular weight peak.

### Substrate polymerisation

Study of the paper substrate isolated from the reaction was carried out by FT-IR and SEM. Figure 60 shows the IR spectrum of paper (blue line), in which a shoulder centred at  $1732\text{ cm}^{-1}$  can be observed; the region gives indication that the laterally attached polymer brushes are present on the paper surface.

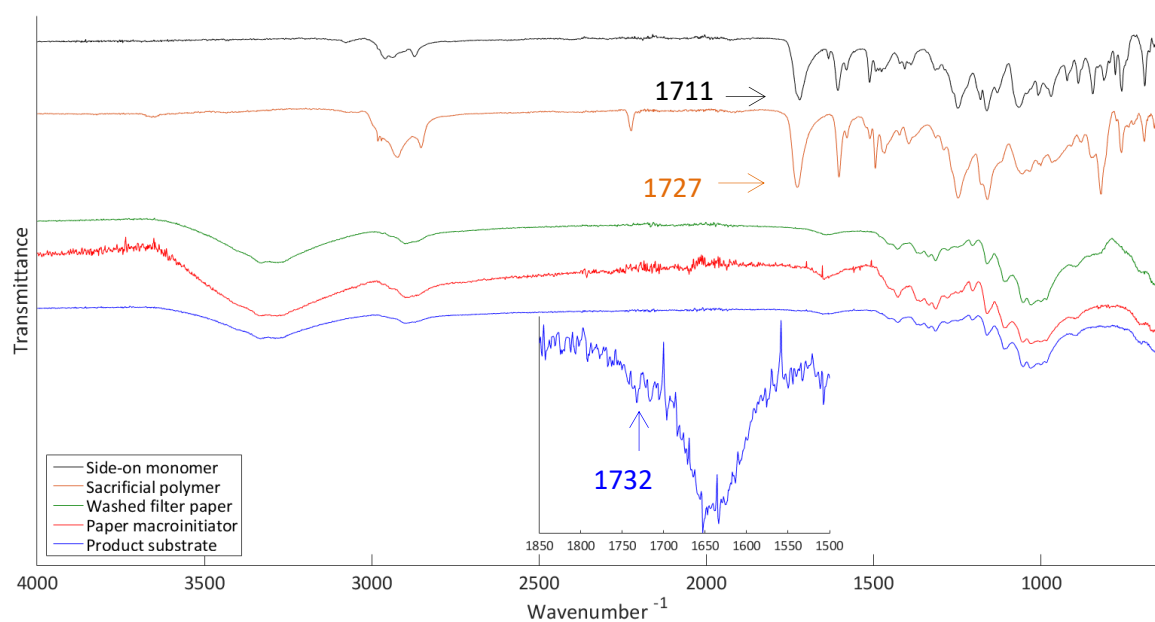
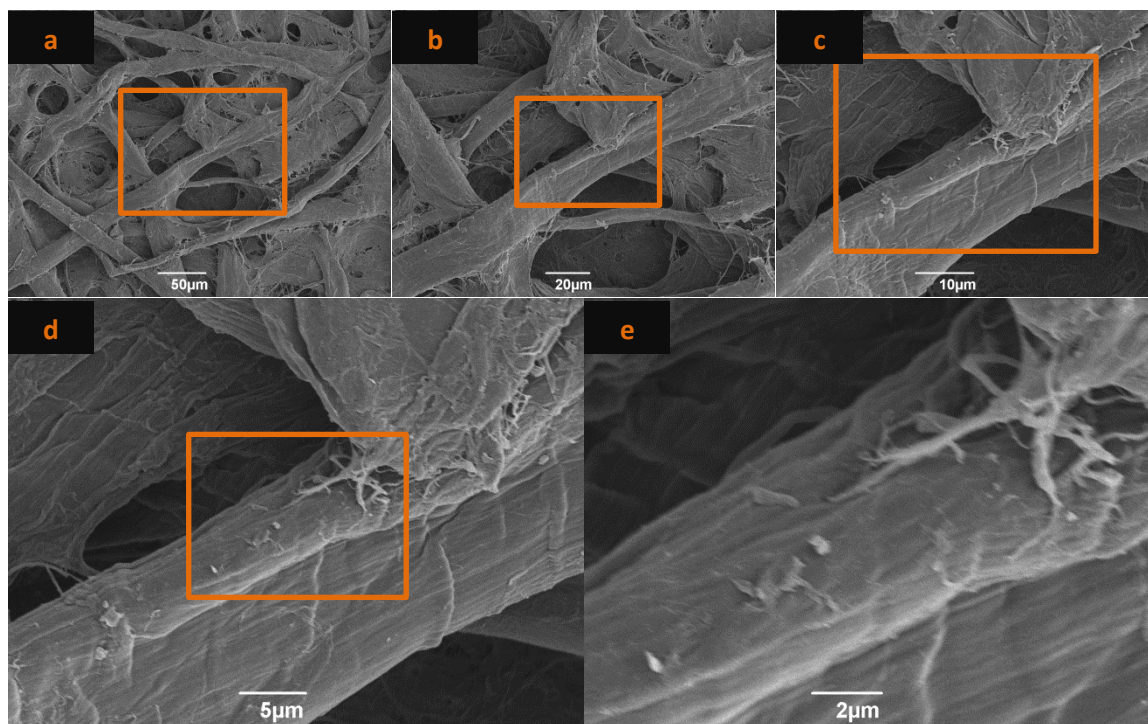


Figure 60: FT-IR of from the substrate achieved via the SI-ARGET ATRP of compound **6**, with an inset showing the carbonyl region for the product substrate (blue).

Comparisons of the SI-ARGET ATRP of the side-on acrylate against the SI-ARGET ATRP end-on acrylate polymerisations shows a slightly weaker stretch in the FT-IR, of the former, corresponding to a lower number of carbonyls in the grown polymers. For each monomer unit, three carbonyls are present, for a sample with the same degree of polymerisation, a greater carbonyl stretch would be expected. The lower than expected signal can be partially accounted for by the stoichiometry (*ca.* 2:3) added to the reaction and the termination reactions observed in the  $^1\text{H}$  NMR spectrum. The FT-IR data indicates that lower loadings of polymer have been achieved on the surface. This could mean that the grafted polymer chains are shorter, or that there are less sites grafted. With the data available it is not possible to discern between these two potential scenarios.

SEM images appears to show a significant loss of the finest substrate microfibers and a smoothing of the surface (Figure 61).



*Figure 61: SEM images of the surface obtained from the SI-ARGET ATRP reaction of compound 6 with [Cu(II)/PMDETA] – ascorbic acid in the presence of sacrificial initiator in anisole (Entry 8) at a. 330x, b. 750x, c. 2000x, d. 3000x, and e. 8000x magnification.*

Prominent ridges and features from interacting fibres continue to be observed through the smoothing attributable to thin layers of grafted polymer. Microfibril bundles appear to be retained but with a greatly reduced abundance. The surface observations by SEM corroborate the information obtained from FT-IR, this is, that some of the amorphous cellulose regions might have been detached from the surface.

## Conclusions

Each of the analytical methods used for the characterisation of the polymerisation indicate a successful polymerisation. To the best of our knowledge this represents the first successful graft-from polymerisation with a side-on LC monomer from cellulose.

SEM analysis appears to show a higher than expected smoothing effect for the relatively weak carbonyl signal in the FT-IR spectrum compared to the terminal attached polymer. This could be a result of thinner polymer layers, made up of more bulky constituent chains, as expected from with laterally attached side groups. The thinner loading can account for the continued detail clarity of the underlying fibre contours. The over expression of polymer character could alternatively derive from a more defined polymer chain due to rigidity of the laterally attached LC side-groups with a shorter spacer length.

The GPC retention volume ranges are similar for the side-on polymerisation and the end-on polymerisation. A similar retention volume indicates a similar range for the hydrodynamic

volume. A comparable hydrodynamic volume suggests a comparable volume of side-on polymers has been achieved from each initiation site.

A similar hydrodynamic volume from the bulkier side-on acrylate would imply a lower number of repeat units. The greater retention time for the side-on polymerisation is therefore clear evidence of a lower degree of polymerisation.

In this work the impact of the increased lateral component of the molecular shape and short spacer were shown to not prevent grafting. A comparison of the measured  $M_n$  of 15,200 from the ARGET ATRP side-on polymerisation results relative to  $M_n = 4,613$  for the ARGET ATRP end-on polymerisation results suggest that polymerisation has been limited in the second case. The change to a trimodal peak suggests, in the context of the  $^1\text{H}$  NMR resonance at 5.58 ppm, that the alternative termination mechanisms are resulting in two distinct molecular weight distributions. Disproportionation terminations, as suggested by the  $^1\text{H}$  NMR resonance at 5.58 ppm, would represent the loss of end chain functionality and 'living' polymer character. The trimodal shape reflects those seen in random coupling of living chains in the absence of monomer. Random coupling could reflect the low loading of the monomer used in this reaction or result from a reduced rate of monomer coupling; due to increased steric bulk, relative to a similar or reduced rate of chain deactivation. It is likely that the reduction in monomer stoichiometry allows the termination mechanisms to be more influential.

Alternatively, it could be speculated that the distribution, as suggesting that the increased strain, due to the graft chains acting as springs<sup>51</sup>, may lead to the elongation of the springs from the surface until the point of eventual detachment of amorphous cellulose graft-from initiated polymer chains, along with the attached cellulose<sup>49, 103</sup>. This would be most likely to occur in amorphous regions of the cellulose surface, contributing to the apparent loss of the finest/most delicate fibres and the prominent presence of ridges on the cellulose fibres (Figure 61). If the degradation of the surface is confirmed this could represent an intrinsic limitation of the side-on graft from approach for such bulky monomer units on restricted substrates such as cellulose fibres. This could account for higher  $M_w$  polymers present (since chains of cellulose would act as macroradicals themselves yielding much higher molecular  $M_w$  polymers).

### 3.9. Vacuum Alternative to Mechanical Stirring (VALMS)

Concerns regarding the mechanical damage observed to the cellulose substrates mean that alternative, less abrasive, methods for the mixing of the polymerisation would be needed before current work can be conducted without fear of damaging the substrate before advancing substrates more delicate than paper. Modified reaction equipment has been developed in order to separate stirrers from the reaction substrates.<sup>110</sup>

Due to the ability of the ARGET system to regenerate Cu(I) and tolerate oxygen, the ability to perform polymerisations under a passive vacuum presented an opportunity for a novel model of mixing. Performing the ARGET polymerisation with residual toluene in anisole under vacuum resulted in the refluxing of the solvent. Whether this is attributable to an azeotrope of the toluene and anisole or simply the boiling and condensing of the toluene component of the solvent was not investigated.

It was observed that when a solution of 100  $\mu\text{L}$  in 0.5 mL toluene in anisole was heated under a passive vacuum, with the solvent level matching the level of oil in a heating oil bath, the reaction mixture boiled gently. With the reaction Schlenk tube submerged further to heat some of the vessel walls where the solvent was condensing, the boiling stopped and the mixture was static. By raising the Schlenk tube to only heat the lower part of the solvent, the observed rate of boiling increased.

In all cases where boiling was observed, the cellulose substrate was visibly but gently agitated by the developing effervescence. The ability of the observed boiling to mix the substrate and solution combined with the ability to control the rate of observed boiling allows for controlled mixing of the reaction without the need for mechanical stirring devices (i.e. without magnetic stirrer).

### 3.10. ARGET-ATRP in the absence of controlled mixing (Entry 5).

Having observed a promising basis for a potential alternative mixing which it was hoped might reduce the mechanical fatigue experienced by the cellulose substrates, it was important to understand the contribution of mixing to the polymerisation results. In light of this similar conditions were used to explore the contribution of mixing to the polymerisation. Cu(II)Br<sub>2</sub>/PMDETA (2.1 μmol:17 μmol), ascorbic acid (21.1 μmol) and end-on acrylate monomer (0.940 mmol) in anisole, in presence of sacrificial initiator, EBIB (11 μmol), were used for the polymerisation with no controlled mixing mechanism.

#### Solution polymerisation

Figure 62 shows the <sup>1</sup>H NMR monitoring region for the crude sacrificial polymer isolated from the reaction.

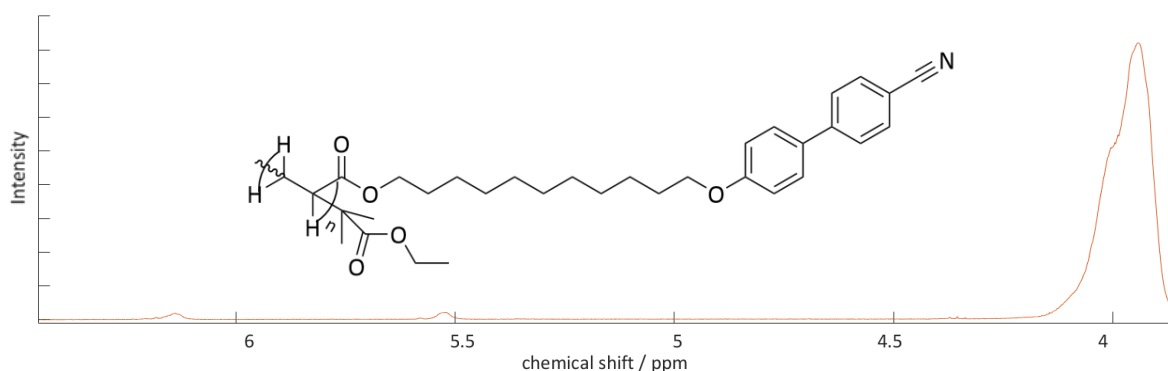


Figure 62: Monitoring region of the sacrificial polymer <sup>1</sup>H NMR monitoring region from the synthesis of substrate 7 via the ARGET polymerisation of compound 2 in the absence of controlled mixing.

<sup>1</sup>H NMR showed significant but not yet complete conversion of the monomer to conjugated species after the 16 hour reaction period, the monitoring ratio was calculated as 40.2:1. This is consistent with polymerisation controlled by diffusion of the substrates. Additionally, FT-IR of the crude sacrificial polymer shows an absorption at  $\nu = 1727 \text{ cm}^{-1}$  instead of the  $\nu_{\text{CO}} = 1711 \text{ cm}^{-1}$  monomer (Figure 64), consistent with successful polymerisation.

The successful polymerisation was ascertained by GPC, as shown in figure 63.

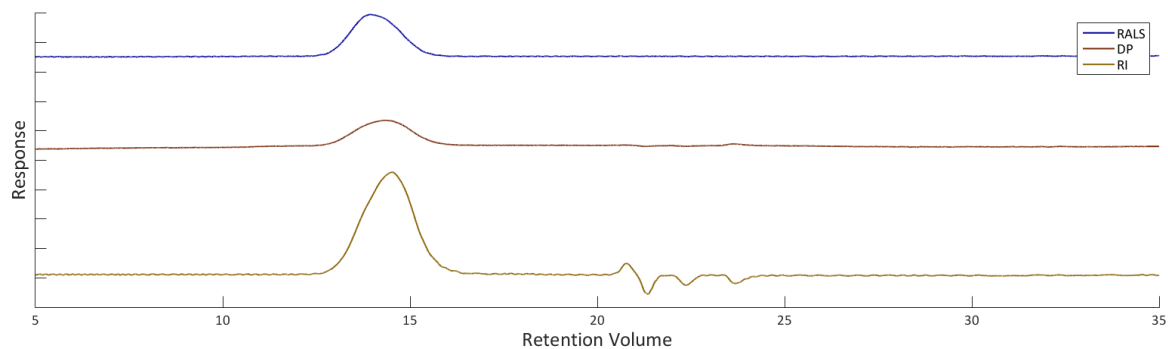


Figure 63: GPC triple detection trace of sacrificial initiator from the synthesis of substrate 7 via the ARGET polymerisation of compound 2 in the absence of controlled mixing: showing right angle light scattering (RALS), differential pressure (DP) and refractive index (RI).

The GPC trace shows no evidence of residual monomer, and a broad polymer peak of RV = 14.51 mL corresponding to  $M_{n,meas}$  7,080;  $M_{w,meas}$  13,300 with a calculated polydispersity of 1.88 even without stirring, with a symmetrical weight distribution. This would suggest to the robustness of the polymeric control achievable *via* ARGET-ATRP.

### Substrate polymerisation

The IR spectrum of paper substrate (blue line) shows no indication of a carbonyl band on the surface (Figure 64).

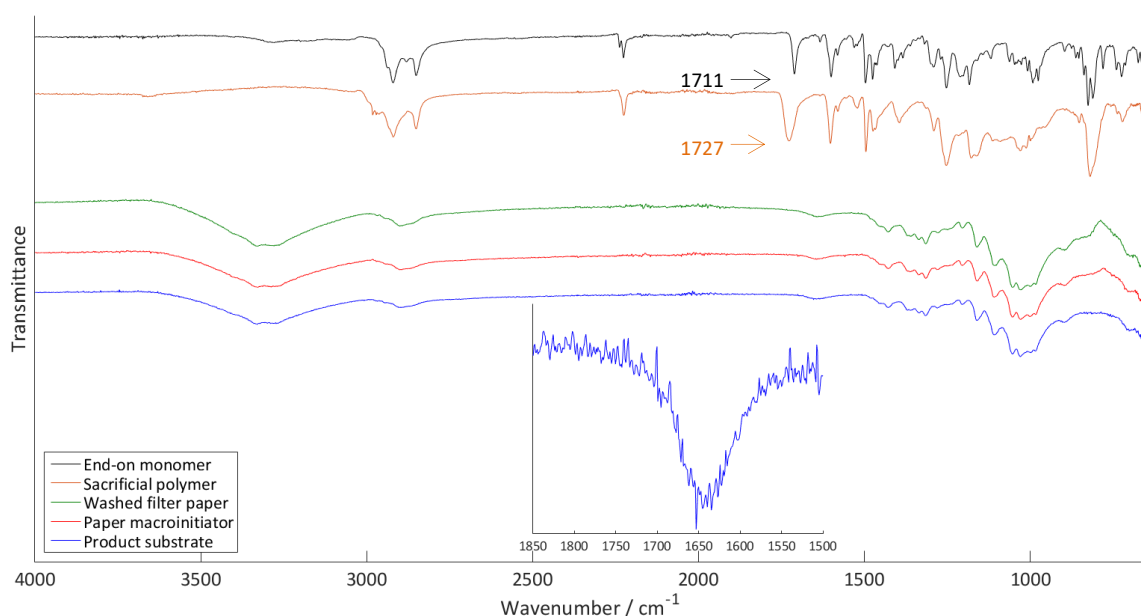


Figure 64: FT-IR of the substrate obtained from the synthesis of substrate 7 via the ARGET polymerisation of compound 2 in the absence of stirring, with an inset showing the carbonyl region for the product substrate (blue).

In contrast to the positive polymerisation results deduced from analysis sacrificial polymerisation, by  $^1\text{H}$  NMR GPC and FT-IR, the FT-IR of the surface shows no discernible evidence of

polymerisation. This contradiction can be seen starkly in Figure 64. As was seen for Figure 48 in Section 3.5 SEM can provide insights into the surface morphology where the FT-IR evidence is inconclusive. SEM images of the surface obtained are shown in Figure 65.

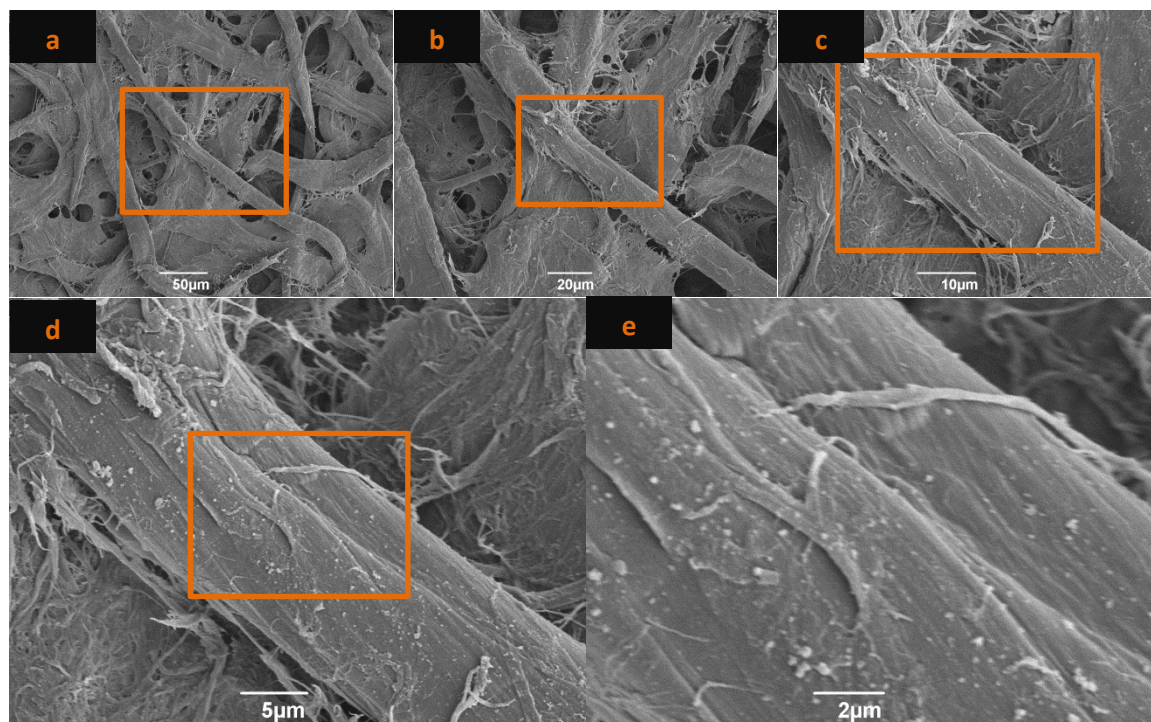


Figure 65: SEM images of the surface obtained from the SI-ARGET ATRP reaction of compound 2 with [Cu(II)/PMDETA] – ascorbic acid, in the presence of sacrificial initiator in anisole (Entry 5), without controlled mixing, at a. 330 $\times$ , b. 750 $\times$ , c. 2000 $\times$ , d. 3000 $\times$ , and e. 8000 $\times$  magnification.

The SEM appears to show a surface comparable to the failed polymerisation of Cu(I)/PMDETA in anisole this supports the FT-IR interpretation that the polymerisation has failed to reach a sufficient loading to be detectable or has failed to initiate on the surface.

## Conclusions

In this experiment, the reaction accidentally became exposed to the atmosphere and was subsequently evacuated and restarted.

It is clear from the sacrificial polymer obtained that the polymerisation had initiated successfully in solution, with a relatively low calculated polydispersity. This would be consistent with the highly controlled nature of the controlled radical polymerisations, specifically ARGET ATRP in this context.

In contrast, there is no convincing evidence of successful polymerisation from the cellulose surface. Taking into account that the reaction became exposed to oxygen and later restarted, to reconcile both the highly successful polymerisation in the solution and the unsuccessful polymerisation on the surface; it is important to consider the reliance on diffusion might not have

an appreciably negative effect in solution but might have dramatically affected the polymerisation initiated from the surface.

### 3.11. ARGET-ATRP with vacuum assisted mixing (Entry 6).

Having established a control condition for the ARGET-ATRP, with both stirring and non-stirring conditions, the potential of the vacuum assisted mixing could be ascertained with a study using compound **2** under the conditions of vacuum assisted mixing. Cu(II)Br<sub>2</sub>/PMDETA (2.2 μmol:17 μmol), ascorbic acid (22.6 μmol) and end-on acrylate monomer (0.940 mmol) in anisole/toluene, in presence of sacrificial initiator, EBIB (11 μmol), were used with vacuum assisted mixing.

#### Solution polymerisation

The sacrificial polymer obtained in the reaction was analysed by <sup>1</sup>H NMR (Figure 66) and GPC (Figure 67).

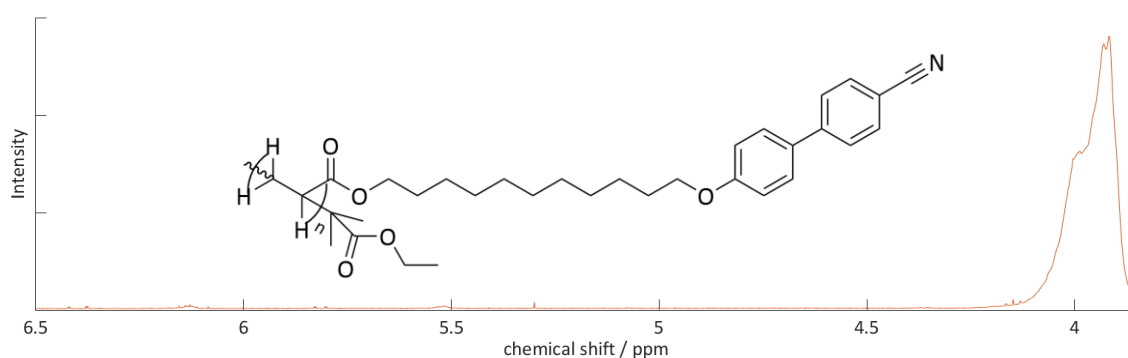


Figure 66: Monitoring region of the sacrificial polymer <sup>1</sup>H NMR monitoring region from the synthesis of substrate **8** via the ARGET-ATRP of compound **2** with vacuum assisted mixing.

The <sup>1</sup>H NMR of the solution phase shows that the polymerisation has been successful; there are minimal traces of the initial monomer by integration. The ratio of the aliphatic protons at 3.85-4.20 against the acrylate protons between 5.77-6.44 in the monitoring region was 26.3:1, this would suggest a very high conversion of monomer to polymer.

The high conversion observed by <sup>1</sup>H NMR is confirmed by the GPC (Figure 67).

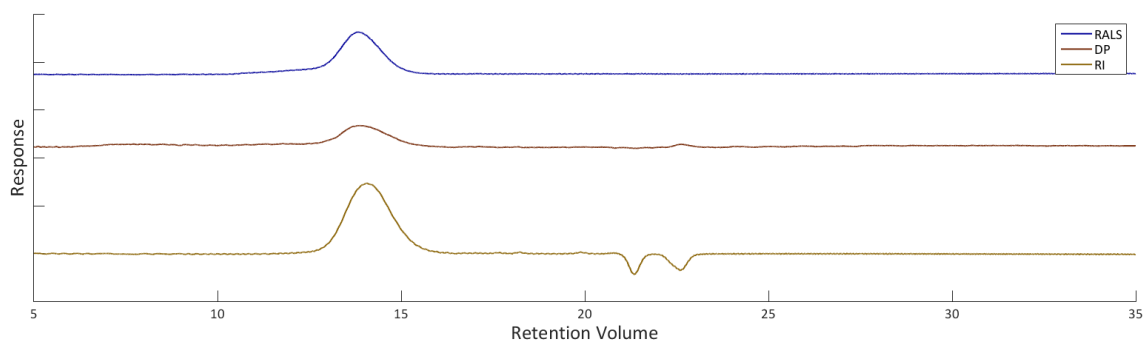


Figure 67: GPC triple detection trace of sacrificial initiator from the synthesis of substrate **8** via the ARGET polymerisation of compound **2** mixed utilising the vacuum alternative to mechanical stirring: showing right angle light scattering (RALS), differential pressure (DP) and refractive index (RI).

No residual monomer is seen in the GPC with a single apparently normally distributed peak eluting at 14.06 mL;  $M_{n_{meas}}$  10,412;  $M_{w_{meas}}$  18,607 with a calculated polydispersity of 1.79. This represents a higher degree of polymerisation, with a lower polydispersity compared to Entry 5 with very similar condition apart from the mixing. This suggests a very successful polymerisation with good control, compared to both the stirred and non-mixed reactions.

### Substrate polymerisation

The FT-IR of the surface was analysed by FT-IR and SEM. The FT-IR shows the sacrificial polymer and resultant cellulose substrate (Figure 68).

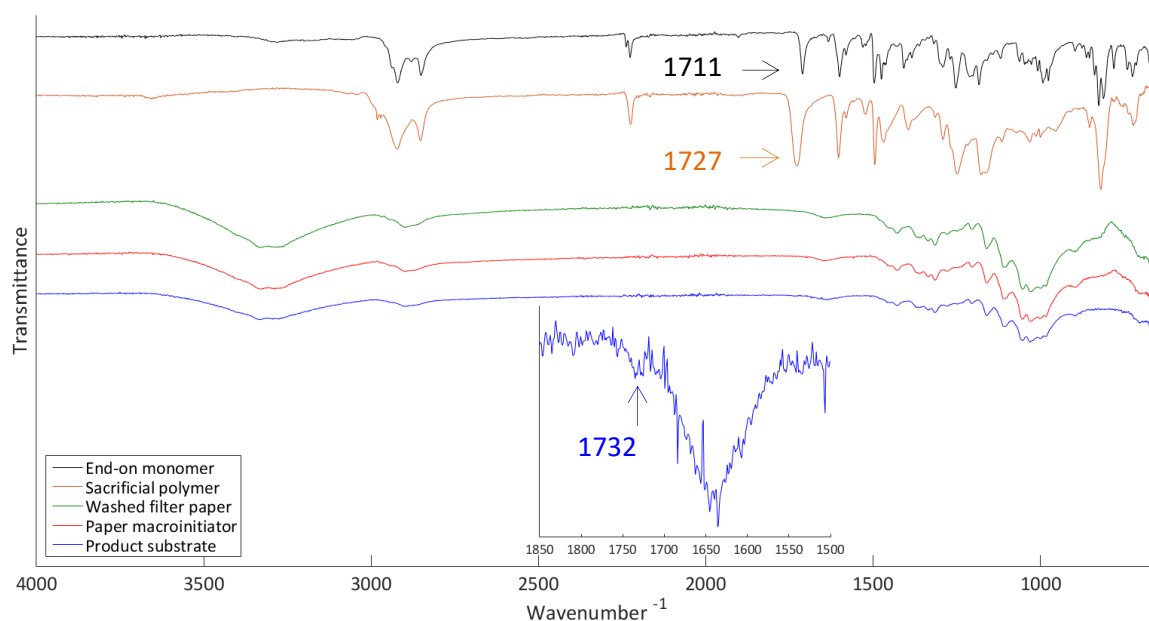


Figure 68: FT-IR of the substrate achieved from the synthesis of substrate **8** via the ARGET polymerisation of compound **2** mixed utilising the vacuum alternative to mechanical stirring.

FT-IR of the substrate showed a clear peak assigned as  $1732\text{ cm}^{-1}$ , assigned to the carbonyl stretch due to the polymer chains grafted on the surface.

Analysis of the surface by SEM is shown in Figure 69.

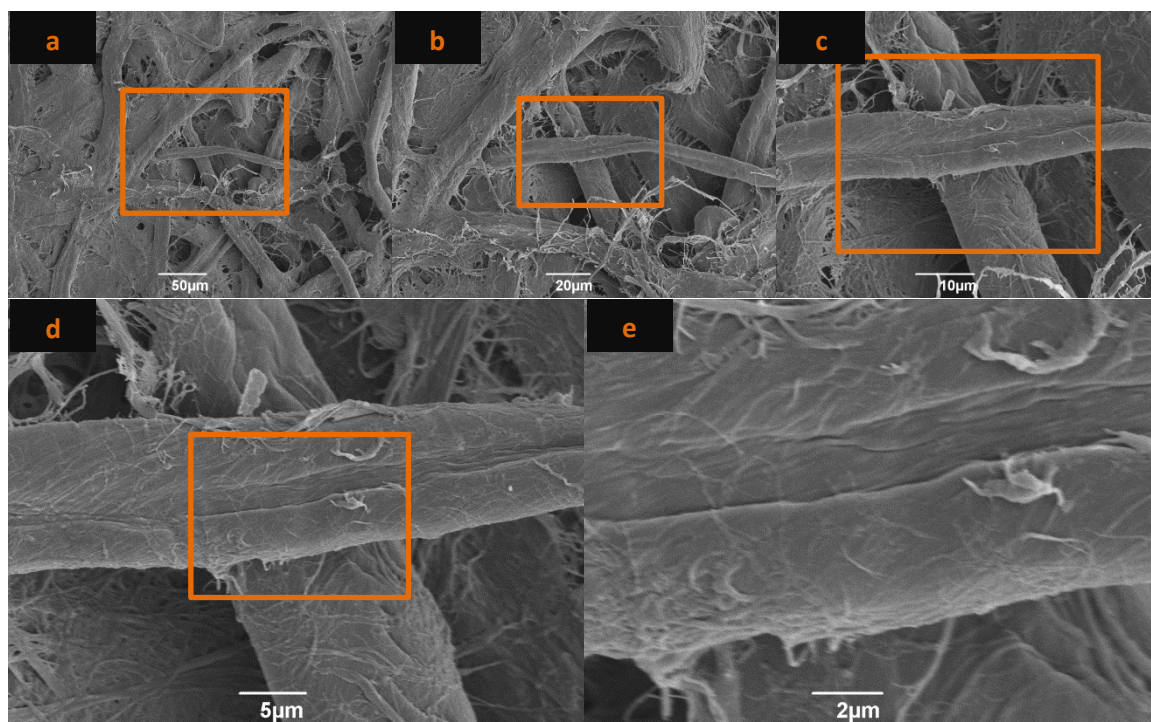


Figure 69: SEM images of the surface obtained from the SI-ARGET ATRP reaction of compound 2 with [Cu(II)/PMDETA] – ascorbic acid, in the presence of sacrificial initiator in anisole/toluene (Entry 6), with VALMS at a. 330 $\times$ , b. 750 $\times$ , c. 2000 $\times$ , d. 3000 $\times$ , and e. 8000 $\times$  magnification.

SEM showed significant smoothing of the surface as well as the development of trenches alongside the development of a valley with apparent curvature along the fibre in Figure 69e. Observations of microfibril bundles were minimal.

## Conclusions

The results observed for the vacuum mixed polymerisation of the surface initiated ARGET-ATRP of compound 2 from a paper macroinitiator are much more comparable to the mechanically stirred polymerisation than those of the non-mixed system. It is clear that the vacuum assisted mixing provided sufficient mixing to support the successful surface grafting of the LC polymer.

The mechanically stirred polymerisation appears to have been more successful on the surface by the measure of FT-IR, this reflects the higher degree of polymerisation achieved in the bulk. The mechanical stirring of the paper substrate has caused some mechanical damage this is consistent with the topologies observed with SEM of both surfaces (see Figures 65 & 69). To protect the mechanical properties of the surface it is therefore true that the vacuum alternative may offer a preferable compromise to the more abrasive mechanical stirring. Extending this argument, it is sensible to decide that for more delicate substrates the vacuum alternative would represent the best explored conditions, without resorting to specifically modified reaction vessels.

### 3.12. Model Substrates

The ability to achieve comparable results for polymerisations avoiding mechanical stirring opens up the possibility of exploring less mechanically robust model substrates to understand the surface properties obtained. To this end we extended our studies to include electrospun cellulose fibres. Electrospun fibres provide homogenous nanofibers with a high surface-to-volume ratio<sup>111</sup>. The nanofibril nature allows for corresponding nanoscales analysis of surface properties<sup>112</sup>.

The cellulose acetate electrospun fibres are homogenous tubular nanofibrils, with relatively narrow diameter dispersity. The cellulose acetate polymer used to produce the electrospun fibres had an average degree of substitution of 2.3 (if every OH group of the glucose unit is substituted the maximum degree of substitution, 3, is present). Although cellulose acetate electrospun fibres have been functionalised successfully, the degree maximum functionalisation achieved is more limited. To aid easy detection of the surface species the acetate groups were hydrolysed to obtain cellulose as a polymerisation substrate for this work. The hydrolysis process is mild enough to preserve the morphology of the fibres (it is likely some or all of the resultant constituent cellulose microfibrils were the cellulose II polymorph<sup>23</sup>), yielding a substrate that is amenable to higher loadings.

SEM images of the cellulose acetate fibres, as used, are shown in figure **70**.

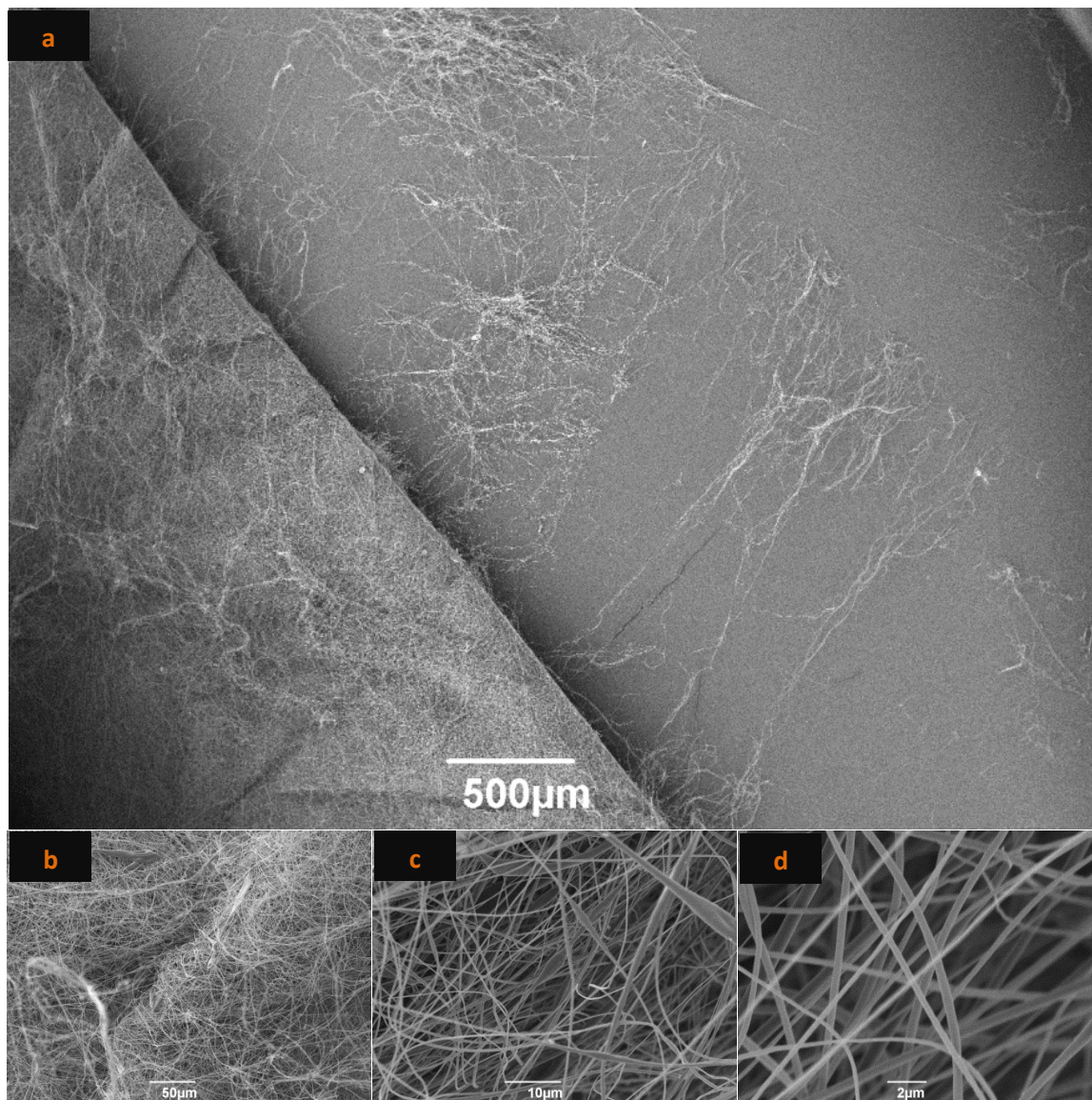


*Figure 70: SEM images of ESF cellulose acetate mat, at a. 70× b. 330×, c. 2000× and d. 8000× magnification. Analysed following the boiling toluene, ethanol wash cycle.*

### 3.13. Regeneration of cellulose from cellulose acetate ESF.

The cellulose acetate electrospun fibres were hydrolysed with sodium hydroxide  $0.05 \text{ mol dm}^{-3}$  to generate cellulose electrospun fibres (referred to as regenerated electrospun fibres, RegC) in accordance with well-established practices<sup>32, 113, 114</sup>. The RegC was analysed with SEM and FT-IR.

The SEM images of regenerated cellulose fibres are shown in Figure 71.

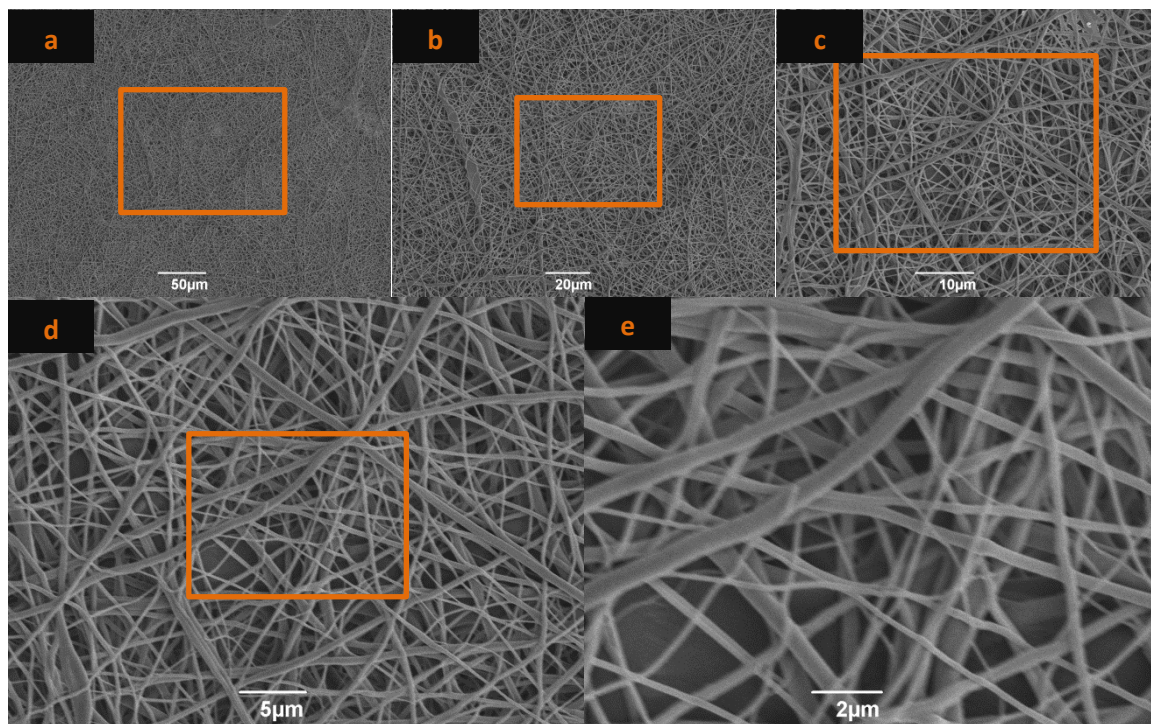


Figure 71: SEM images of the regenerated cellulose fibres obtained from the NaOH treatment of cellulose acetate ESF. at a. 330x, b. 750x, c. 2000x, d. 3000x, and e. 8000x magnification.

SEM of the regenerated electrospun fibres (Figure 71) showed no significant changes from the pretreated fibres (Figure 72). The fibre surface became slightly less uniform and the fibres became more compacted. This is consistent with the mercerization (hydrolysis) process. FT-IR showed the loss of the  $1740 \text{ cm}^{-1}$  carbonyl stretching (Figure 72). This reflects that during the hydrolysis process the acetate groups are removed, resulting in the uncapped hemiacetal and glycol hydroxyl groups of the cellulose being regenerated. The fibres are likely to have become cellulose II polymorphs.<sup>23</sup>

### 3.14. Polymer grafting from regenerated cellulose ESF

End-on polymerisations were performed from the regenerated electrospun fibres with no stirring and with the vacuum alternative to mechanical stirring respectively.

#### Solvent selection

From the initial screening of the substrate tolerance to solvents it was clear that our previous washing protocols required modification. In our previous reactions to anchor initiator on the cellulose surface THF was used as a solvent; however the cellulose acetate ESF is soluble in THF, giving rise to concerns that the grafted-from substrates may dissolve upon grafting. From the limited solvents available to carry out the initiation and polymerisation reactions, which do not dissolve the cellulose acetate substrate, toluene proved successful for the anchoring of the initiator.

In order to eliminate the polymer produced in solution from the fibre, a thorough washing protocol is needed. Based on the preferable solvents, a washing with toluene, isopropanol, water, isopropanol, and hexane similar to that used in the paper functionalisation was selected. As with the paper polymerisations, control samples were produced to ascertain the effectiveness of the washing protocol. The fibre mats were suspended in solutions of the terminal SCLCP and lateral SCLCP sacrificial polymers from Entry **7** and Entry **8**, in anisole (0.5 mL) and toluene (100  $\mu$ L), respectively and heated to 100 °C for sixteen hours. These control reactions show that the initial washing was not sufficient to remove physisorbed polymer from the surface. An additional, more robust wash was conducted using boiling toluene four times, followed by ethanol at room temperature three times. Following the subsequent washing, it appeared by SEM and FT-IR that physisorbed laterally attached polymer was mostly washed away and removed from the surface (very localised deposits remained in one region), however physisorbed terminally attached polymer was persistent. Full characterisation of the substrates was deemed to be desirable before further exploration of potentially compromising washing techniques. The results presented in this work represent show the substrates following the subsequent 'rigorous' washing protocols.

Detection of the grafted bromoisobutyryl bromide (bibb) initiation unit was only conclusive for substrate 12c (used in the ESF initiated ARGET-ATRP with the side-on acrylate monomer (Figure **83**). The FT-IR of the cellulose acetate mat (a), regenerated cellulose mat (b) and a typical macroinitiator substrate (12a, used in the ESF initiated ARGET-ATRP with the end-on monomer using the VALMS technique are shown in Figure **72**.

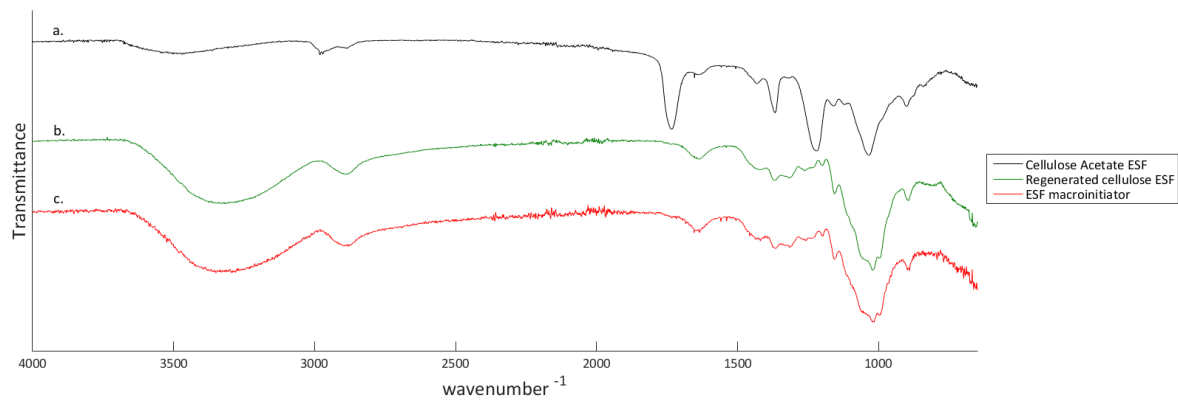


Figure 72: FT-IR showing a. the initial cellulose acetate, b. the regenerated cellulose ESF and c. an ESF macroinitiator (substrate **12b**).

Figure 72 shows the  $\nu_{\text{CO}}$  of cellulose acetate at  $1740 \text{ cm}^{-1}$  is lost after hydrolysis (Figure 72b.). Loading of the initiator (BIB) by esterification of the OH groups does not change the IR spectrum (no  $\nu_{\text{CO}}$  is observed) since the substitution ratio is very low.

### 3.15. ReGC-ESF graft-from ARGET ATRP polymerisation of the end-on acrylate monomer, **2**, in the absence of controlled mixing (Entry 9)

As with the paper substrate counterparts, ARGET ATRP of compound **2** from an regenerated cellulose electrospun fibre (ReGC ESF) macroinitiator in absence of controlled mixing was monitored by infrared spectroscopy and SEM of the surface, alongside GPC and  $^1\text{H}$  NMR of the sacrificially polymer produced in the reaction. The polymerisation was conducted with  $\text{Cu(II)Br}_2/\text{PMDETA}$  (2.1  $\mu\text{mol}$ :17  $\mu\text{mol}$ ), ascorbic acid (21.1  $\mu\text{mol}$ ) and end-on monomer (0.950 mmol) in anisole/toluene, in presence of sacrificial initiator, EBIB (11  $\mu\text{mol}$ ), using vacuum assisted mixing.

#### Solution polymerisation

The  $^1\text{H}$  NMR of the crude isolated from the polymerisation solution shows mostly unreacted monomer (Figure **73**); only traces of the broad resonance at  $\sim 4$  ppm due to the oligomer or polymer aliphatics is observed. The ratio of 3.85-4.20 ppm to 5.77-6.44 ppm is 1.63:1, which indicates very limited polymerisation.

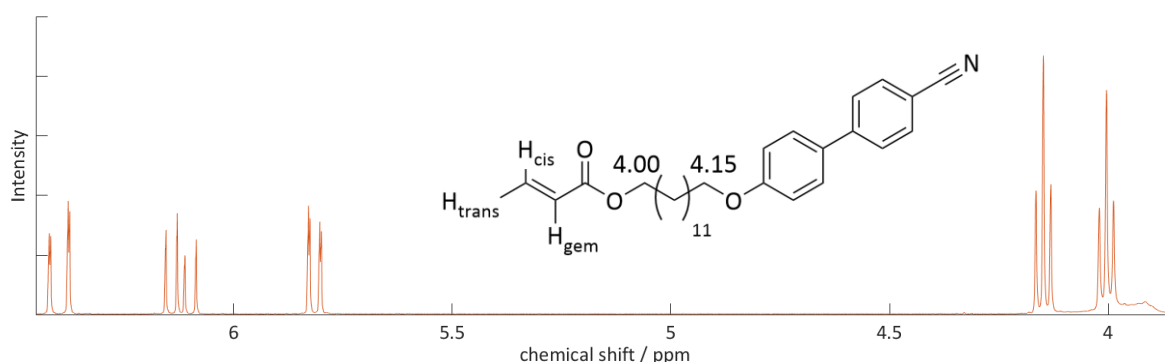


Figure **73**:  $^1\text{H}$  NMR monitoring region from the synthesis of substrate **13** via the ARGET-ATRP polymerisation of compound **2** in the absence of stirring.

However, evidence of polymerisation can be seen in the GPC trace of the reaction crude Figure **74**.

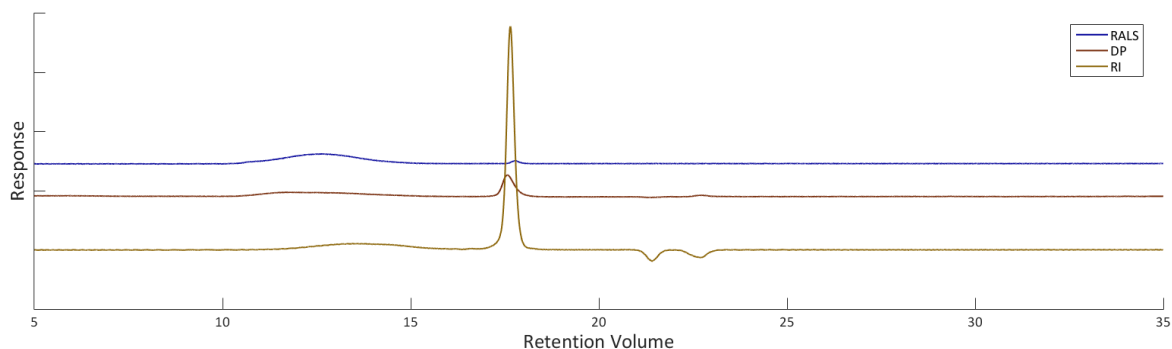
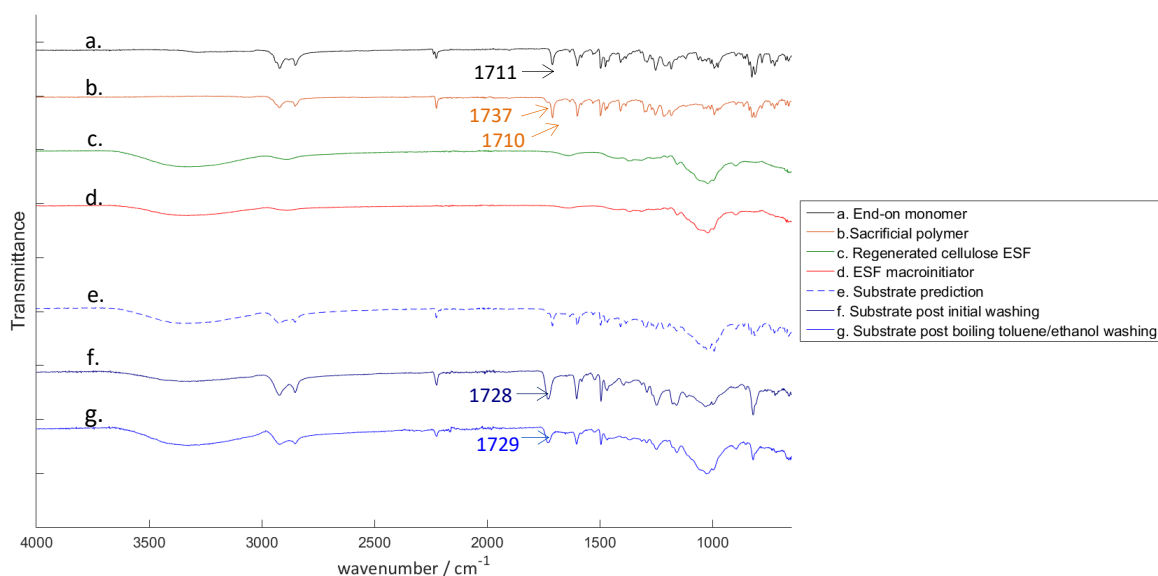


Figure 74: GPC triple detection trace of sacrificial initiator from the synthesis of substrate **13** via the ARGET polymerisation of compound **2** in the absence of stirring: showing rightv angle light scattering (RALS), differential pressure (DP) and refractive index (RI).

The GPC showed two elution events, one minor event at higher molecular weight and one major event at lower molecular weights. The higher molecular weight event occurred at 13.6 mL corresponding to  $M_{n_{meas}} = 16,000$  ,  $M_{w_{meas}} = 56,607$  with a calculated polydispersity of 3.54. The lower molecular weight peak occurring at 17.61 mL is identified as the unreacted monomer by comparison with the pure acrylate **2** Section 3.1.1).

### Substrate polymerisation

Figure 75 shows the IR spectra of the solid species capable of contributing to the FT-IR signal of the product substrate and spectra of the "predicted", initial and final ESF product substrates. and the electrospun fibres obtained from the SI-ARGET ATRP of the end-on monomer, **2**.



**Figure 75:** FT-IR of a. Compound **2**, b. Sacrificial polymer from the monitoring of the graft-from modification of substrate **13**, c. Regenerated electrospun fibre, d. Electrospun fibre macroinitiator, e. scaled summation of **b.** and **c.** to predict the infrared spectra of sacrificially formed polymer physisorbed on the substrate surface, f. substrate **13** synthesised via the ARGET-ATRP of compound **2** in the absence of stirring following the initial washing, g. substrate **13** following an additional washing procedure of boiling toluene and ethanol.

During the drying, following the initial washing the substrate became strongly adhered to the sample vial causing severe damage to the substrate during separation.

Following the polymerisation the crude solution showed a higher wavenumber shoulder on the carbonyl signal at  $\nu_{\text{CO}} = 1737 \text{ cm}^{-1}$ , this is identified as the polymer contribution; a similar shoulder was seen on the  $\nu_{\text{Ar}} = 1600 \text{ cm}^{-1}$  signal (Figure **75b**).

In order to aid the interpretation of the product substrate spectrum, the sacrificial polymer spectrum was scaled (according to the rough ratios of the cellulose OH stretch and the polymer CH stretches in the substrate spectra) and added, mathematically, to the spectrum of the regenerated cellulose ESF to give a prediction of a spectrum of sacrificial polymer and substrate with no interaction between the two species (Figure **75e**). This provides a reference of what overlapping, non-interacting, signals would present as.

The IR spectrum of the regenerated cellulose fibre after polymerisation showed very strong C=O band corresponding to the polymer. The carbonyl band was observed at  $1728 \text{ cm}^{-1}$  after the initial wash and after the subsequent washing no meaningful change was observed with  $\nu_{\text{CO}} = 1729 \text{ cm}^{-1}$ . In addition, bands at  $2923 \text{ cm}^{-1}$  (CH Ar),  $2852 \text{ cm}^{-1}$  (CH Ar),  $2224 \text{ cm}^{-1}$  (CN) and  $1603 \text{ cm}^{-1}$  (CH Ar) are present, which correspond to the functionalities of the side-group.

The subsequent washing resulted in a reduction of the intensity of the  $\nu_{\text{CO}}$  and other polymer signals against the background fibre intensity; however a significant degree of polymer character was retained. This can be attributed to the loss of physisorbed polymer. However, given that

significant degradation of the fibres occurred during the subsequent washing, it is also possible that this loss can be attributed to the mechanical degradation of the surface cellulose, which might be expected to show the greatest graft density in comparison to the deeper fibres.

The SEM showed a film in localised regions of the substrate (Figure 76). The surface was highly inhomogeneous with entire regions unmodified and others totally “wetted” by a film. It is possible that some of the inhomogeneity arose from the washing procedure. The polymer was not limited to the surface layer; this is evidenced by the clear development of films at different depths (Figure 76e). There is evidence of grain like material on the surface of some fibres. These grains could be either polymer or (given the roughness of the grains) catalyst which became “encased” in the polymer film and was not washed away during the washing cycles.

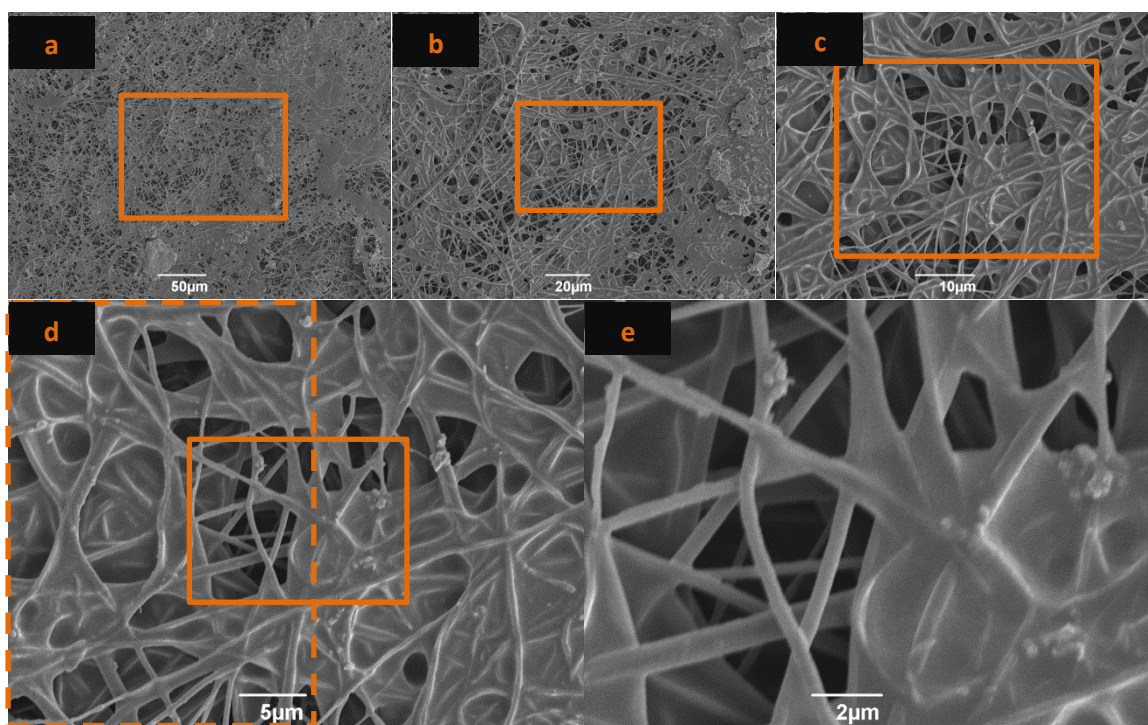


*Figure 76: SEM images of the surface obtained from the SI-ARGET ATRP reaction of compound 2 with [Cu(II)/PMDETA] – ascorbic acid, in the presence of sacrificial initiator in anisole (Entry 9), without controlled mixing, at a. 330x, b. 750x, c. 2000x, d. 3000x, and e. 8000x magnification. Analysed following the boiling toluene, ethanol wash cycle.*

## Conclusions

These results show that the inhomogeneous retention of adsorbed polymer occurs in the ARGET-ATRP process without stirring. This is in contrast to the polymerisation (ATRP and ARGET ATRP) on paper where no free polymer is retained on the surface and SEM appears to show broadly regular surfaces variations.

Due to the lack of effectiveness of the washing protocol we cannot be confident that the material observed on the substrate surface by SEM is grafted. FT-IR shows a small change of the  $V_{CO}$  of the

polymer on the surface following polymerisation, this appears to be a response to the adsorption (grafted, physisorbed or both).

It appears, that polymer character represents a greater contribution of the carbonyl stretch for the surface than the solution. The polymer may be a result of the polymer being formed preferentially on the surface or strongly deposited on the surface. If the polymer is preferentially formed on the substrate it is likely that either the monomer or another reaction species has strong interactions with the surface. This could explain the deposition of the grainy material, observed in SEM, on the surface. The material may be 'trapped' catalyst or ascorbic acid, which would lead to an increase in active catalyst and in turn monomer radicals at the surface.

Alternatively, the discrepancy could arise from preferential interaction of the mesogenic species. Strong monomer interactions would result with high degrees of polymerisation at the surface limiting the growth observed the solution. Additionally, larger polymers may have strong interactions with the fibres; this could be investigated against a form of the BET isotherm.

### 3.16. ReGC-ESF graft-from ARGET ATRP polymerisation of the end-on acrylate monomer, **2**, with vacuum assisted mixing (Entry 10)

Having observed inhomogenous deposition of polymer on the electrospun fibre surface in the absence of mixing, the gentle VALMS mixing method was used to mix the SI-ARGET ATRP from the RegC ESF macroinitiator. The polymerisation was conducted with Cu(II)Br<sub>2</sub>/PMDETA (2.3 μmol:18 μmol), ascorbic acid (22.0 μmol) and end-on acrylate monomer (0.98 mmol) in anisole/toluene, in presence of sacrificial initiator, EBIB (22 μmol), were used with vacuum assisted mixing.

#### Solution polymerisation

The <sup>1</sup>H NMR of the crude isolated from the polymerisation solution is shown in figure 77. The absence of acrylate monomer indicates that the polymerisation had gone to completion. This is reflected in the monitoring ratio of 3.85-4.20 ppm to 5.77-6.44 ppm calculated at 9.63:1, however, this is lower than for the VALMs SI-ARGET ATRP from paper, with the same monomer.

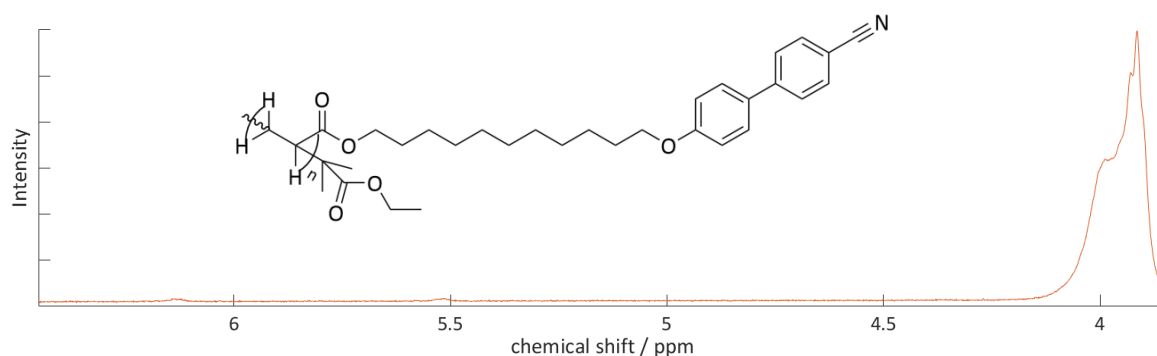


Figure 77: Monitoring region of the sacrificial polymer <sup>1</sup>H NMR monitoring region from the synthesis of substrate **14** via the ARGET-ATRP of compound **2** mixed utilising the vacuum alternative to mechanical stirring.

The GPC trace agrees with the <sup>1</sup>H NMR showing no detectable monomer signal. The polymer signal elutes at 13.51 mL, corresponding to Mn<sub>meas</sub> = 13,900, Mw<sub>meas</sub> = 42,200, and a calculated polydispersity of 3.03 (Figure 78). The GPC trace shows a multi-modal distribution of polymer. One main peak is seen by all detection methods. A minor shoulder of lower molecular weight is seen in RI and DP and a higher molecular weight is seen in RALS and DP. This reflects the sensitivity of each technique. The higher molecular weight peak in the RALS appears to show a plateau, this could reflect a physical process affecting the sacrificial polymer or the constructive signal of two peaks with a coincidental degree of resolution.

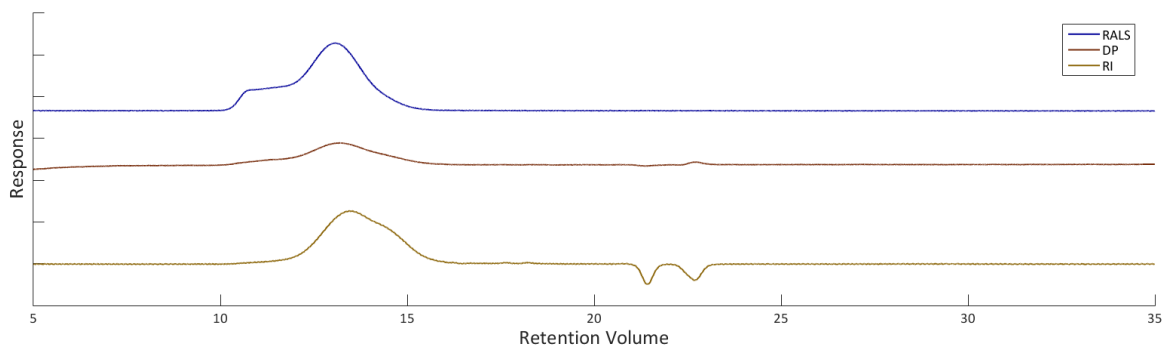


Figure 78: GPC trace of sacrificial initiator from the synthesis of substrate **14** via the ARGET atom transfer radical polymerisation of compound **2** mixed utilising the vacuum alternative to mechanical stirring: showing right angle light scattering (RALS), differential pressure (DP) and refractive index (RI).

### Substrate polymerisation

The FT-IR of the fibres achieved with VALMS is similar to that achieved without mixing as is shown in Figure 79.

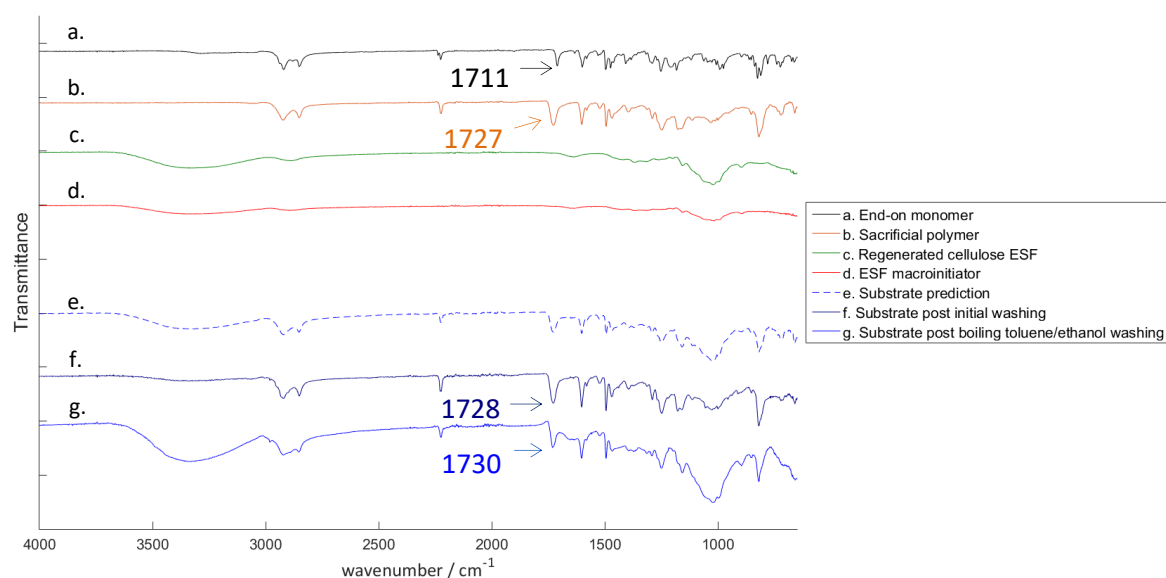


Figure 79: FT-IR of a. Compound **2**, b. Sacrificial polymer from the monitoring of the graft-from modification of substrate **14**, c. Regenerated electrospun fibre, d. Electrospun fibre macroinitiator, e. scaled summation of **b.** and **c.** to predict the infrared spectra of sacrificially formed polymer physisorbed on the substrate surface, f. substrate **14** synthesised via the ARGET-ATRP of compound **2** in the absence of stirring following the initial washing, g. substrate **14** following an additional washing procedure of boiling toluene and ethanol.

The substrate FT-IR shows the identified peaks associated with the polymer. Following the initial washing protocol the polymer contribution to the spectrum was significantly stronger (comparing the cellulose OH and sacrificial polymer CH contributions) than that of the background cellulose, even more so than for the unmixed polymerisation. Following the more rigorous washing the two contributions to the IR absorption became comparable. This is consistent with our understanding of the washing procedure from the control washes. The carbonyl peak was observed at  $1728\text{ cm}^{-1}$

after the initial wash and at  $1730\text{ cm}^{-1}$  upon subsequent washing. This could indicate an increase in the polymer contribution to the signal composition. An increased contribution to the carbonyl peak from the grafted polymer relative to the free polymer would be consistent with the explanation of non-grafted species being washed off. Following the subsequent washing the other identified polymer functionalities were observed at  $2921\text{ cm}^{-1}$  (CH Ar),  $2853\text{ cm}^{-1}$  (CH Ar),  $2225\text{ cm}^{-1}$  (CN) and  $1603\text{ cm}^{-1}$  (CH Ar).

The SEM of the surface achieved shows a more homogenous coating across the surface than the unmixed SI-ARGET ATRP from electropun fibres Figure 80. The individual fibres are thicker with webbing between them; some of the fibres appear to have fused together, from the control observations, it can be interpreted that webbed physisorbed polymer contributes to this observation.

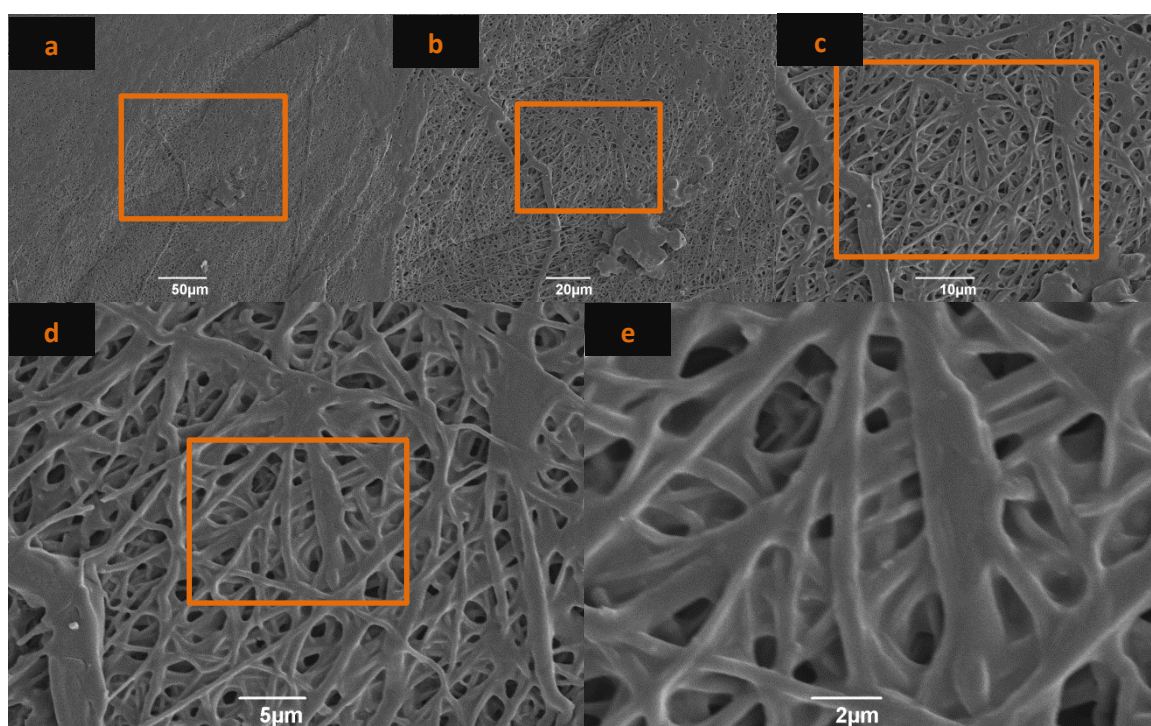


Figure 80: SEM images of the surface obtained from the SI-ARGET ATRP reaction of compound 2 with [Cu(II)/PMDETA] – ascorbic acid, in the presence of sacrificial initiator in anisole (Entry 10), with VALMS, at a. 330x, b. 750x, c. 2000x, d. 3000x, and e. 8000x magnification. Analysed following the boiling toluene, ethanol wash cycle.

## Conclusions

A more homogenous distribution of polymer was achieved on the surface using the VALMS technique. Webbing was observed in the SEM. This is likely caused by physisorbed polymer. Comparing the fibre thicknesses from the two end-on monomer polymerisations by SI-ARGET ATRP it appears that the VALMS polymerisation, which proceeded to a higher conversion, and thicker layer growth from the fibres. This would explain the webbing observed in SEM and the very high initial loadings on polymer observed on the surface by FT-IR. The cause of the fibre

thickening cannot be unambiguously ascertained with the current washing protocol. A BET isotherm might distinguish between increased physisorption interactions and a successful covalent graft.

### 3.17. ReGC-cellulose ESF graft-from ARGET ATRP polymerisation of the side-on acrylate monomer, **6**, with vacuum assisted mixing (Entry 11)

Having the potential of the vacuum alternative for mechanical for polymerisation from ESF macroinitiator a polymerisation of side-on monomer **6** from the ESF macroinitiator was conducted. The polymerisation was conducted with Cu(II)Br<sub>2</sub>/PMDETA (2.2 μmol:17 μmol), ascorbic acid (22.0 μmol) and side-on acrylate monome (0.62 mmol) in anisole/toluene, in presence of sacrificial initiator, EBIB (22 μmol), were used with vacuum assisted mixing.

#### Solution polymerisation

The <sup>1</sup>H NMR of the crude solution shows high levels of conversion of the monomer (Figure 81).

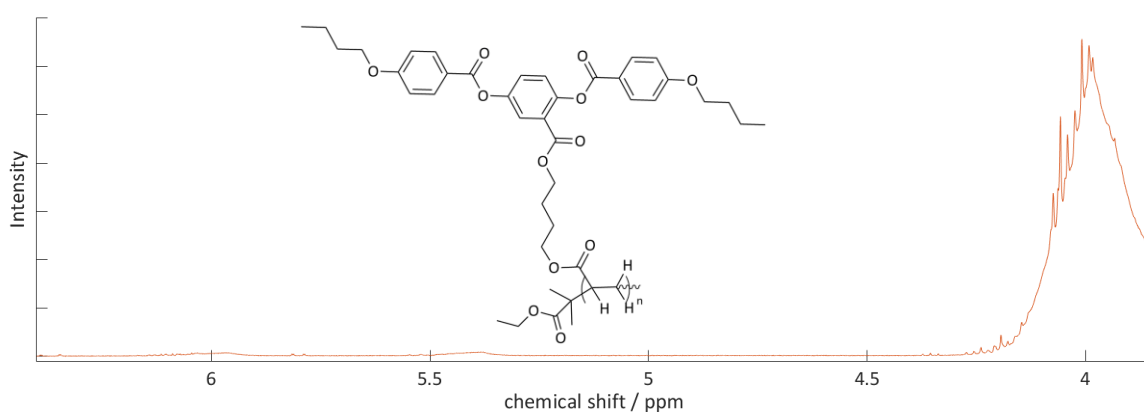


Figure 81: Monitoring region of the sacrificial polymer <sup>1</sup>H NMR monitoring region from the synthesis of substrate **15** via the ARGET ATRP of compound **6** mixed utilising the vacuum alternative to mechanical stirring.

The <sup>1</sup>H NMR of the sacrificially obtained polymer showed a high conversion of the monomer, as identified by the loss of olefin signals and the growth of a broad multiplet of increased intensity, at ~ 4 ppm, due to the increase in aliphatic protons. Very small concentrations of monomer remained unreacted a monitoring ratio of 26.3:1 for the 3.85-4.20 ppm to 5.77-6.44 ppm, which is very high indicating a successful polymerisation, however it is smaller than that observed with the paper substrate, indicating a lower degree of polymerisation.

GPC was used to provide information about the comparative molecular weight achieved (Figure 82).

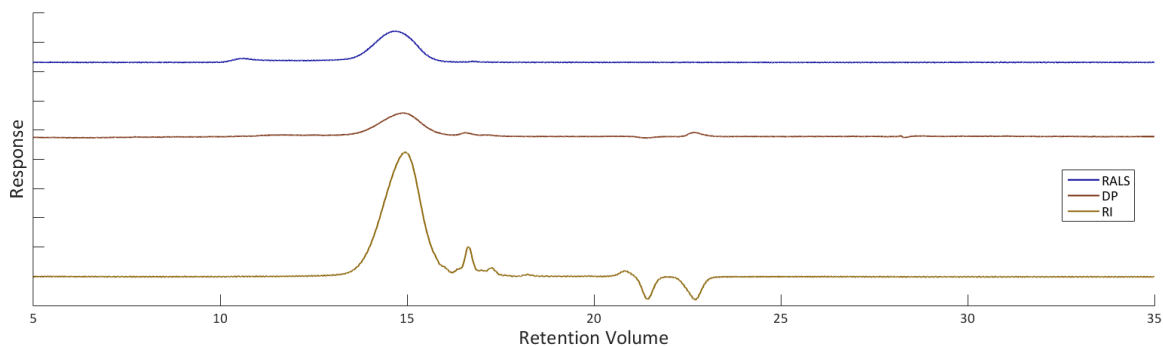


Figure 82: GPC trace of sacrificial initiator from the synthesis of substrate **15** via the ARGET atom transfer radical polymerisation of compound **6** mixed utilising the vacuum alternative to mechanical stirring: showing right angle light scattering (RALS), differential pressure (DP) and refractive index (RI).

Evidence of polymerisation can be seen in the GPC trace of the sacrificially initiated polymer present in the polymerisation of compound **6** from electrospun fibre, see Figure 82, a high molecular weight peak elutes at 13.5 ml. Comparison against the polystyrene standard gave  $M_{n,meas} = 5,020$ ,  $M_{w,meas} = 7,760$  and a calculated polydispersity of 1.55. A lower molecular weight species eluted at 16.6 mL, 17.3 mL the latter is identified as unreacted monomer. This is the lowest calculated polydispersity for an ARGET ATRP in this study, potentially reflecting the contribution of the increased number of initiator sites loaded on the surface.

## Substrate polymerisation

The FT-IR of the substrate showed clear evidence of the side-group functionality on the surface (Figure 83), as observed by the strong  $\nu_{\text{CO}} = 1743$  band on the surface of the thoroughly washed substrate (Figure 83g).

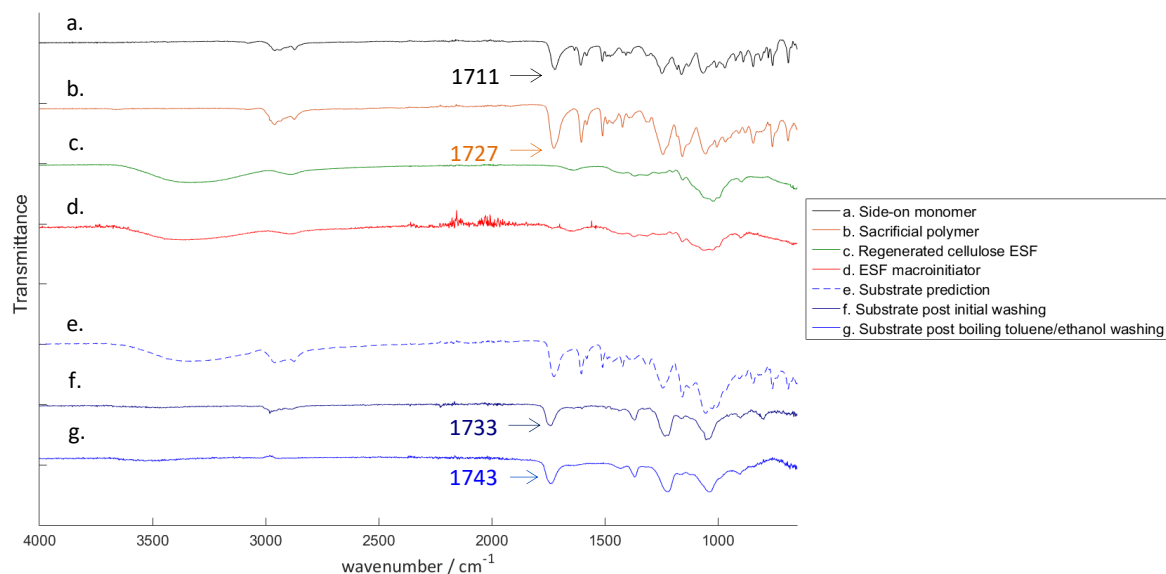


Figure 83: FT-IR of a. Compound 6, b. Sacrificial polymer from the monitoring of the graft-from modification of substrate 15, c. Regenerated electrospun fibre, d. Electrospun fibre macroinitiator, e. scaled summation of b. and c. to predict the infrared spectra of sacrificially formed polymer physisorbed on the substrate surface, f. substrate 15 synthesised via the ARGET-ATRP of compound 6 in the absence of stirring following the initial washing, g. substrate 15 following an additional washing procedure of boiling toluene and ethanol.

The FT-IR of the crude isolated from the reaction solution shows it to be composed of sacrificial polymer and unreacted monomer, this is indicated by a broad carbonyl band  $\nu_{\text{CO}} = 1727 \text{ cm}^{-1}$  relative to the same band in the paper initiated ARGET ATRP with the same monomer Section 3.8. The bib unit was clearly identifiable on the macroinitiated sacrificial initiator from a signal at  $1734 \text{ cm}^{-1}$ . This shows that the initiation conditions were successful. Following the polymerisation and initial washing, a spectrum reflecting a simplified sacrificial polymer spectrum dominated the substrate profile with the cellulose peaks reduced to the baseline and strong signals at  $1742 \text{ cm}^{-1}$ ,  $1370 \text{ cm}^{-1}$ ,  $1234 \text{ cm}^{-1}$  and  $1052 \text{ cm}^{-1}$ . The cellulose OH stretch ( $\nu_{\text{OH}} \sim 3300 \text{ cm}^{-1}$ ) is barely observed. Following the boiling toluene/ethanol washing procedure the spectrum was further simplified, the retained carbonyl peak remained ( $\sim 1740 \text{ cm}^{-1}$ ). The monomer CH stretches were no longer visible.

FT-IR suggests a thorough polymer coverage this was corroborated by SEM (Figure 84).

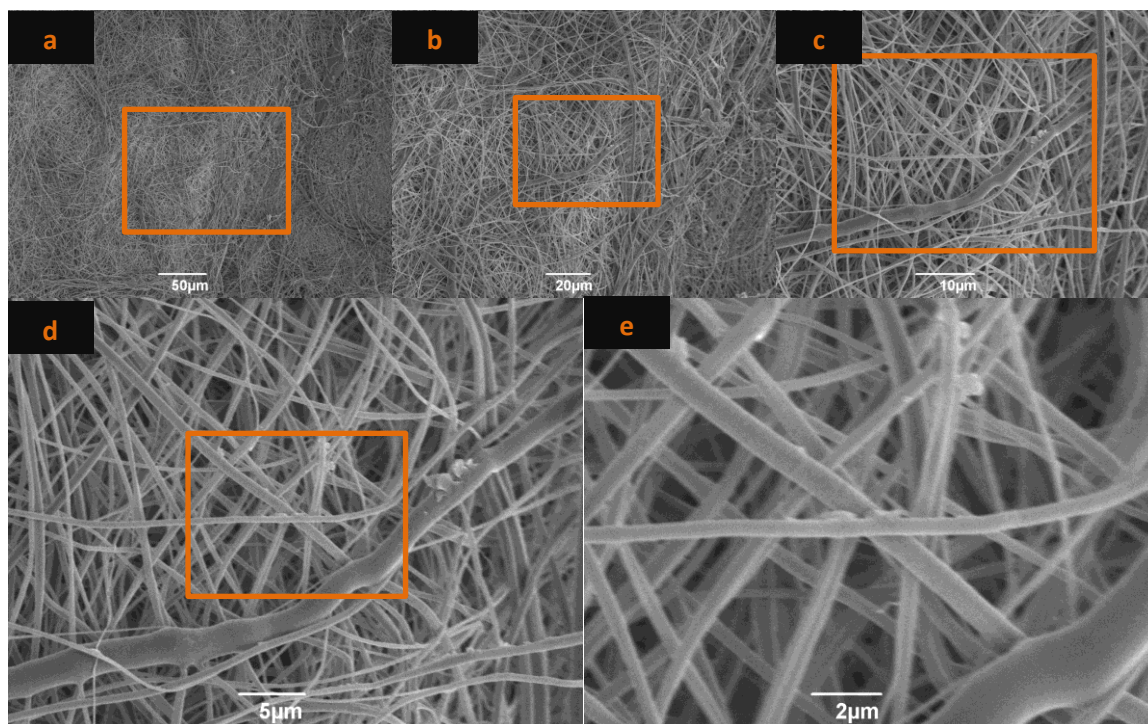


Figure 84: SEM images of the surface obtained from the SI-ARGET ATRP reaction of compound 6 with [Cu(II)/PMDETA] – ascorbic acid, in the presence of sacrificial initiator in anisole (Entry 11), with VALMS, at a. 330x, b. 750x, c. 2000x, d. 3000x, and e. 8000x magnification. Analysed following the boiling toluene, ethanol wash cycle.

SEM showed retention and thickening of the fibres compared to the RegC ESF. Analysis of comparable regions in the RegC ESF showed fibres with a larger diameter, than the pristine regenerated cellulose and a broadly smooth surface with some localised obtrusions. These observations were not seen in the control samples. The webbing/fusing of fibres observed in the mixed end-on monomer polymerisation (Entry 10) is not observed.

## Conclusions

The bib unit was positively identified on the macroinitiator providing confidence that the attachment procedure was successful. The attachment of bib unit on the surface means that the ESF macroinitiators and paper macroinitiators had the same surface chemistry prior to the polymerisation. The washing procedure for the ESF substrate mixed with the sacrificial polymer from Entry 8 was shown to be effective for the control sample. The successful washing of the control sample allows us to be confident that polymer detection on the substrate by SEM and FT-IR reflects chemically grafted polymer. The polymer was characterised with a relatively low calculated polydispersity of 1.13, if a relatively low polydispersity is confirmed in subsequent analysis. This could indicate that the more porous substrate less adversely affected the polydispersity or reflect the increase in initiation sites on the surface.

## 4. Mesophase behaviour of polymeric materials

### 4.1. Sacrificial polymer properties

The sacrificial polymers were subjected to minimal work-up to ensure that the composition remained as similar as possible to that formed *in situ*. The solution reaction mixture was passed through a short alumina column to eliminate the copper catalyst and ligand, and the crude polymer obtained by evaporating the solvent to dryness. This protocol avoids the fractionation of the polymer. The mesophase behaviour was analysed by DSC and POM.

The choice to analyse that sacrificial polymer in the *in situ* composition means that there is, in most cases, a degree of unreacted acrylate monomer present. On the substrate there should not be any persistent monomer present as the substrates were subjected to a washing protocol expected to efficiently remove the low molar mass species.

### 4.1.1. End-on (terminally attached) sacrificial polymer characterisation

#### Differential Scanning Calorimetry

For the reactions with the end-on monomer the thermal behaviour of the crude products was analysed by DSC without further purification as this would result in the fractionation of the polymer distribution. The samples with residual monomer polymerised on heating to the clearing point of the polymer, this resulted in a thermal polymer. The sacrificial crude for polymerisations where the initial analysis showed that the polymerisation had approached completion, and would therefore have a negligible thermal component, were analysed by DSC.

The DSC traces of the sacrificial polymer from Entries **3**, **5**, **6**, **7** and **10** are presented in figures **85**, **86**, **87**, **88**, and **89** respectively. Phases were identified by POM of the polymer from Entries 7 and 10 and previous literature<sup>90, 115, 116</sup> (Figure **85-89**).

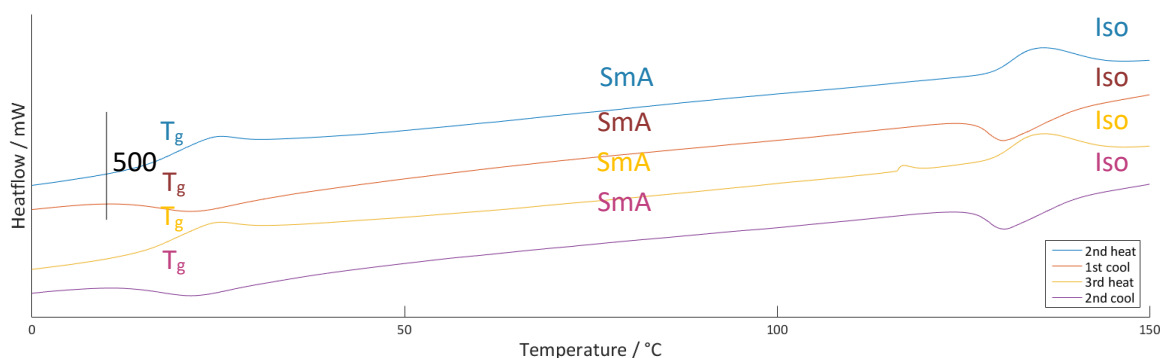


Figure **85**: DSC trace of the sacrificial polymer (1.22 mg) formed in the CuI/Me6TREN catalysed polymerisation of the end-on monomer acrylate (Entry **3**), showing the: second heat (blue), first cool (red), third heat (yellow) and second cooling (purple) cycles.

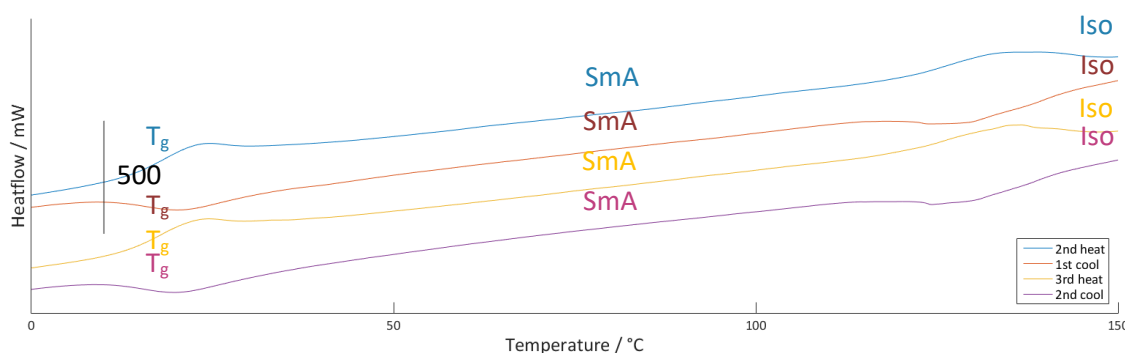


Figure **86**: DSC trace of the sacrificial polymer (1.37 mg) formed in the ARGET-ATRP reaction in the absence of controlled mixing (Entry **5**), showing the: second heat (blue), first cool (red), third heat (yellow) and second cooling (purple) cycles.

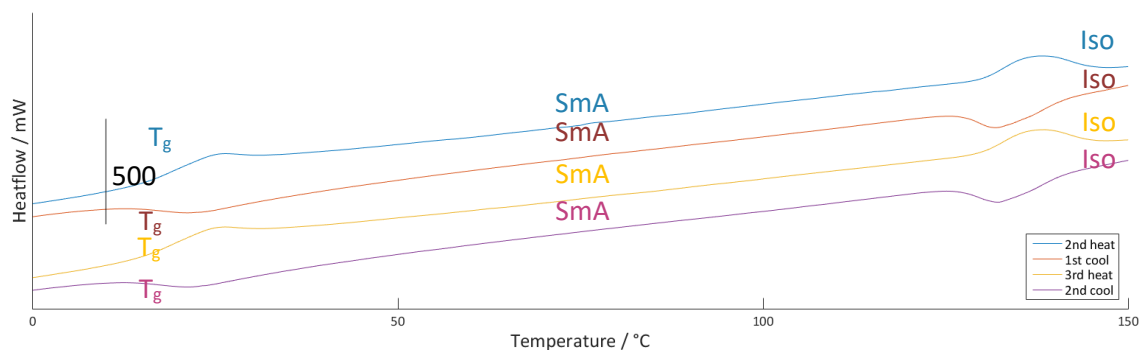


Figure 87: DSC trace of the sacrificial polymer (1.12 mg) formed in the ARGET-ATRP reaction with vacuum assisted mixing (Entry 6), showing the: second heat (blue), first cool (red), third heat (yellow) and second cooling (purple) cycles.

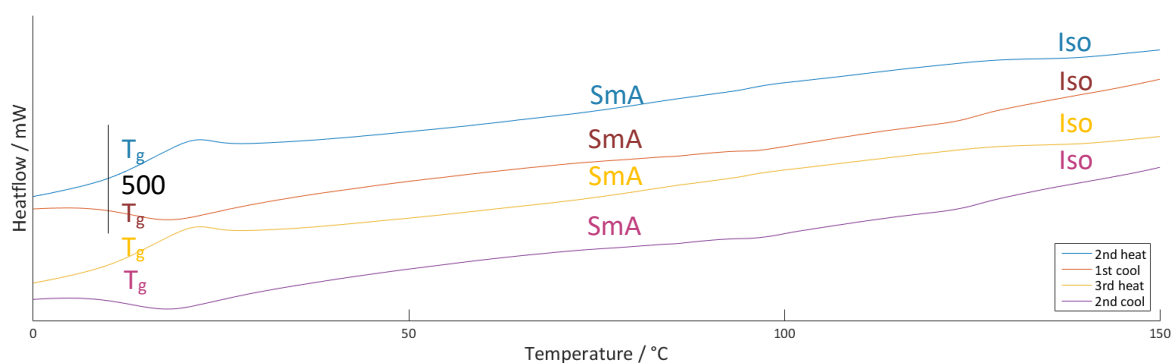


Figure 88: DSC trace of the sacrificial polymer (1.78 mg) formed in the surface initiated (SI) ARGET ATRP of the end-on acrylate monomer (Entry 7), showing the: second heat (blue), first cool (red), third heat (yellow) and second cooling (purple) cycles.

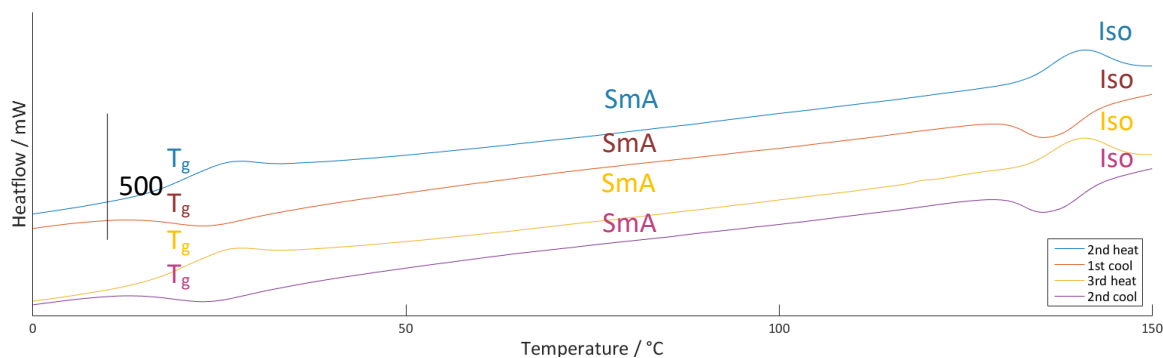


Figure 89: DSC trace of the sacrificial polymer (1.04 mg) formed in ReGC-ESF graft-from ARGET ATRP polymerisation of the end-on acrylate monomer with vacuum assisted mixing (Entry 10), showing the: second heat (blue), first cool (red), third heat (yellow) and second cooling (purple) cycles.

All DSC traces show a glass transition followed by a higher temperature first order phase transition. The phases were identified by POM of entries 7 and 10, and 9 (not presented in DSC due to the low conversion of the monomer), (Section 3.15). The sacrificial polymer from entry 7 (Figure 88) shows broader responses for the Iso-SmA phase transition, which is consistent with the bimodal distribution of the polymer observed in GPC (Figure 55). Due to the polymeric nature of the species, the phase transitions are broad relative to low molecular weight species.

Table 3: Phase transition temperatures of the sacrificial polymers, showing good conversion of the end-on acrylate monomer thermal properties were taken as an average of the first and second cooling cycles, with a cooling rate of 10 °C min<sup>-1</sup>. Transition temperatures were taken from the peak on cooling. The SmA-SmC phase transition could not be observed by DSC.

Entry	Mn	PDI	glass/(SmC)	T / °C	SmA	T / °C	Iso
				$\Delta C_p / J g^{-1} K^{-1}$		$\Delta H / J g^{-1}$	
3	9,730	1.60	●	21.87	●	130.76	●
				(-330.26)		(-5181.21)	
5	7,090	1.88	●	20.54	●	129.8	●
				(-299.50)		(-6019.84)	
6	10,400	1.79	●	22.20	●	132.42	●
				(-284.13)		(-5201.59)	
7	15,200	3.52	●	18.31	●	122.75	●
				(-448.58)		(-562.44)	
10	13,900	3.03	●	23.69	●	136.33	●
				(-327.65)		(-5457.96)	

The similar polydispersity of entries 5 and 6 appear to indicate the importance of the Mn on the glass transition with the higher molar mass polymer 6 showing a higher onset. In contrast the comparably higher molar mass polymer of entries 7 and 10 show a decrease in the glass transition, this is attributable to the decreased packing efficiency due to the higher polydispersity.

On cooling the DSC traces showed the polymer exhibits a mesophase between approximately 140-145 °C and 30-40 °C on both heating and cooling.

## Polarising Optical Microscopy

The sacrificial polymers produced from the stirred ARGET-SIATRP with the side-on monomer from a paper macroinitiator and both reported ARGET-SIATRP from RegC ESF macroinitiators were analysed by POM. These experiments cover the best conditions for each substrate and aid interpretation of the substrate properties for the grafted RegC ESF substrates.

The POM of the sacrificial polymer from all three reactions showed clearly defined focal-conic fan textures. Focal conics exhibiting elliptical and hyperbolic lines of optical discontinuity are characteristic of a SmA phase.

The smectic A texture nucleates in the form of bâtonnets, which coalesce to build up the focal-conic texture, as seen in Figure 91. Within each focal conic domain molecules arrange in smectic layers. The layers arrange around a geometrically inverted torus. The plane of the ellipse is seen side on, resulting in extinctions under POM. Discontinuities result in the observation of the hyperbola (Figure 90).

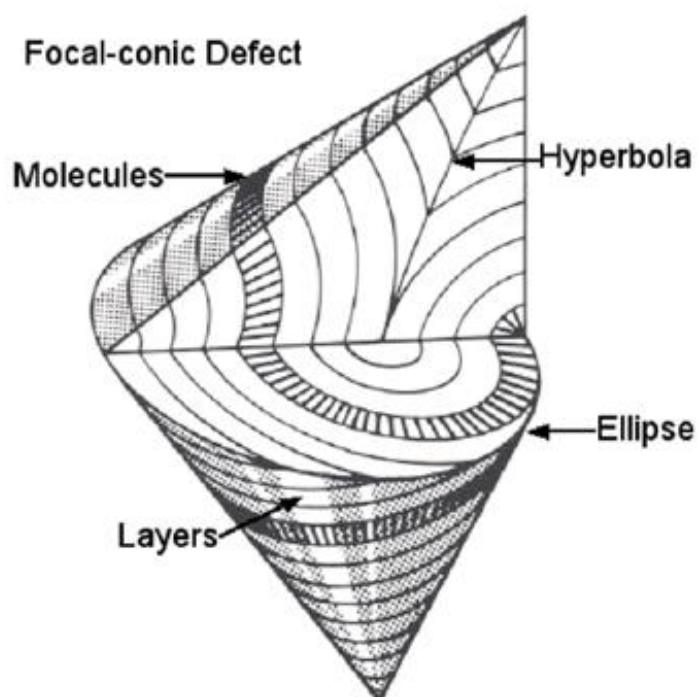
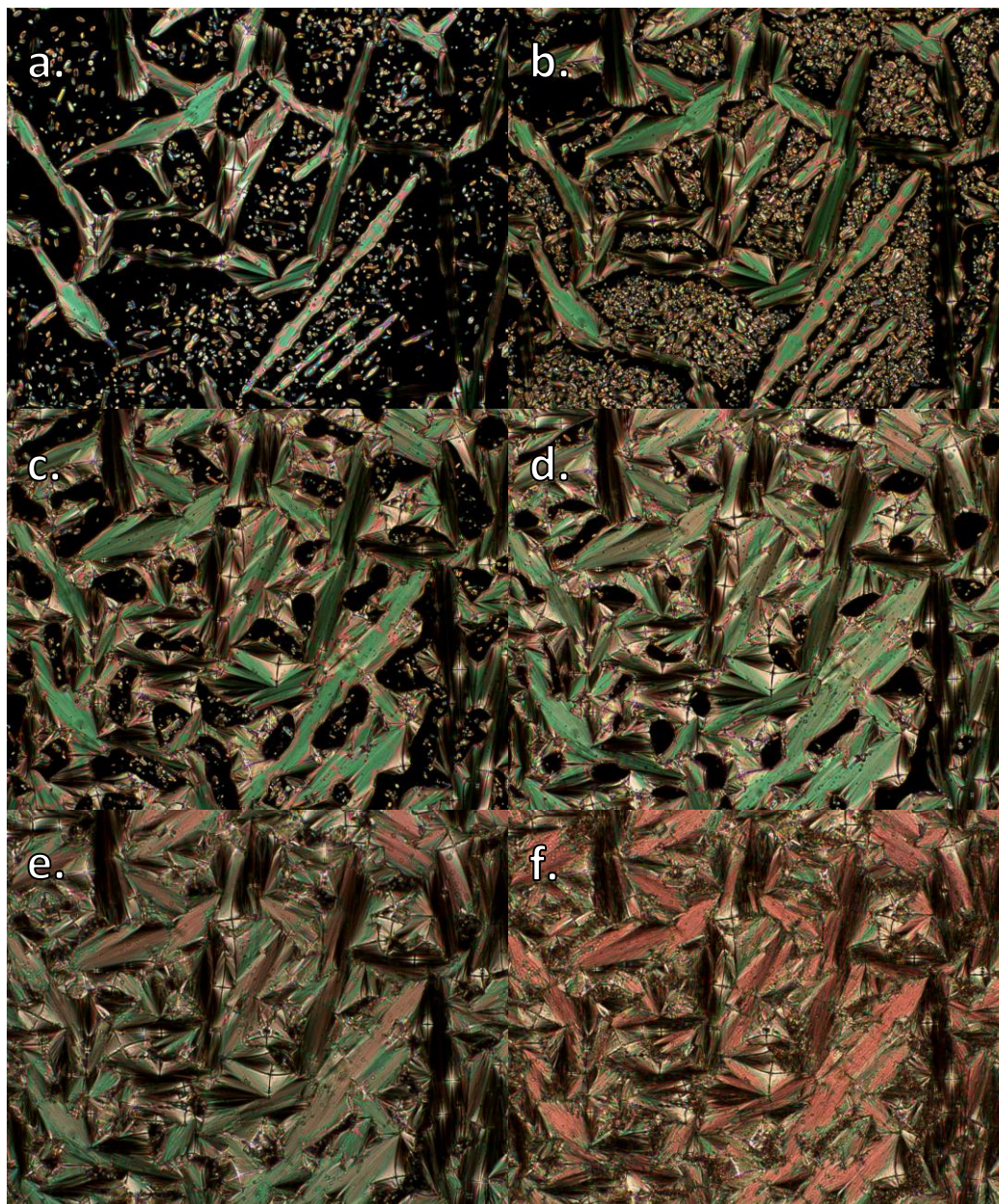


Figure 90: Focal-conic domain and sections through the domain for the case of an ellipse and hyperbola [reproduced from 117].

POM images of the sacrificial polymer obtained from the sacrificially initiated polymerisation in the presence of the paper initiated ARGET ATRP (Entry 7) is shown in figure 91.



*Figure 91: Photomicrographs of sacrificial polymer from the paper initiated ARGET ATRP of compound **2**, with stirring (Entry 7), showing the development of the SmA phase on cooling from the isotropic liquid at 122.3 (a), 117.7 (b), 110.0 (c), 100.5 (d), 92.8 (e), 72.5 (f) °C, at magnification  $\times 100$ .*

The sacrificial polymer from the SI-ARGET ATRP of end-on monomer, **2**, from paper, showed the typical growth a focal-conic fan texture from bâtonnets, to reveal a smectic A texture (Figure 92). The transition occurred over a broad range with two apparent onsets. This corresponds to the DSC results, showing two transitions over this range.

The sacrificial polymer from the SI-ARGET ATRP reaction from RegC ESF with compound **2** in the absence of controlled mixing, shown in Figure 90, showed Maltese crosses at the onset and upon further cooling showed focal conic defects.

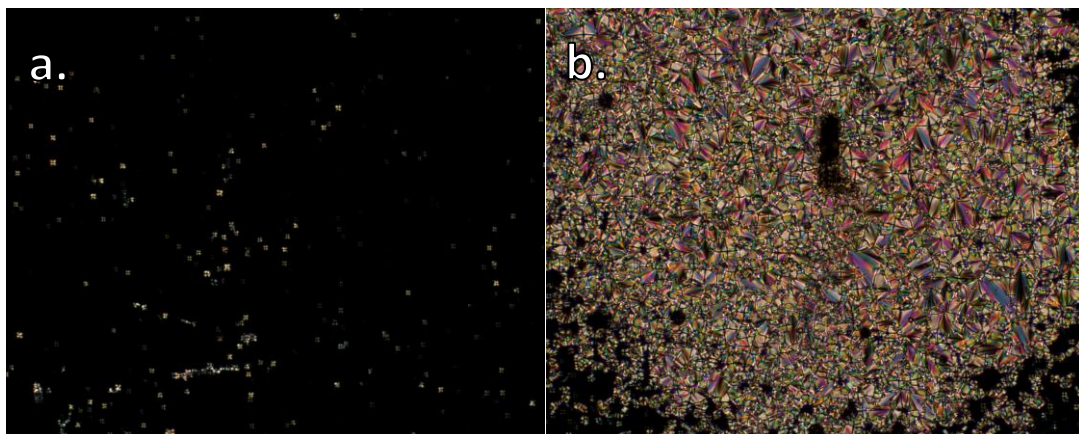


*Figure 92: Photomicrographs of sacrificial polymer from the RegC ESF initiated ARGET ATRP of compound **2**, in the absence of mixing (Entry **9**), showing the development of the SmA phase on cooling from the isotropic liquid at 115.8 °C and 110.0 °C, at magnification  $\times 100$ .*

The sacrificial polymer from the SI-ARGET ATRP of monomer, **2**, from RegC ESF with mixing showed a smectic A phase upon cooling from the isotropic liquid and before the glass, a smectic C phase was observed, identified by 'broken' fans, originating as a result of the tilting of the smectic layers in the fans. An example of the unconstrained polymer showing focal-conic domains is shown in figure **93**, this is able to be observed in polymers due to higher surface tension.

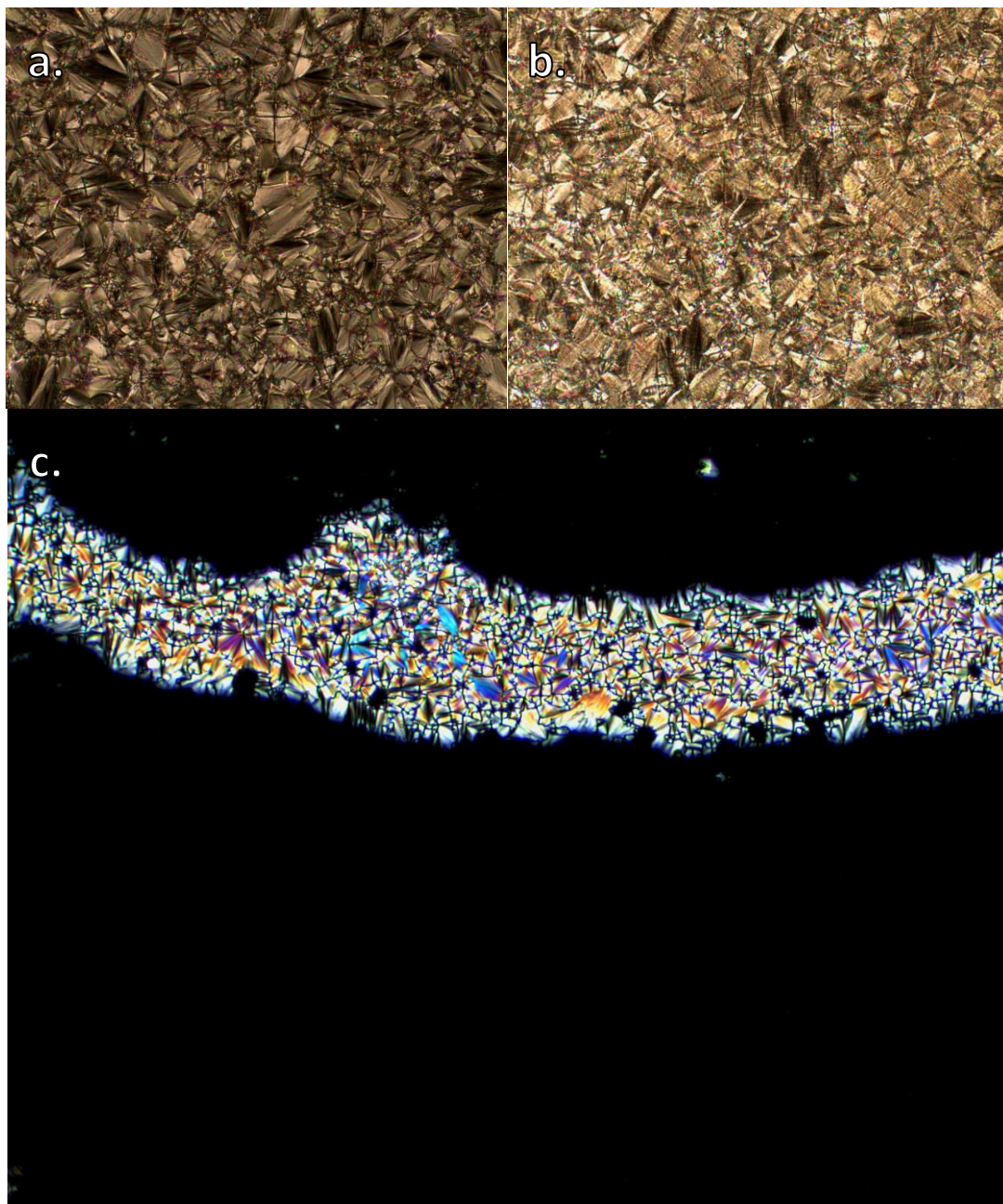


*Figure 93: Photomicrographs of sacrificial polymer from the RegC ESF initiated ARGET ATRP of compound 2, with VALMS (Entry 10), on cooling from the isotropic liquid. Showing a focal conic texture of the SmA phase at 131.9 °C (a) and the broken-fan texture of the SmC phase at 28.8 °C (b) confined between two layers, and the SmA phase at 131.9 °C (c) on a single surface at magnification  $\times 100$ . Note different regions are observed in all photomicrographs.*

Upon cooling each sample analysed showed a frozen smectic texture (Figure 94). For the polymers crystallisation is inhibited. As the mesophase is cooled the thermal energy of the molecules is reduced and the medium becomes less mobile. Eventually molecular motion is frozen out and a glass is formed; if this process occurs quickly enough the molecular arrangement of the mesosphere can be retained, resulting in a more opaque 'frozen' texture.

The phase transition temperatures observed by POM in the polymer films were delayed compared to the transitions measured by DSC, this could potentially be related to the 'slip mechanism' of delayed glassification.<sup>118, 119</sup>

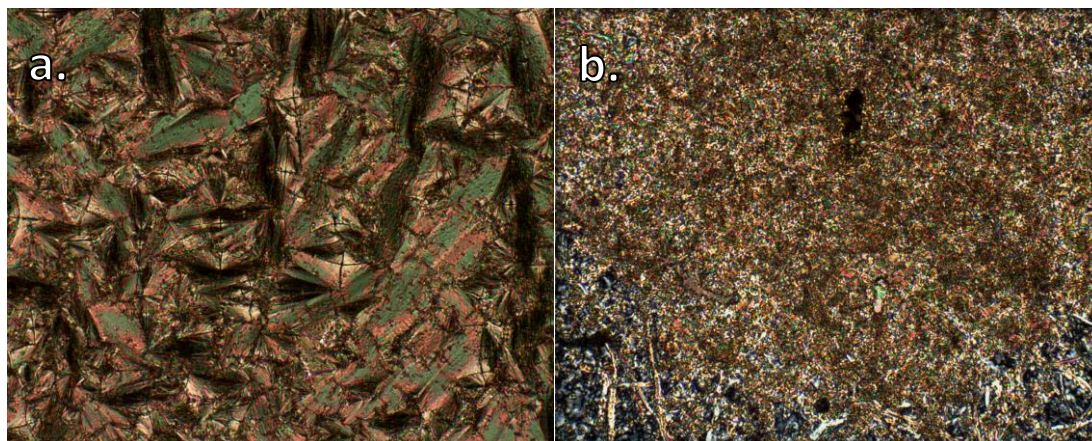


Figure 94: Photomicrographs of the 'Frozen' smectic (glass) phases observed from the cooling ( $\sim 5$  °C (a) and room temperature for one week (b)) of a. paper initiated, with stirring (Entry 7) and b. ESF initiated without mixing (Entry 9) at magnification  $\times 100$ . For the same regions previously observed.

Relating the results from the sacrificial polymers analysis by POM and DSC traces, it can be seen that the end-on (terminally attached) liquid crystal polymers exhibit a smectic A phase.

The observation of the smectic phase for the end-on polymerisations is consistent with the previous work conducted *via* conventional ATRP<sup>90</sup> and other work conducted with the monomer<sup>116</sup>.

A smectic C phase is expected between twenty and thirty centigrade, although this was difficult to observe by POM due to the onset of the glass transition.<sup>90</sup> The broken fan texture of the smectic C was observed for the sacrificial polymer from both well-mixed systems (Entries 9 & 10), a similar phase was observed in the non-mixed ESF polymer, however the domains were too small for a conclusive assignment.

For a side-chain liquid crystal polymer to exhibit a stable liquid crystal phase the antagonistic factors, of the backbone entropy and the mesogenic groups desire to maximise interactions, must be sufficiently decoupled using a spacer unit<sup>15</sup>. From the observations of the phase it is evidence that this is the case for the C<sub>11</sub> spacer with the cyanobiphenyloxy group used in this work.

With end-on, terminally attached, structural units - where decoupling is observed, the spatially restrained mesogenic groups arrange to maximise their interactions, this results in the formation of layers. Sufficiently close adjacent layers can, depending on their specific chemistry, adopt interdigitated or double layers. Where they are not sufficiently close the two parallel layers exist in isolation. The backbone is likely, but not necessarily, accommodated between the layers (Figure 95).

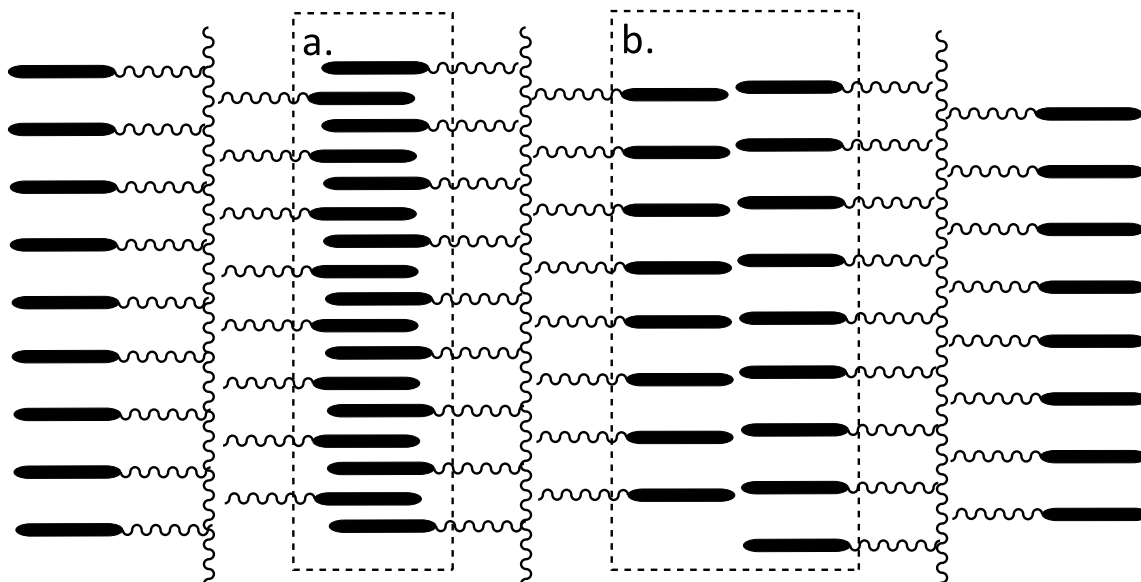


Figure 95: Schematic representation of the interdigitated (a) and double-layer (b) alternatives for mesogenic group

For the cyanobiphenyloxy group used as the mesogenic unit in the end-on side-groups the interdigitated layers are preferable (Figure 95a)<sup>120</sup> as a result of interacting dipoles an interdigitated smectic phase, all else being equal, is preferable to maximise the intermolecular  $\pi$ - $\pi$  stacking and dipole interactions (Figure 96).<sup>121</sup>

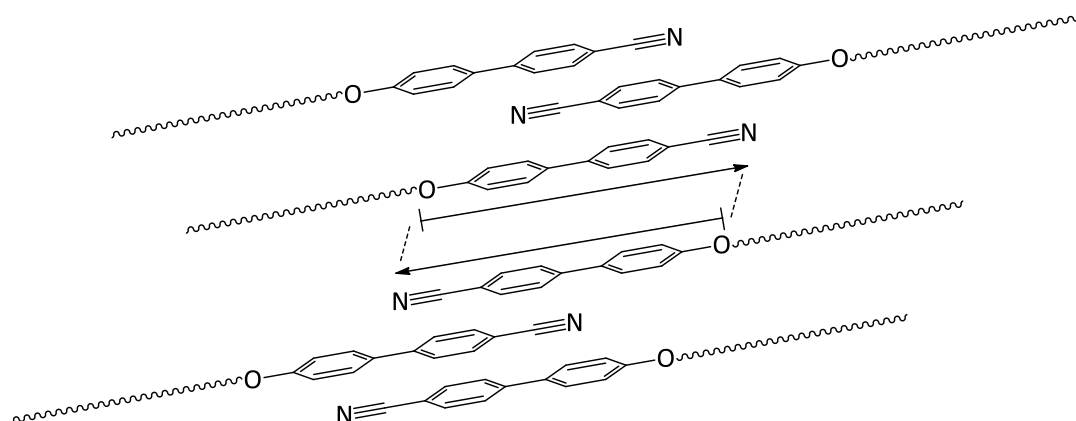


Figure 96: Representation of the intermolecular interactions between adjacent cyanobiphenyloxy groups in an interdigitated smectic phase.

#### 4.1.2. Side-on (laterally attached) sacrificial polymer characterisation

In terms of liquid crystal polymers, the nematic phase is much less common, but is seen in laterally appended side-chain polymers.<sup>122</sup> Where the decoupling of the backbone to the mesogenic unit is significant two trends operate. In the first mechanism the entropy of the backbone is dominant; the backbone entropy disrupts the ability of the mesogenic side-groups to assemble with orientational alignment.<sup>123</sup>

In the second mechanism, the interactions between the side-groups are dominant. In order to maximise these interactions, the backbone is forced to straighten out to allow the side-groups to adopt their preferred positions relative to their neighbours. Once the lateral arrangements of the neighbouring side-groups has been established, any orientational behaviour results in a smectic phase.

In order to form the nematic phase the backbone must be decoupled from the mesogenic unit, by a sufficiently long and flexible spacer. In end-on systems the increase of the spacer tends to destabilise the nematic phase with respect to the smectic phase, as would be expected of small molecule systems; where the spacer increases the favourability of segregating the aliphatic and aromatic components leading to smectic layering. The favourability of laterally attached side-groups towards the nematic phase offers an alternative approach.

It has been reported previously that the side-on (laterally attached) liquid crystal elastomers prepared from laterally attached acrylate mesogen **6**, show the nematic phase.<sup>99</sup>

Polymerisations were performed using the laterally attached acrylate mesogen under ARGET-ATRP conditions (Sections **3.8** & **3.17**). The sacrificial polymers were analysed for their mesogenic properties to elucidate our understanding of the grafts achieved on the surface.

#### Differential Scanning Calorimetry

The sacrificial polymer from the polymerisations with the side-on monomer were analysed by DSC. As with the reactions with the end-on monomer no attempt was made to purify the polymer. The crude sacrificial polymers showed that the polymerisations had approached completion therefore both were analysed by DSC.

The DSC traces of the sacrificial polymer from Entries **8** and **11** are presented in figures **97**, and **98** respectively. Phases were identified by POM. It should be noted that the phase transitions are, due to the polymeric lengths, broad.

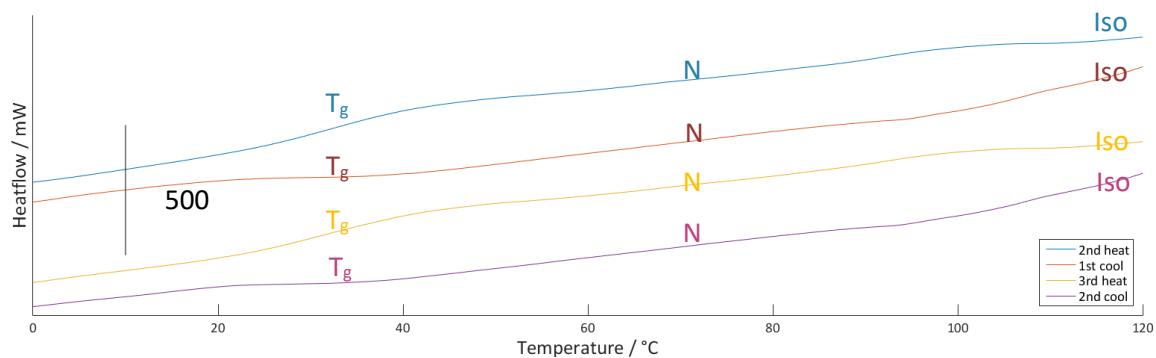


Figure 97: DSC trace of the sacrificial polymer (1.63 mg) formed in the surface initiated (SI) ARGET ATRP of the side-on acrylate monomer (Entry 8), showing the: second heat (blue), first cool (red), third heat (yellow) and second cooling (purple) cycles.

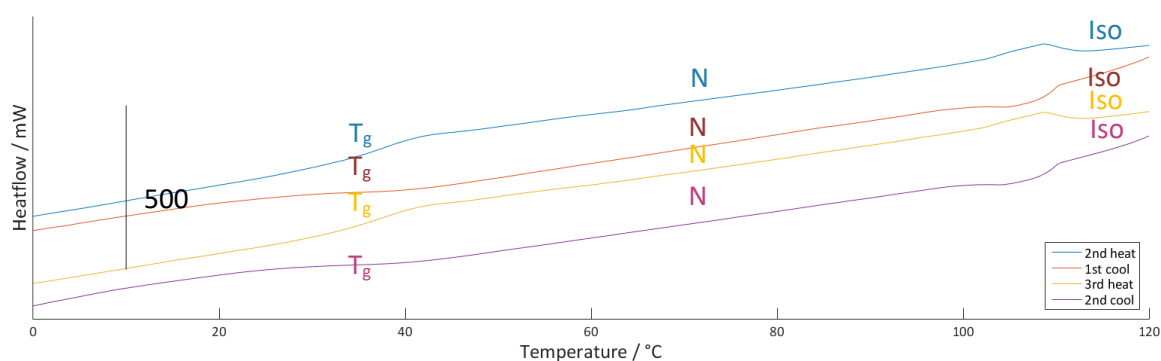


Figure 98: DSC trace of the sacrificial polymer (2.28 mg) formed in the ReGC-cellulose ESF graft-from ARGET ATRP polymerisation of the side-on acrylate monomer with vacuum assisted mixing (Entry 11), showing the: second heat (blue), first cool (red), third heat (yellow) and second cooling (purple) cycles.

The transitions observed by DSC are summarised in Table 4.

Table 4: Phase transition temperatures of the sacrificial polymers, showing good conversion of the side-on acrylate monomer thermal properties were taken as an average of the first and second cooling cycles, with a cooling rate of 10 °C min<sup>-1</sup>. Transition temperatures were taken from the peak on cooling.

Entry	Mn	PDI	glass	T / °C	N	T / °C	Iso
				$\Delta C_p / J g^{-1} K^{-1}$		$\Delta H / J g^{-1}$	
8	4,610	3.56	●	29.45	●	95.18	●
				(-271.23)		(-2532.45)	
11	5,020	1.55	●	34.71	●	105.91	●
				(-252.97)		(-1347.75)	

The higher polydispersity and lower polydispersity sacrificial species produced in the polymerisation with the paper and ESF substrates respectively both showed similar phase transition. The lower Mn, higher PDI sacrificial species from entry 8 had reduced phase transition temperatures as would be expected. On cooling, the DSC traces showed the polymer had a mesophase, assigned as the nematic by POM, between approximately 110 °C and 35 °C on both heating and cooling.

### Polarising Optical Microscopy

The sacrificial polymers from all reported experiments with the side-on monomer were analysed by POM. Figures **99** and **100** show photomicrographs of the sacrificial polymer entries **8** and **11**, on cooling, respectively.

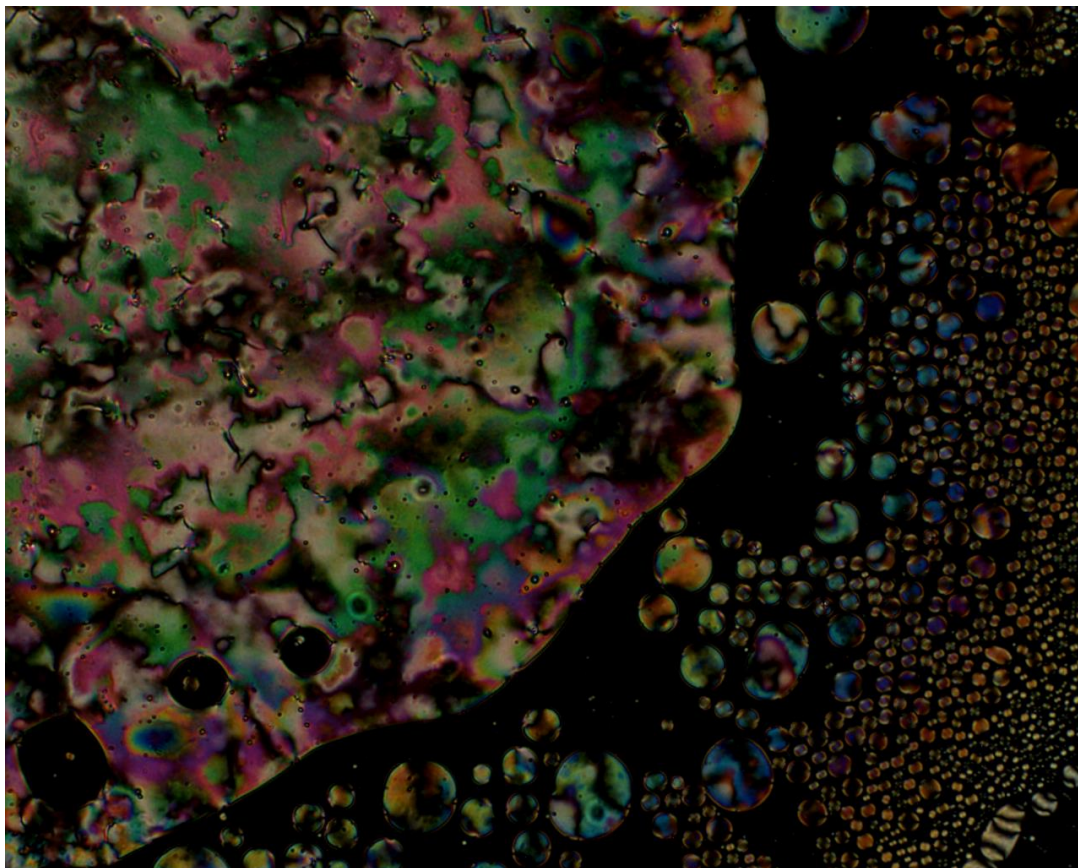


*Figure 99: Photo micrographs of sacrificial polymer from the paper initiated ARGET ATRP of compound 6, with stirring, on cooling from the isotropic liquid at 103.6 °C on a single surface at magnification  $\times 100$ .*

The POM of the sacrificial polymer from the graft-from polymerisation with laterally-attached side groups showed nematic mesophases. This is consistent with previous literature<sup>99</sup> and work within the group. The sacrificial polymer formed from the paper reaction showed large nematic domains with some elongated defects. Typical nematic droplets were identified, growing from the isotropic (Figure 99). These identified the phase as the nematic phase unequivocally. For the sacrificial polymer from the RegC ESF macroinitiator a characteristic nematic Schlieren texture was observed. As with the focal-conic phase, discussed in Section 4.1.1., disclinations are seen in nematic phases, this results in the Schlieren texture observed. Nematic regions (domains), with an average director, grow until they meet each other. At the interface of two nematic domains a conflict arises causing the molecular alignments to pass through an extinction orientation. These extinction, or disclination, regions can result in either 4- or 2- brush defects. The Schlieren texture observed showed 4-brush and 2-brush defects with both positive and negative singularities representing both directions that the director rotates, these were confirmed by varying the angle between the polarisers (Figure 100). The nematic phase is unambiguously assigned to the sacrificial polymer from the RegC ESF macroinitiator and for the sacrificial polymer from the paper macroinitiator.

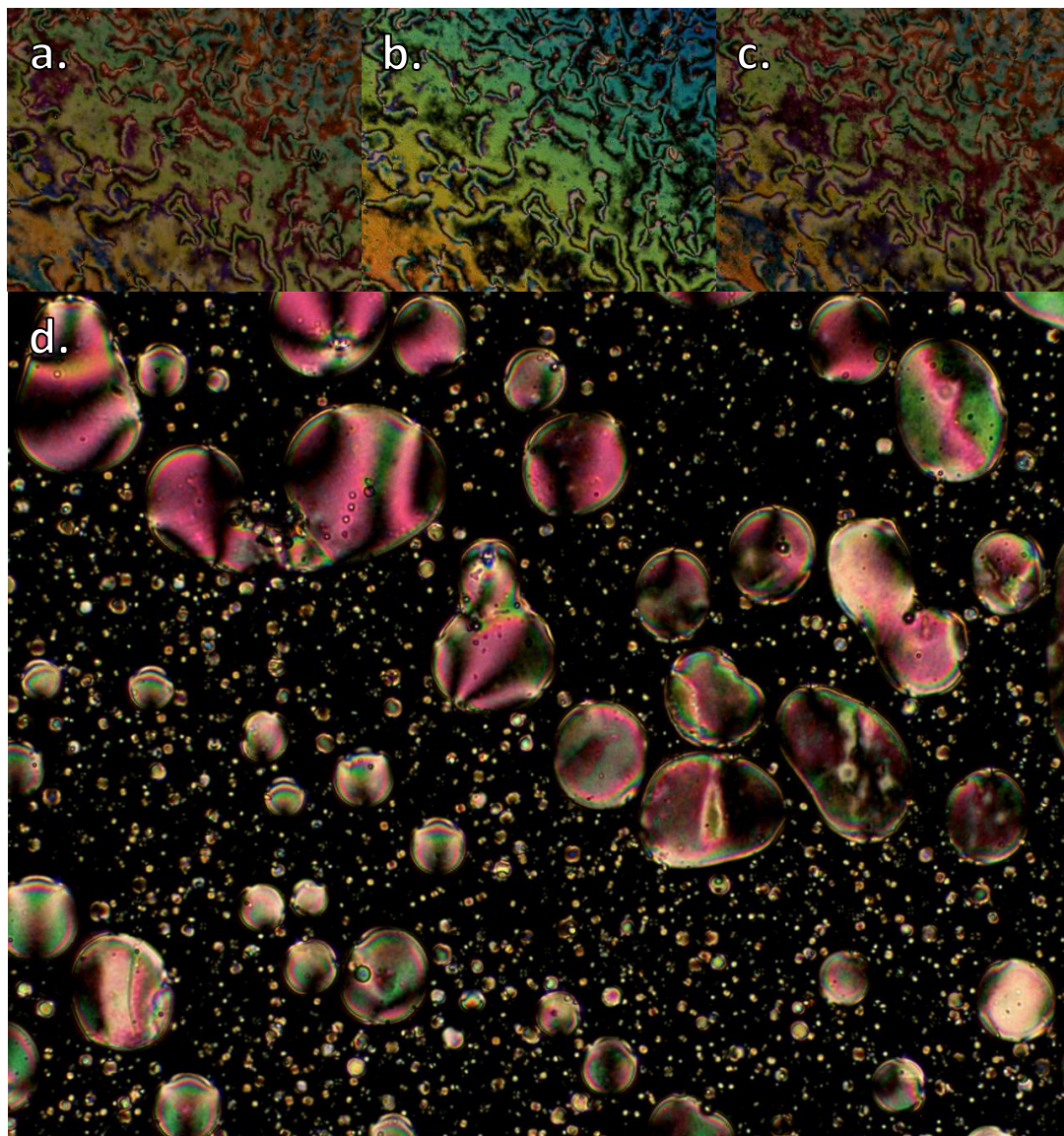


*Figure 100: Photo micrographs of sacrificial polymer from the RegC ESF initiated ARGET ATRP of compound 6, with VALMS, with the cross polarisers at 50° (a), 90° (b) and 130° (c) and at 105.0 °C and on cooling from the isotropic liquid at 105.5 °C under crossed polarisers (d) at magnification  $\times 100$ .*

Upon cooling both samples below the glass transitions, a frozen nematic texture was observed (Figure 101). This texture results from the same physical process as the ‘frozen’ smectic discussed in Section 4.1.1.

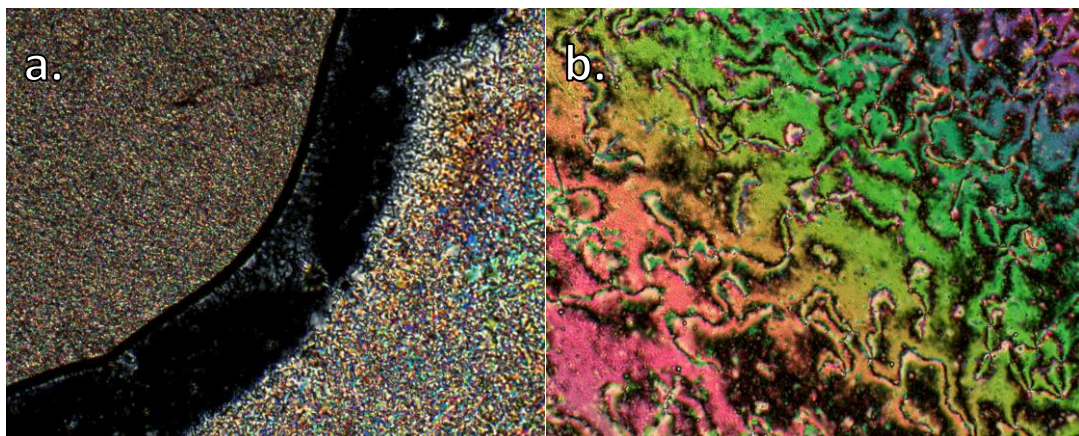


Figure 101: Photomicrographs of the 'Frozen' nematic (glass) phases observed from cooling ( $\sim 5$  °C (a) and room temperature for one week (b)) of sample paper initiated (a), and RegC initiated (b) ARGET ATRP at magnification  $\times 100$ .

The phase transitions observed by POM for the laterally-attached side-group polymers agreed more closely with the transition ranges measured by DSC than the terminally-attached side-group polymers.

The contribution of undesired C5 spacer in the ratio C4 to C5 of 13.8:1 has not been sufficient for the odd-even effect to prevent the nematic phase, previously observed for the liquid crystal elastomer with the same monomer.<sup>99</sup>

For laterally attached side-group polymerisations with acrylates, the lateral unit length is significantly great than the increase in backbone length.

A consequence of the resulting bulk is that the mesogenic side-groups are offset against, but still overlapping, the next side-group along the chain. In order to accommodate the neighbouring mesogenic group it is likely that the side-groups are not at regular angular positions around the backbone. This results in the jacketing of the polymer and only the nematic phase is observed. The nematic phase observed in this work is therefore the result of positive coupling in the N phase.<sup>124</sup> The N phase tells us that the backbone polymer is prolate - lengthened in the direction of the director.

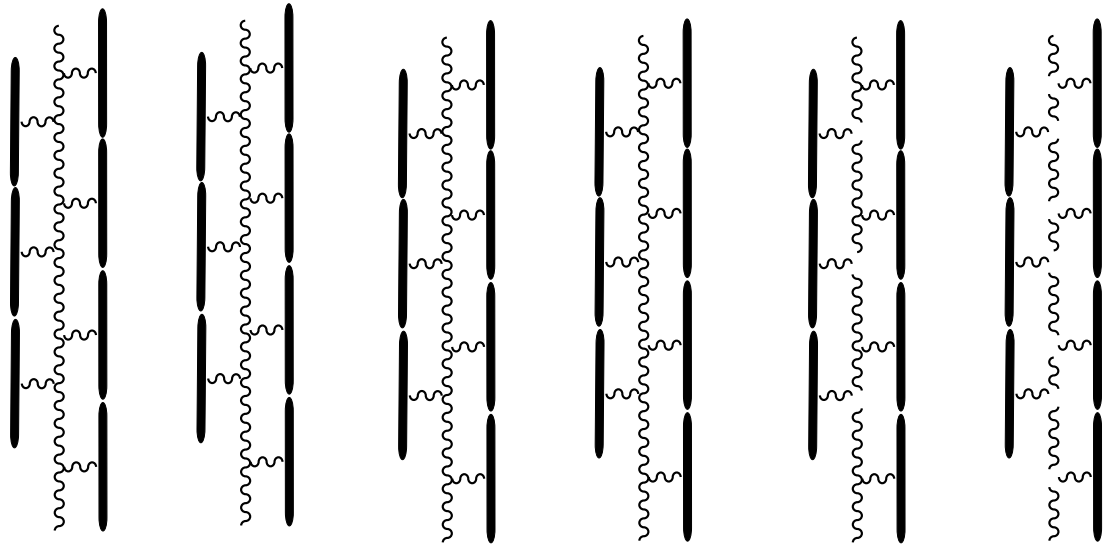


Figure 102: Schematic representation of the backbone jacketing by laterally attached mesogenic side-groups.

#### 4.2. Properties of the substrate from the ReGC-ESF graft-from ARGET ATRP polymerisation of the end-on acrylate monomer in the absence of controlled mixing (Entry 9).

A thin region of the electrospun fibre substrate from the unmixed graft-from polymerisation of monomer, **2**, was analysed for birefringent character by POM (Figure 103).

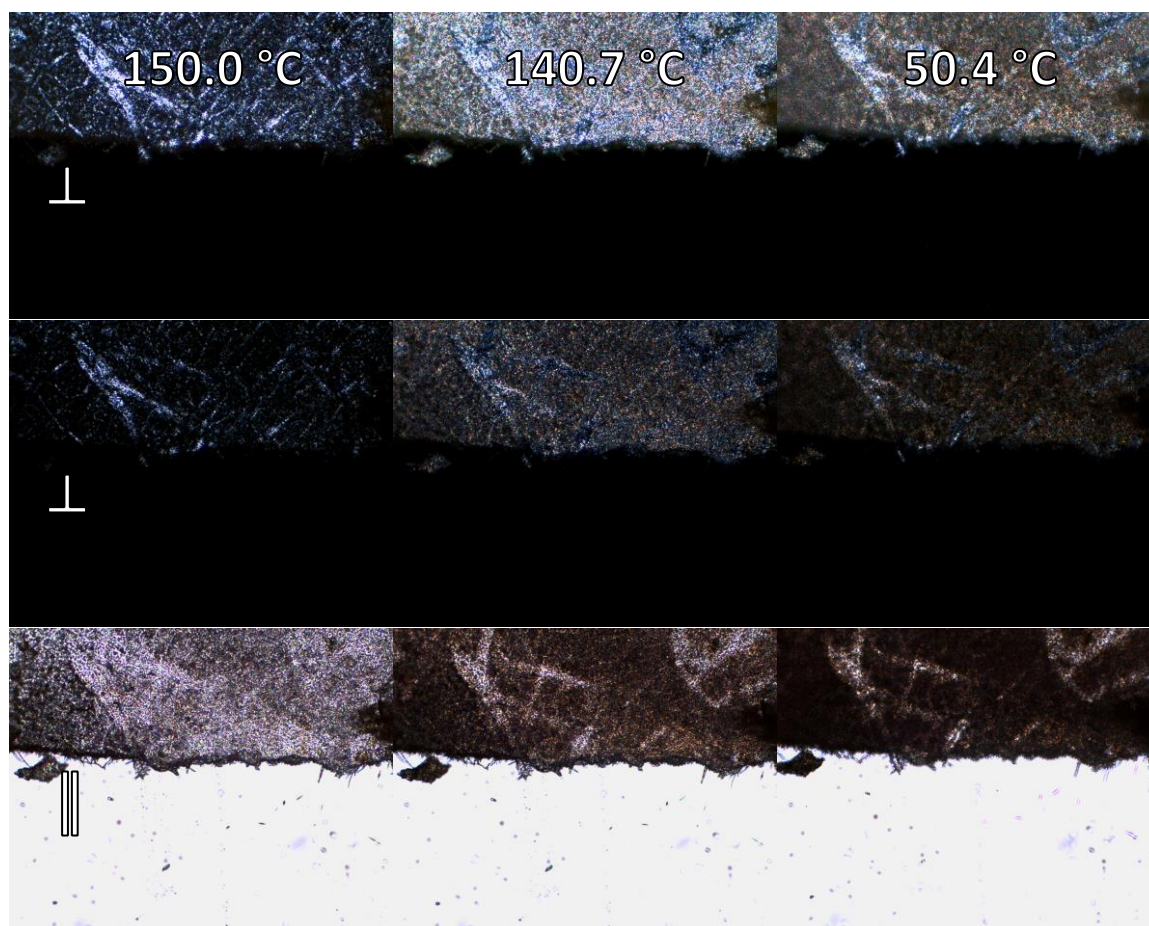


Figure 103: Photomicrography of substrate **14** taken at (left to right) 150.0 °C, 140.7 °C and 50.4 °C at (from top to bottom) 1008 ms exposure, crossed polarisers, 304 ms exposure crossed polarisers and 144 ms exposure parallel polarisers. All photomicrographs were taken with the bright field at the same illumination.

From observation by POM it is apparent that the substrate has birefringent character. The domains present are too small to obtain a positive characterisation by POM. The lack of domain growth is likely due to the nanofibers acting as defects preventing the growth of extended domains.

In order to try and interpret whether the birefringence is resulting from surface LCP the previous tested washing technique was used (Section 3.14). FT-IR and SEM show that polymer is present on the surface (Figures 74 & 76). Whether the source of the polymer is physisorption, chemical grafting or a combination remains ambiguous (Section 3.14).

The background birefringence of the RegC ESF was ascertained with the unactivated RegC ESF. Regardless of the source of the polymer, it is evident that the interactions with the surface are not preventing additional birefringent character. On cooling the substrate became less transparent, potentially indicating a glass.

The introduced birefringence disappears on heating to 150 °C and reappears on cooling below 142.5 °C, and continues to be observed, with some reduction in the definition of the texture and reduced transmittance of light through the substrate, to room temperature. The observations correspond accurately with the transition onset temperatures observed by DSC.

The adsorption of the polymer on the surface is not homogenous; which agrees with the observations, on the local scale, by SEM (Figure 76).

The specific sacrificial polymer from this reaction is not appropriate for direct comparison as there is a low component of polymer (and a lot of monomer), regardless of the method of accumulation only the polymer is expected to be retained on the surface after the washing of unreacted monomer.

### 4.3. Properties of the substrate from the ReGC-ESF graft-from ARGET ATRP polymerisation of the end-on acrylate monomer with VALMS (Entry 10).

As with Entry 9, a thin region of the electrospun fibre substrate from the unmixed graft-from polymerisation of monomer, 2, was analysed for birefringent character by POM (Figure 104).

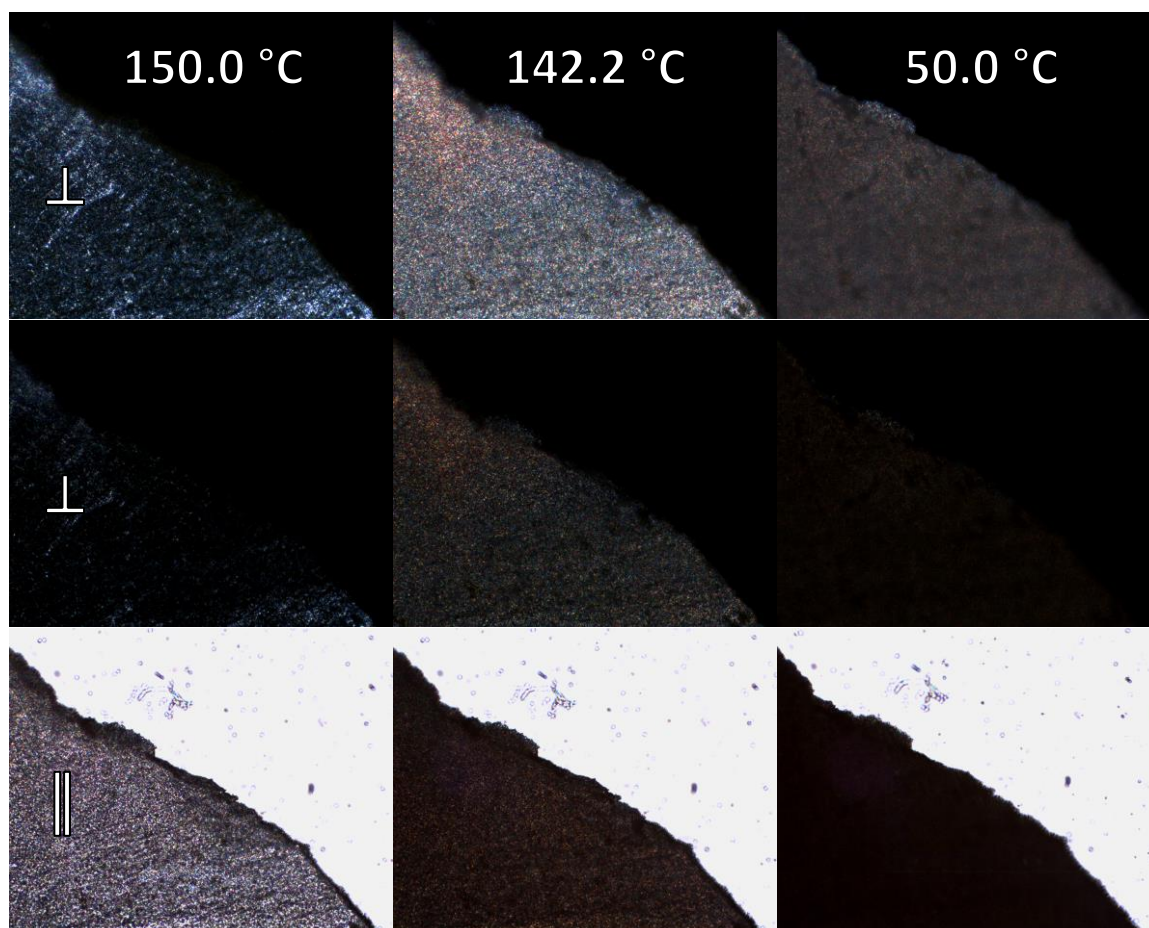


Figure 104: Photomicrography of substrate 15 taken at (left to right) 150.0 °C, 142.2 °C and 50.0 °C) at (from top to bottom) 1008 ms exposure, crossed polarisers, 304 ms exposure crossed polarisers and 144 ms exposure parallel polarisers. All photomicrographs were taken with the bright field at the same illumination.

At 150 °C the substrate appeared dark under cross-polars with residual birefringence from the cellulose background (as ascertained for Section 4.2). Cooling the fibres saw the emergence of birefringence, as with the previous non-mixed polymerisation (Section 4.2). Differing from the non-mixed polymerisation substrate, the cellulose birefringence of the fibres was obscured by the additional incoming birefringence contribution. This is consistent with the increased homogeneity observation by SEM (Figure 80) and interpretation of a more even effective coverage. As with the substrate produced by the un-mixed method the birefringent character assigned to the polymer became less transparent upon further cooling, this is consistent with a glass transition as was observed in the sacrificial polymer. An increased melting point for the glass on both substrates

could potentially be understood in terms of more order chains resulting from the tethering process.

Relative to the non-mixed polymerisation conditions, the substrate produced showed a more homogenous distribution of the adsorbed polymer. This is consistent with the observations by SEM. In the non-mixed substrate, high loadings or deposition events were seen in some regions with sparse/no covering of other regions, by contrast the mixed polymerisation showed a substrate with a more homogenous coating, with reductions in the birefringence extremes.

#### 4.4. Properties of the substrate from the ReGC-ESF graft-from ARGET ATRP polymerisation of the side-on acrylate monomer with VALMS (Entry 11).

The POM of the electrospun fibres obtained from the laterally-attached monomer graft from ReGC ESF (Section 3.17) are shown in Figure 105.

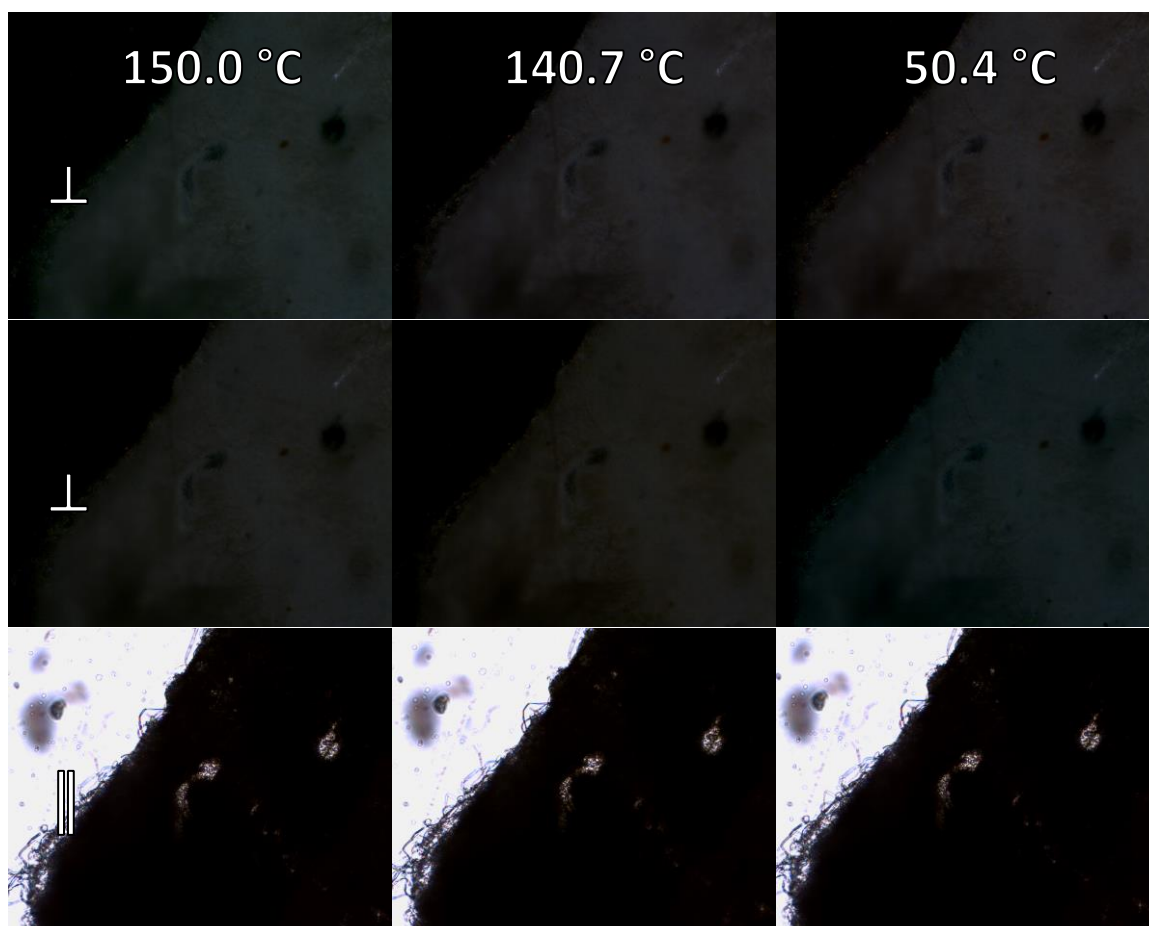


Figure 105: Photomicrography of substrate **16** taken at (left to right) 150.0 °C, 140.7 °C and 50.4 °C) at (from top to bottom) 1008 ms exposure, crossed polarisers, 304 ms exposure crossed polarisers and 144 ms exposure parallel polarisers. All photomicrographs were taken with the bright field at the same illumination.

The development of an appropriate washing technique confirms that polymer present on the surface is the chemically grafted laterally-attached polymer. It was observed that the sacrificial polymer showed a broad nematic phase, for the side-on graft from polymerisation with RegC ESF initiator as the primary substrate. The substrate was heated to 150 °C and returned to room temperature, with observation under a polarised optical microscope. The substrate showed no visible birefringent character, this is counter to the expectations from the sacrificial polymer.

The degree of polymerisation for the side-on monomer is, confirmed by the sacrificial polymers to be, less than that for the end-on monomer. It could be the case that the sacrificial polymer loading is not sufficient for birefringence to be observed.

The nematic phase exhibited by the LCP is deduced to originate from macromesogenic units. In order to ensure the nematic phase can be supported it might prove necessary to introduce spacers for the macromesogens, to separate the LCP and surface systems. This has previously been achieved with cellulose macro-initiated graft-from liquid crystal polymers in the group.<sup>90</sup> The previous work shows the potential of grafted block copolymers constituted from PMMA and liquid crystal polymer.

It is possible the addition of surface constraints could impede the less ordered nematic phase. High density polymer brushes, achievable by SI-ATRP, can induce ordering in the form of chains stretching to minimise the free energy.<sup>10, 11</sup> If this is occurring then lower the graft density would be expected to relieve some of the graft-chain stretching,<sup>125-127</sup> and potentially allow the chains to 'relax' into the 'mushroom' regime which would allow for arrangements similar to the free N<sub>III</sub> phase to be adopted.<sup>49</sup>

Close to the surface it would be expected that the backbone influence would be significant as high density grafts represent a confined system. As the polymer becomes elongated the early backbone might act to reduce the surface influences on the more distant parts of the polymer.<sup>128</sup> It could be the case that the side-groups have not been sufficiently decoupled from the surface to have a persistent mesophase in spite of the successful surface grafting. If the less ordered nematic phase is being impeded by tethering, the grafting of MMA-SCLCP block co-polymers, as previously conducted with terminal side-group from paper,<sup>90</sup> or longer chains might provide a route to decoupling the nematic LCP from the surface.

#### **4.5. Liquid Crystal behaviour conclusions**

Birefringence was observed for the RegC derived substrates produced in the graft-from polymerisations with the end-on monomer. The birefringence changes were consistent with the transitions observed for the sacrificial polymer by DSC, this implies that the phase properties were maintained. A more homogenous coating of the substrate was achieved using a vacuum induced bubbling alternative to mechanical stirring.

Unambiguous assignment of the polymer adsorption as either, physisorbed polymer, grafted polymer or a combination of the two was not possible with the washing regime used. The chemical similarities of the paper and cellulose substrates, combined with the control reactions and observed polymer pooling by DSC make it likely a combination of the two is being observed.

The substrate produced by the SI-ATRP of the side-on monomer from the RegC ESF showed no birefringent character; the birefringence observed in the RegC ESF was suppressed by the polymer and no polymer birefringence was observed. Our control conditions provide us with confidence that retained polymer is a result of grafting. It is therefore possible that the polymer tethering is suppressing both sources of birefringence.

From the lack of birefringence in for the laterally attached SCLCP, questions are raised as to whether any birefringence would be observed for the terminally attached surface where all physisorbed polymer to be washed under conditions confirmed to remove physisorbed polymer.

Different polymer cross-sectional areas, degrees of polymerisation are both factors that could affect the demonstration of birefringent behaviour.

## 5. Conclusion

The ARGET-ATRP and preceding ATRPs in this work demonstrate a proof of principle; no attempt has been made to optimise the conditions beyond that necessary to demonstrate successful grafting of polymer. To the best of our knowledge this work contains the first example of a nematic LCP being grafted at a cellulose surface and contains the first LCP grafts at (specifically from a cellulose) electrospun fibre graft reactions have been performed for both nematic and smectic LCPs.

For stirred substrates  $\text{Cu}^{\text{I}}/\text{Me}_6\text{TREN}$  was used to produce polymers with a measured polydispersity of 1.60.

Successful application of ARGET ATRP allowed us to utilise the reportedly favourable polymeric control of  $\text{Cu}^{\text{II}}/\text{PMDETA}$  systems, including low catalytic loadings and increased oxygen tolerance. The use of  $\text{Cu}^{\text{II}}/\text{PMDETA}$ , ascorbic acid and anisole/toluene under vacuum has been demonstrated to allow graft-from polymerisations, with gentle solvent mediated mixing, in the absence of mechanical stirring, resulting in more homogenous coverage.

Having established favourable conditions PDIs of 3.52 from paper and as low as 3.03 for the polymer grafts from ESFs with a laterally-attached side groups LCP. For the terminally-attached side-group graft from paper and ESF polydispersities of 3.56 and 1.55 were achieved under similar conditions.

The ESF from the SI-ARGET-ATRP of the end-on monomer exhibited birefringence, for a temperature range corresponding to the nematic phase of the sacrificial polymer. With the side-on monomer, no birefringence was observed despite the sacrificial polymer exhibiting a nematic phase. It is not clear if the discrepancy arises from the terminally attached LCP demonstrated birefringence resulting from physisorbed sacrificial polymer or if the grafted laterally-attached side-group LCP is inhibited likely due to a lower degree of polymerisation.

This work has demonstrated the adsorption of LCPs with laterally-attached and terminally-attached side groups, which in the bulk show nematic and smectic phases respectively at the cellulose ESF surface including the confident interpretation of grafting for the laterally-attached LCP.

### 5.1. Future Work

In order to make a quantitative assessment of the sacrificial polymers used to monitor the reactions in this study, the samples have been retained to allow for fresh analysis once instrumental issues have been resolved.

The conditions presented in this work have not been optimised, further optimisation of both the reagent ratios and solvent ratios are required. It is well reported that the solvent composition can have significant effects on the rate of ATRP reactions, so optimisation of reagent ratios will be best performed once the solvent ratios have been established. Both  $\text{Cu}^{\text{I}}/\text{Me}_6\text{TREN}$  and the ARGET ATRP conditions warrant further investigation for stirred and VALMS conditions respectively.

In order to differentiate the effects of physisorbed and chemically grafted LCP, it will be vital that a rigorous washing technique is developed for each SI-ATRP process and variant. The terminally attached LCP washing from ESF is one such process. Boiling toluene was used for the washes presented; having indicated a potentially improved wetting of the surface anisole (as used as the reaction solvent) may prove more successful at displacing physisorbed LCP.

## **6. Experimental**

Percentage yields were calculated from the moles of obtained product as a comparison to the moles of limiting reagent in the reaction.

All reagents and solvents used in the synthesis of the monomers and in the dispersion polymerisations were readily available commercially and were used as supplied without any further purification. Accurate weights were obtained using a Mettler Toledo XS 105 dual range balance.

### **6.1. Chemical analysis and purification**

#### **6.1.1. Nuclear Magnetic Resonance (NMR) Spectroscopy**

<sup>1</sup>H NMR spectra were recorded using a JEOL EX400 NMR Spectrometer operating at a frequency of 400 MHz, all monitoring NMRs were conducted on 1024 scans. <sup>13</sup>C NMR spectra were recorded using a JEOL EX400 NMR Spectrometer at a frequency of 100 MHz. The  $\delta$  values were recorded in ppm, relative to the residual protic solvent peak, and the coupling constants quoted in Hertz (Hz).

#### **6.1.2. Fourier Transformed Infrared (FT-IR) Spectroscopy**

FT-IR analyses were conducted on a Shimadzu IR Prestige-21 FTIR Spectrometer with a Specac "Golden Gate" ATR crystal adaptor.

#### **6.1.3. Mass Spectrometry (MS)**

Mass spectra were recorded using a Bruker micrOTOF MS-Agilent series 1200LC spectrometer (ESI).

#### **6.1.4. High Performance Liquid Chromatography (HPLC)**

High performance liquid chromatography (HPLC) analysis was carried out on a Shimadzu Prominence HPLC composed of a LC-20A liquid chromatograph, a DGU-20A5 and DGU-20B degasser, a CTO-20A column oven, a SPO-20A dual wavelength detector, a CBM-20A communications bus and an C18 column (5  $\mu$ m pore size, 10  $\times$  250 nm).

#### **6.1.5. Scanning Electron Microscopy (SEM)**

Scanning electron microscopy (SEM) photomicrographs were taken in the Biology Technology Facility at the University of York. For SEM, the samples were mounted on conductive stubs with silicon wafers and sputter coated with approximately 7 nm of gold/palladium using a Quorum SC7640 sputter coater before being analysed with a JEOL JSM6490-LV instrument, operating under high vacuum in secondary electron mode at 5 kV, with a working distance of 10 mm.

### **6.1.6. Gel Permeation Chromatography (GPC)**

Gel Permeation Chromatography (GPC) was completed using a triple detection GPC fitted with a Viscotek VE3580 RI detector and a Viscotek 270 dual detector with a 670 nm laser and a 100  $\mu\text{L}$  viscoGEL™ column with THF as the mobile phase against a polystyrene standard (PolyCAL™ Polystyrene Standard PS99K) at a flow rate of 1 mL min<sup>-1</sup>.

### **6.1.7. Thin Layer Chromatography (TLC)**

Merck TLC Silica Gel 60 F254, aluminium sheets were used for thin layer chromatography. TLC plates were examined using a UVGL-58 lamp that emits light at 254 or 365 nm.

### **6.1.8. Column Chromatography**

Column Chromatography was used to purify materials and was carried out using Fluka, 70-230 mesh silica gel with a 63-200  $\mu\text{m}$ . When desirable increased flow rate was achieved *via* the use of dry vacuum flash column chromatography.<sup>129</sup>

## **6.2. Characterisation of Liquid Crystal behaviour**

### **6.2.1. Polarising Optical Microscopy (POM)**

A Zeiss axioskop 40 polarised light microscope with a Mettler Toledo FP82HT hotstage and Mettler FP90 CPU was used to investigate the mesomorphic behaviour of the compounds and mixtures described herein. Photomicrographs were captured using an InfinityX 21 Megapixel digital camera with Infinity Capture Software at a magnification of 100 times.

### **6.2.2. Differential Scanning Calorimetry (DSC)**

A Mettler Toledo DSC 822e equipped with an autosampler operating with Star<sup>e</sup> software was used to observe phase transitions temperatures of the sacrificial liquid crystal polymers synthesised and to calculate the associated enthalpies. The instrument was calibrated using an indium standard of mass 6.36 mg,  $\Delta H = 28.45 \pm 0.40 \text{ Jg}^{-1}$ , onset  $156.56^\circ\text{C} \pm 0.20^\circ\text{C}$ .<sup>130</sup>

### 6.3. Synthesis of Monomers

#### 6.3.1. Compound 1: 4'-((11-hydroxyundecyl)oxy)-[1,1'-biphenyl-yl]carbonitrile<sup>100</sup>

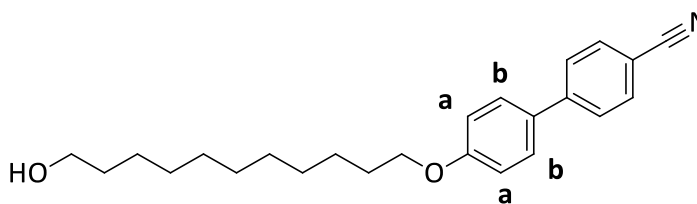


Figure 106: 4'-((11-hydroxyundecyl)oxy)-[1,1'-biphenyl-yl]carbonitrile.

A solution of KOH (1.25 g, 22.3 mmol) and KI (0.24 g, 1.44 mmol) in water (10 mL) was added at once to a stirred solution of 4-hydroxy-4'-cyanobiphenyl (4.25 g, 21.8 mmol) and 11-bromoundecanol (5.60 g, 22.3 mmol) in a mixture of EtOH/water 4:1 (200 mL) the reaction was heated to reflux (20 hours). The solution was cooled to room temperature and the resulting white crystals formed were collect by filtration, washed with cold ethanol and dried *in vacuo*.

Yield: 5.50 g (69.1 %).

<sup>1</sup>H NMR (400 MHz, CDCl<sub>3</sub>) δ<sub>H</sub>: 1.27 – 1.40 (m, 10H, CH<sub>2</sub>), 1.47 (quint, 4H, *J* = 7.9 Hz, CH<sub>2</sub>), 1.57 (quint, 2H, *J* = 6.8 Hz, CH<sub>2</sub>) 1.81 (quint, 2H, *J* = 7.1 Hz, CH<sub>2</sub>) 3.64 (t, 2H, *J* = 6.6 Hz, CH<sub>2</sub>OH) 4.00 (t, 2H, *J* = 6.6 Hz, CH<sub>2</sub>OAr), 6.99 (AA'BB', 2H, *J* = 8.9 Hz, ArH<sub>a</sub>), 7.52 (AA'BB', 2H, *J* = 8.8, ArH<sub>b</sub>), 7.64 (AA'BB', 2H, *J* = 8.4 Hz, ArH), 7.68 (AA'BB', 2H, *J* = 8.4 Hz, ArH).

OH is not observed.

ESI-MS: C<sub>24</sub>H<sub>32</sub>NO<sub>2</sub> calculated [M + H] *m/z* 366.2428, found 366.2417.

FTIR ν cm<sup>-1</sup>: 3281 (C–H Ar), 2920, 2851, 2238 (CN), 2226 (CN), 1711, 1634, 1600, 1581, 1496, 1475, 1408, 1384, 1253, 1183, 1118, 1062, 1008, 991, 976, 896, 862, 854, 838, 811, 780, 740, 724, 674, 663.

### 6.1.1. Compound 2: 11-((4'-cyano-[1,1'-biphenyl]-4-yl)oxy)undecyl acrylate<sup>100</sup>

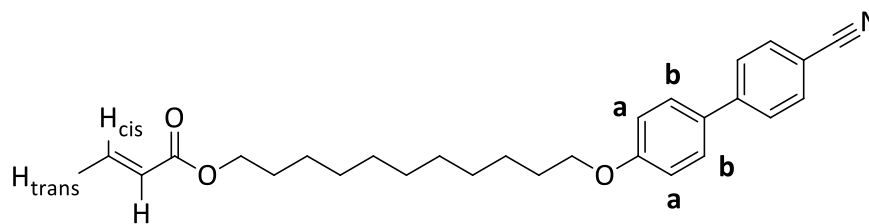


Figure 107: 11-((4'-cyano-[1,1'-biphenyl]-4-yl)oxy)undecyl acrylate.

Acryloyl chloride (1.73 g, 16.2 mmol) was added to a stirred solution of 4'-(11-hydroxyundecyloxy)-[1,1'-biphenyl]-4-carbonitrile, **2** (7.00 g, 19.2 mmol) and triethylamine (7.7 mL, 55 mmol) in dry dichloromethane (200 mL) under a nitrogen atmosphere (16 hr). The mixture was filtered and the filtrate evaporated to dryness. The crude was purified *via* flash column chromatography over silica gel using DCM as eluent and the compound was recrystallised from toluene with hexane (ca. 1:4) to form a fine white solid. Yield: 3.44 g (42.8 %).

<sup>1</sup>H NMR (400 MHz, CDCl<sub>3</sub>) δ<sub>H</sub>: 1.24 – 1.41 (m, 10H, CH<sub>2</sub>), 1.47 (quint, 4H, J = 7.3 Hz, CH<sub>2</sub>), 1.67 (quint, J = 7.1 Hz, 2 H) 1.81 (quint, J = 7.1 Hz, 2H) 4.00 (t, J = 6.5 Hz, 2H, CH<sub>2</sub>OOC) 4.15 (t, J = 6.8 Hz, 2H, CH<sub>2</sub>OAr), 5.81 (dd, J = 10.4, 1.5 Hz, 1H, CH<sub>cis</sub>=), 6.12 (dd, J = 17.1, 10.4 Hz, 1H, CH=), 6.40 (dd, J = 17.3, 1.5 Hz, 1H, CH<sub>trans</sub>=), 6.99 (AA'BB', J = 8.8 Hz, 2H, ArH<sub>a</sub>) 7.52 (AA'BB', J = 8.8, 2H ArH<sub>b</sub>), 7.68 (AA'BB', J = 8.6 Hz, 2H, ArH), 7.68 (AA'BB', J = 8.6 Hz, 2H, ArH).

<sup>13</sup>C (101 MHz, ) δ<sub>C</sub>: 26.0, 26.1, 28.7, 29.3, 29.3, 29.5, 29.6, 29.6, 64.8, 68.2, 110.1, 115.1, 119.2, 127.1, 127.1, 128.4, 128.7, 130.6, 131.2, 132.6, 145.3, 159.9, 166.4.

ESI-MS: C<sub>27</sub>H<sub>34</sub>NO<sub>3</sub> calculated [M + H] *m/z* 420.2533, found 420.2514.

FTIR ν cm<sup>-1</sup>: 3281 (C–H Ar), 2920, 2851, 2238 (CN), 2226(CN), 1711, 1634, 1600, 1581, 1496, 1475, 1408, 1384, 1253, 1183, 1118, 1062, 1008, 991, 976, 896, 862, 854, 838, 826, 811, 780, 740, 724, 674, 663.

### 6.1.1. Compound 3: Benzyl-2,5-dihydroxybenzoate<sup>99</sup>

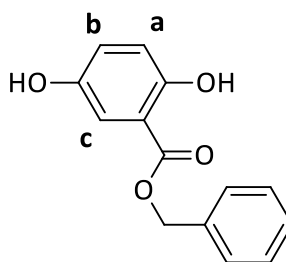


Figure 108: Benzyl-2,5-dihydroxybenzoate.

NaHCO<sub>3</sub> (32.00 g, 0.38 mol) was added to a solution of 2,5-dihydroxybenzoic acid (23.00 g, 0.16 mol) in DMF (500 mL) and heated to 70 °C (1hr). Benzyl bromide (26 g, 0.15 mol) was added and the suspension was heated to 70 °C (16 hr). The reaction was cooled to room temperature and diluted with water (400 mL). The mixture was extracted three times with 50:50 hexane/ethyl acetate (3 × 100 mL). Residual DMF was removed from the organic phase with water extraction; the organic phase was subsequently dried over Na<sub>2</sub>SO<sub>4</sub>. The solid was filtered off and the solution evaporated to dryness to yield a pale yellow solid. The product was recrystallised from ethanol and washed with cold ethanol, yielding an off white solid. Yield: 13.50 g (55.3 %).

<sup>1</sup>H NMR (400 MHz, ) δ<sub>H</sub>: 4.53 (s, 1H, OH), 5.37 (s, 2H, CH<sub>2</sub>O), **a** 6.89 (d, 1H, 8.9 Hz, ArH), **b** 7.01 (dd, 1H, J = 8.9 Hz, 3.1 Hz, ArH), **c** 7.32 (d, 1H, J = 3.2 Hz, ArH), 7.34-7.46 (m, 5H, ArH), 10.33 (s, 1H, OH).

ESI-MS: C<sub>14</sub>H<sub>13</sub>O<sub>4</sub> calculated [M + H] *m/z* 245.0808, found 245.0809.

C<sub>14</sub>H<sub>12</sub>NaO<sub>4</sub> calculated [M + Na] *m/z* 267.0628, found 267.0633.

FTIR ν cm<sup>-1</sup>: 3388 (OH), 2982, 2941, 2922, 2852 (CH), 1669 (C=O), 1624, 1600 (Ar), 1476 (CH), 1354, 1303, 1271, 1079, 959, 909, 874, 862, 828, 795, 781, 745.

### 6.1.1. Compound 4: Benzyl-2,5-di(4-butoxybenzoyloxy)benzoate<sup>99</sup>

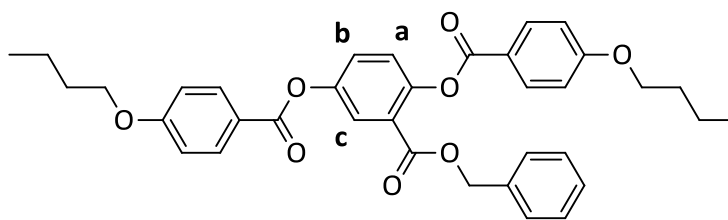


Figure 109: Benzyl-2,5-di(4-butoxybenzoyloxy)benzoate.

A solution of benzyl-2,5-dihydroxybenzoate, **3** (5.03 g, 20.6 mmol), 4-butoxybenzoic acid (8.90 g, 45.8 mmol), EDAC (8.91 g, 57.3 mmol) and DMAP (0.56 g) in dichloromethane (300 mL) was stirred at room temperature for several days. The solvent was evaporated to dryness, the crude was dissolved in minimum dichloromethane and purified *via* flash column chromatography over silica gel using DCM as eluent, the isolated product was recrystallised from ethanol. A white microcrystalline product was collected by filtration. Yield: 11.1 g (90.4 %)

<sup>1</sup>H NMR (400 MHz, CDCl<sub>3</sub>) δ<sub>H</sub>: 1.00 (t, 3H, *J* = 7.4 Hz, CH<sub>3</sub>), 1.01 (t, 3H, *J* = 7.4 Hz, CH<sub>3</sub>), 1.53 (m, 4H, CH<sub>2</sub>), 1.82 (m, 4H, CH<sub>2</sub>), 4.06 (t, 4H, *J* = 6.5 Hz, CH<sub>2</sub>O), 5.19 (s, 2H, ArCH<sub>2</sub>), 6.94 (AA'BB', 4H, *J* = 2.45, ArH), 7.24-7.25 (m, 5H, ArH) **a** 7.29 (d, 1H, *J* = 8.7 Hz, ArH), **b** 7.46 (dd, 1H, *J* = 8.9 Hz, *J* = 3.1 Hz, ArH), **c** 7.90 (d, 1H, *J* = 2.9 Hz, ArH), 8.07 (m AA'BB', 2H, *J* = 8.9 Hz, ArH), 8.13 (m AA'BB', 2H, *J* = 8.9 Hz, ArH).

ESI-MS: C<sub>29</sub>H<sub>30</sub>NaO<sub>8</sub> calculated [M + H] *m/z* 529.183289, found 529.182343.

FTIR ν cm<sup>-1</sup>: 2959, 2933, 2873, 1722, 1606, 1582, 1511, 1492, 1457, 1420, 1354, 1323, 1303, 1270, 1079, 1047, 959, 946, 909, 873, 862, 828, 795, 781, 745, 668.

### 6.1.1. Compound 5: 2,5-bis((4-butoxybenzoyl)oxy)benzoic acid<sup>99</sup>

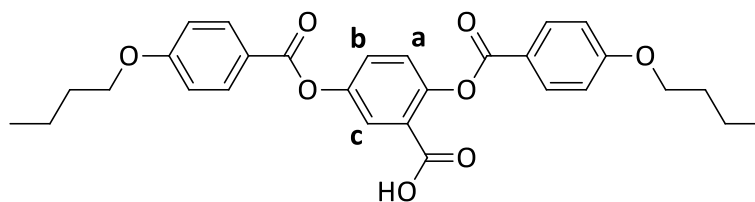


Figure 110: 2,5-bis((4-butoxybenzoyl)oxy)benzoic acid.

Dry THF (250 mL) and ethanol (5 mL) were added to a flask charged with benzyl-2,5-di(4-butyloxybenzoyloxy)benzoate, 4 (10.57 g, 17.77 mmol) and palladium-on-carbon (0.45 g). The reaction mixture was degassed and the atmosphere filled with hydrogen three times. The reaction was stirred under hydrogen (24 hr, r.t.). The reaction mixture was filtered through celite, the solvent dried *in vacuo* and the white crystalline product recrystallised from ethanol. Yield 7.34 g (81.8 %)

<sup>1</sup>H NMR (400 MHz, CDCl<sub>3</sub>) δ<sub>H</sub>: 0.99 (t, 3H, *J* = 7.4 Hz, CH<sub>3</sub>), 1.00 (t, 3H, *J* = 7.4 Hz, CH<sub>3</sub>), 1.52 (sex, 2H, *J* = 7.4 Hz, CH<sub>2</sub>), 1.52 (sex, 2H, *J* = 7.4 Hz, CH<sub>2</sub>), 1.81 (quint, 2H, *J* = 7.0 Hz, CH<sub>2</sub>), 1.82 (quint, 2H, *J* = 7.0 Hz, CH<sub>2</sub>), 4.05 (t, 2H, *J* = 6.5 Hz, CH<sub>2</sub>O), 4.06 (t, 2H, *J* = 6.5 Hz, CH<sub>2</sub>O), 6.97 (AA'BB', 4H, *J* = 8.0, ArH), a 7.29 (d, 1H, *J* = 8.7 Hz, ArH), b 7.50 (dd, 1H, *J* = 8.8 Hz, *J* = 2.9 Hz, ArH), c 7.93 (d, 1H, *J* = 2.9 Hz, ArH), 8.14 (m AA'BB', 4H, *J* = 8.9 Hz, ArH).

COOH not observed

ESI-MS: C<sub>29</sub>H<sub>30</sub>NaO<sub>8</sub> calculated [M + H] *m/z* 529.183289, found 529.182343.

FTIR ν cm<sup>-1</sup>: 2957, 2928, 2874, 2232, 1728, 1688, 1605, 1580, 1511, 1493, 1492, 1468, 1453, 1423, 1313, 1246, 1186, 1162, 1128, 1025, 1008, 968, 924, 887, 844, 819, 793, 756, 690.

**6.3.2. Compound 6: 2-((4-(acryloyloxy)butoxy)carbonyl)-1,4-phenylene bis(4-butoxybenzoate)<sup>99</sup>**

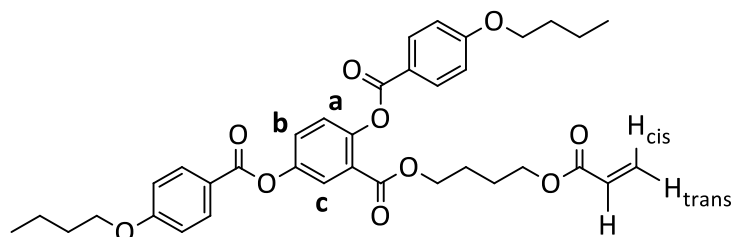


Figure 111: 2-((4-(acryloyloxy)butoxy)carbonyl)-1,4-phenylene bis(4-butoxybenzoate).

A solution of 2,5-di(butyloxybenzoyloxy)benzoic acid, **5** (2.43 g, 4.79 mmol), 4-hydroxybutylacrylate 90% (0.67 g, 4.23 mmol), EDAC (1.49 g, 9.59 mmol) and DMAP in dichloromethane (100 mL) was stirred for several days at room temperature. The solvent was removed *in vacuo*, the product was dissolved in minimal dichloromethane, loaded onto celite and purified *via* dry vacuum flash column chromatography over silica gel using DCM as eluent. The solvent was removed *in vacuo*, to yield an oil. The product was recrystallized from toluene/hexane to yield a white powder. Yield: 1.29 g (48.2 %).

<sup>1</sup>H NMR (400 MHz, CDCl<sub>3</sub>) δ<sub>H</sub>: 1.00 (t, *J* = 7.4 Hz, CH<sub>3</sub>)×2, 6H), 1.52 (m, 4H, CH<sub>2</sub>), 1.61 (m, 2H, CH<sub>2</sub>), 1.82 (m, 6H, CH<sub>2</sub>), 4.03 (t, 2H, *J* = 6.2 Hz, CH<sub>2</sub>O), 4.06 (t, 2H, *J* = 6.5 Hz, CH<sub>2</sub>O), 4.06 (t, 2H, *J* = 6.5 Hz, CH<sub>2</sub>O), 4.20 (t, 2H, *J* = 6.2 Hz, CH<sub>2</sub>), 5.80 (dd, 1H, *J* = 10.4, 1.5 Hz, CH<sub>cis</sub>=), 6.08 (dd, 1H, *J* = 17.4, 10.4 Hz, CH=), 6.40 (dd, 1H, *J* = 17.4, 1.5 Hz, CH<sub>trans</sub>=), 6.98 (m AA'BB', 4H, *J* = 8.9, ArH), **a** 7.26 (d, 1H, *J* = 8.7 Hz, ArH), **b** 7.46 (dd, 1H, *J* = 8.8 Hz, *J* = 2.9 Hz, ArH), **c** 7.89 (d, 1H, *J* = 2.9 Hz, ArH), 8.15 (m AA'BB', 4H, ArH).

ESI-MS: C<sub>36</sub>H<sub>41</sub>O<sub>10</sub> calculated [M + H] *m/z* 633.269424, found 633.267666.

C<sub>36</sub>H<sub>40</sub>NaO<sub>10</sub> calculated [M + H] *m/z* 655.251368, found 655.252854.

HPLC: a. 92.7 %, b. 6.7%

Smaller contribution is attributed to higher chain length spacers from the 4-hydroxybutylacrylate 90%.

FTIR ν cm<sup>-1</sup>: 2956, 2872, 1726, 1684, 1607, 1584, 1510, 1490, 1454, 1422, 1313, 1245, 1188, 1171, 1129, 1072, 1024, 1009, 969, 924, 888, 845, 819, 793, 774, 758, 690.

#### 6.4. Substrate Synthesis

Paper preparation: Whatmann filter paper (20 mm diameter, 3.8 mL Area, surface area 7.6 cm<sup>2</sup>) was washed with acetone with shaking (3 × 5 cm<sup>2</sup>) and dichloromethane with shaking (5 × 5 cm<sup>2</sup>) and dried in a desiccator (> 12 hr).

Electrospun fibre: Cellulose acetate (Degree of Substitution: 2.3) electrospun fibre mats were provided by the Soft and Biofunctional Materials group at the New University of Lisbon Cellulose acetate ESF was used as received.

All stirred reactions were stirred using a magnetic follower, with pivot ring (diameter, size 12 mm × 4.5 mm).

All macroinitiator syntheses were performed in stoppered round bottom flasks.

All polymerisations were performed in stoppered Schlenk tubes.

Freeze-thaw cycles were performed until no further effervescence was observed. Typically this was four times, in all cases it was between three and five.

All substrates were dried, and activated substrates stored for up to two days, in a desiccator with self-indicating silica gel as the desiccant.

All washes of paper substrates were performed in a separating funnel - with the exception of substrate 2, which was washed *via* agitation (ca. 5 min) and decantation from the reaction flask.

All ESF washes were performed *via* swirling and decantation from the reaction flask.

Agitation was performed on an IKA vibrax VXR at 100 rpm, with the reaction flask secured to the reaction flask to the agitator.

Prior to polymerisations the acrylate species was eluted through activated alumina (aluminium oxide, activated, basic, Brockmann I, ca. 2.5 cm diameter, ca. 6 cm depth) with THF and dried *in vacuo* (40 °C) and evaporated to dryness.

Polymerisations solutes were eluted through activated alumina (aluminium oxide, activated, basic, Brockmann I, ca. 2.5 cm diameter, ca. 6 cm depth) with THF and dried *in vacuo* (40 °C) and further dried *in vacuo* (16 hr).

Where a substrate has been produced by the same procedure in multiple batches one is presented. If the substrate is used as a reagent a letter is assigned to each batch. If more than one substrate is produced in a batch each substrate is assigned a number (eg. i, ii).

#### 6.4.1. Substrate 1: Representative of single cellulose(paper) macroinitiator preparation<sup>90</sup>

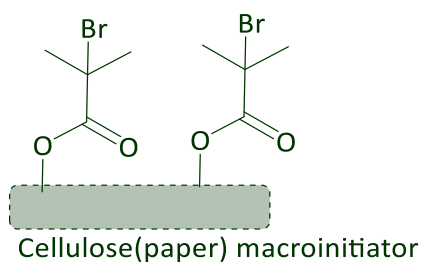


Figure 112: Cellulose(paper) macroinitiator.

Washed filter paper (Whatman (I)) (6.89 mg, 425  $\mu\text{mol}$ ) was submerged in a stirred solution of THF (5 mL), triethylamine (21  $\mu\text{L}$ , 0.15 mmol), and DMAP the headspace was flushed with argon and the suspension was subjected to sonication (6 min). The suspension headspace was freshly flushed with argon and 2-bromoisobutyryl bromide (16  $\mu\text{L}$ , 0.13 mmol) was added, the system was closed under argon and stirred (16 hr, R.T.).

The substrate was washed sequentially with acetone and DCM and dried *in vacuo* (12 hr).

Substrate mass                      6.92 mg

mass change %                      +0.44%

FTIR  $\nu$   $\text{cm}^{-1}$ :                      No detectable change.

#### 6.4.2. Substrate 2: Multiple cellulose(paper) macroinitiator preparation

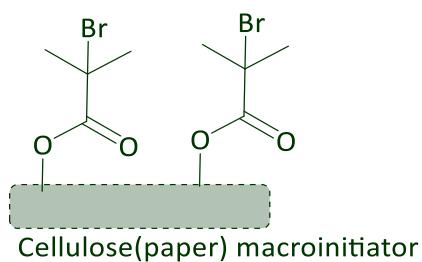


Figure 113: Cellulose(paper) macroinitiator.

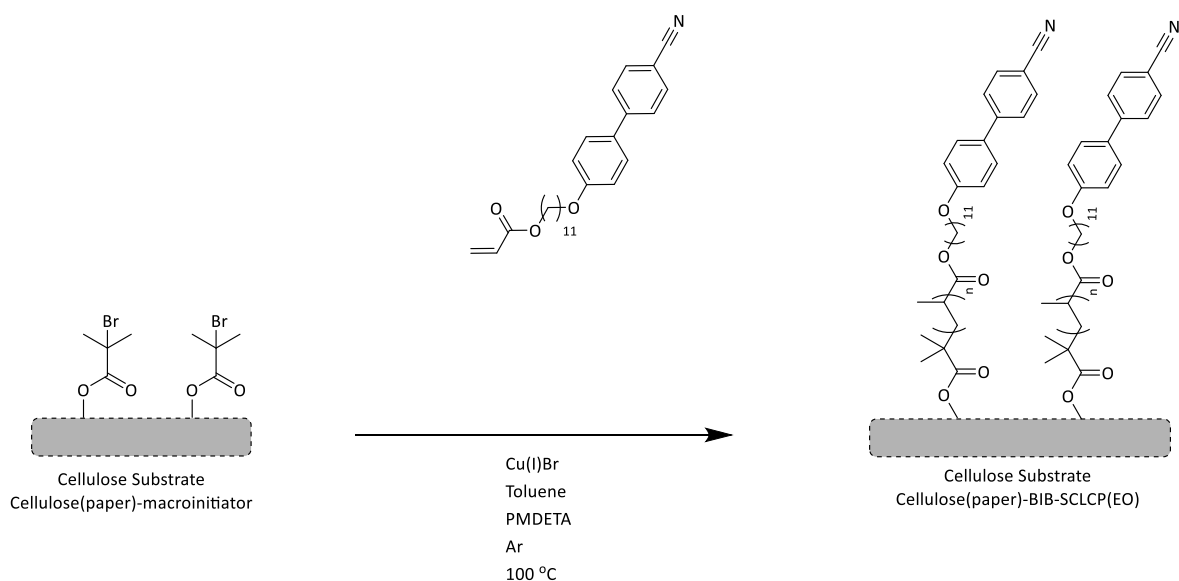
Washed filter paper (Whatman (I)) (261.6 mg, 38 pieces, 1.61 mmol) was submerged in a well-mixed solution of THF (30 mL), TEA (86  $\mu$ L, 0.61 mmol), and DMAP (cat.), the headspace was flushed with argon and the suspension was subjected to sonication (6 min). The suspension headspace was freshly flushed with argon and 2-bromoisobutyl bromide (67  $\mu$ L, 0.54 mmol) was added. The system was closed under argon and agitated (16 hr, R.T.). The paper-macroinitiators were washed collectively, sequentially with acetone (5  $\times$  30 mL) and dichloromethane (3  $\times$  30 mL) and dried *in vacuo* (12 hr).

Collective substrate mass    256.20 mg [1 piece dropped during work up]

mass change %                N/A

FTIR  $\nu$   $\text{cm}^{-1}$ :                No detectable change.

**6.4.3. Substrate 3: SI-ATRP of compound 2, from cellulose (paper) macroinitiator using Cu(I)/PMDETA in toluene, under argon (with stirring). (Entry 1).**



*Scheme 12: SI-ATRP of compound 2, from cellulose (paper) macroinitiator using Cu(I)/PMDETA in toluene, under argon (with stirring).*

11-((4'-Cyano-[1,1'-biphenyl]-4-yl)oxy)undecyl acrylate (2.00 g, 4.77 mmol), Cu(I)Br (15.52 mg, 0.1080 mmol) and Substrate 1a (6.10 mg, whole, [37.6  $\mu$ mol, assuming substituent mass is negligible]) were placed in a Schlenk tube and the atmosphere was degassed and refilled with argon. Toluene (3 ml) and PMDETA (20  $\mu$ L, 96  $\mu$ mol) were added to the Schlenk tube *via* syringe and stirred (5 min). The suspension was degassed and refilled with argon (x3). The reaction was heated, with stirring (100 °C, 16 hr).

The reaction was allowed to cool to room temperature and opened to the atmosphere. The reaction mixture was diluted with THF (10 mL) and the substrate was removed. The reaction mixture was sonicated and eluted through activated alumina in THF and dried *in vacuo*, resulting in a white powder (1.97 g).

The substrate was thoroughly washed with THF, water, THF/water (50:50), THF and ethanol sequentially. The substrate was dried *in vacuo* (16 hr).

**Substrate**

mass: 5.78 mg [mass loss].

FT-IR  $\nu$   $\text{cm}^{-1}$ : ~ 1730 (C=O).

**Sacrificial Polymer**

GPC: RV:13.210\*

RV: 17.600; Mn 397; Mw 5,450; Mw/Mn 363

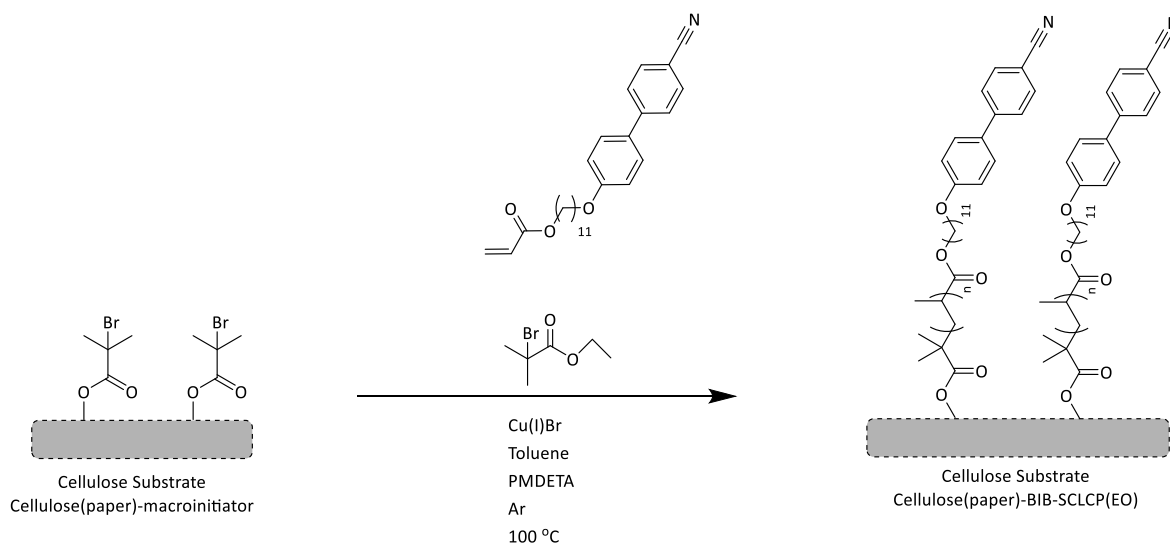
$^1\text{H}$  NMR monitoring ratio (400 MHz, 1.36:1

$\text{CHCl}_3$ ), 3.85 – 4.20:5.77 – 6.44  $\delta_{\text{H}}$ :

FTIR  $\nu$   $\text{cm}^{-1}$ : 3085 (C-H Ar), 2923, 2853, 2226 (CN), 1710, 1634, 1600, 1532, 1498.

\*Not meaningfully characterised

**6.4.4. Substrate 4: SI-ATRP of compound 2, from cellulose (paper) macroinitiator using Cu(I)/PMDETA in toluene, with sacrificial initiator (ebib) under argon (with stirring). (Entry 2).**



*Scheme 13: SI-ATRP of compound 2, from cellulose (paper) macroinitiator using Cu(I)/PMDETA in toluene, with sacrificial initiator (ebib) under argon (with stirring).*

11-((4'-Cyano-[1,1'-biphenyl]-4-yl)oxy)undecyl acrylate (0.46 g, 1.1 mmol), Cu(I)Br (3.17 mg, 22.1  $\mu\text{mol}$ ) and Substrate 1b (1.79 mg, quart, [11.0  $\mu\text{mol}$ , assuming substituent mass is negligible]) were placed in a Schlenk tube and the atmosphere was degassed and refilled with argon. Ethyl-2-bromoisobutyrate (9.6  $\mu\text{L}$ , 65  $\mu\text{mol}$ ) was dissolved in toluene (2 ml) and degassed/refilled with argon (3x). The ethyl-2-bromoisobutyrate solution (1 ml, 33  $\mu\text{mol ml}^{-1}$ ) and PMDETA (5.1  $\mu\text{L}$ , 35  $\mu\text{mol}$ ) were added to the Schlenk tube *via* syringe and stirred (5 min) the flask suspension was degassed (freeze/thaw) until no further gas was evolved and refilled with argon. The reaction was heated, with stirring (100°C, 16 hr).

The reaction was allowed to cool to room temperature and opened to the atmosphere. The reaction mixture was diluted with THF (10 mL) and the substrate was removed, the reaction mixture was sonicated and eluted through activated alumina in THF and dried *in vacuo*, resulting in a white powder (0.44 g).

The substrate was thoroughly washed with THF, water, THF/water (50:50), THF and ethanol sequentially. The substrate was dried *in vacuo* (16 hr).

**Substrate**

mass: 1.75 mg [mass loss].

FT-IR  $\nu$   $\text{cm}^{-1}$ : N/A.

**Sacrificial Polymer**

GPC: RV:14.317\*

RV: 17.613; Mn 304; Mw; 453 Mw/Mn 1.49

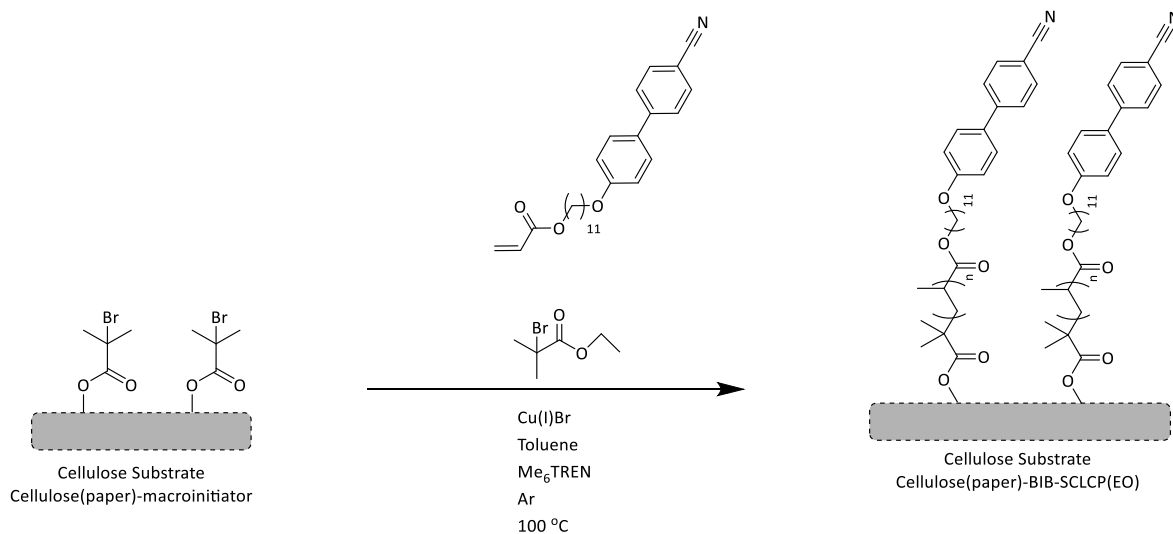
$^1\text{H}$  NMR monitoring ratio (400 MHz, 1.44:1

$\text{CHCl}_3$ ), 3.85 – 4.20:5.77 – 6.44  $\delta_{\text{H}}$ :

FTIR  $\nu$   $\text{cm}^{-1}$ : 3085 (C-H Ar), 2923, 2852, 2226 (CN), 1730, 1710, 1634, 1600, 1532, 1498.

\*Not meaningfully characterised

**6.4.5. Substrate 5: SI-ATRP of compound 2, from cellulose (paper) macroinitiator using Cu(I)/Me<sub>6</sub>TREN in toluene, with sacrificial initiator, ebib, under argon (with stirring). (Entry 3).**



*Scheme 14: SI-ATRP of compound 2, from cellulose (paper) macroinitiator using Cu(I)/Me<sub>6</sub>TREN in toluene, with sacrificial initiator, ebib, under argon (with stirring).*

11-((4'-Cyano-[1,1'-biphenyl]-4-yl)oxy)undecyl acrylate (353.67 mg, 843.00  $\mu\text{mol}$ ), Cu(I)Br (2.68 mg, 18.7  $\mu\text{mol}$ ) and Substrate 1c (1.55 mg, quart, [9.56  $\mu\text{mol}$ , assuming substituent mass is negligible]) were placed in a Schlenk tube and the atmosphere was degassed and refilled with argon. Ethyl-2-bromoisobutyrate (12.8  $\mu\text{L}$ , 87.2  $\mu\text{mol}$ ) was dissolved in toluene (2 ml) and degassed/refilled with argon (3x). The ethyl-2-bromoisobutyrate solution (0.5 ml, 44  $\mu\text{mol ml}^{-1}$ ) and Me<sub>6</sub>TREN (5.0  $\mu\text{L}$ , 21  $\mu\text{mol}$ ) were added to the Schlenk tube *via* syringe and stirred (5 min). The flask suspension was degassed (freeze/thaw) until no further gas was evolved and refilled with argon. The reaction was heated, with stirring (100°C, 16 hr).

The reaction was allowed to cool to room temperature and opened to the atmosphere. The reaction mixture was diluted with THF (10 mL) and the substrate was removed. The reaction mixture was sonicated and eluted through activated alumina in THF and dried *in vacuo*, resulting in a white solid (0.33 g).

The substrate was thoroughly washed with THF, water, THF/water (50:50), THF and ethanol sequentially. The substrate was dried *in vacuo* (16 hr).

**Substrate**

mass: 1.55 mg.  
FT-IR  $\nu$   $\text{cm}^{-1}$ : 1730 (C=O).

**Sacrificial Polymer**

GPC: RV 14.030: Mn 9,732; Mw 15,556; Mw/Mn 1.60.

RV 17.613\*

$^1\text{H}$  NMR monitoring ratio (400 MHz, 30.3:1

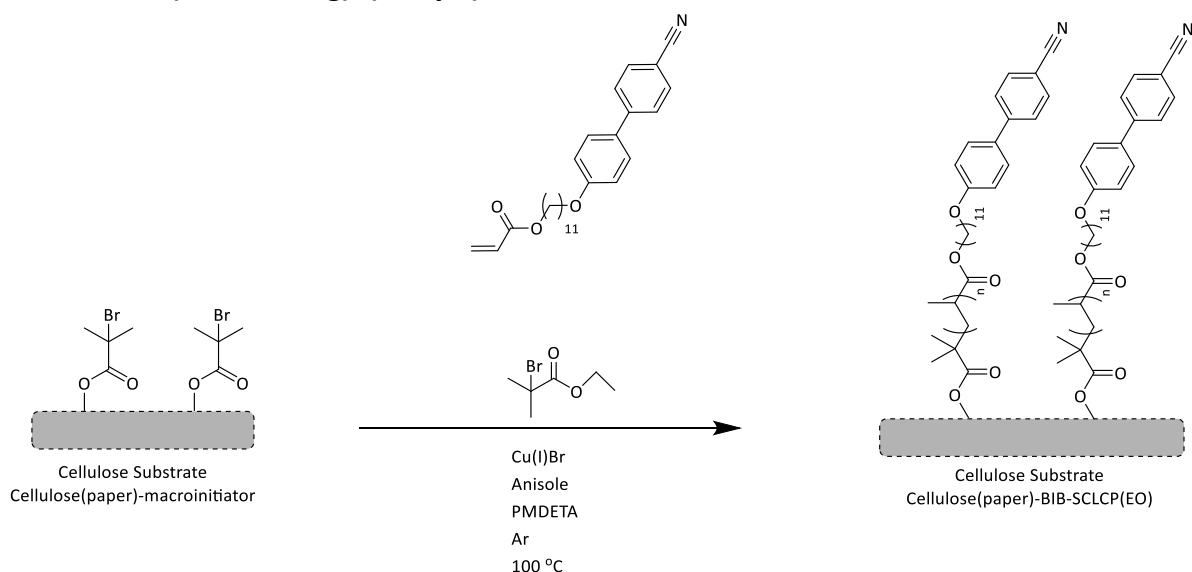
$\text{CHCl}_3$ ), 3.85 – 4.20:5.77 – 6.44  $\delta_{\text{H}}$ :

Thermal Properties DSC:  $T_g$  12.4 SmC 37.3 SmA 142.0 Iso Liq. °C

FT-IR: 2982 2920, 2852, 2224 (CN), 1729, 1710, 1603, 1523,  
1495.

\*Not meaningfully characterised

**6.4.6. Substrate 6: SI-ATRP of compound 2, from cellulose (paper) macroinitiator using Cu(I)/PMDETA in anisole, with sacrificial initiator, ebib, under argon (with stirring). (Entry 4).**



*Scheme 15: SI-ATRP of compound 2, from cellulose (paper) macroinitiator using Cu(I)/PMDETA in anisole, with sacrificial initiator, ebib, under argon (with stirring).*

11-((4'-Cyano-[1,1'-biphenyl]-4-yl)oxy)undecyl acrylate (353.35 mg, 842.00  $\mu\text{mol}$ ), Cu(I)Br (2.64 mg, 18.4  $\mu\text{mol}$ ) and Substrate 1c (1.98 mg, quart, [12.2  $\mu\text{mol}$ , assuming substituent mass is negligible]) were placed in a Schlenk tube and the atmosphere was degassed and refilled with argon. Ethyl-2-bromoisobutyrate (12.8  $\mu\text{L}$ , 87.2  $\mu\text{mol}$ ) was dissolved in anisole (2 mL) and degassed/refilled with argon (3 $\times$ ). The ethyl-2-bromoisobutyrate solution (0.5 mL, 44  $\mu\text{mol ml}^{-1}$ ) and PMDETA (3.6  $\mu\text{L}$ , 17  $\mu\text{mol}$ ) were added to the Schlenk tube *via* syringe and stirred (5 min). The flask suspension was degassed (freeze/thaw) until no further gas was evolved and refilled with argon. The reaction was heated, with stirring (100°C, 16 hr).

The reaction was allowed to cool to room temperature and opened to the atmosphere. The reaction mixture was diluted with THF (10 mL) and the substrate was removed. The reaction mixture was sonicated and eluted through activated alumina in THF and dried *in vacuo*, resulting in a white powder (0.34 g).

The substrate was thoroughly washed with THF, water, THF/water (50:50), THF and ethanol sequentially. The substrate was dried *in vacuo* (16 hr).

**Substrate**

mass: 1.96 mg [mass loss].

FT-IR  $\nu$   $\text{cm}^{-1}$ : N/A.

**Sacrificial Polymer**

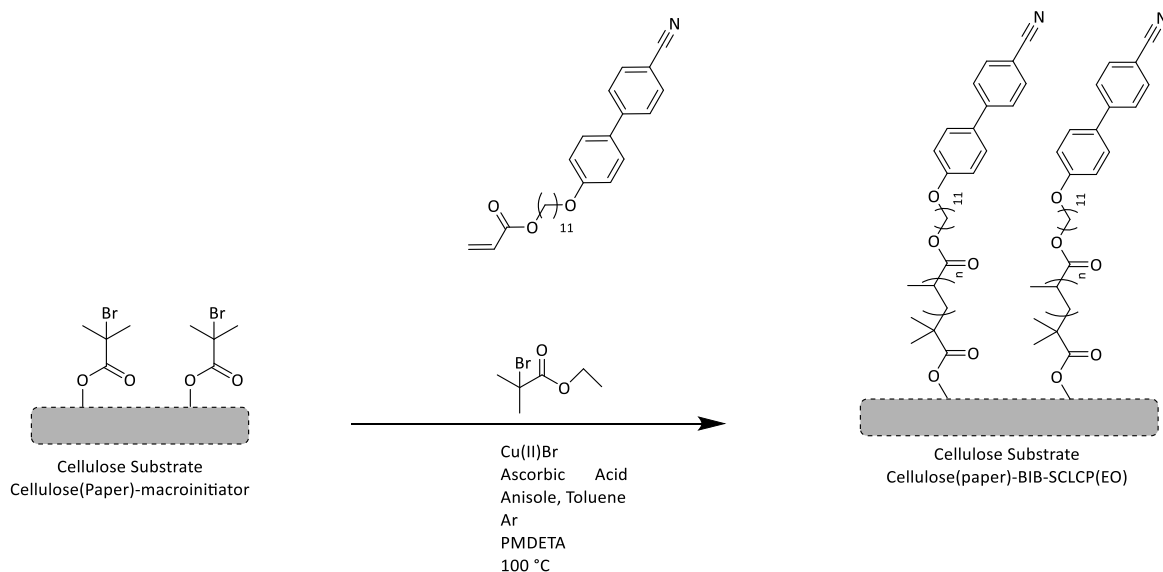
GPC: RV 17.603;; Mn 384; Mw 762; Mw/Mn 1.96

$^1\text{H}$  NMR monitoring ratio (400 MHz, 1.35:1

$\text{CHCl}_3$ ), 3.85 – 4.20:5.77 – 6.44  $\delta_{\text{H}}$ :

FT-IR 2982, 2922, 2852, 2226 (CN), 1710, 1633, 1599, 1532, 1498.

**6.4.7. Substrate 7: SI-ARGET ATRP of compound 2, from cellulose (paper) macroinitiator using Cu(II)/PMEDTA – ascorbic acid in anisole/toluene, with sacrificial initiator, ebib, under argon (without mechanical mixing). (Entry 5).**



*Scheme 16: SI-ARGET ATRP of compound 2, from cellulose (paper) macroinitiator using Cu(II)/PMEDTA – ascorbic acid in anisole/toluene, with sacrificial initiator, ebib, under argon (without mechanical mixing).*

11-((4'-Cyano-[1,1'-biphenyl]-4-yl)oxy)undecyl acrylate (395.08 mg, 942.00  $\mu\text{mol}$ ), Cu(II)Br (0.46 mg, 2.1  $\mu\text{mol}$ ), ascorbic acid (3.71 mg, 21.1  $\mu\text{mol}$ ) were washed into a dry Schlenk tube in dry toluene, the solution was concentrated *in vacuo*. Substrate 1d (1.70, quart, [10.5  $\mu\text{mol}$ , assuming substituent mass is negligible]) was introduced to the Schlenk tube and the atmosphere was degassed and refilled with argon. Ethyl-2-bromoisobutyrate (9.6  $\mu\text{L}$ , 65  $\mu\text{mol}$ ) was dissolved in anisole (3 mL) and degassed/refilled with argon (3x). The ethyl-2-bromoisobutyrate solution (22  $\mu\text{mol mL}^{-1}$ , 0.5 mL), toluene (100  $\mu\text{L}$ ) and PMDETA (3.6  $\mu\text{L}$ , 17  $\mu\text{mol}$ ) were added to the Schlenk tube *via* syringe the flask suspension was degassed (freeze/thaw) until no further gas was evolved, the reaction was refilled with argon and isolated before heating, no mixing mechanism was employed (100 °C, 1.5 hr). Due to a pressure build up the reaction became open to air. The reaction was cooled and stoppered (20 hr), the flask suspension was degassed (freeze/thaw) until no further gas was evolved, the reaction was refilled with argon and isolated before heating, no mixing mechanism was employed (100 °C, 16 hr).

The reaction was allowed to cool to room temperature and opened to the atmosphere. The reaction mixture was diluted with toluene (10 mL) and the substrate was removed. The reaction

mixture was further diluted with THF (5 mL), sonicated and eluted through activated alumina in THF and dried *in vacuo*, resulting in a white solid (0.38 g).

The substrate was thoroughly washed with toluene, isopropanol, water, isopropanol and hexane sequentially. The substrate was dried *in vacuo* (16 hr).

### Substrate

mass: 1.65 mg [mass loss]

FT-IR  $\nu$   $\text{cm}^{-1}$ : N/A.

### Sacrificial Polymer

GPC: RV 14.510: Mn 7,088; Mw 13,312; Mw/Mn 1.88.

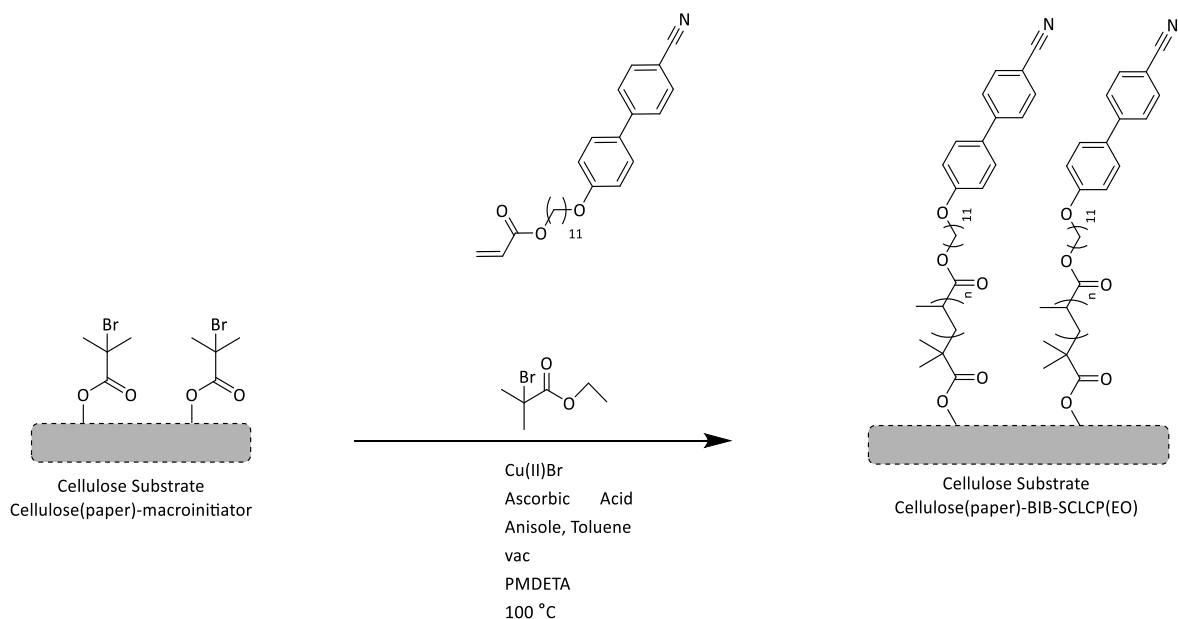
$^1\text{H}$  NMR monitoring ratio (400 MHz, 40.2:1

$\text{CHCl}_3$ ), 3.85 – 4.20:5.77 – 6.44  $\delta_{\text{H}}$ :

Thermal Properties DSC:  $T_g$  12.7 SmC 37.4 SmA 145.1 Iso Liq.  $^{\circ}\text{C}$

FT-IR: 2982, 2919, 2851, 2225 (CN), 1727, 1602, 1521, 1495.

**6.4.8. Substrate 8: SI-ARGET ATRP of compound 2, from cellulose (paper) macroinitiator using Cu(II)/PMDETA – ascorbic acid in anisole/toluene, with sacrificial initiator, ebib, under vacuum (without mechanical mixing). (Entry 6).**



*Scheme 17: SI-ARGET ATRP of compound 2, from cellulose (paper) macroinitiator using Cu(II)/PMDETA – ascorbic acid in anisole/toluene, with sacrificial initiator, ebib, under vacuum (without mechanical mixing).*

11-((4'-Cyano-[1,1'-biphenyl]-4-yl)oxy)undecyl acrylate (395.67 mg, 943.04  $\mu\text{mol}$ ), Cu(II)Br (0.49 mg, 2.2  $\mu\text{mol}$ ), ascorbic acid (3.98 mg, 22.6  $\mu\text{mol}$ ) were washed into a dry Schlenk tube in dry toluene, the solution was concentrated *in vacuo*. Substrate 1d (1.49 mg, quart, [9.19  $\mu\text{mol}$ , assuming substituent mass is negligible]) was introduced to the Schlenk tube and the atmosphere was degassed and refilled with argon. Ethyl-2-bromoisobutyrate (9.6  $\mu\text{L}$ , 65  $\mu\text{mol}$ ) was dissolved in anisole (3 mL) and degassed/refilled with argon (3x). The ethyl-2-bromoisobutyrate solution (22  $\mu\text{mol mL}^{-1}$ , 0.5 mL), toluene (100  $\mu\text{L}$ ) and PMDETA (3.6  $\mu\text{L}$ , 17  $\mu\text{mol}$ ) were added to the Schlenk tube *via* syringe the flask suspension was degassed (freeze/thaw) until no further gas was evolved, on the final cycle the reaction left under a passive vacuum and heating (100 °C, 16 hr).

The reaction was allowed to cool to room temperature and opened to the atmosphere. The reaction mixture was diluted with THF (10 mL) and the substrate was removed. The reaction mixture was sonicated and eluted through activated alumina in THF and dried *in vacuo*, resulting in a white solid (0.37 g).

The substrate was thoroughly washed with THF, water, THF/water (50:50), THF and ethanol

sequentially. The substrate was dried *in vacuo* (16 hr).

### Substrate

mass: 1.48 mg [mass loss].

FT-IR  $\nu$   $\text{cm}^{-1}$ : 1732 (C=O).

### Sacrificial Polymer

GPC: RV 14.057; Mn 10,412; Mw 18,607; Mw/Mn 1.79.

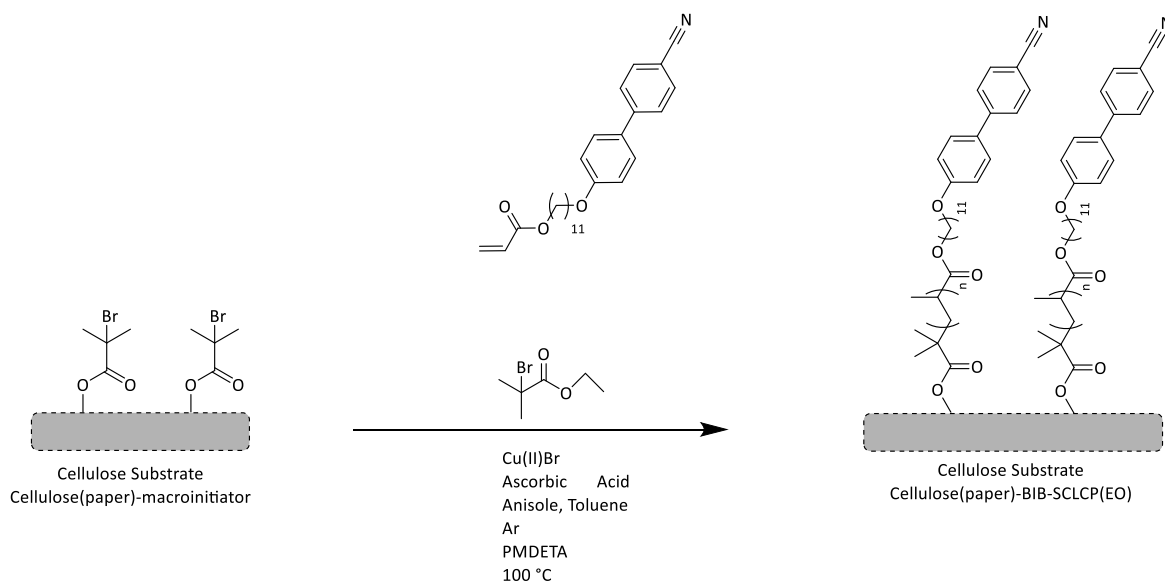
$^1\text{H}$  NMR monitoring ratio (400 MHz, 26.3:1

$\text{CHCl}_3$ ), 3.85 – 4.20:5.77 – 6.44  $\delta_{\text{H}}$ :

Thermal Properties DSC:  $T_g$  14.4 SmC 36.5 SmA 143.4 Iso Liq.  $^{\circ}\text{C}$

FT-IR: 2982, 2922, 2852, 2223 (CN), 1727 (C=O), 1603, 1524, 1495.

**6.4.9. Substrate 9: SI-ARGET ATRP of compound 2, from cellulose (paper) macroinitiator using Cu(II)/PMDETA – ascorbic acid in anisole, with sacrificial initiator, ebib, under argon (with stirring). (Entry 7).**



*Scheme 18: SI-ARGET ATRP of compound 2, from cellulose (paper) macroinitiator using Cu(II)/PMDETA – ascorbic acid in anisole, with sacrificial initiator, ebib, under argon (with stirring).*

11-((4'-Cyano-[1,1'-biphenyl]-4-yl)oxy)undecyl acrylate (0.41 g, 0.98 mmol), Cu(II)Br (0.45 mg, 2.0 mmol), ascorbic acid (3.86 mg, 21.9  $\mu\text{mol}$ ) and Substrate 2a (1.99 mg, quart, [12.3  $\mu\text{mol}$ , assuming substituent mass is negligible]) were washed into a dry Schlenk tube in dry toluene, the toluene was removed *in vacuo* and the atmosphere was degassed and refilled with argon. Ethyl-2-bromoisobutyrate (19.2  $\mu\text{L}$ , 0.13 mmol) was dissolved in anisole (3 mL) and degassed/refilled with argon (3x). The ethyl-2-bromoisobutyrate solution (43  $\mu\text{mol mL}^{-1}$ , 0.5 mL), and PMDETA (3.6  $\mu\text{L}$ , 17  $\mu\text{mol}$ ) were added to the Schlenk tube via syringe, the flask suspension was degassed (freeze/thaw) until no further gas was evolved and refilled with argon. The reaction was heated, with stirring (100 °C, 16 hr).

The reaction was allowed to cool to room temperature and opened to the atmosphere. The reaction mixture was diluted with THF (10 mL) and the substrate was removed. The reaction mixture was sonicated and eluted through activated alumina in THF and dried *in vacuo*, resulting in a white solid (0.41 g).

The substrate was thoroughly washed with THF, water, THF/water (50:50), THF and ethanol sequentially. The substrate was dried *in vacuo* (16 hr).

**Substrate**

mass: 2.00 mg.

FT-IR  $\nu$   $\text{cm}^{-1}$ : 1730 (C=O).

**Sacrificial Polymer**

GPC: RV: 13.403; Mn: 15,230; Mw: 53,611; Mw/Mn: 3.52.

RV: 17.600\*

$^1\text{H}$  NMR monitoring ratio (400 MHz, 2.38:1

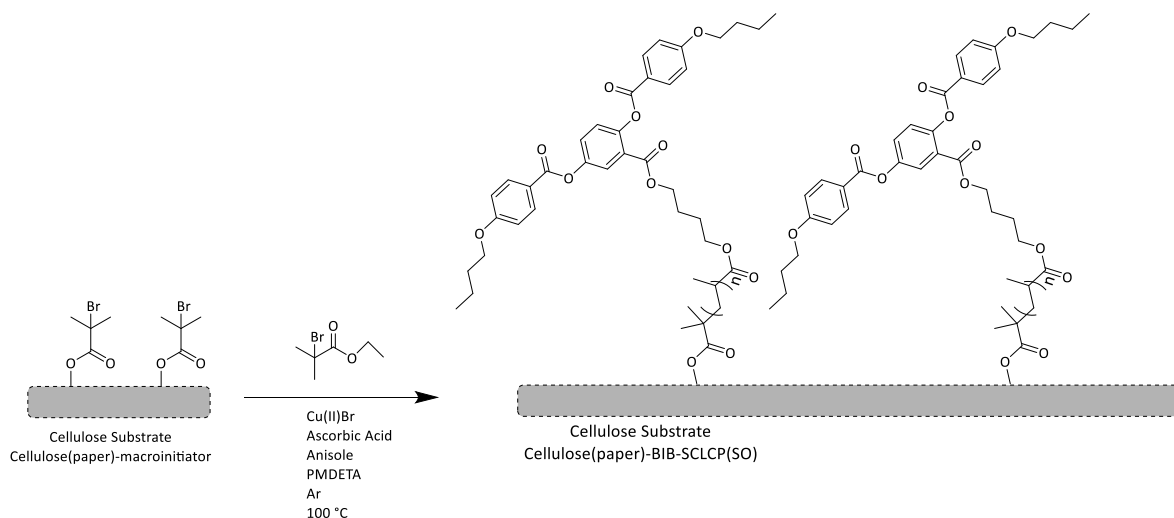
$\text{CHCl}_3$ ), 3.85 – 4.20:5.77 – 6.44  $\delta_{\text{H}}$ :

Thermal Properties DSC:  $T_g$  8.5 SmC 40.1 SmA 144.3 Iso Liq. °C

FT-IR: 3085 (C-H Ar), 2982, 2921, 2852, 2224 (CN), 1727, 1710, 1603, 1523, 1495.

\*Not meaningfully characterised

**6.4.10. Substrate 10: SI-ARGET ATRP of compound 6, from cellulose (paper) macroinitiator using Cu(II)/PMDETA – ascorbic acid in anisole, with sacrificial initiator, ebib, under argon (with stirring). (Entry 8).**



*Scheme 19: SI-ARGET ATRP of compound 6, from cellulose (paper) macroinitiator using Cu(II)/PMDETA – ascorbic acid in anisole, with sacrificial initiator, ebib, under argon (with stirring).*

Compound 6; 2-((4-(acryloyloxy)butoxy)carbonyl)-1,4-phenylene bis(4-butoxybenzoate) (0.39 g, 0.62 mmol), Cu(II)Br (0.48 mg, 2.1  $\mu\text{mol}$ ), ascorbic acid (4.16 mg, 23.6  $\mu\text{mol}$ ) and Substrate 2ai (1.75 mg, quart, [10.8  $\mu\text{mol}$ , assuming substituent mass is negligible]) were washed into a dry Schlenk tube in dry toluene, the toluene was removed *in vacuo*. And the atmosphere was degassed and refilled with argon. Ethyl-2-bromoisobutyrate (19.2  $\mu\text{L}$ , 0.13 mmol) was dissolved in anisole (3mL) and degassed/refilled with argon (3x). The ethyl-2-bromoisobutyrate solution (43  $\mu\text{molml}^{-1}$ , 0.5 mL), toluene (100  $\mu\text{L}$ ) and PMDETA (3.6  $\mu\text{L}$ , 17  $\mu\text{mol}$ ) were added to the Schlenk tube *via* syringe and stirred (5 min) the flask suspension was degassed (freeze/thaw) until no further gas was evolved, the reaction was refilled with argon, isolated and heated, with stirring (100 °C, 16 hr).

The reaction was allowed to cool to room temperature and opened to the atmosphere. The reaction mixture was diluted with THF (10 mL) and the substrate was removed. The reaction mixture was sonicated and eluted through activated alumina in THF and dried *in vacuo*, resulting in a white solid (0.38 g).

The substrate was thoroughly washed with THF, water, THF/water (50:50), THF and ethanol sequentially. The substrate was dried *in vacuo* (16 hr).

**Substrate**

mass: 3.29 mg (Substrate damaged during drying).

FT-IR  $\nu$   $\text{cm}^{-1}$ : 1732 (C=O).

**Sacrificial Polymer**

GPC: RV: 14.557 ml; Mn: 4,613; Mw: 16,431; Mw/Mn: 3.56.

RV: 16.670 ml\*

RV: 17.277 ml\*

$^1\text{H}$  NMR monitoring ratio (400 MHz, 37.0:1

$\text{CHCl}_3$ ), 3.95 – 4.25:5.75 – 6.40  $\delta_{\text{H}}$ :

Thermal Properties DSC:  $T_g$  27.4 N 109.5 Iso Liq.  $^{\circ}\text{C}$

FT-IR: 2982, 2925, 2853, 2224, 1727, 1603, 1511, 1495, 1467,  
1395, 1248, 1159, 1055.

\*Not meaningfully characterised

6.4.11. Substrate 11: Regeneration of electrospun fibre<sup>113</sup>



Regenerated cellulose ESF mat

Figure 114: Regenerated cellulose ESF mat.

Electrospun cellulose acetate was suspended in sodium hydroxide (110 mL, 0.050 mol dm<sup>-3</sup>), agitated (24 hr) and thoroughly washed with deionised water and dried *in vacuo* (85 °C).

FTIR  $\nu$  cm<sup>-1</sup>:                      Loss of 1740 (C=O).

#### 6.4.12. Substrate 12: Preparation of Cellulose(electrospun fibre) macroinitiator.<sup>84</sup>

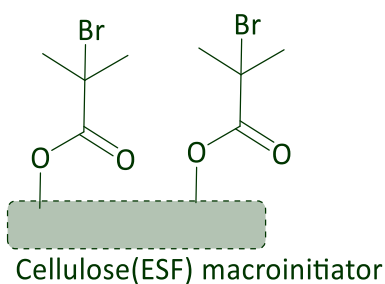


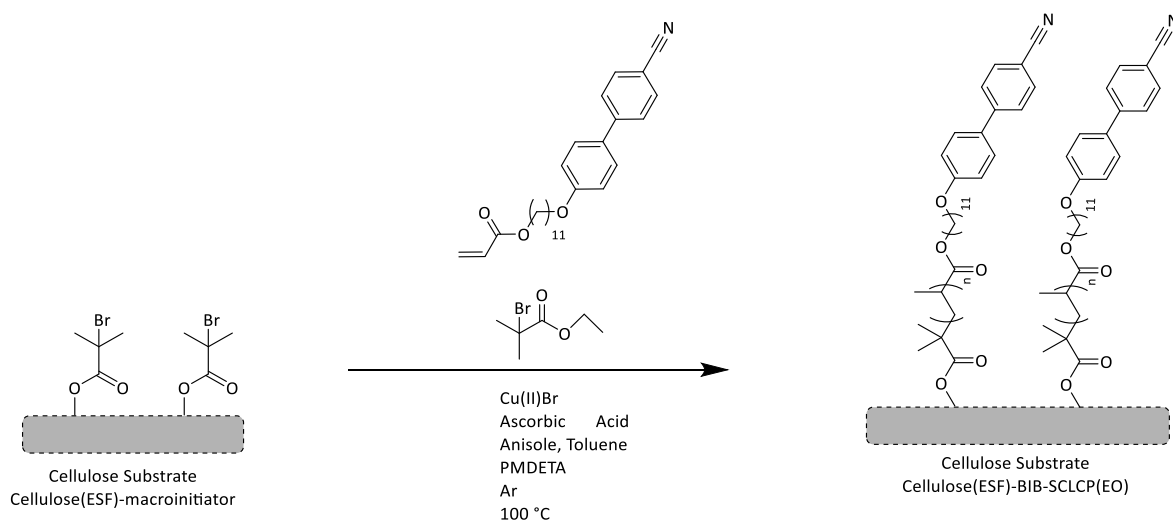
Figure 115: Cellulose(ESF) macroinitiator.

DMAP (cat.) was added to a well-mixed solution of toluene (5 mL) and TEA (21  $\mu$ L, 0.15 mmol), the headspace was flushed with argon and the solution was subjected to sonication (6 min). Substrate 11a (1.13 mg, 6.97  $\mu$ mol) was submerged in the solution. The suspension headspace was freshly flushed with argon and 2-bromoisobutyryl bromide (16  $\mu$ L, 0.13 mmol) was added, the system was closed under argon and agitated (16 hr). The substrate was washed sequentially with toluene, water, and hexane and dried *in vacuo* (12 hr). 1.15 mg

mass change %                    +1.8 %

FTIR  $\nu$   $\text{cm}^{-1}$ :                    (1733).

**6.4.13. Substrate 13: SI-ARGET ATRP of compound 2, from cellulose (ESF) macroinitiator using Cu(II)/PMDETA – ascorbic acid in anisole/toluene, with sacrificial initiator, ebib, under argon (without mixing). (Entry 9)**



*Scheme 20: SI-ARGET ATRP of compound 2, from cellulose (ESF) macroinitiator using Cu(II)/PMDETA – ascorbic acid in anisole/toluene, with sacrificial initiator, ebib, under argon (without mixing).*

11-((4'-Cyano-[1,1'-biphenyl]-4-yl)oxy)undecyl acrylate (400.51 mg, 954.6  $\mu\text{mol}$ ), Cu(II)Br (0.46 mg, 2.1  $\mu\text{mol}$ ), ascorbic acid (3.71 mg, 21.1  $\mu\text{mol}$ ) were washed into a dry Schlenk tube in dry toluene, the solution was concentrated *in vacuo*. Substrate 12a (1.54 mg, [9.50  $\mu\text{mol}$ , assuming substituent mass is negligible]) was introduced to the Schlenk tube and the atmosphere was degassed and refilled with argon. Ethyl-2-bromoisobutyrate (9.6  $\mu\text{L}$ , 65  $\mu\text{mol}$ ) was dissolved in anisole (3 mL) and degassed/refilled with argon (3x). The ethyl-2-bromoisobutyrate solution (22  $\mu\text{mol mL}^{-1}$ , 0.5 mL), toluene (100  $\mu\text{L}$ ) and PMDETA (3.6  $\mu\text{L}$ , 17  $\mu\text{mol}$ ) were added to the Schlenk tube via syringe. The flask suspension was degassed (freeze/thaw) until no further gas was evolved, the reaction was refilled with argon and isolated before heating. The no mixing method was employed (100 °C, 16 hr).

The reaction was allowed to cool to room temperature and opened to the atmosphere. The reaction mixture was diluted with toluene (10 mL) and the substrate was removed. The reaction mixture was further diluted with THF (5 mL), sonicated and eluted through activated alumina in THF and dried *in vacuo*, resulting in a white solid (0.39 g).

The substrate was thoroughly washed with toluene, isopropanol, water, isopropanol and hexane sequentially. The substrate was dried *in vacuo* (16 hr). (3.29 mg, substrate damaged during drying). The substrate was subsequently subjected to further washing boiling toluene (4  $\times$  25 mL)

and ethanol (4 × 25 mL) and dried *in vacuo* (> 16hr).

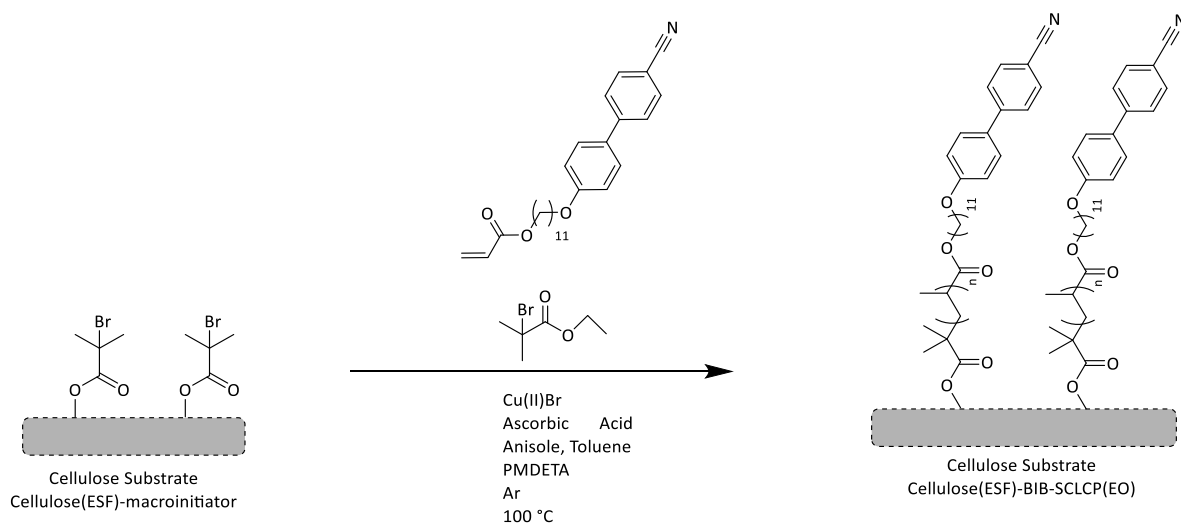
### Substrate

mass: 3.03 mg [damaged substrate].  
FT-IR  $\nu$  cm<sup>-1</sup>: 2923 (CH Ar), 2852 (CH Ar), 2224 (CN), 1729, 1603 (CH Ar),  
1526, 1495, 1291, 1248, 820.  
Thermal Properties, POM: Birefringence<sub>LC</sub> 142.5 Birefringence<sub>Background</sub> °C

### Sacrificial Polymer

GPC: RV: 13.587 ml; Mn: 15,987; Mw: 56,607; Mw/Mn: 3.54.  
RV: 17.603 ml; Mn: 1; Mw: 1; Mw/Mn: 1.  
<sup>1</sup>H NMR monitoring ratio (400 MHz, CHCl<sub>3</sub>), 3.85 – 4.20:5.77 – 6.44  $\delta$ <sub>H</sub>: 1.63:1  
FT-IR: 2922, 2853, 2226 (CN), 1737, 1710, 1635, 1600, 1531,  
1497.

**6.4.14. Substrate 14: SI-ARGET ATRP of compound 2, from cellulose (ESF) macroinitiator using Cu(II)/PMDETA – ascorbic acid in anisole/toluene, with sacrificial initiator, ebib, under argon (without mixing). (Entry 9)**



*Scheme 21: SI-ARGET ATRP of compound 2, from cellulose (ESF) macroinitiator using Cu(II)/PMDETA – ascorbic acid in anisole/toluene, with sacrificial initiator, ebib, under argon (without mixing).*

11-((4'-Cyano-[1,1'-biphenyl]-4-yl)oxy)undecyl acrylate (400.51 mg, 954.6  $\mu\text{mol}$ ), Cu(II)Br (0.46 mg, 2.1  $\mu\text{mol}$ ), ascorbic acid (3.71 mg, 21.1  $\mu\text{mol}$ ) were washed into a dry Schlenk tube in dry toluene, the solution was concentrated *in vacuo*. Substrate 12a (1.54 mg, [9.50  $\mu\text{mol}$ , assuming substituent mass is negligible]) was introduced to the Schlenk tube and the atmosphere was degassed and refilled with argon. Ethyl-2-bromoisobutyrate (9.6  $\mu\text{L}$ , 65  $\mu\text{mol}$ ) was dissolved in anisole (3 mL) and degassed/refilled with argon (3x). The ethyl-2-bromoisobutyrate solution (22  $\mu\text{mol mL}^{-1}$ , 0.5 mL), toluene (100  $\mu\text{L}$ ) and PMDETA (3.6  $\mu\text{L}$ , 17  $\mu\text{mol}$ ) were added to the Schlenk tube via syringe. The flask suspension was degassed (freeze/thaw) until no further gas was evolved. The reaction was refilled with argon and isolated before heating, no mixing mechanism was employed (100 °C, 16 hr).

The reaction was allowed to cool to room temperature and opened to the atmosphere. The reaction mixture was diluted with toluene (10 mL) and the substrate was removed. The reaction mixture was further diluted with THF (5 mL), sonicated and eluted through activated alumina in THF and dried *in vacuo*, resulting in a white solid (0.39 g).

The substrate was thoroughly washed with toluene, isopropanol, water, isopropanol and hexane sequentially. The substrate was dried *in vacuo* (16 hr). (3.29 mg, substrate damaged during drying). The substrate was subsequently subjected to further washing boiling toluene (4  $\times$  25 mL)

and ethanol (4 × 25 mL) and dried *in vacuo* (> 16hr).

### Substrate

mass: 3.03 mg [damaged substrate].

FT-IR  $\nu$   $\text{cm}^{-1}$ : 2923 (CH Ar), 2852 (CH Ar), 2224 (CN), 1729, 1603 (CH Ar), 1526, 1495, 1291, 1248, 820.

Thermal Properties, POM: Birefringence<sub>LC</sub> 142.5 Birefringence<sub>Background</sub> °C

### Sacrificial Polymer

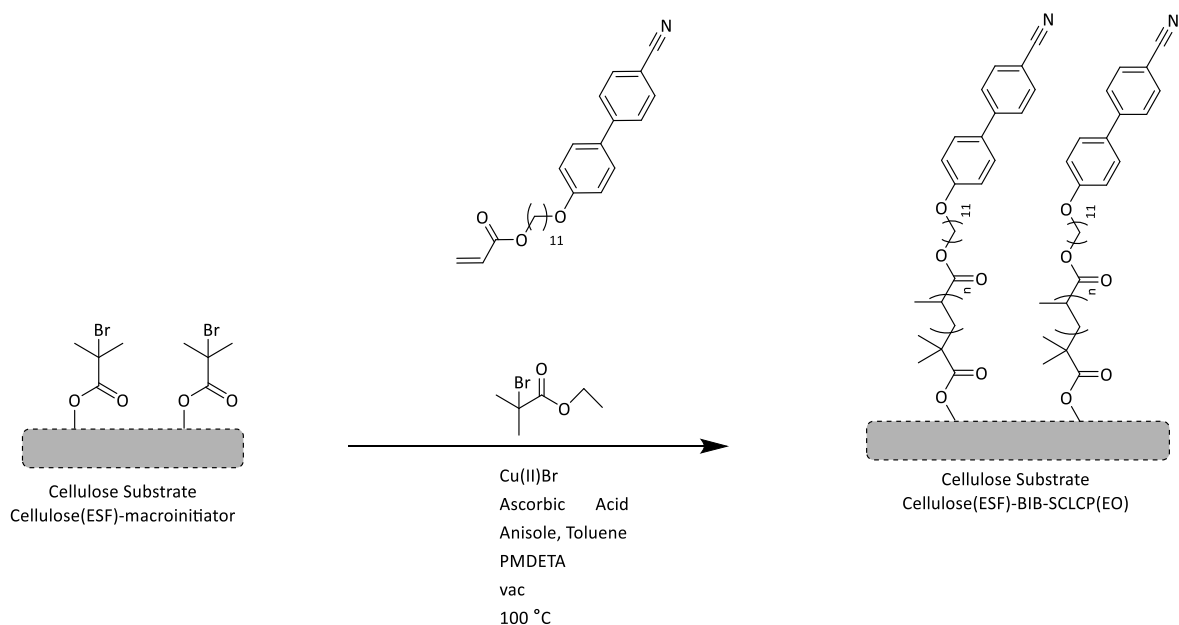
GPC: RV: 13.587 ml; Mn: 15,987; Mw: 56,607; Mw/Mn: 3.54.  
RV: 17.603 ml\*

<sup>1</sup>H NMR monitoring ratio (400 MHz, CHCl<sub>3</sub>), 3.85 – 4.20:5.77 – 6.44  $\delta_{\text{H}}$ : 1.63:1

FT-IR: 2922, 2853, 2226 (CN), 1737, 1710, 1635, 1600, 1531, 1497.

\*Not meaningfully characterised

**6.4.15. Substrate 15: SI-ARGET ATRP of compound 2, from cellulose (ESF) macroinitiator using Cu(II)/PMDETA – ascorbic acid in anisole/toluene, with sacrificial initiator, ebib, under vacuum (without mechanical mixing). (Entry 10)**



*Scheme 22: SI-ARGET ATRP of compound 2, from cellulose (ESF) macroinitiator using Cu(II)/PMDETA – ascorbic acid in anisole/toluene, with sacrificial initiator, ebib, under vacuum (without mechanical mixing).*

11-((4'-Cyano-[1,1'-biphenyl]-4-yl)oxy)undecyl acrylate (409.9 mg, 977.0  $\mu\text{mol}$ ), Cu(II)Br (0.52 mg, 2.3  $\mu\text{mol}$ ), ascorbic acid (3.88 mg, 22.0  $\mu\text{mol}$ ) were washed into a dry Schlenk tube in dry toluene, the toluene was removed *in vacuo*. Substrate 12b (2.19 mg, [13.5  $\mu\text{mol}$ , assuming substituent mass is negligible]) was introduced to the Schlenk tube and the atmosphere was degassed and refilled with argon. Ethyl-2-bromoisobutyrate (9.6  $\mu\text{L}$ , 65  $\mu\text{mol}$ ) was dissolved in anisole (1.5 mL) and degassed/refilled with argon (3x). The ethyl-2-bromoisobutyrate solution (43  $\mu\text{mol mL}^{-1}$ , 0.5 mL), toluene (100  $\mu\text{L}$ ) and PMDETA (3.8  $\mu\text{L}$ , 18  $\mu\text{mol}$ ) were added to the Schlenk tube via syringe. The flask suspension was degassed (freeze/thaw) until no further gas was evolved, on the final cycle the reaction left under a passive vacuum and heating (100  $^\circ\text{C}$ , 16 hr).

The reaction was allowed to cool to room temperature and opened to the atmosphere. The reaction mixture was diluted with toluene (10 mL) and the substrate was removed. The reaction mixture was further diluted with THF (5 mL), sonicated and eluted through activated alumina in THF and dried *in vacuo*, resulting in a white solid (0.40 g).

The substrate was thoroughly washed with toluene, isopropanol, water, isopropanol and hexane sequentially. The substrate was dried *in vacuo* (16 hr). The substrate was subsequently subjected to further washing boiling toluene (4 × 25 mL) and ethanol (4 × 25 mL) and dried *in vacuo* (> 16hr).

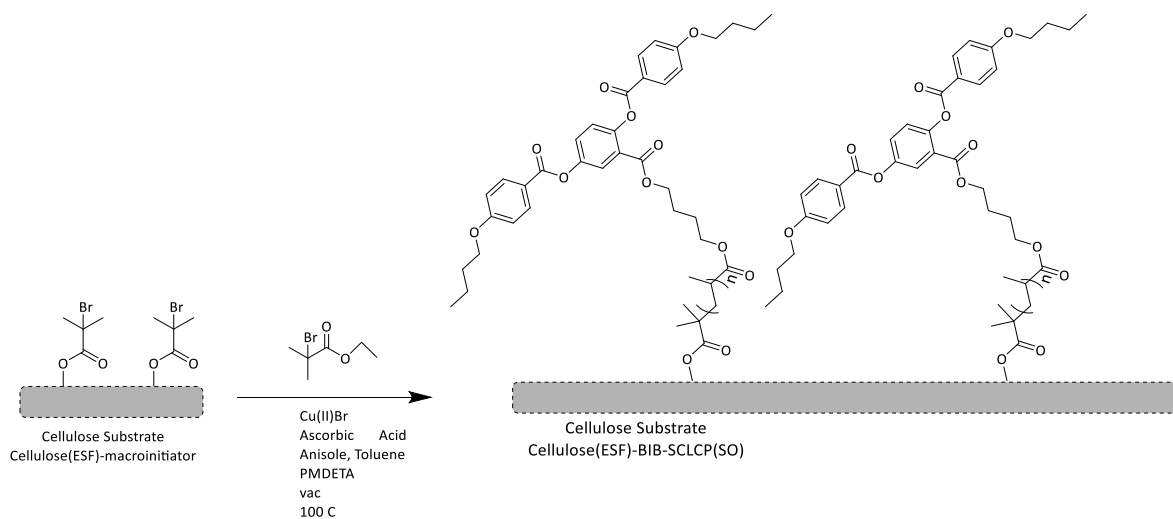
### Substrate

mass:	4.87 mg.
FT-IR $\nu$ $\text{cm}^{-1}$ :	2982, 2921 (CH Ar), 2853 (CH Ar), 2225 (CN), 1730, 1603 (CH Ar), 1524, 1495.
Thermal Properties, POM:	Birefringence <sub>LC</sub> 142.8 Birefringence <sub>Background</sub> °C

### Sacrificial Polymer

GPC:	RV: 13.513; Mn: 13,928; Mw: 42,216; Mw/Mn: 3.03
$^1\text{H}$ NMR monitoring ratio (400 MHz, $\text{CHCl}_3$ ), 3.85 – 4.20:5.77 – 6.44 $\delta_{\text{H}}$ :	9.63:1
Thermal Properties DSC:	$T_g$ 14.2 SmC 37.3 SmA 147.4 Iso Liq °C
FT-IR:	2922, 2852, 2225 (CN), 1727, 1603, 1522, 1495.

**6.4.16. Substrate 16: SI-ARGET ATRP of compound 6, from cellulose (ESF) macroinitiator using Cu(II)/PMDETA – ascorbic acid in anisole/toluene, with sacrificial initiator, ebib, under vacuum (without mechanical mixing). (Entry 11)**



*Scheme 23: SI-ARGET ATRP of compound 6, from cellulose (ESF) macroinitiator using Cu(II)/PMDETA – ascorbic acid in anisole/toluene, with sacrificial initiator, ebib, under vacuum (without mechanical mixing).*

Compound 6; 2-((4-(acryloyloxy)butoxy)carbonyl)-1,4-phenylene bis(4-butoxybenzoate) (401.12 mg, 0.62 mmol), Cu(II)Br (0.49 mg, 2.2  $\mu\text{mol}$ ), ascorbic acid (3.96 mg, 22.5  $\mu\text{mol}$ ) were washed into a dry Schlenk tube in dry toluene, the toluene was removed *in vacuo*. Substrate 12c (1.15 mg, [7.09  $\mu\text{mol}$ , assuming substituent mass is negligible]) was introduced to the Schlenk tube and the atmosphere was degassed and refilled with argon. Ethyl-2-bromoisobutyrate (19.2  $\mu\text{L}$ , 0.13 mmol) was dissolved in anisole (3 mL) and degassed/refilled with argon (3x). The ethyl-2-bromoisobutyrate solution (43  $\mu\text{mol mL}^{-1}$ , 0.5 mL), toluene (100  $\mu\text{L}$ ) and PMDETA (3.6  $\mu\text{L}$ , 17  $\mu\text{mol}$ ) were added to the Schlenk tube via syringe. The flask suspension was degassed (freeze/thaw) until no further gas was evolved, on the final cycle the reaction left under a passive vacuum and heating (100  $^{\circ}\text{C}$ , 16 hr).

The reaction was allowed to cool to room temperature and opened to the atmosphere. The reaction mixture was diluted with toluene (10 mL) and the substrate was removed. The reaction mixture was further diluted with THF (5 mL), sonicated and eluted through activated alumina in THF and dried *in vacuo*, resulting in a white solid (0.39 g).

The substrate was thoroughly washed with toluene, isopropanol, water, isopropanol and hexane sequentially. The substrate was dried *in vacuo* (16 hr). The substrate was subsequently subjected

to further washing boiling toluene (4 × 25 mL) and ethanol (4 × 25 mL) and dried *in vacuo* (> 16hr).

### Substrate

mass: 1.23 mg.  
FT-IR  $\nu$   $\text{cm}^{-1}$ : 1739 (CO), 1636, 1433, 1369, 1227, 1039.  
Thermal Properties, POM: -

### Sacrificial Polymer

GPC: RV 14.943: Mn 5,022; Mw 7,759; Mw/Mn 1.55.  
RV: 16.643\*  
RV: 17.26\*  
 $^1\text{H}$  NMR monitoring ratio (400 MHz,  $\text{CHCl}_3$ ), 3.85 – 4.20:5.77 – 6.44  $\delta_{\text{H}}$ : 26.3:1  
Thermal Properties DSC:  $T_g$  27.6 N 110.6 Iso Liq. °C  
FT-IR 2960, 2874, 1725 (C=O), 1604, 1510, 1423, 1243, 1157, 1053.

\*Not meaningfully characterised

Table 5a: Overview of polymerisation variables

	Entry 1	Entry 2	Entry 3	Entry 4	Entry 5	Entry 6
Substrate Type	Paper MI	Paper MI	Paper MI	Paper MI	Paper MI	Paper MI
Substrate Preparation	Substrate 1a	Substrate 1b	Substrate 1c	Substrate 1c	Substrate 1d	Substrate 1d
Size/Shape	whole/circle	quarter	quarter	quarter	quarter	quarter
mass / mg	6.10	1.79	1.55	1.98	1.70	1.49
Monomer Acrylate	EO	EO	EO	EO	EO	EO
mass / g (mmol)	2.00 (4.77)	0.46 (1.09)	0.35 (0.840)	0.35 (0.840)	0.40 (0.940)	0.40 (0.940)
Sacrificial Initiator	N/a	EBIB	EBIB	EBIB	EBIB	EBIB
Volume / $\mu\text{L}$ ( $\mu\text{mol}$ )		4.8 (33)	3.2 (22)	3.2 (22)	1.6 (11)	1.6 (11)
Ligand	PMDETA	PMDETA	Me <sub>6</sub> TREN	PMDETA	PMDETA	PMDETA
Volume / $\mu\text{L}$ ( $\mu\text{mol}$ )	20 (96)	5.1 (35)	5.0 (21)	3.6 (17)	3.6 (17)	3.6 (17)
Copper species	Cu(I)Br	Cu(I)Br	Cu(I)Br	Cu(I)Br	Cu(II)Br <sub>2</sub>	Cu(II)Br <sub>2</sub>
Mass / mg ( $\mu\text{mol}$ )	15.52 (108.0)	3.17 (22.1)	2.68 (18.7)	2.68 (18.4)	0.46 (2.1)	0.49 (2.2)
Solvent	Toluene	Toluene	Toluene	Anisole	Anisole	Anisole
Volume / mL	3.0	1.0	0.5	0.5	0.5	0.5
(Additional Component)	N/a	N/a	N/a	N/a	N/a	Toluene
Volume / $\mu\text{L}$						100
Reducing Agent	N/a	N/a	N/a	N/a	Asc Acid	Asc Acid
mass / mg ( $\mu\text{mol}$ )					3.71 (21.1)	3.98 (22.6)
Atmosphere	V/Ar	F-T/Ar	F-T/Ar	F-T/Ar	F-T/Ar	F-T/Ar
Mixing	Stirring	Stirring	Stirring	Stirring	None	Bubbling

Table 5b: Overview of polymerisation variables continued.

	Entry 7	Entry 8	Entry 9	Entry 10	Entry 11
Substrate Type	Paper MI	Paper MI	ESF MI	ESF MI	ESF MI
Substrate Preparation	Substrate 2ai	Substrate 2ai	Substrate 12a	Substrate 12b	Substrate 12c
Size/Shape	quarter	quarter	square	square	square
mass / mg	1.99	1.75	1.54	2.19	1.15
Monomer Acrylate	EO	SO	EO	EO	SO
mass / g (mmol)	0.41 (0.980)	0.39 (0.62)	0.40 (0.950)	0.41 (0.98)	0.40 (0.62)
Sacrificial Initiator	EBIB	EBIB	EBIB	EBIB	EBIB
Volume / $\mu\text{L}$ ( $\mu\text{mol}$ )	3.2 (22)	3.2 (22)	1.6 (11)	3.2 (22)	3.2 (22)
Ligand	PMDETA	PMDETA	PMDETA	PMDETA	PMDETA
Volume / $\mu\text{L}$ ( $\mu\text{mol}$ )	3.6 (17)	3.6 (17)	3.6 (17)	3.8 (18)	3.6 (17)
Copper species	Cu(II)Br <sub>2</sub>				
Mass / mg ( $\mu\text{mol}$ )	0.45 (2.0)	0.48 (2.1)	0.46 (2.1)	0.52 (2.3)	0.49 (2.2)
Solvent	Anisole	Anisole	Anisole	Anisole	Anisole
Volume / mL	0.5	0.5	0.5	0.5	0.5
(Additional Component)	N/a	N/a	Toluene	Toluene	Toluene
Volume / $\mu\text{L}$			100	100	100
Reducing Agent	Asc Acid				
mass / mg ( $\mu\text{mol}$ )	3.86 (21.9)	4.16 (23.6)	3.71 (21.1)	3.88 (22.0)	3.96 (22.5)
Atmosphere	F-T/Ar	F-T/Ar	F-T/Ar	F-T/PV	F-T/PV
Mixing	Stirring	Stirring	None	Bubbling	Bubbling

## Abbreviations

ARGET	Activator ReGenerated by Electron Transfer
Asc acid	Ascorbic Acid
ATRP	Atom Transfer Radical Polymerisation
BIB	Grafted bromoisobutyrate functionality
BIBB	$\alpha$ - Bromoisobutyryl bromide
DP	Degree of Polymerisation / Differential Pressure
DMAP	4-Dimethylaminopyridine
DSC	Differential scanning calorimetry
EBIB	Ethyl $\alpha$ -bromoisobutyrate
EDAC	1-Ethyl-3-(3-dimethylaminopropyl)carbodiimide
ESF	ElectroSpun Fibre
ESI	Electrospray ionization
FT-IR	Fourier transform infrared spectroscopy
G	Glass
GPC	Gel permeation chromatography
HMTETA	1,1,4,7,10,10-Hexamethyltriethylenetetramine
Iso	Isotropic
MCLCP	Main Chain Liquid Crystal Polymer
MS	Mass Spectrometry
LC	Liquid Crystal
LRP	“Living” Radical Polymerisation
MALDI	Matrix-assisted laser desorption/ionization
Meas	Measured
Me <sub>6</sub> TREN	Tris[2-(dimethylamino)ethyl]amine
MMA	Methylmethacrylate

Mn	Number Average Molecular Weight
Mw	Weight Average Molecular Weight
N	Nematic
NMP	Nitroxide mediated radical polymerization
NMR	Nuclear Magnetic Resonance
PDI	Polydispersity Index
PLC	Polymeric Liquid Crystal
PMA	Poly(methyl acrylate)
PMDETA	N,N,N',N'',N''-Pentamethyldiethylenetriamine
POM	Polarising Optical Microscopy
Prev	Previous
RAFT	Reversible addition–fragmentation chain-transfer
RALS	Right Angle Light Scattering
RI	Refractive Index
ROP	Ring Opening Polymerisation
RegC	Regenerated Cellulose
SCLCP	Side Chain Liquid Crystal Polymer
SEM	Scanning Electron Microscopy
SI	Surface Initiated
SmA	Smectic A
SmC	Smectic C
THF	Tetrahydrofuran

## References

1. C.-F. Huang, *Polym. J. (Tokyo, Jpn.)*, 2016, **48**, 341-350.
2. P. J. Collings and M. Hird, in *Introduction to Liquid Crystals Chemistry and Physics*, Taylor & Francis, London, Editon edn., 1997, pp. 43-77.
3. P. G. De Gennes, *Mol. Cryst. Liq. Cryst.*, 1973, **21**, 49-76.
4. A. Wulf, *Phys. Rev. A*, 1975, **11**, 365-375.
5. W. L. McMillian, *Phys. Rev. A*, 1973, **8**, 1921- 1929
6. P. J. Collings and M. Hird, in *Introduction to Liquid Crystals Chemistry and Physics*, Taylor & Francis, London, Editon edn., 1997, pp. 271-288.
7. G. Moad and D. H. Solomon, *The Chemistry of Radical Polymerization*, second edn., Elsevier Ltd, Oxford, 2006.
8. W. A. Braunecker and K. Matyjaszewski, *Prog. Polym. Sci.*, 2007, **32**, 93-146.
9. G. Moad, E. Rizzardo and S. H. Thang, *Acc. Chem. Res.*, 2008, **41**, 1133-1142.
10. R. F. T. Stepto, *Pure Appl. Chem.*, **81**, 351-353.
11. M. Rogosic, H. J. Mencer and Z. Gomzi, *Eur. Polym. J.*, 1996, **32**, 1337-1344.
12. V. N. Tsvetkov, *Polymer Science U.S.S.R.*, 1977, **19**, 2485-2508.
13. L. Noirez, H. Mendil-Jakani, P. Baroni and J. H. Wendorff, *Polymers*, 2012, **4**, 1109-1124.
14. T. Ganicz and W. Stańczyk, *Mater. Corros.*, 2009, **2**, 95-128.
15. H. Finkelmann, H. Ringsdorf, W. Siol and J. H. Wendorff, in *Mesomorphic Order in Polymers and Polymerization in Liquid Crystalline Media*, ed. A. Blumstein, American Chemical Society, Washington D.C., Editon edn., 1978, vol. 74 of ACS Symp. Ser., pp. 22-32.
16. H. Finkelmann, H. Ringsdorf and J. H. Wendorff, *Makromol. Chem.*, 1978, **179**, 273-276.
17. H. Finkelmann, H. Ringsdorf, W. Siol and J. H. Wendorff, *Makromol. Chem.*, 1978, **179**, 829-832.
18. P. J. Collings and M. Hird, in *Introduction to Liquid Crystals Chemistry and Physics*, Taylor & Francis, London, Editon edn., 1997, pp. 93-110.
19. X.-F. Chen, Z. Shen, X.-H. Wan, X.-H. Fan, E.-Q. Chen, Y. Ma and Q.-F. Zhou, *Chem. Soc. Rev.*, 2010, **39**, 3072-3101.
20. J. Tani, T. Takagi and J. Qiu, *Appl. Mech. Rev* 1998 **51**, 505-521.
21. Y. Nishiyama, P. Langan and H. Chanzy, *J. Am. Chem. Soc.*, 2002, **124** 9074–9082.
22. G. Siqueira, J. Bras and A. Dufresne, *Polymer*, 2010, **2**, 728-765.
23. N. Lavoine, I. Desloges, A. Dufresne and J. Bras, *Carbohydr. Polym.*, 2012, **90**, 735-764.
24. K. Ohkawa, *Molecules*, 2015, **20**, 9139-9154.
25. F. J. Schmied, C. Teichert, L. Kappel, U. Hirn, W. Bauer and R. Schennach, *Scientific Reports*, 2013, **3**, 2432.
26. J. R. Barnett and V. A. Bonham, *Biol. Rev.*, 2004, **79**, 461-472.
27. A. Isogai, T. Saito and H. Fukuzumi, *Nanoscale*, 2011, **3**, 71-85.
28. I. Siró and D. Plackett, *Cellulose*, 2010, **17**, 459-494.
29. M. E. Vallejos, M. S. Peresin and O. J. Rojas, *J. Polym. Environ.*, 2012, **20**, 1075-1083.
30. W. E. Teo and S. Ramakrishna, *Nanotechnology*, 2006, **17**, R89.
31. Z. Ma, M. Kotaki and S. Ramakrishna, *J. Membr. Sci.*, 2005, **265**, 115-123.
32. M. W. Frey, *Polym. Rev. (Philadelphia, PA, U. S.)*, 2008, **48**, 378-391.
33. J. P. F. Lagerwall, J. T. McCann, E. Formo, G. Scalia and Y. Xia, *Chem. Commun.*, 2008, **42**, 5420-5422.
34. D. K. Kim, M. Hwang and J. P. F. Lagerwall, *J. Polym. Sci. B. Polym. Phys.*, 2013, **51**, 855-867.
35. C. G. Reyes, A. Sharma and J. P. F. Lagerwall, *Liq. Cryst.*, 2016, **43**, 1986-2001.
36. M. M. Hamed, V. E. Campbell, P. Rothemund, F. Güder, D. C. Christodouleas, J.-F. Bloch and G. M. Whitesides, *Adv. Funct. Mater.*, 2016, **26**, 2446-2453.
37. J. Mu, C. Hou, H. Wang, Y. Li, Q. Zhang and M. Zhu, *Science Advances*, 2015, **1**.
38. A. A. Kumar, J. W. Hennek, B. S. Smith, S. Kumar, P. Beattie, S. Jain, J. P. Rolland, T. P. Stossel, C. Chunda-Liyoka and G. M. Whitesides, *Angew. Chem. Int. Ed.*, 2015, **54**, 5836-5853.

39. F. Güder, A. Ainla, J. Redston, B. Mosadegh, A. Glavan, T. J. Martin and G. M. Whitesides, *Angew. Chem. Int. Ed.*, 2016, **55**, 5727-5732.
40. S. C. Fox, B. Li, D. Xu and K. J. Edgar, *Biomacromolecules*, 2011, **12**, 1956-1972.
41. K. J. Edgar, C. M. Buchanan, J. S. Debenham, P. A. Rundquist, B. D. Seiler, M. C. Shelton and D. Tindall, *Prog. Polym. Sci.*, 2001, **26**, 1605-1688.
42. H. P. S. Abdul Khalil, A. H. Bhat and A. F. Ireana Yusra, *Carbohydr. Polym.*, 2012, **87**, 963-979.
43. A. Hebeish and J. T. Guthrie, in *The Chemistry and Technology of Cellulosic Copolymers*, Springer Berlin Heidelberg, Berlin, Heidelberg, Editon edn., 1981, pp. 196-244.
44. Y. Yang, K. Yan, C. Zhi-nan, S. Xiao-feng and Y. Jin-ying, *Journal of Cellulose Science and Technology*, 2009, 53-58.
45. C. Jian, Q. Ye, M. Huo and J. Yuan, in *Cellulose-Based Graft Copolymers: structure and chemistry*, ed. V. K. Thakur, CRC Press, New York, Editon edn., 2015, pp. 65-78.
46. T. Govindarajan and R. Shandas, *Polymers*, 2014, **6**, 2309.
47. T. Ge and M. Rubinstein, *Macromolecules*, 2015, **48**, 3788-3801.
48. J. Gomez, J. Jiang, A. Gujral, C. Huang, L. Yu and M. D. Ediger, *Soft Matter*, 2016, **12**, 2942-2947.
49. Y. Tsujii, K. Ohno, S. Yamamoto, A. Goto and T. Fukuda, in *Surface-Initiated Polymerization I*, ed. R. Jordan, Springer Berlin Heidelberg, Berlin, Heidelberg, Editon edn., 2006, pp. 1-45.
50. T. Zhou, H. Qi, L. Han, D. Barbash and C. Y. Li, *Nature Communications*, 2016, **7**, 11119.
51. S. T. Milner, *Science*, 1991, **251**, 905-914.
52. M. I. Montañez, Y. Hed, S. Utsel, J. Ropponen, E. Malmström, L. Wågberg, A. Hult and M. Malkoch, *Biomacromolecules*, 2011, **12**, 2114-2125.
53. R. Meena and A. Bhattacharya, in *Cellulose-Based Graft Copolymers: structure and chemistry*, ed. V. K. Thakur, CRC Press, New York, Editon edn., 2015, pp. 13-39.
54. A. Yu, J. Shang, F. Cheng, B. A. Paik, J. M. Kaplan, R. B. Andrade and D. M. Ratner, *Langmuir*, 2012, **28**, 11265-11273.
55. J. Hafrén, W. Zou and A. Córdova, *Macromol. Rapid Commun.*, 2006, **27**, 1362-1366.
56. D. Roy, M. Semsarilar, J. T. Guthrie and S. Perrier, *Chem. Soc. Rev.*, 2009, **38**, 2046-2064.
57. M. Szwarc, *Nature*, 1956, **178**, 1168-1169.
58. H. Fischer, *Chem. Rev.*, 2001, **101**, 3581-3610.
59. W. Tang, N. V. Tsarevsky and K. Matyjaszewski, *J. Am. Chem. Soc.*, 2006, **128**, 1598-1604.
60. A. Rabea and S. Zhu, *Polymers*, 2015, **7**, 819.
61. M. Abbasian and S. E. Shoja, *Braz. J. Chem. Eng.*, 2012, **29**, 285-294.
62. K. Matyjaszewski and N. V. Tsarevsky, *Nat. Chem*, 2009, **1**, 276-288.
63. K. Matyjaszewski, *Curr. Org. Chem.*, 2002, **6**, 67-82.
64. M. Kato, M. Kamigaito, M. Sawamoto and T. Higashimura, *Macromolecules*, 1995, **28**, 1721-1723.
65. J.-S. Wang and K. Matyjaszewski, *J. Am. Chem. Soc.*, 1995, **117**, 5614-5615.
66. N. V. Tsarevsky and K. Matyjaszewski, *Chem. Rev.*, 2007, **107**, 2270-2299.
67. *Atom Transfer Radical Polymerization (ATRP)*, <http://www.cmu.edu/maty/chem/fundamentals-atrp/atrp.html> Accessed March 2016.
68. W. Tang, Y. Kwak, W. Braunecker, N. V. Tsarevsky, M. L. Coote and K. Matyjaszewski, *J. Am. Chem. Soc.*, 2008, **130**, 10702-10713.
69. W. Tang and K. Matyjaszewski, *Macromolecules*, 2007, **40**, 1858-1863.
70. K. Matyjaszewski and J. Xia, *Chem. Rev.*, 2001, **101**, 2921-2990.
71. T. J. Zerk and P. V. Bernhardt, *Dalton Trans.*, 2013, **42**, 11683-11694.
72. M. Fantin, A. A. Isse, A. Gennaro and K. Matyjaszewski, *Macromolecules*, 2015, **48**, 6862-6875.
73. W. A. Braunecker, N. V. Tsarevsky, A. Gennaro and K. Matyjaszewski, *Macromolecules*, 2009, **42**, 6348-6360.
74. M. Horn and K. Matyjaszewski, *Macromolecules*, 2013, **46**, 3350-3357.

75. K. Min, H. Gao and K. Matyjaszewski, *J. Am. Chem. Soc.*, 2005, **127**, 3825-3830.
76. Y. Kwak and K. Matyjaszewski, *Polym. Int.*, 2009, **58**, 242-247.
77. W. Jakubowski, K. Min and K. Matyjaszewski, *Macromolecules*, 2006, **39**, 39-45.
78. K. Min, H. Gao and K. Matyjaszewski, *Macromolecules*, 2007, **40**, 1789-1791.
79. T. Kreer, *Soft Matter*, 2016, **12**, 3479-3501.
80. M. Ejaz, S. Yamamoto, K. Ohno, Y. Tsujii and T. Fukuda, *Macromolecules*, 1998, **31**, 5934-5936.
81. C. J. Fristrup, K. Jankova and S. Hvilsted, *Soft Matter*, 2009, **5**, 4623-4634.
82. N. Çankaya, in *Cellulose - Fundamental Aspects and Current Trends*, eds. M. Poletto and H. L. Ornaghi, InTech, Editon edn., (2015).
83. A. Carlmark and E. Malmström, *J. Am. Chem. Soc.*, 2002, **124**, 900-901.
84. Q. Feng, D. Hou, Y. Zhao, T. Xu, T. J. Menkhaus and H. Fong, *ACS Appl. Mater. Interfaces*, 2014, **6**, 20958-20967.
85. T. J. Menkhaus, H. Varadaraju, L. Zhang, S. Schneiderman, S. Bjustrom, L. Liu and H. Fong, *Chem. Commun. (Cambridge, U. K.)*, 2010, **46**, 3720-3722.
86. J. M. Geary, J. W. Goodby, A. R. Kmetz and J. S. Patel, *J. Appl. Phys.*, 1987, **62**, 4100-4108.
87. M. P. Stewart, F. Maya, D. V. Kosynkin, S. M. Dirk, J. J. Stapleton, C. L. McGuinness, D. L. Allara and J. M. Tour, *J. Am. Chem. Soc.*, 2004, **126**, 370-378.
88. H. A. Haque, S. Kakehi, M. Hara, S. Nagano and T. Seki, *Langmuir*, 2013, **29**, 7571-7575.
89. W. A. Stańczyk, A. Szeląg, J. Kurjata, E. Nowinowski-Kruszelnicki and A. Walczak, *Mol. Cryst. Liq. Cryst.*, 2010, **526**, 18-27.
90. R. Westlund, A. Carlmark, A. Hult, E. Malmstrom and I. M. Saez, *Soft Matter*, 2007, **3**, 866-871.
91. X. Chen, Y. Huang, H. Zhang, M. Gauthier and G. Yang, in *Cellulose-based graft copolymers: structure and chemistry*, ed. T. V. K., CRC Press, Florida, Editon edn., 2015, pp. 455-466.
92. D. Lee, A. J. Nolte, A. L. Kunz, M. F. Rubner and R. E. Cohen, *J. Am. Chem. Soc.*, 2006, **128**, 8521-8529.
93. D. Wang, J. Tan, H. Kang, L. Ma, X. Jin, R. Liu and Y. Huang, *Carbohydr. Polym.*, 2011, **84**, 195-202.
94. A. Donald, A. Windle and S. Hanna, in *Liquid Crystalline Polymers*, Cambridge University Press, Cambridge, Editon edn., 2006, pp. 44-46.
95. *A guide to multi-detector gel permeation chromatography*, <http://www.agilent.com/cs/library/primers/public/5990-7196EN.pdf>, Accessed November 2016.
96. S. Hansson, E. Östmark, A. Carlmark and E. Malmström, *ACS Appl. Mater. Interfaces*, 2009, **1**, 2651-2659.
97. T. A. von Werne, D. S. Germack, E. C. Hagberg, V. V. Sheares, C. J. Hawker and K. R. Carter, *J. Am. Chem. Soc.*, 2003, **125**, 3831-3838.
98. C.-F. Huang, *Polym J*, 2016, **48**, 341-350.
99. D. L. Thomsen, P. Keller, J. Naciri, R. Pink, H. Jeon, D. Shenoy and B. R. Ratna, *Macromolecules*, 2001, **34**, 5868-5875.
100. P. L. Barny, J. C. Dubois, C. Friedrich and C. Noel, *Polym. Bull.*, 1986, **15**, 341-348.
101. C. Chang and C. Pugh, *Macromolecules*, 2001, **34**, 2027-2039.
102. H. Zhang, Z. Yu, X. Wan, Q. F. Zhou and E. M. Woo, *Polymer*, 2002, **43**, 2357-2361.
103. H. Zhao, J. H. Kwak, Z. Conrad Zhang, H. M. Brown, B. W. Arey and J. E. Holladay, *Carbohydr. Polym.*, 2007, **68**, 235-241.
104. I. M. Saez, Editon edn., 2016.
105. D. Gaspar, S. N. Fernandes, A. G. d. Oliveira, J. G. Fernandes, P. Grey, R. V. Pontes, L. Pereira, R. Martins, M. H. Godinho and E. Fortunato, *Nanotechnology*, 2014, **25**, 094008.
106. K. Matyjaszewski, H. Dong, W. Jakubowski, J. Pietrasik and A. Kusumo, *Langmuir*, 2007, **23**, 4528-4531.

107. Y. Nakamura, R. Lee, M. L. Coote and S. Yamago, *Macromol. Rapid Commun.*, 2016, **37**, 506-513.
108. H. Sato, N. Ichieda, H. Tao and H. Ohtani, *Anal. Sci.*, 2004, **20**, 1289-1294.
109. C. Yoshikawa, A. Goto and T. Fukuda, in *e-Polymers*, Editon edn., 2002, vol. 2, p. 172.
110. R. Lacheretz, D. G. Pardo and J. Cossy, *Org. Lett.*, 2009, **11**, 1245-1248.
111. S. Ramakrishna, K. Fujihara, W.-E. Teo, T. Yong, Z. Ma and R. Ramaseshan, *Materials Today*, 2006, **9**, 40-50.
112. L. E. Aguirre, A. de Oliveira, D. Seč, S. Čopar, P. L. Almeida, M. Ravnik, M. H. Godinho and S. Žumer, *Proceedings of the National Academy of Sciences*, 2016, **113**, 1174-1179.
113. Y. Nakamori, G. Kitahara, K. Miwa, S. Towata and S. Orimo, *Applied Physics a-Materials Science & Processing*, 2005, **80**, 1-3.
114. A. P. Mathew, A. Chakraborty, K. Oksman and M. Sain, in *Cellulose Nanocomposites*, American Chemical Society, Editon edn., 2006, vol. 938, pp. 114-131.
115. A. M. Kasko, S. R. Grunwald and C. Pugh, *Macromolecules*, 2002, **35**, 5466-5474.
116. A. M. Kasko, A. M. Heintz and C. Pugh, *Macromolecules*, 1998, **9297**, 256-271.
117. G. W. Gray and J. W. Goodby, in *Smectic Liquid Crystals*, Leonard Hill, Glasgow, Editon edn., 1984, pp. 1-22.
118. P. G. de Gennes, *Eur. Phys. J. E*, 2000, **2**, 201-205.
119. C. R. de Gennes, *Acad. Sci. Paris, ser. IV* 2000, **1**, 1179-1186.
120. M. F. Palermo, A. Pizzirusso, L. Muccioli and C. Zannoni, *J. Chem. Phys.*, 2013, **138**, 204901.
121. M. Walker and M. R. Wilson, *Soft Matter*, 2016, **12**, 8876-8883.
122. X.-J. Wang and Q.-F. Zhou, *Liquid Crystalline Polymers*, World Scientific, Singapore, 2004.
123. A. Donald, A. Windle and S. Hanna, in *Liquid Crystalline Polymers*, Cambridge University Press, Cambridge, Editon edn., 2006, pp. 229-291.
124. X.-J. Wang and M. Warner, *J. Phys. A.*, 1987, **20**, 713-731.
125. T. Wu, K. Efimenko, P. Vlček, V. Šubr and J. Genzer, *Macromolecules*, 2003, **36**, 2448-2453.
126. A. Milchev, J. P. Wittmer and D. P. Landau, *J. Chem. Phys.*, 2000, **112**, 1606-1615.
127. P. Tadeusz, *Macromol. Symp.*, 1999, **139**, 49-56.
128. S. Yamamoto, Y. Tsujii and T. Fukuda, *Macromolecules*, 2002, **35**, 6077-6079.
129. D. S. Pedersen and C. Rosenbohm, *Synthesis*, 2001, **16**, 2431-2434
130. E. Gmelin and S. M. Sarge, *Pure & Appl. Chem*, 1995, **67**, 1789-1800.